IN VITRO LONG TERM TIME-LAPSE IMAGING STUDIES OF THE MCF-10 MAMMARY CANCER CELL PROGRESSION MODEL USING A CUSTOM INCUBATOR MICROSCOPE

A Dissertation

Presented to the Faculty of the Graduate School

of Cornell University

In Partial Fulfillment of the Requirements for the Degree of

Doctor of Philosophy

by

Julian Palacios Goerger

August 2015

© 2015 Julian Palacios Goerger

IN VITRO LONG TERM TIME-LAPSE IMAGING STUDIES OF THE MCF-10 MAMMARY CANCER CELL PROGRESSION MODEL USING A CUSTOM INCUBATOR MICROSCOPE

Julian Palacios Goerger, Ph.D.

Cornell University 2015

Time-lapse imaging of cells has been historically limited to a few hours because of the difficulty associated with maintaining the appropriate physiological pH and temperature of the cells during prolonged imaging. Carbon dioxide produced by cellular respiration changes the pH of the medium, and sodium bicarbonate based buffers typically used for cell culture require an atmosphere of 5% CO2 to maintain a physiologically appropriate pH. Microscope stage incubators can provide such an atmosphere in an encapsulated box set up on the microscope stage, but researchers often complain about temperature instability and gradients that arise in such systems. Additionally, the price and complexity of such systems led us to develop an inexpensive alternative consisting of a miniaturized microscope and stage that fits inside a conventional CO2 incubator. In addition to the optical and mechanical parts, I created a user-friendly computer program that allows for the design of custom imaging sessions and protocols, developed autofocusing algorithms, and the associated electronics for instrument control and communication between the computer and the microscopes. I placed special emphasis on giving the microscopes the capability to perform fluorescent imaging because fluorescence has become the workhorse of molecular studies in cell biology in recent times.

My primary use of the microscopes that I built centered on studies of a human-derived mammary cancer cell line, the MCF cell progression model of cancer, which provides a model of increasing tumorigenicity in cells all arising from the same genetic background. By tracking single cells I find that cancer cells have heterogeneous subpopulations of cells with varied division potential, mitotic errors and aberrant nuclei, which I quantified and categorized. I describe a method for quantifying the absence of contact inhibition of growth in cancer cells in cocultures, and I find that cancer cells affect the morphology of normal cells. I

find that the cancer cells are better at creating invasive strands in Matrigel, and these invasions are temporally correlated with the change of cell culture medium. Additionally, an absence of serum causes the retraction of normal cells but promotes the invasion of the cancer cells.

BIOGRAPHICAL SKETCH

Julian was born in downtown Madrid, Spain on February 24, 1983 where he grew up with his three siblings and parents. He spent his childhood summers in southern France where his mother was born. It was there that he probably developed a love for rural landscapes, forests and streams that would eventually lead him to travel to Ithaca. At age 13 he became tennis champion of the Madrid tournament. However, he was more interested in understanding what was this thing called gravity that makes the ball go down. So Julian graduated from Runnymede High School in 2001 obtaining his British A-levels in Physics and Math and then went on to obtain his bachelor's degree in Physics from Complutense University in 2008, with an emphasis in Astronomy. By that time he had developed an interest in biology so he obtained his Master's degree in Biophysics from Autonoma University a year later. He spent the 2004 academic year in Germany at the Johannes Gutenberg University in Mainz where he successfully completed the corresponding physics curriculum in German. Mainz is a setting similar to Ithaca, but with a huge Rhine river supplanting Ithaca's Cayuga Lake, a nice cathedral and some roman ruins, and a large international Campus like Cornell's. In 2008 he was awarded a fellowship to pursue an advanced degree in the United States from the competitive "la Caixa" Foundation based in Barcelona. He chose Cornell over Yale and Boston because of the excellent engineering facilities available at Cornell as well as the beautiful campus and scenic landscapes. Also, Ithaca allowed for his favorite pass times: gorge hiking, biking and anything water related in the summer and skiing in the winter. His biggest interests during alternating points in his life were Airplanes, Astronomy, Quantum Physics, Microscopes, Cellular biology and Computer Programming. Someone once said happiness results when you find a job that intersects four things: what you're good at, what you like to do, what you think you should do, and what actually pays you. Julian's problem is probably that he's interested in too many things, but he feels fulfilled and lucky by this thesis that has covered a number of his interests.

To all the people who share my passion for building things and the progress of science and discovery

ACKNOWLEDGMENTS

I'd like to thank all the people that have made it possible for me to write this thesis. Firstly my parents, who have almost daily asked me if I had finished it, and who, during my life, have given me the support and freedom necessary to pursue any of my interests. Secondly, to my advisor Warren Zipfel who has *also* given me the freedom necessary to pursue my interests, and whose extraordinary support has made this thesis a reality. I have been lucky to work with many people that have used my microscope, and thanks to them I have seen amazing things with it, from neuronal growths to heart beating cells to fusion of myotubes, to just name a few, giving me a wide range of experiences with time-lapse culture of cells that I think few people have. In the lab, Avtar Singh has been a constant and friendly source of help as he is the person that I have turned to by default. I'd also like to thank Becky Williams for contributing to all the group meeting discussions with interesting comments. Finally I am also grateful for the "La Caixa" Foundation which supported my first two years at Cornell.

TABLE OF CONTENTS

Biographical Sketch iii
Acknowledgments v
Table of Contents vi
Chapter 1: Introduction 1
Chapter 2: Custom Microscope Designs For Optimal Long Term Cell Imaging Experiments 7
Introduction 7
General description of the instrument 8
Building a Microscope 11
Tube Lens 13
Brightfield Light Source 14
Inclined Illumination 17
Space Considerations 19
Adding Darkfield and Fluorescence Capabilities 23
Adding Fluorescence Capability 27
Motorization of Focusing and Stages 36
The 1-Color Fluorescence Microscope 48
The 2-Color Fluorescence Microscope 50
Other Aspects of the Microscope 52
Light Emitting Diodes and Electronics 52
Upright Microscope 56
Reduction of hot pixel noise 57
Calibration of the two-color microscope 58
Resolution 59
Condensation 59
Plastic versus glass dishes 60
Incubator vibrations 61
Chapter 3: Software: IncuScope and ImageJ Programs 63
IncuScope – The Program That Runs The Incubator Microscope 63
Main Functions 65
Secondary Functions 71
Algorithms 77
Image Analysis Programs Written In The ImageJ Macro Language 82
Methods for tracking cells 82
Methods for correction of vibrations via image alignments 91

Other programs for image analysis 95
Chapter 4: In Vitro Long Term Imaging Studies Of The MCF Cell Progression Model Of Cancer 99
Abstract 99
Introduction 99
Results 103
Cellular features characteristic of MCF10CA1a cells. 103
Analysis of tripolar divisions in MCF10CA1a cells 119
Origin of giant MCF10CA1a cells 123
Other features of MCF10CA1a cells 126
Experiments using co-cultures of MCF10A and MCF10CA1a cells 133
The morphology of MCF10A cells is affected by the presence of MCF10CA1a cells 137
Co-cultures show contact inhibited growth in 10A and 10AT cells, but not in CA1a cells 140
Laser ablation of a CA1a cell 144
Growth of cells in Matrigel 146
Migrating sheets of cells originating from CA1a acini 152
Coculture of 10A and CA1a cells in Matrigel: Invasive strands 154
CA1a cells are the leader cells of invasive strands in cocultures 155
CA1a cells affects the morphology of 10A acini 157
Sheet outgrowths reveal dynamic response of cells to new medium 161
Invasion is induced by serum depravation and by EGF 163
Chapter 5: Conclusions 166
APPENDIX A: Other aspects of the 10A, 10AT and CA1a cell lines 172
Other aspects of growth on Matrigel 172
Cell movements in Matrigel 175
Hypoxia inhibits growth 176
Discussion on tubules 179
Growth on Collagen 179
Effect of light on cell growth: MCF10A vs MCFCA1a 181
Sheet Migration: A problem to overcome when measuring cell migration speed 183
Average Migration Speed 186
Test for cell senescence is negative 189
Search for markers of cancer stem cells 191
Different modes of growth 193
The effect of a thin layer of Matrigel on 10A cells 194
Effect of density on cell migration speed and cell growth 195
Scratch assays 197

APPENDIX B: Other applications of the microscope 198
Submitted co-authored Papers 198
A microRNA miR-34a-Regulated Bimodal Switch Targets Notch in Colon Cancer Stem Cells. 198
Recruitment of mesenchymal stem cells by bone marrow concentrate and platelet rich plasma. 199
Other preliminary collaborative data 201
Triggering X-ray computed tomography with real time image analysis of heart beats in chicken embryo vessels 201
Horse mesenchymal bone marrow primary cells- Cornell Vet School Nixon Lab 204
Cardiomyocytes and cell stress 210
Keratinocyte culture from Hair Follicle 212
Scratch assays reveal that migration inhibits division 214
Darkfield illumination can detect subpopulations of primary cells 216
APPENDIX C: Additional Information 217
Parts List for a simple non-fluorescent Microscope 217
Additional Components needed for fluorescence and incubator use as described in the thesis 224
Supplementary Information 227
Programming codes for IncuScope, Arduino, ImageJ 228
A program to sort PubMed results 229
References 230

CHAPTER 1: INTRODUCTION

Existing options for long term time-lapse imaging of cells in biology are either expensive or don't provide sufficient control of both temperature and CO2. To overcome these issues I developed a small microscope that can be assembled from commercially available parts and, optionally, also from custom made parts, which fits inside a conventional CO2 incubator that is commonly found in every biological laboratory. At an estimated cost of $14000 (of which $10000 is the motorized stage) the microscope is much cheaper than for example, an Olympus incubator microscope system which ranges in the hundreds of thousands of dollars. Other companies have, over the past 5 years, introduced into the market microscopes that fit inside incubators. None of them has chosen the same design that I have and they are all more expensive and offer less features. For example, there doesn't exist one that includes a motorized focusing solution at a low price point. The same applies to 2-color fluorescence capability.

A crucial aspect of an incubator microscope is that it has to be able to withstand the temperature and the high humidity inside the incubator for long periods of time. It is conceivable that the optics, camera or electronics would deteriorate over time in such conditions. However, my microscope continues to work after several years without signs of deterioration. Nonetheless it was designed to have easy and cheap replacements given that the harsh conditions inside the incubator are expected to eventually lead to some deterioration in the long run. In this thesis I will describe various models of varying complexity with price tags that makes them affordable to any laboratory while the quality of the images is good enough for publications in peer-reviewed journals. A considerable part of the development of this microscope has turned out to be the development of a computer program that serves to control the microscope and acquire images. This program, which I have named IncuScope, can be made available to any lab that wishes to use it.

The thesis is divided into three chapters, each of which comprises about 33% of my work. The first chapter describes building the microscope. It illustrates some of the optical concepts and shows various prototype microscopes leading up to the final 1-color and 2-color microscopes, which are the two final microscopes that are currently in operation, and which have been used by a number of labs at Cornell. An advantage of the microscopes that I have built is that they have a horizontal configuration so that they can fit in the space between the trays of an incubator, leaving other trays available for cell culture. Another advantage of the 2-color fluorescent microscope is that it can switch between the two colors without any mechanical movements because it uses two cameras and additional mirrors. This is especially useful for long-term imaging where we want to reduce any mechanical movements that could eventually deteriorate due to tear and wear.

The third chapter describes the software developed for the microscope and the image analysis. I don't include any code but rather I describe the main features of the programs. First there is a description of IncuScope, the main program that manages the microscope. This program runs on a computer and displays the acquired images in real time. With it we can schedule imaging sessions and acquire images from different positions in multiple dishes or at different focal positions. We can select the type of illumination, we can move the stage, and we can move the objective up or down in order to focus. It contains autofocusing algorithms so it can also focus on its own at each programed position. It also contains many other functions that are useful for long-term imaging and all of these are described in detail so that it is clear for potential future users. In this chapter I also include image analysis programs that are independent of IncuScope and that are used for post-acquisition analysis, for example, a program to track fluorescently labeled nuclei.

Whereas the first chapters are engineering chapters, chapter 4 is dedicated to science and the study of cancer cells. The fourth chapter is also the longest and so I will describe it here in more detail. The focus of my study has been three MCF10 cell lines (10A, 10AT and CA1a) that form a model of the progression of breast cancer from normal non-tumorigenic to aggressive metastatic cells. The three cell lines originally derive from a single donor who did not have cancer, but who had fibrocystic changes (a condition where

fibrous tissue and cysts appear and is dependent on hormonal changes, but which is present in up to half of all woman). The interesting thing about this cell line is that it became spontaneously immortalized while maintaining non-tumorigenicity. Immortalization is a necessary requirement for long-term study of a cell line. Given that the three cell lines share a common genetic background, we can expect them to share certain characteristics, which will make the features of tumorigenic cells stand out.

For breast cancer, there exists a grading system called the Nottingham Histologic Score (or "Elston Grade") which grades the cancer from 1 to 3 based on three features: Nuclear Pleomorphism (variation in shape and size), Mitotic Count (number of cells in mitosis), and Differentiation State (which reflects how much the tumor cells differ from the cells of the normal tissue they have originated from). However, these only apply to histological fixed sections of human tumors.

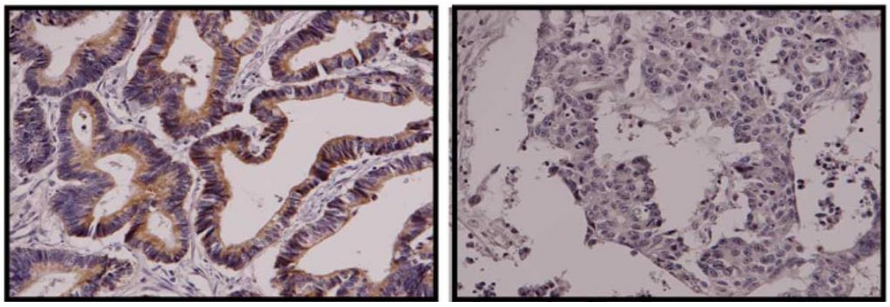

Figure 1.1 Examples of tissue sections of a well differentiated carcinoma (left image) and a poorly differentiated carcinoma (right image). The poorly differentiated carcinoma has lost the characteristic structures of the tissue and is associated with a higher grade of cancer.

This grading system is not generally used for xenograft studies in mice (where other grading systems are used), and they apply even less so to cell cultures. For example, when a cell line is implanted into a mouse, the mouse can develop tumors of different grades ranging from benign tumors to aggressive metastasis. Therefore a single cell line doesn't have a grade, but rather a probability of a grade. For 10AT cells, the probability of invasive carcinoma is 25%. Nevertheless, the grading system tells us what is most important for a pathologist in determining the severity of a cancer, namely variations in nuclear morphology, the proliferation rate, and the differentiation state. I will now discuss what I have found regarding these three criteria for the MCF cell lines.

Changes in differentiation state between the three cell lines are not immediately apparent. In fact the 10AT cells form acinar and tubular structures faster than the 10A cells (which would not be expected if we follow the grading scale) but this makes sense if we realize that 10AT cells grow faster than 10A cells (which *would* be expected using the grading scale). On the other hand, CA1a cells do show a change in tissue architecture. This change is the disassembly of acinar structures due to invasion into surrounding space. This does not happen immediately but rather after a week of culture, once the acini have had time to form. This is in line with the grading scale, as a high grade, malignant cancer such as those found in CA1a cell mouse transplantation studies, are expected to not be able to produce or maintain tissue architecture. It turns out that CA1a cells in culture can produce structures but can't maintain them after one week.

Another grading criterion: variations in nuclear shape and size, is definitely apparent in CA1a cells with respect to the other cell types. CA1a cells have a subpopulation of cells with large and amorphous nuclei, which corresponds to a higher grade of cancer.

The third criterion is mitotic count. Interestingly CA1a cells did not grow faster than the other cells when grown in plastic dishes. On the other hand, when grow on Matrigel, the acinar structures did become larger than in the case of the other cell lines. However, the difference was not necessarily that they grow faster, but rather that they continued to grow long after the 10A acini had stopped growing. Most interestingly, I found that even though CA1a cells grow slower than the other cells in plastic, when they are cocultured together with confluent normal 10A cells they end up growing more than normal cells. This is because a confluent layer of cells causes normal cells to stop growing, whereas CA1a cells will continue to grow on top of the confluent layer of cells.

To a great extent, chapter 4 is an extension or a continuation of a paper by Imbalzano et al.[17] which compares the same three MCF cell lines as I do. They culture the cells in both in plastic and on Matrigel. When cultured on Matrigel the differences that they found between the acinar structures of the three cell lines were as expected: larger acini and more irregular shapes for the more tumorigenic the cell lines. When cultured on plastic, the main difference between the three cell lines is that CA1a cells contains large cells

that are often vacuolated. I start chapter 4 of this thesis with a close look at these large, aberrant, vacuolated cells that are characteristic of the CA1a cell line. I perform time-lapse imaging on these cells and it's progeny as an illustration of the wide array of phenomena that can occur. For example, I find multinucleated cells that undergo multipolar divisions, cell fusions, and failed mitosis events. Some of these cells go on to become, within a week, the large, aberrant cells that I have mentioned earlier. With the time-lapse data, I trace back in time 18 giant cells to analyze how they have developed. I find that the most commonly visible original error is a mitosis event whereby a mononucleated cell becomes a binucleated cell. It seems that this error is brought about by cells not being able to segregate into two daughter cells at the cytokinesis step of mitosis. The second most common error at mitosis is a mononuclear cell that enters mitosis but also does not complete cytokinesis and produces only a single mononucleated cell, likely due to an error at either the anaphase or telophase.

The chapter continues with an analysis comparing the number of viable progeny of CA1a cells versus 10A cells. I find that CA1a cells have a subset of cells that divide a lot, while also having a subset of cells that die quickly. On the other hand, the 10A cells are more homogenous. Interestingly, both CA1a cells and 10A cells have a similar number of cell fusion and tripolar divisions. The percentage of tripolar divisions (1%) is low compared to other cell types found in the literature. The tripolar divisions, however, don't include the highly aberrant divisions that are commonly found in the CA1a cells line, but these usually develop later during cell culture. This implies that giant, highly aberrant cells don't survive the passaging with trypsin. Also found in both cell types are chromosomal bridges that link nuclei during mitosis. These are likely part of the phenomenon known as the Breakage-Fusion-Bridge cycle which features fusions between chromosomes due to short telomeres. This phenomenon could be responsible for the failed mitosis events.

The next section of the thesis analyzes cocultures of normal cells with cancer cells. I find that the cancer cells affect the morphology of the normal cells. I used a focused laser beam to ablate one of these cancer

cells. Doing so results in a recovery of the normal cells to their original morphology. The speed with which they recover suggests that it is the physical contact between the cells that was affecting their morphology.

The rest of the thesis concerns the growth of the cells when plated on a thick layer of Matrigel. I focus on cells plated on top of Matrigel rather than embedded within the Matrigel to follow the procedure of Imbalzano et al.[17] which leads to invasive outgrowths in the CA1a cell line. I look at cocultures where normal cells outnumber cancer cells to simulate more closely an incipient tumor. I find that the acini have invasive strands, both in the case of 10AT and CA1a cells. However, the leading cell of the invasive strand is almost always a CA1a cell. 10AT cells are only half as often the leader cell. (These are always cocultures with 10A cells at a ratio of 4:1, which means that 10AT cells are more likely to be the leader cells than 10A cells). This is a major difference between the malignant cancer cells and the premalignant cells. I also find that the normal cells will often follow the leader cell. This leads to changes in the morphology of the acini when there is a high number of invasive cells.

An unexpected finding was that the invasive outgrowths of the CA1a cells happen at the moment when the medium is renewed (the medium of culture dishes is renewed every 3 days). When the interval between medium renewals is increased, there is more invasion. This suggests that a depletion of nutrients could be causing the invasion. By comparing invasion with and without serum I confirm that lack of serum causes the cells to start invading. Interestingly, doing the same with and without EGF (epidermal growth factor) shows that EGF is in fact also causing the invasion. Therefore we can conclude that there is a component of serum, that isn't the EGF, that is preventing the invasion of the cells. (Other growth factors, such as TGF-alpha, can compete with EGF binding to its receptor, but may not activate the same signaling program).

CHAPTER 2: CUSTOM MICROSCOPE DESIGNS FOR OPTIMAL LONG TERM CELL IMAGING EXPERIMENTS

Introduction

Existing options for long term time-lapse imaging of live cells are either expensive or don't provide the level of control of temperature and CO2 needed for imaging over days or weeks. To overcome these issues we developed a small microscope that can be assembled from commercially available parts (and, optionally, from custom made parts), that fits inside conventional CO2 incubators commonly found in biological laboratories. A crucial aspect of an incubator microscope is that it is able to function properly for long periods of time at the elevated temperature and the high humidity found inside cell incubators. Although we initially had concerns that the optics, camera and/or electronics would deteriorate over time in such conditions, our microscopes have continued to function for several years without signs of deterioration. A considerable part of the development of this type of incubator microscope turned out to be the development of computer software that both locally and remotely controls the microscope and acquires images. This program (Incuscope.exe), written primarily in Visual Basic, along with microscope designs based on the findings presented in this thesis will be made available to any lab that wishes to use it.

General description of the instrument

Image acquisition

The microscope is designed to work inside an incubator and therefore it has no eyepiece. This reduces the price and complexity with respect to traditional microscopes, as well as reducing the size, which is a critical factor for an imaging device that resides inside an incubator. Instead, there is a megapixel camera that captures the images and sends the data (via USB) to a computer where the images are saved. The camera (Pointgrey Chameleon) selected for the design is physically small (4 cm by 4 cm), inexpensive (~$300) and has sufficient sensitivity to detect fluorescent signals. In addition to that, it is fully enclosed in an airtight casing and can be easily mounted onto the tube of the microscope using a standard microscope C-mount. Most important of all, this model has been able to withstand the temperature and humidity for years and still function correctly.

Illumination

The grabbing of images has to be synchronized with the source of illumination and the illumination has to be as short as possible to prevent damage to the cells due to photo-toxicity. Light emitting diodes (LEDs) were used both as the source for brightfield illumination and for excitation of fluorescence. However, it is important to use low power (standard) LEDs for brightfield and higher power "super-bright" LEDs for fluorescence excitation. There is a significant difference in the intensities generated by low and high powers LEDs, and while low powered LEDs can illuminate the cells continuously without affecting them, high powered LEDs can quickly damage the cells. The LEDs are inexpensive (less than $10) and can be turned on and off rapidly for efficiently taking images of cells for long periods of time while minimizing photo-toxicity while imaging in fluorescence excitation mode. Whenever possible the brightfield LEDs are chosen to emit in red since this wavelength does not harm the cells, as higher energy (bluer) wavelengths can.[4-6]

Rather than using phase contrast or differential interference, we use inclined off-axis illumination for brightfield illumination, which is less expensive and simpler to implement, but provides similar contrast levels and enhances topological features. Additionally, this method allows for the easy adjustment and optimization of contrast by simply rotating the LED, which cannot be done with the other contrast enhancing methods.

In addition to bright field and fluorescence modes, the microscope can also acquire darkfield images by the use of a ring of LEDs placed slightly above and around the sample. Darkfield illumination makes it easier to visualize the cells and their organelles or nuclei. All three modes of imaging (fluorescence, brightfield and darkfield) can be used simultaneously and then the images in different colors can be merged into one.

Automation

Unlike conventional microscopes, the microscopes I built reside inside a CO2 incubator and must be highly automated. For example, if the user had to open the door of the incubator to operate the stage or the focus, the atmosphere inside the incubator would be compromised. Therefore, all the focusing and stage functions must be performed from and controlled by the computer. A nice offshoot of this fact is that the microscope can effectively be operated over the internet from a distant location. The system designed allows for cell phone or laptop control though the internet, and allows for assessment of the current state of the imaging experiment as well as the ability to change or adjust the settings for the current imaging session. LEDs and the focusing motors are controlled by lab-built custom electronics situated outside of the incubator that is connected to the microscope via cables routed through the standard access hole found in the back of CO2 incubators. As in the case of the camera, the circuit board is also connected to the computer via USB. The synchronization between the LEDs and camera(s) is achieved by the computer program, which controls all the camera settings and the time-lapse acquisition settings.

The microscopes I designed are capable of acquiring images in multiple wells in a single experiment by the use of motorized XY stages that move multi-well plates or dishes. Lateral motion over millimeter

distances produces focusing artifacts and autofocus capability is critical for these instruments. Autofocusing requires the implementation of an algorithm that operates through feedback and controls the focusing motor which moves the objective automatically up and down at each user-defined position. It is also possible to tile the images together to form larger fields of view. Many of the image processing tasks such as merging of multiple fluorescence channels, conversion of images into movies and image analysis I have simplified by the creation of programs in the ImageJ macro language.

The three main components of the microscope are depicted in Figure 2.1, and they are shown in the order in which they will be described: first A) the microscope, followed by B) the electronics that control the microscope, and finally C) the computer software that runs the microscope.

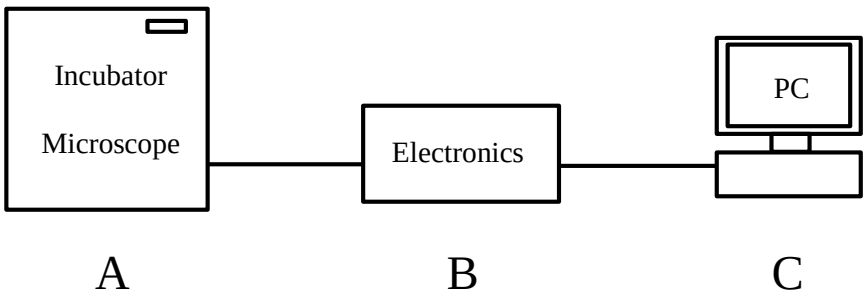

Figure 2.1. Overview of the main components of the system. A) microscope inside an incubator, B) electronics, and C) computer software.

Building a Microscope

In its most simple form, the microscope can be built from just three parts: a) a light source (LED), b) an objective lens and c) a camera, as shown in Figure 2.2. This pertains especially to older objective lenses that don't need an additional tube lens. Elements will be added to this scheme as we proceed.

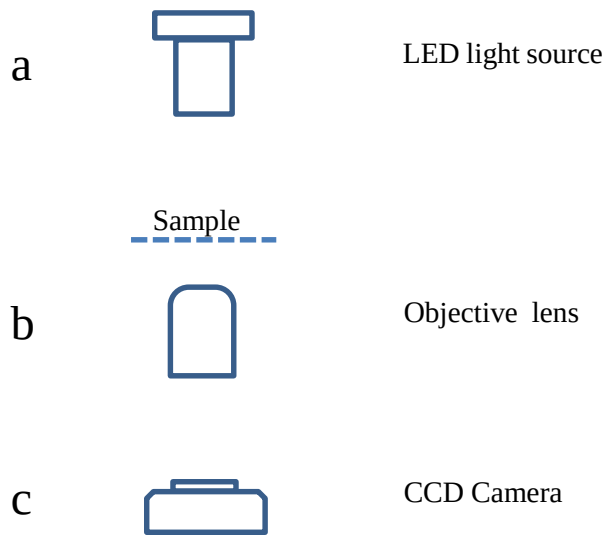

Figure 2.2 The simplest microscope set-up involves just three main components: a) an LED light source, b) an objective lens and c) a camera

This is not the recommended set-up for current objective lenses which are designed to work with an additional lens that is placed between the objective lens and the camera, but nonetheless this simple set-up illustrates the fact that the objective lens can be regarded as a simple lens, and Figure 2.3 shows that decent images can be obtained with this set-up even for objectives that are designed to require tube lens although this is not recommended.

In order to build a microscope from the three components mentioned above we require a supporting framework that supports both the components of the microscope and the specimen to be imaged. The most basic set-up illustrated in Figure 2.3 consists of metal bars that provide support for each of the components. Additionally in Figure 2.3 we have used a support to hold the dish that is being imaged, and this support can be adjusted with a micrometer to facilitate focusing.

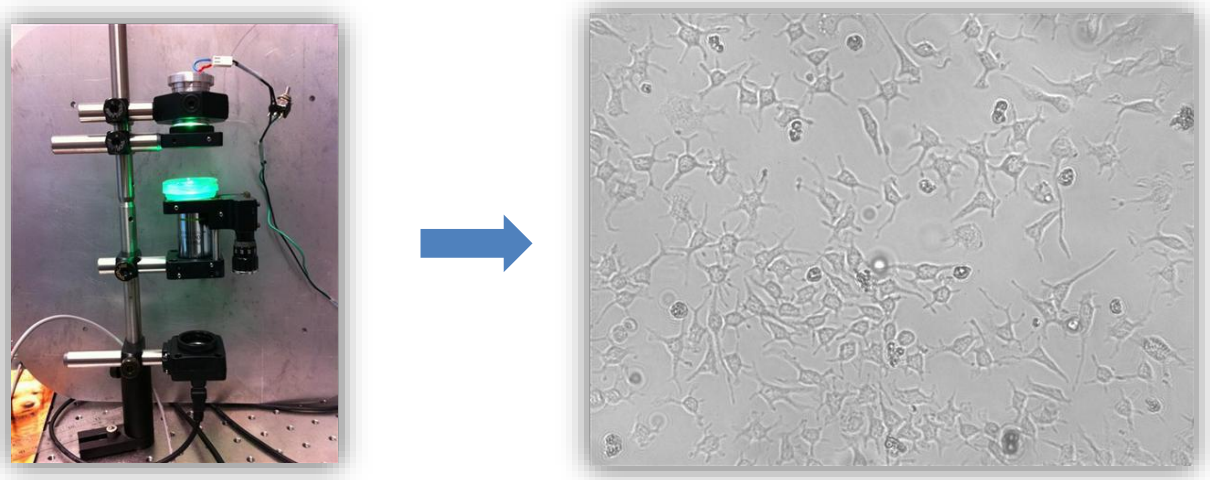

Figure 2.3 Simplest possible microscope set-up and the corresponding image obtained with it.

Thus the microscope doesn't require complex contrast enhancing mechanisms like phase contrast or DIC, in fact we can still obtain images like the one shown in Figure 2.3 without using a condenser or Kohler illumination or a tube lens. However a tube lens is essential when working with higher N.A. objectives and when working with fluorescence and therefore it will be added to the microscope. Additionally, even though not perceptible, there is a slight distortion in Figure 2.3. If we shorten the distance between the camera and the objective lens the field of view will be larger and the radial barrel distortion will become more apparent (Figure 2.4).

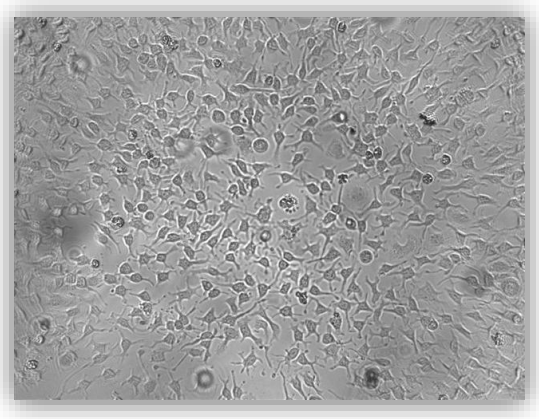

Figure 2.4. Example of radial barrel distortion.

Tube Lens

Present day objective lenses are made so that rays emerge parallel from the back aperture of the objective. Therefore they require a tube lens to focus the light to form an image. This makes it possible to add optical elements between the objective and the tube lens (termed "infinity-space") and minimizing aberrations. The position of the tube-lens is shown in Figure 2.5.

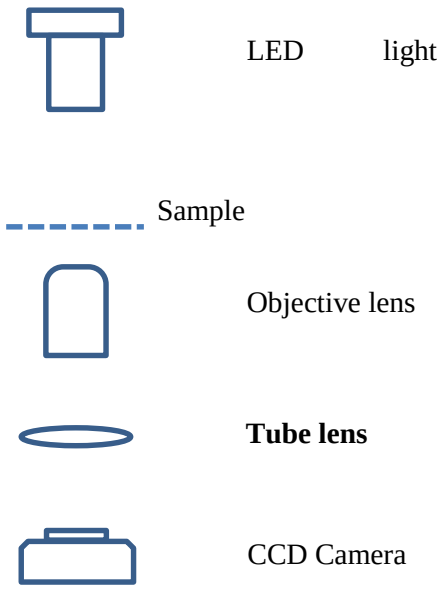

Figure 2.5 The tube lens is located between the objective lens and the camera. Modern objectives lenses are designed to work with a tube lens, without which the numerical aperture and working distance of the lens are compromised and aberrations would ensue.

The distance between the sample and the objective lens is known as the working distance of the objective lens and is specified by the manufacturer of the objective lens and is often written on the objective lens itself. The distance between the objective lens and the tube lens is variable and is where optional optical elements such as dichroic mirrors and filters should be placed. The distance between the tube lens and the camera should be the focal length of the tube lens. Olympus objective lenses are manufactured to work with a tube lens of 180cm of focal length, but given space constraints inside the incubator, focal lengths as low as 150cm are possible without significant loss of image quality, with the added benefit that the intensity of the image is greater because the rays of light fall onto a smaller area on the camera's CCD chip and the field of view is increased. The reason the field of view is larger is because the magnification will have changed. The magnification is M = $f_{\text{tube lens}}$ / $f_{\text{objective}}$ where M is the magnification and f is the focal length. However aberrations will become apparent when changing the distances by large amounts.

Brightfield Light Source

As mentioned earlier, ideally a low power LED should be used as the brightfield light source. A 3 Volt 20mA 10mm-wide diffuse LED that provides red, green and blue light and costs less than $1 is a surprising ideal choice. Especially given that you can switch between the different colors to match the excitation filter's frequency and avoid useless radiation to the cells. If a diffuse light LED is not available, or if you have a point light source (the previously mentioned LED is not a point source because it is relatively large which helps to diffuse light and is also placed relatively close to the cells), a component that I have successfully used in my microscopes is a frosted filter. The frosted filter diffuses the light coming from the LED and effectively increases the angle of incidence and N.A. of the light that illuminates the sample. (Ideally the N.A. of the incoming light should match the N.A. of the objective lens although deviations from this will not have any noticeable effect unless working with very high N.A. objective lenses). The

filter is placed just above the sample as shown in Figure 2.6, although it is not necessary if using a diffuse light LED.

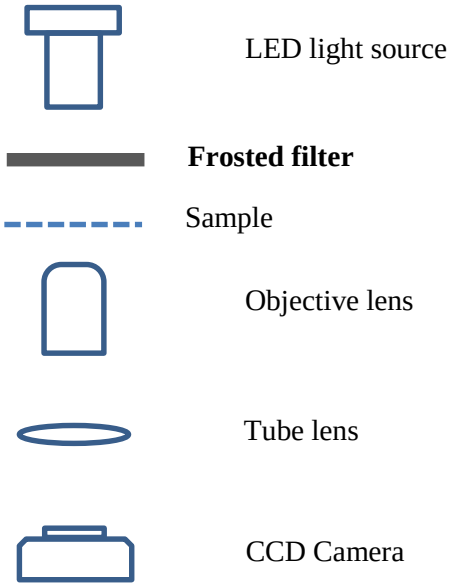

Figure 2.6 The frosted filter is placed between the LED light and the sample, it's position can vary but it exerts a greater effect when placed close to the sample. An alternative is to use an LED that already provides diffuse light.

The frosted filter performs a job similar to a condenser lens in that it increases the angle of incidence (or N.A.) of some of the incoming rays and has the benefit that the image appears cleaner because features that are outside of the focal plane will no longer be visible (it decreases the focal depth). In some instances where we are interested in having a large focal depth we can remove the frosted filter. Figure 2.7 is an example of the improvement in image quality due to the use of the frosted filter.

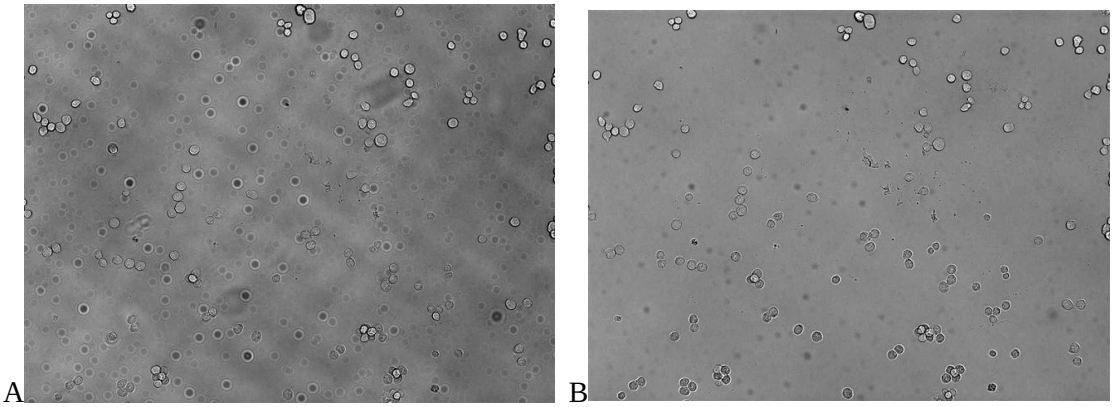

Figure 2.7 The frosted filter greatly improves the quality of the image by fading out objects that are out of focus (This was done with a small-sized high power LED). A) No frosted filter. B) Frosted filter

Another benefit of using the frosted filter is that it effectively removes the ripples caused by the diffraction of light, shown in Figure 2.8.

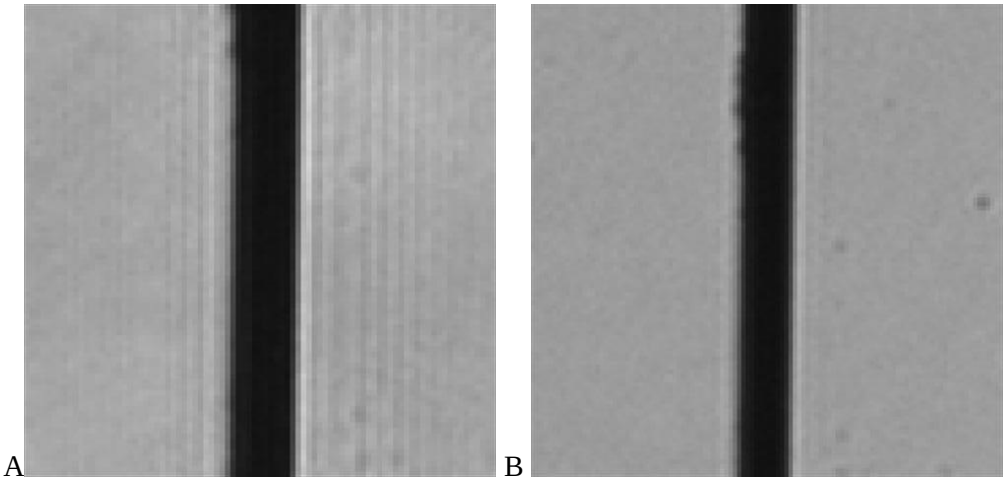

Figure 2.8 Ripples caused by diffraction of light disappear when using a frosted filter. A) No frosted filter. B) Frosted filter.

The filter is only required for point-source illumination and is not required when using large LEDs which already have a diffusing coating but in some circumstances, point-source illumination can give better contrast, for example, when imaging in low magnification 3D cultures of cells in Matrigel.

Inclined Illumination

Adjusting the source of illumination so that it is slightly off-axis results in inclined illumination. Figure 2.9 shows the direction of illumination in inclined illumination as well as in bright field, dark field and epifluorescence modes.

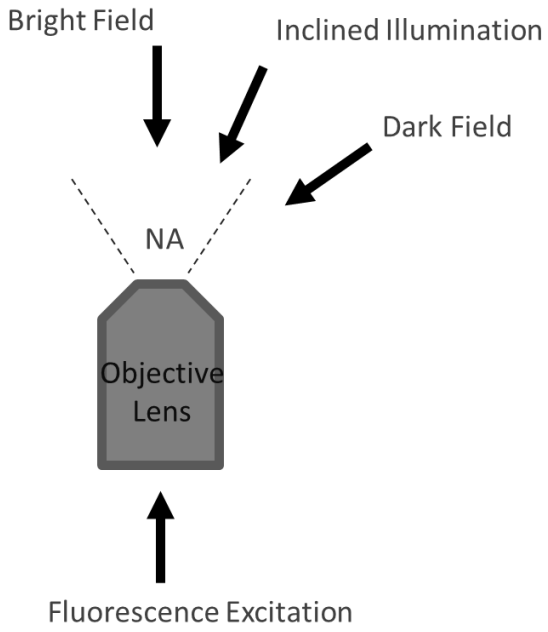

Figure 2.9 Direction of illumination in inclined illumination as well as in bright field, dark field and epifluorescence modes. The dotted lines represent the angle corresponding to the Numerical Aperture (N.A.) of the objective lens.

Inclined illumination can be very beneficial in some cases to increase the contrast required to visualize cells and results in beautiful images. The relief-contrast generated is very similar to DIC (Differential Interference Contrast microscopy) and can enhance the contrast like Phase contrast microscopy without the associated complexity or price. However, inclined illumination will not always work. Figure 2.10 shows that inclined illumination does not work well with the Olympus 4x 0.1NA objective because of the appearance of a gradient, but it works very well with the Olympus 10x 0.3NA objective lens.

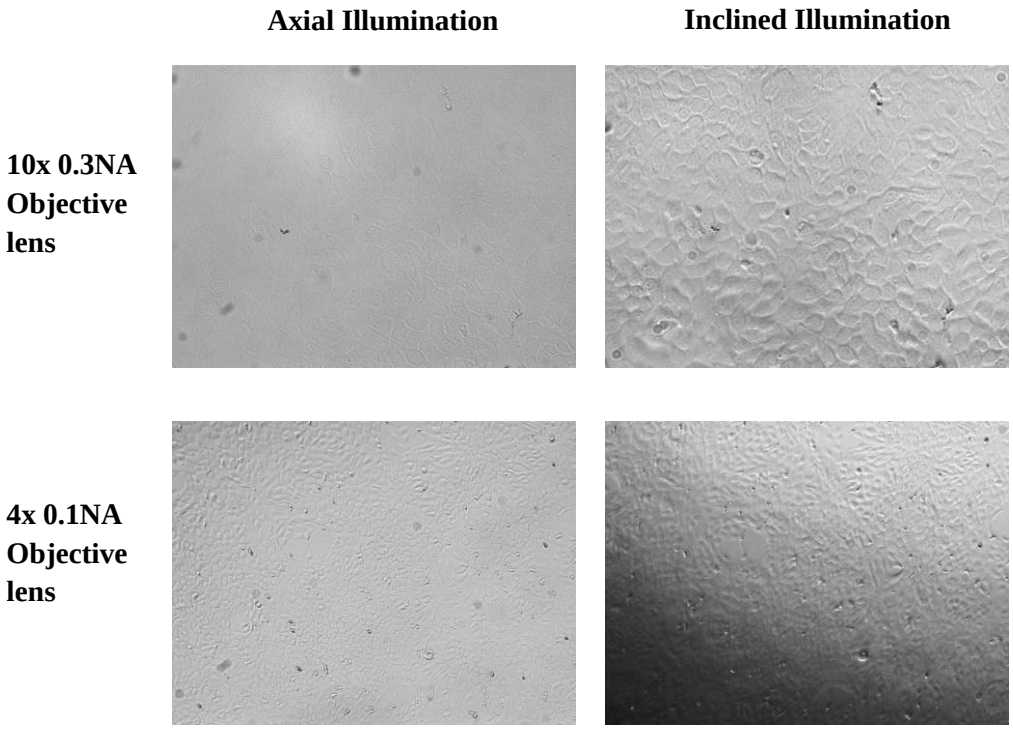

Figure 2.10 Inclined illumination gives very good results with some objective lenses (upper images). In the case where it doesn't improve the image because of the appearance of a gradient (lower images) it is not required as much because there is already some contrasts present with axial illumination (left panel).

An alternative option to off-axis illumination which has an equal effect can be obtained by blocking part of the back aperture of the lens as shown in Figure 2.11. However, off-axis illumination is much simpler to implement.

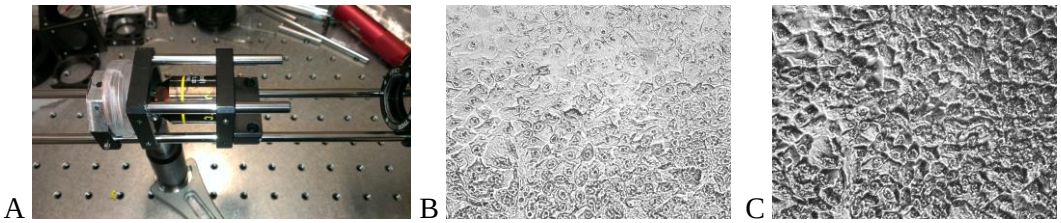

Figure 2.11 Partial blockage of the back aperture of the objective yields improved contrast and produce an effect similar to DIC.

Space Considerations

Given that the microscope has space constraints inside the incubator we have to find ways to make the microscope as small as possible. It would be better if the microscope is horizontal instead of vertical. This way the microscope will occupy only one tray inside the incubator leaving the other trays free for regular cell culture or for other people to use. This can be achieved by employing a mirror that reflects the light coming from the objective by 90 degrees. The location of this mirror, which can be purchased from Thorlabs, is shown in Figure 2.12.

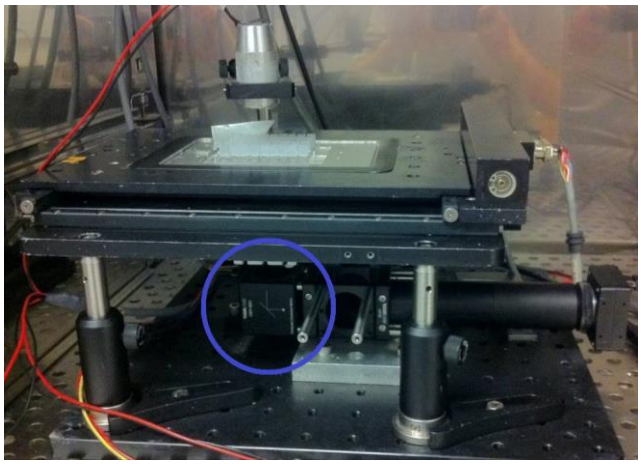

Figure 2.12 A mirror located behind the objective lens allows a horizontal configuration that makes the height of the microscope as reduced as possible which is important inside an incubator.

As mentioned earlier the distance between the tube lens and the camera is determined by the manufacturer and should be close to the focal length of the tube lens but can be reduced somewhat depending on our goals. On the other hand the distance between the light source (the LED) and the objective lens is not critical and can be varied to a great degree which means that we can place it as close as we want to the sample. This is a benefit of using very low power LED that will not heat up and potentially harm the cells. Finally there is the so-called "infinity-space" between the objective lens and the tube lens. It is important to know whether we can reduce the distance between the objective lens and the tube lens without affecting the quality of the image. To figure this out, since the distance between the sample and the objective lens is defined by the manufacturer of the lens, I fixed this distance as well as the distance between the tube

lens and the camera and varied the distance between the objective lens and the tube lens as shown in Figure 2.13. Figure 2.14 shows that a short tube length can induce some glare artifacts in some objective lenses.

Figure 2.13 Experimental set up for varying the distance between objective and tube lens, showing two extremes. A) Large infinity space. B) No infinity space.

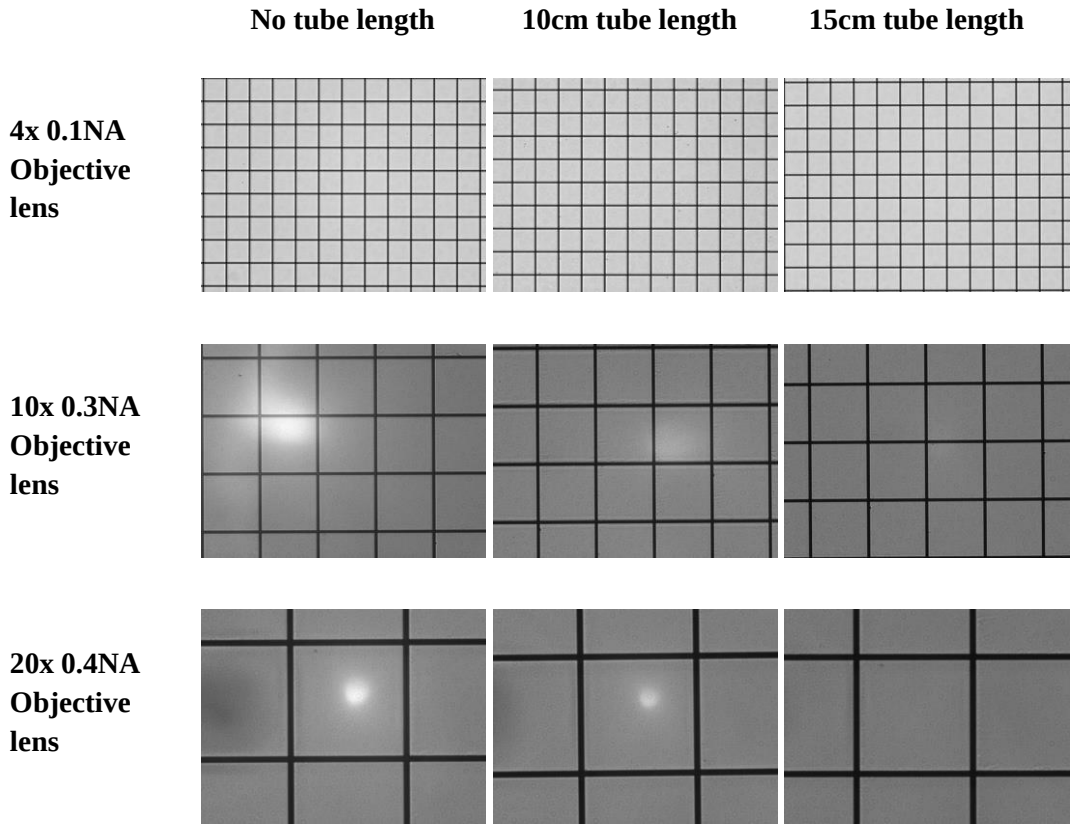

Figure 2.14 Comparison of 3 objectives when changing the tube length. Illumination glare appear with the some objectives at 0cm and 10cm tube lengths but not at 15cm. 4x objective shows no difference from 0cm to 15cm tube lengths.

As the figure shows the result is that the distance can be varied from 15cm all the way to 0cm for the 4x objective lens without affecting image quality whereas for the 10x and 20x objectives there is a bright spot of illumination. This can be partially corrected by using a diffuser as shown in the following figure:

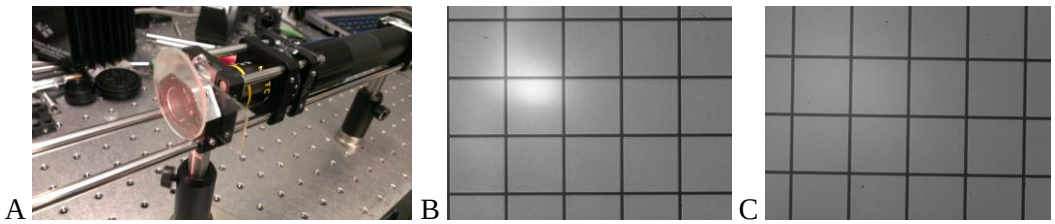

Figure 2.15 Diffusor corrects the illumination glare. A) Diffusor. B) Glare without diffusor. C) Glare with diffusor.

Further correction can also be achieved by moving the lamp away from its axis to achieve inclined illumination (See Figure 2.16).

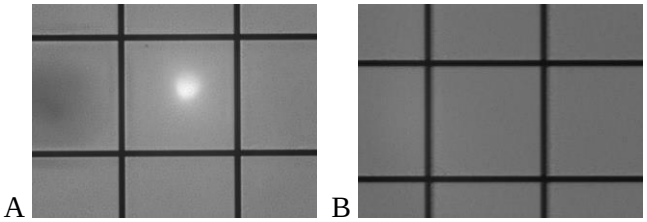

Figure 2.16 The glare can be eliminated by inclined illumination. A) On-axis illumination Glare. B) Off-axis illumination.

Here I investigated how small the "infinity space" can be made without affecting image quality because we want to obtain a microscope small enough that can fit inside an incubator. The results vary depending on the objective used. No image distortion is observed in any objective but there can be glare for high N.A. objectives. In fact the glare is due to stray rays of light that bounce off the walls of the tubes. However the tubes cannot be removed because they are important to prevent other sources of light from reaching the camera. The glare could also be removed by using a condenser lens and accurate illumination. However for simplicity we chose to omit the condenser lens and instead use a longer "infinity space" while having in mind that making the "infinity space" too large reduces the number of peripheral light waves collected by the tube lens which will reduce image quality [7] .

A final distance to have in mind that will be important in the next section when we talk about fluorescence is the distance between the fluorescence excitation LEDs and the corresponding optics. I chose to manually select the distance that fills the field of view with excitation illumination light while at the same time avoiding to focus on the LED itself; the LED has a structure that will be visible on the screen resulting in uneven illumination of the sample unless we move the source until it is out of focus.

Adding Darkfield and Fluorescence Capabilities

In order to obtain darkfield images we must illuminate the sample with a light that comes at an angle greater that the N.A. of the objective lens (Illustrated previously in Figure 2.9). This can be done by placing an opaque disk between the condenser and the sample that blocks the incoming rays of light that have an angle lower than the N.A. of the objective lens. The main drawback of this method is that the disk has to be removed each time that a brightfield image is taken because the disk is incompatible with brightfield imaging. This drawback has to be overcome in order to make a completely automatic microscope. The solution is to use a ring of LEDs to illuminate the sample. This approach enables simultaneous use of brightfield and darkfield imaging. The ring is placed at the position shown in Figure 2.17, at a distance from the objective lens where the angle to the LEDs will be greater than the N.A. of the lens.

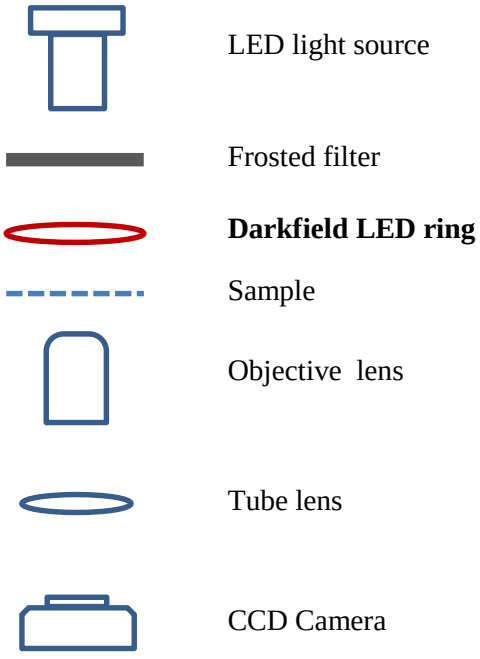

Figure 2.17 The Darkfield LED ring is placed above the sample; its position can vary depending on the N.A. of the objective lens.

The following image shows an early prototype microscope which illustrates the position of all the elements described up to now with the addition of a neutral density filter that serves to reduce the intensity of the light. This is not the final, most optimal, configuration of the microscope (which will be described later) but serves as an illustration of were the different elements are located.

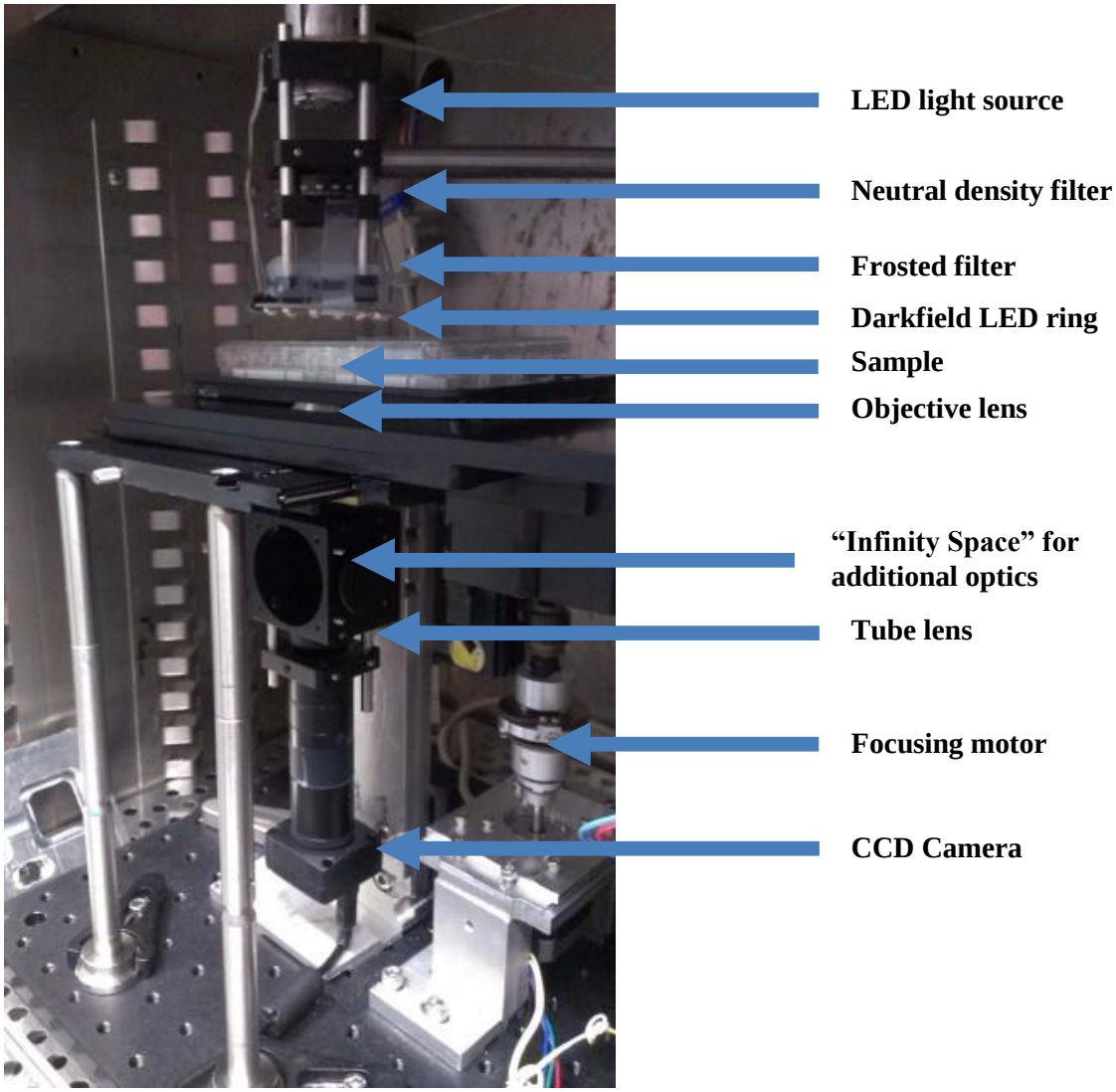

Figure 2.18 An early prototype incubator microscope, to illustrate the position of the elements described up to now.

The utility of the darkfield mode is that it enables visualization of features that are not visible in the brightfield mode. Small vesicles glow especially bright in darkfield and nuclei are more also more discernible (Figure 2.19).

A 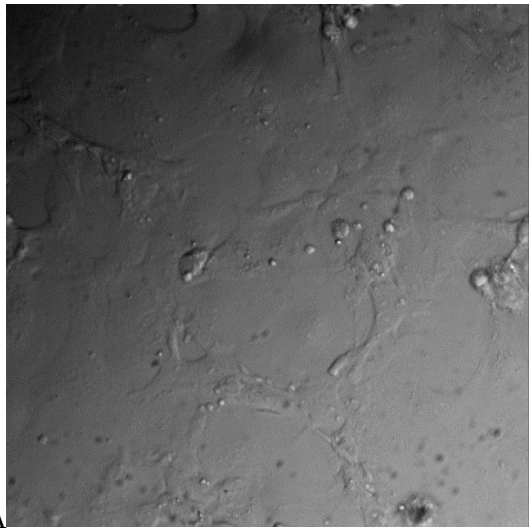 B 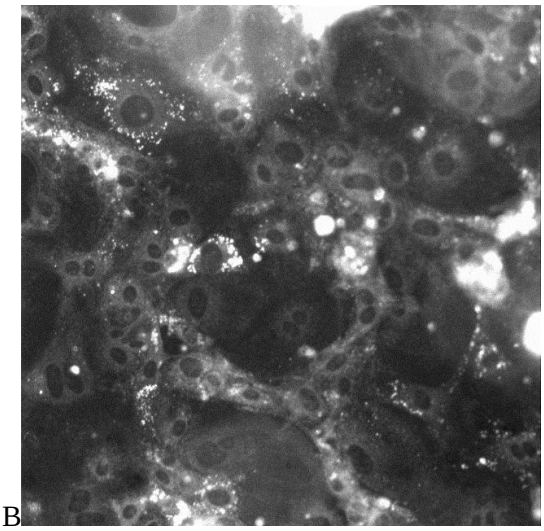

Figure 2.19 Example of the cells imaged with A) Brightfield mode and B) Darkfierld mode. Nuclei are clearly visible in the darkfield mode.

Darkfield and brightfield images can be combined into one as shown in Figure 2.20. It shows how in some circumstances only a subpopulation of cells is visible in darkfield probably because they have a large quantity of vesicles in their cytoplasm. These cells are primary mouse cells that I obtained from the mammary glands but can contain several cells of unknown type that were present inside the mouse.

Improvement in darkfield imaging can be obtained by using a ring of LEDs which consists of diffused illumination instead of individual separated LEDs. These diffuse illumination LEDs are now manufactured for some car models which have circular head or tail position lights and has increased their availability and reduced their price (Figure 2.21).

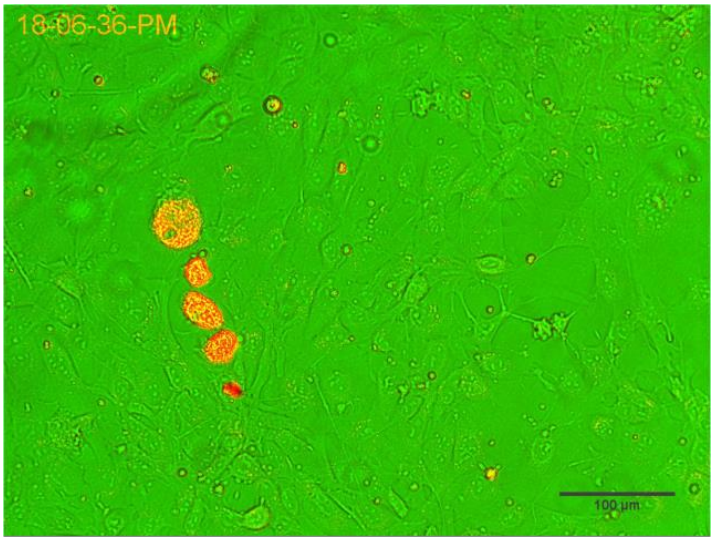

Figure 2.20 Primary mouse mammary gland cells imaged in brightfield (shown in green) and darkfield (shown in red) shows a subpopulaiton of cells that are only visible in darkfield mode (red).

A

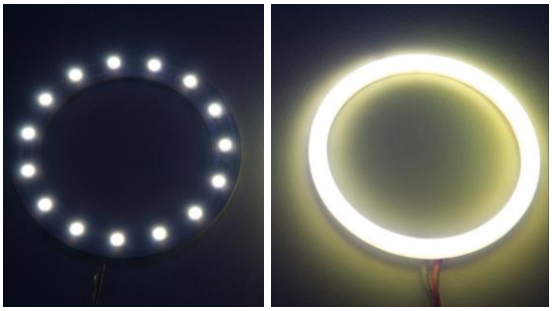

B

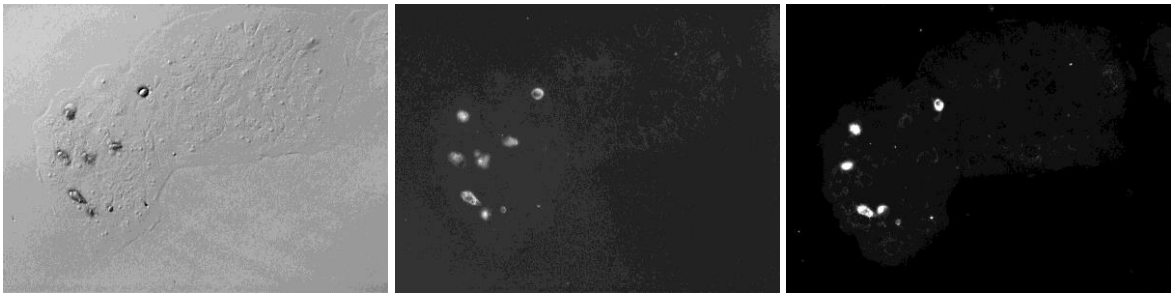

Figure 2.21 A) Newly available LED rings termed COB (chip-on-board) provide diffuse illumination (right image). B) Cells imaged in brightfield, non COB, and COB rings respectively, showing that diffuse illumination COB LED rings provide better contrast.

Adding Fluorescence Capability

In order to obtain images from fluorescent samples we need a new source of illumination that will be responsible for the excitation of the fluorescence. For this we will also use an LED lamp, but it will irradiate the sample from below instead of from above. Illuminating from below is called epifluorescence and is useful because it uses the objective lens to focus the excitation light onto the sample. Focusing the excitation light is important in order to achieve the high levels of intensity necessary to obtain observable fluorescence from the sample. We also need an additional lens to converge the excitation light and a dichroic mirror that reflects the excitation light and transmits the emitted fluorescent light. Their relative positions is shown in Figure 2.22.

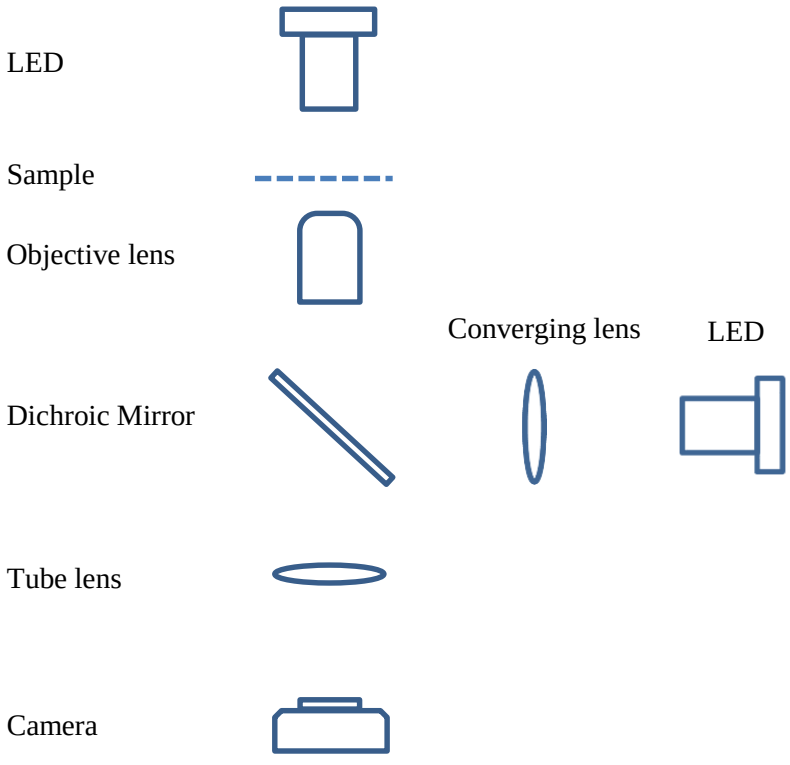

Figure 2.22. The components of the fluorescence microscope. The new components added with respect to previous figures are: a dichroic mirror, a converging lens and the LED for the fluorescence excitation.

The trajectory of the excitation light is illustrated in Figure 2.23A, and the trajectory of the emitted light is illustrated in Figure 2.23B (the colors correspond to GFP imaging).

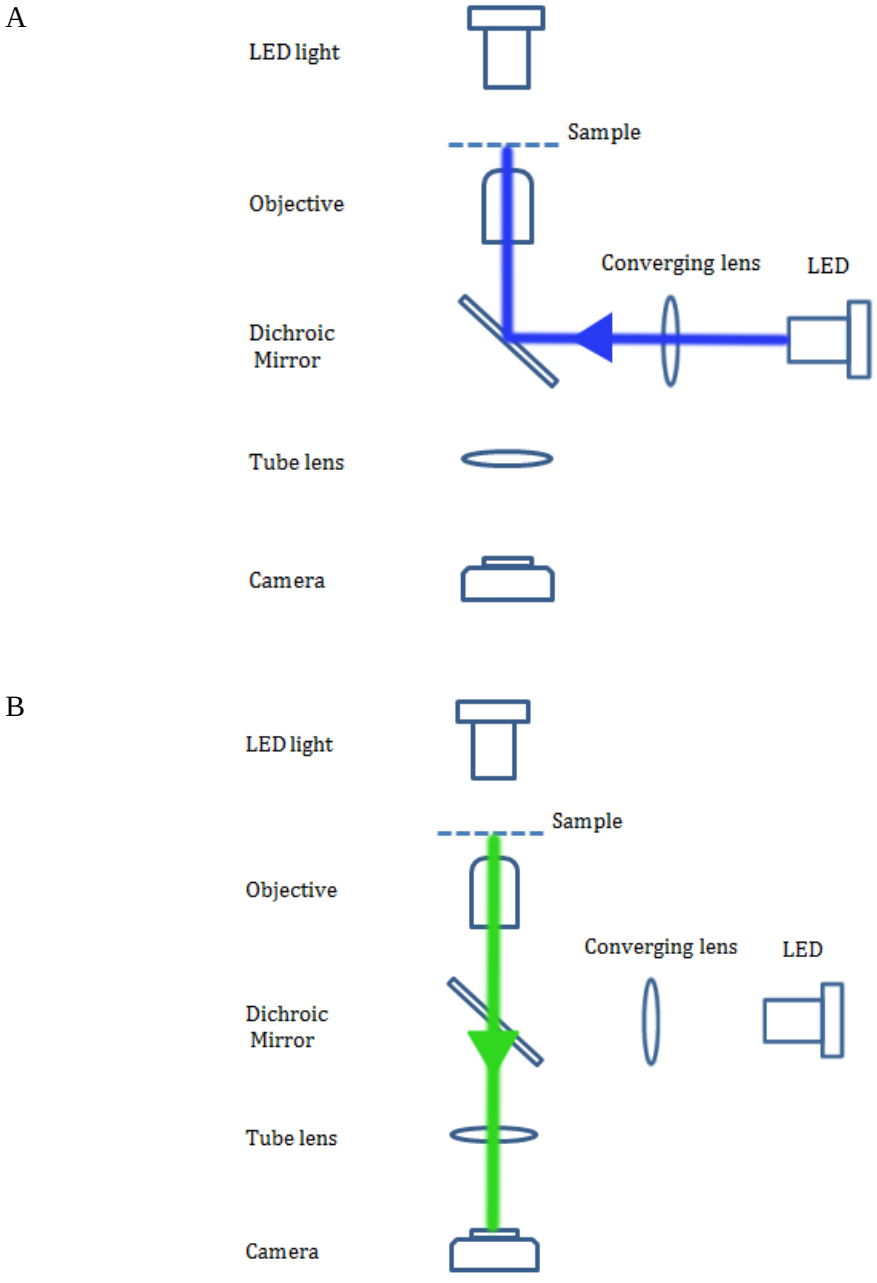

Figure 2.23. A) The dichroic mirror reflects the blue excitation light and directs it toward the sample. B) Then the green fluorescent light coming from the sample is transmitted through the dichroic mirror and into the camera.

Figure 2.24 shows how the previous diagram translates into the real fluorescence microscope with both light paths are superimposed. Please note that the distance between the camera and the tube lens is not the actual distance used in the final microscope which will be described later.

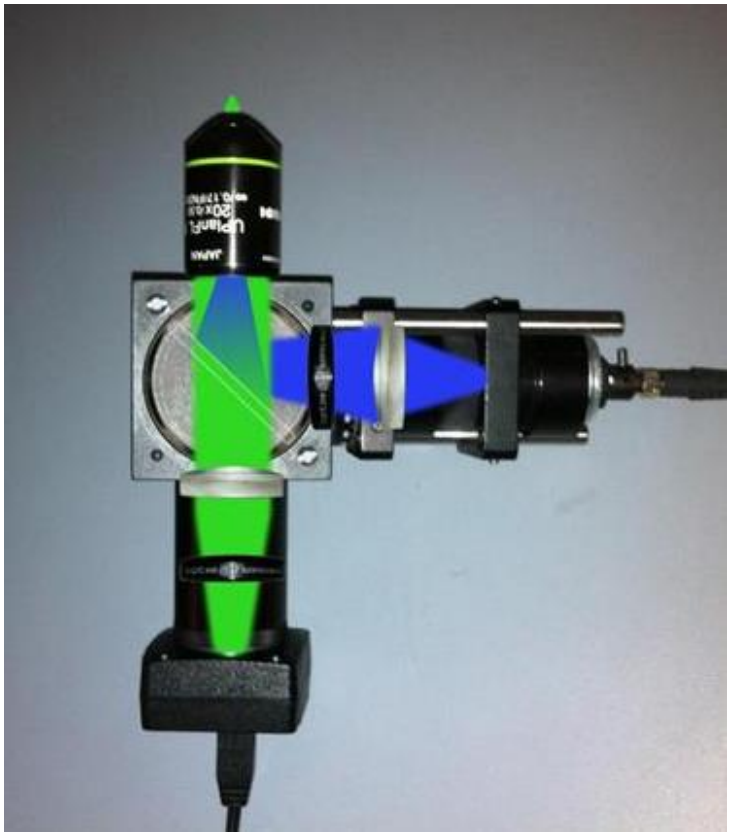

Figure 2.24 Illustration of the excitation (blue) and emission (green) light paths in the microscope. Note that this image is just for illustration purposes and is not the final recommended configuration for the microscope.

Fluorescence also requires the addition of two filters which have the purpose of eliminating the wavelengths of light that are not needed to excite fluorescence or do not come from the emission of the sample. The fact that the filter limits the light that falls on the camera to only the wavelengths of the fluorescence of the sample is important to achieve the level of contrast needed for fluorescence imaging. Some people are lead to think that filters are not needed because the LEDs are low bandwidth but the truth is that the filters are necessary and can make a big difference. Both the filters and the dichroic mirrors have to be selected depending on the color of fluorescence that we are imaging and have to be changed each time that we use a different color. The position of the filters is shown in Figure 2.25.

A description of each component in addition to information on the manufacturer and price is located in the appendix.

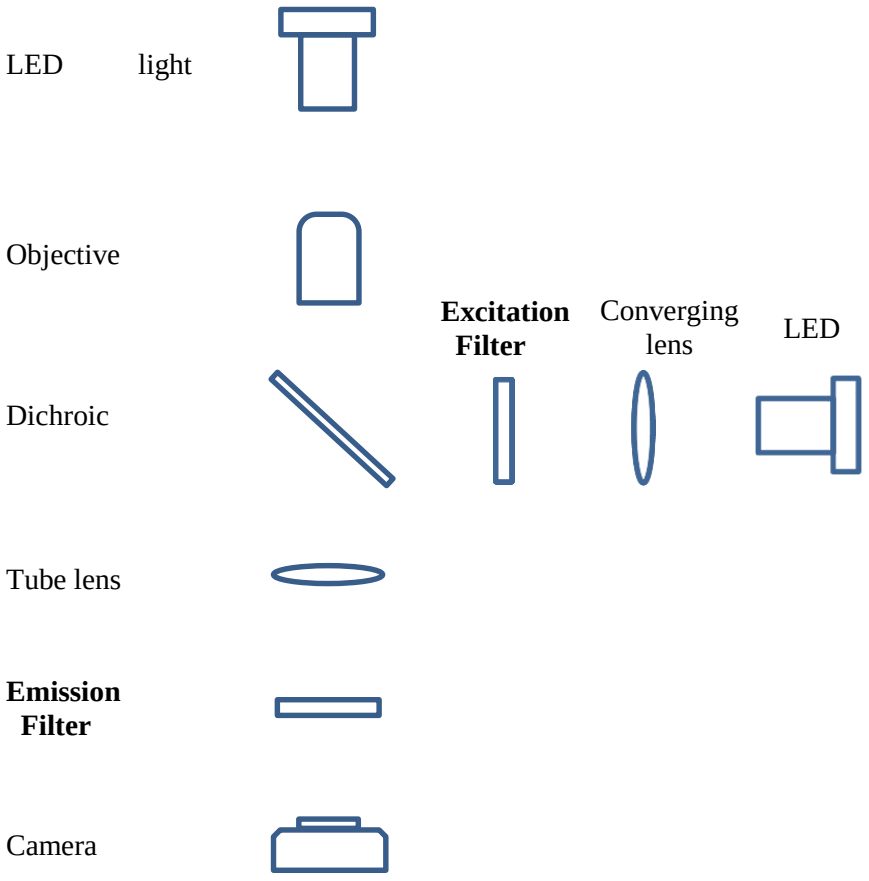

Figure 2.25 The relative position of the excitation and emission filters with respect to the other components of the microscope.

The actual position of the filters is variable. For example, the emission filter can be placed between the tube lens and the dichroic mirror. An important point, however, is that the emission filter should be placed in such a way that no light that doesn't go through it ends up in the camera. In other words, all the light that ends up in the camera should have passed through the emission filter. To achieve this, I use tubes that connect the emission filter to the camera that don't let any light pass through their walls.

As mentioned earlier the distance between the tube lens and the camera should be 180mm for Olympus objective lenses although it is possible to make it lower due to space constraints (approximately 160mm) without sacrificing image quality as long as this distance matches the focal length of the tube lens. The distance between the converging lens and the LED source should be close to the focal length of the converging lens (Figure 2.26) but as we are not utilizing the full field of view of the objective lens (due to the limited size of the CCD of the camera), the distance can be varied in order to maximize the intensity of the fluorescent light at the field of view. This trick enables us to obtain levels of intensity that are sometimes important in certain experiments and which would not be possible to obtain otherwise with the LED light source that we are using.

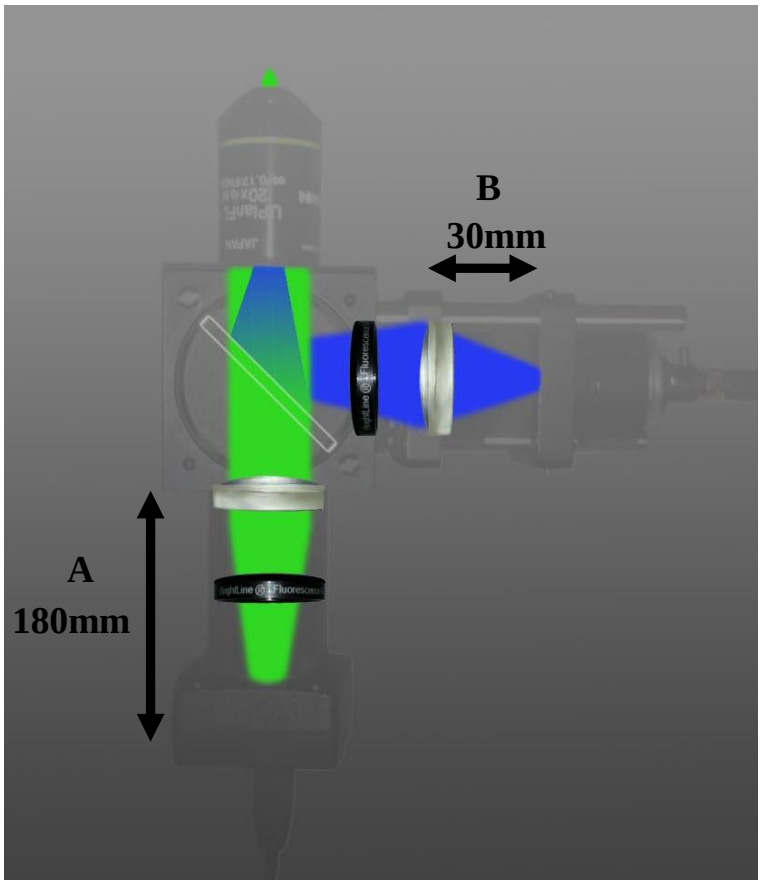

Figure 2.26 Recommended positions of the converging lens (B) and the tube lens (A). Not drawn to scale.

Also highlighted in Figure 2.26 is the position of the two filters. These positions can be varied as I mentioned earlier but another point to have in mind is that they should be placed as close as possible to their corresponding lenses to avoid anything that is on the filter such as scratches or dirt to appear on the image captured by the camera. Additionally this will increase the lifetime of the filter as the light will be more homogeneously spread over the area of the filter.

Aligning of LED light for optimal fluorescence excitation

It is important to focus the fluorescent excitation LED on the specimen to a small spot. By concentrating the light in this way we increase its intensity and we also avoid exposing cells outside the field of view to light. Ideally the spot should be just the size of the field of view and this is done by using an appropriate converging lens that is placed close to the excitation LED. I use a lens with a focal length of 2cm and I move the LED and the mirrors until I see the illumination of the LED on the screen (this is easier if we use a dish with a fluorescent solution). The illumination can also be seen without a fluorescent solution because a small portion of the light is reflected back to the camera and removing the excitation filter makes this easier. An important point to have in mind is that some LEDs have features on the chip itself which will become visible on the illumination of the LED. In our case there are holes within the LED itself that will produce illumination that is not homogeneous and the way to deal with this is to move the LED or lens until the image is slightly out of focus as shown in the next figure.

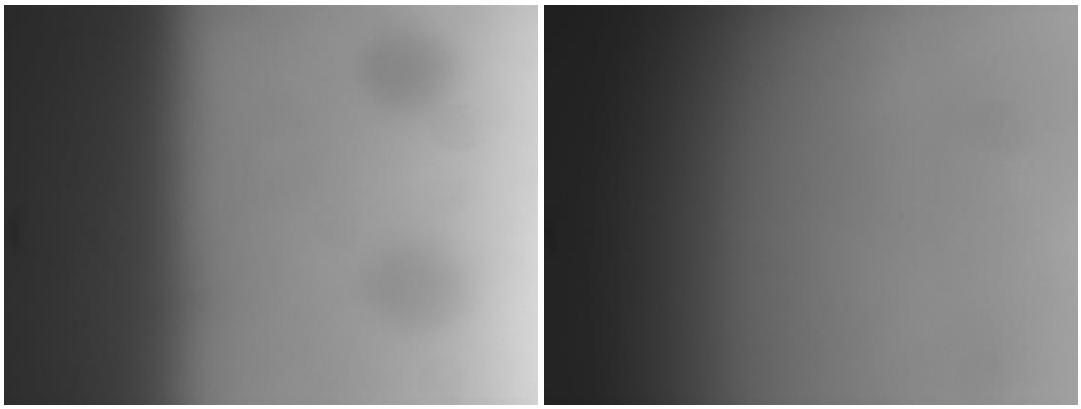

Figure 2.27 Illumination by excitation LED in focused (LEFT) and out of focus (RIGHT) positions. The circles visible on the left image disappear when placed out of focus as shown on the right image, allowing a homogenous illumination of the specimen.

Finally the image should then be centered and adjusted in size until it becomes homogeneous illumination, by moving either the LED, the lens, or the mirrors:

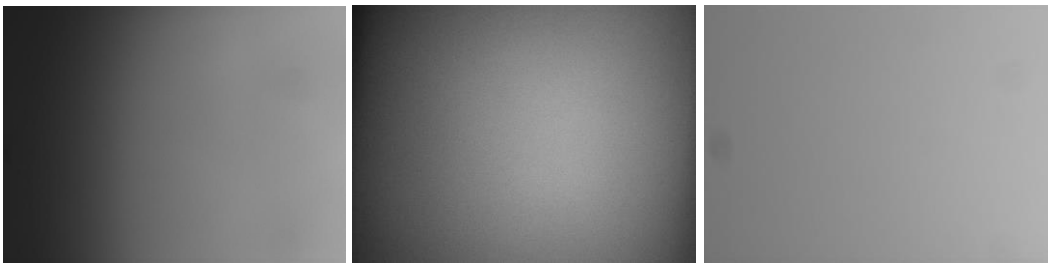

Figure 2.28 Alignment of the excitation LED illumination, followed by enlargement until it is homogeneous.

Custom aluminum parts for the microscope

The supporting structural elements of the microscope could be arranged as I have shown earlier in Figure 2.3 where all the parts can be obtained from a manufacturer. However, it would be highly desirable to be able to change the objective height with a motor in order to focus on the specimen from the computer. This is especially important if the microscope is situated inside an incubator because reaching inside with a hand to change the focus too often would disturb the correct function of the incubator or could be a source of contamination. In our attempt to reduce the cost of the microscope I have not bought any system that is especially designed to focus microscopes, which do exist but are considerably expensive. Instead, I have built the system myself from a mixture of commercially available parts and self-made parts. This makes it difficult to whoever is following these instructions to build the microscope but I will provide help to whoever needs it including the details and models of the parts that will be needed. Alternatively even the self-made parts can be also obtained by making a custom-order at a machine shop. I did not do this because I had the necessary machines at my disposal. To make the aluminum parts I utilized a milling machine and a lathe.

Later sections in this thesis will show some of these parts that were part of prototype microscopes. A later section will show the custom made aluminum parts that are part of the final versions of the 1-color and 2-color microscopes. All the supporting elements that are not self-made can be obtained commercially from Thor Labs. The lenses can also be obtained from Thor Labs or other places, the Appendix contains detailed information.

When using ASI motorized stage, I built plate holders using a milling machine. It is important that everything is well attached especially during long term imaging. Examples of custom made slide and dish holders and attachment techniques are shown in Figure 2.29.

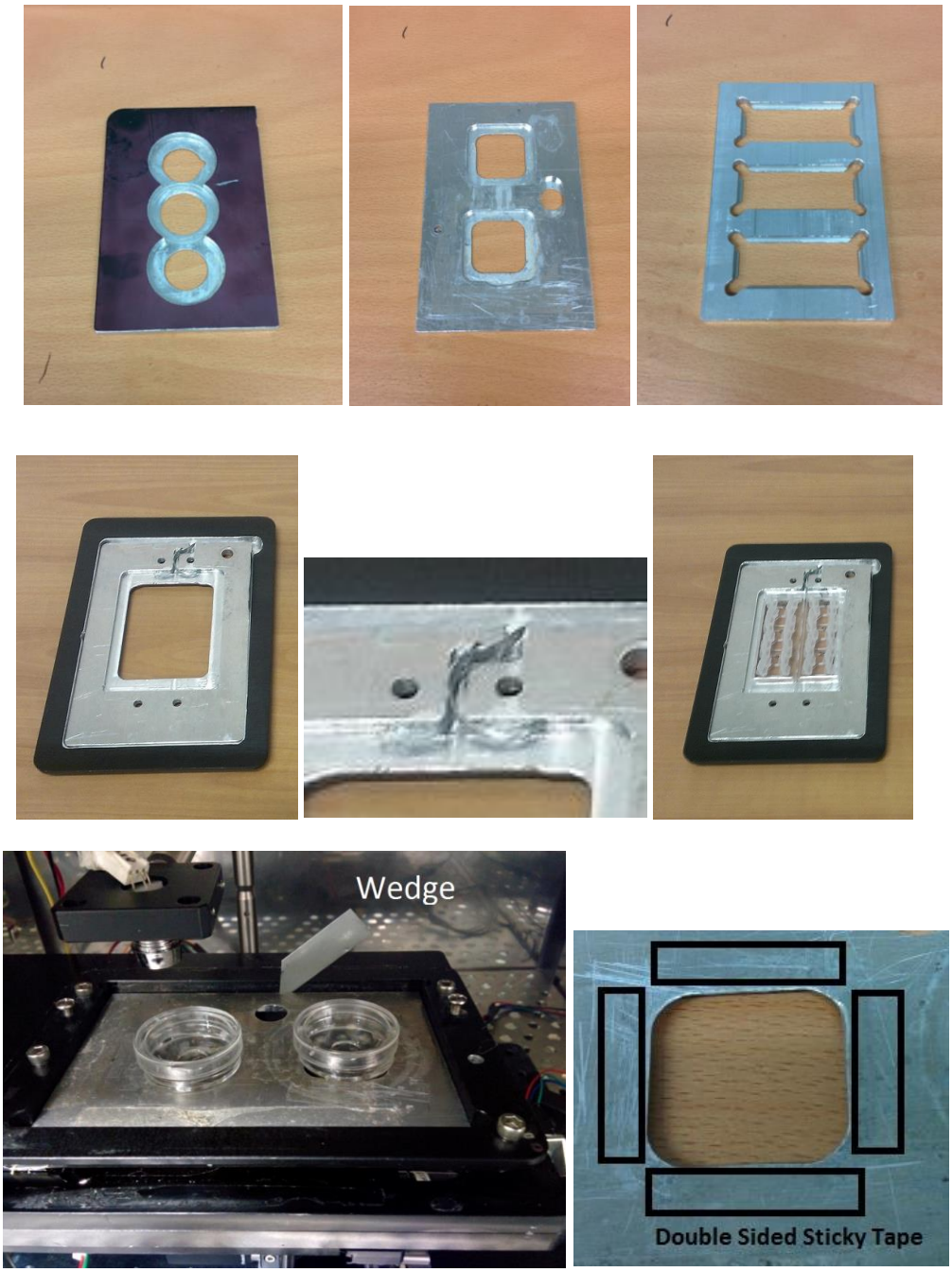

Figure 2.29 Examples of custom made slide and dish holders and attachment techniques. Middle row: a bent piece of aluminum acts as a spring to hold slides firmly in place. Bottom row: A wedge inserted by the dish holder can be important to prevent movements. Right: Double sided sticky tape can be placed under the dishes to hold them in place.

Motorization of Focusing and Stages

In the first version of the motorized incubator microscope I used a DC motor to move the entire microscope up and down in order to focus as shown in Figure 2.30.

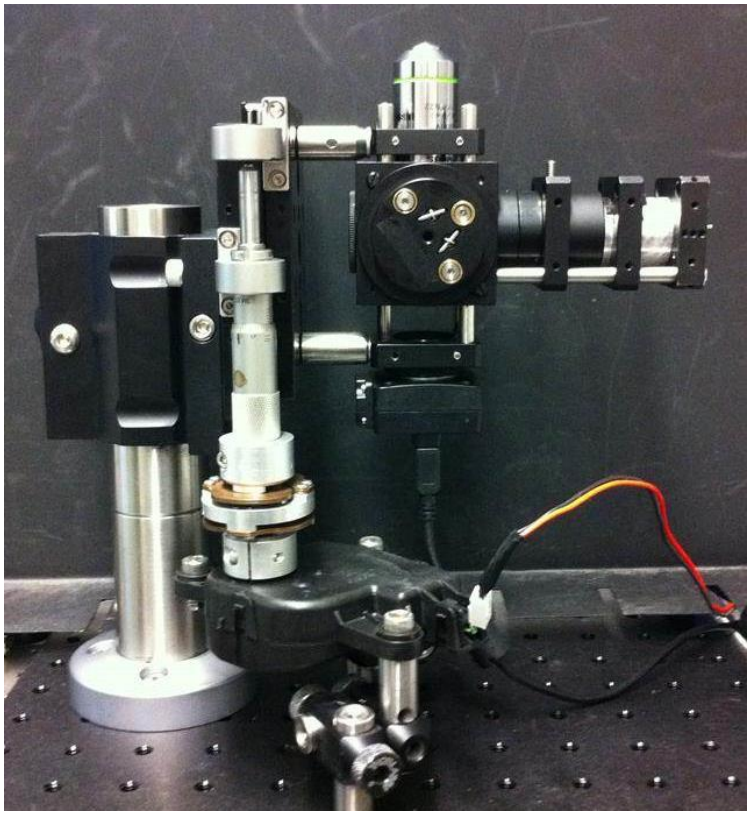

Figure 2.30. First version of a motorized focusing microscope.

The motor, which is commercially used for the motion of car windows, is powerful and weather proof which makes it suitable for the conditions inside an incubator. This microscope worked fine for some time; however it eventually became apparent that there were small changes in the focus for experiments that last for several hours. This was due to two reasons: first, in this design, the entire weight of the microscope is falling on the motor, and second, the motor has no active feedback mechanism to stay in exactly the same position over long periods of time. These are two important points to have in mind when building a microscope for long-term imaging that have to be overcome.

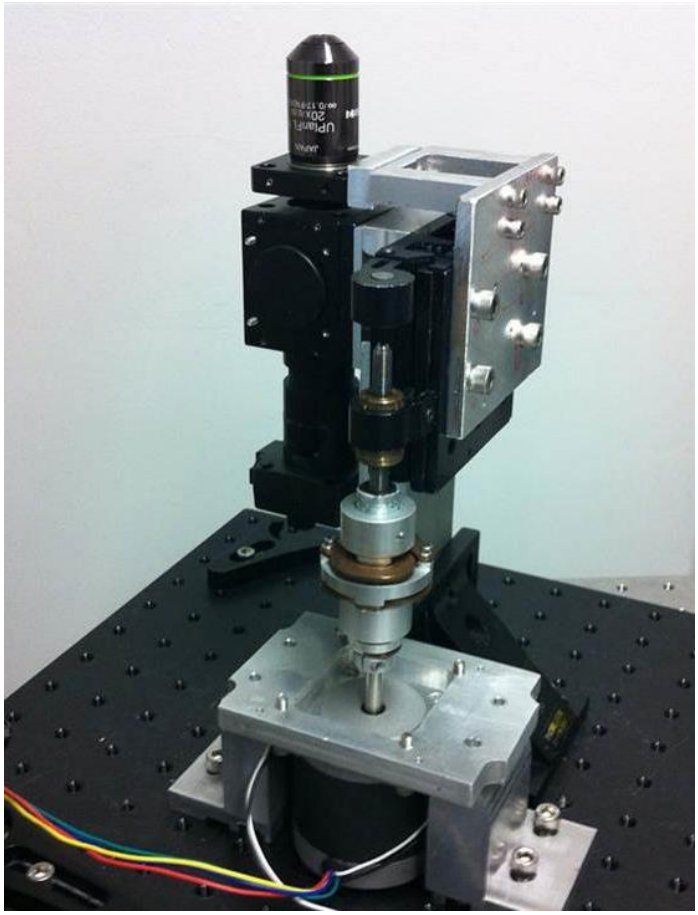

Figure 2.31. A prototype microscope version that includes a stepper motor for focusing.

These two problems are solved in the next version of the microscope which is shown in Figure 2.31. Here instead of a DC motor, a stepper motor is used. A stepper motor has current flowing through it all the time even when it is stopped which makes it suitable for long term accurate positioning. Additionally the motor should not move the whole microscope; instead it only moves the objective lens, as can be seen in Figure 2.31. This increases the accuracy and reproducibility of the focusing system.

The motor is attached to a vertical translational stage via a shaft coupler (the same as in the previous version). The translational stage was chosen because it has the lowest price of all the types of translational stages that are available. However, after some use we realized that their accuracy decreased over time and they were not accurate enough for applications requiring precise focusing such as autofocusing algorithms.

Therefore I built a slightly more expensive version of the microscope which involves using a vertical-positioning stage with a motor attached to a micrometer as shown in Figure 2.32A. The slight disadvantage of this set-up is that the motor has to be clamped so that it doesn't rotate and, at the same time, it also has to be relatively free to slide in and out as the focus changes. The solution that I adopted was to make a horse-shoe shaped aluminum holder for the motor as seen in Figure 2.32A. This way the motor can slide in and out but it cannot rotate.

A 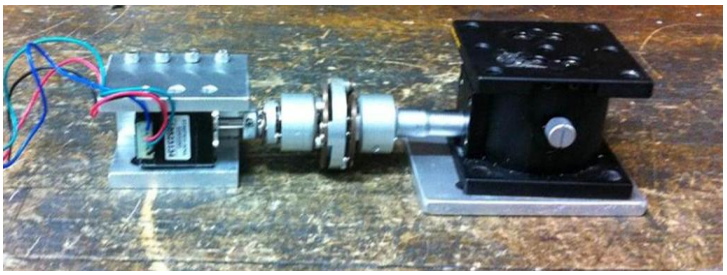

B 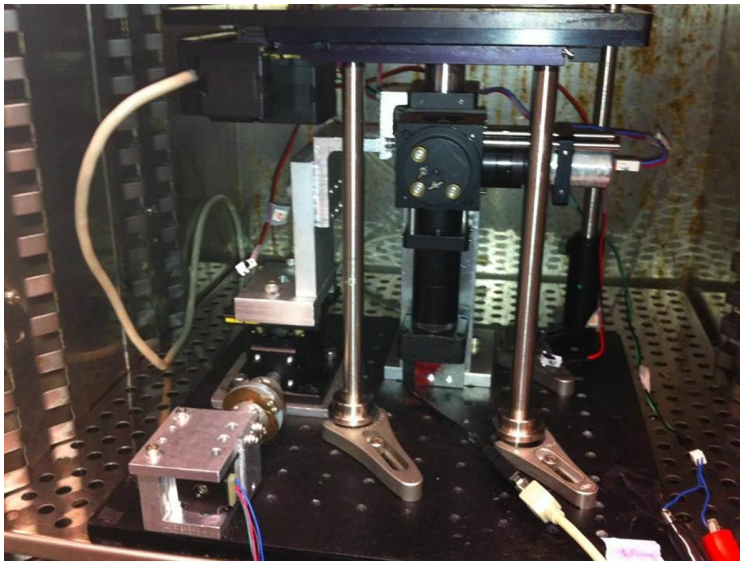

Figure 2.32. A) Motor attached to a vertical-positioning stage. B) Implementation in a microscope. The vertical stage is connected to the objective lens via several L-shaped pieces of aluminum. Note that this is not the final version of the microscope.

This set-up has been successfully used to image cells continuously for weeks inside the incubator and is perfectly suitable for up to 10X 0.3NA objectives. When using objective lenses that have lower depth of focus, for example, a 20X 0.4NA objectives or higher, it is desirable to have a better control of the focusing

motor. In other words, the motor cannot be allowed to rotate freely at all. This I have achieved by mounting the motors on sliders as shown in Figure 2.33. Note that the motor shown in Figure 2.33 is a DC motor while the one shown in the previous figure is a stepper motor. Stepper motors are recommended for the short range movements that require great accuracy such as is the case of focusing. Also note that these rails also involve some self-made parts such as the aluminum part that acts as a support below the rail and the coupler between the motor and the stage shaft. Additionally note that the coupling mechanism in this figure is different and simple than the one shown in previous figures. It involves a commercially available spring-like coupler and a self-made hollow aluminum tube to connect to the shaft. This is the recommended way to do it.

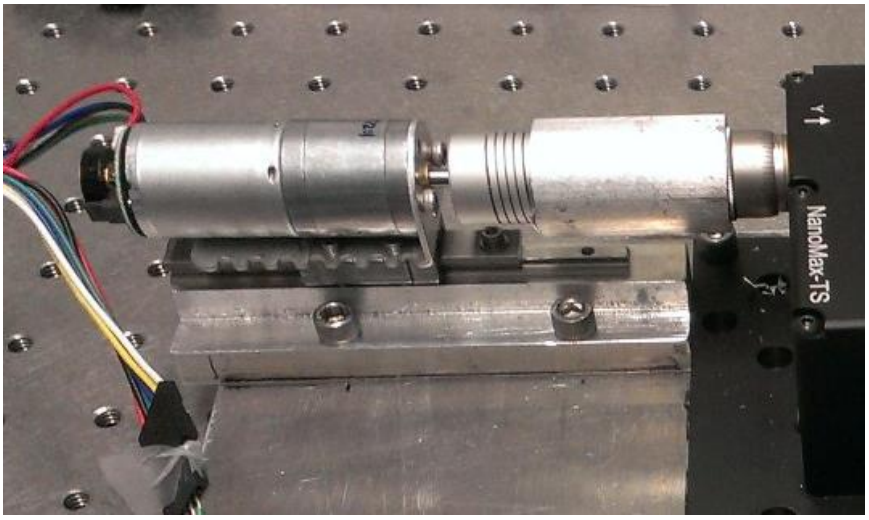

Figure 2.33 Mounting the motors on rails is the best solution for motor that have to slide while rotating such as focusing motors. The IGUS company manufactures these tiny slides that are ideal for use in the microscope as they don't require lubrication.

Here I will describe in more detail the two kinds of motors that I use both for focusing and stage motion. The first type is a stepper motor which I described in the previous section on motorized focusing (Figure 2.34 A). Even though it is a stepping motor, it can also be made to run smoothly by using micro-stepping technology. In order to make the motor work, a pin on the driver has to receive a stepped signal from a microcontroller; I use both Microchip PIC and Arduino as microcontrollers, which have to be programmed to receive a signal from the computer and send the appropriate stepped signal to a pin on the stepper motor driver. The signal can be sent via a USB human interface device or via serial com port. A disadvantage of the stepper motor is that it can quickly overheat when used inside an incubator. An increase of just a couple of degrees can kill the cells. Additionally heat can cause condensation on the petri dish due to heat gradients which will hinder the imaging. The heating can be avoided by transiently turning the motor off or by transiently reducing the current when it is not being used. This is the approach that I use and it has to be implemented in the software of the program that controls the focusing. Stepper motors are also known to miss some steps when high accelerations are used or due to other causes, but I have not had problems of this type. However, there is an alternative to the stepper motor which is to use a geared DC motor with a built-in encoder to measure travel distance (Figure 2.34 B).

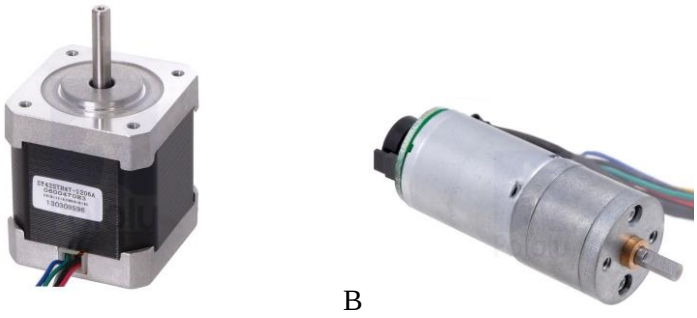

A B

Figure 2.34 Two types of motors that I have used: A) Pololu Stepper 1.2 A at 4 V #1200. B) Geared DC motor 172:1 with 48 CPR encoder #2288.

When using a geared DC motor a gear ratio of more than 1:100 is necessary to move a small stage. To keep track of its position the encoder sends periodic signals to a microcontroller such as the Arduino which must keep track of them. Given that the encoder sends more than 8000 signals per revolution of the shaft

(4000 per second), the microcontroller has to poll the pin that receives the encoder signal at a faster rate than that. This means that the microcontroller will not have time to communicate with the computer via serial com port when the encoder is sending signals because it might miss a step. For example: The Arduino can make around a million arithmetic operations per second. However, this number goes down to 2000 if we include a four character messages via serial com port for every operation at a baud rate of 115200, or down to 200 if the baud rate is 9600. If we increase the baud rate to a million bits per second which is close to the maximum, sending an eight character message every cycle allows 2500 cycles per second. This is not enough for the encoder to work while communicating with the computer. Therefore we have to send a command to the microcontroller and let it drive the motor to that position on its own without the help of the computer.

The stepper motors require drivers that control the current and the timing such as Pololu's A4988 micro-stepping bipolar stepper-motor driver. An example of two of these drivers connected to an Arduino board is shown on Figure 2.35-A. A better way to use this driver is to use is the Dual Bipolar Stepper Motor Shield for Arduino manufactured by Dfrobot, which comes as a shield that can be mounted on top of the Arduino board, and which features two A4988 stepper motor drivers. Figure 2.35-C shows a motor driver that I have used for DC motors (an Arduino shield that is based on the L298 driver). Two main benefits of the A4988 drive are microstepping and current limiting. I use 1/8 microsteps for focusing motors. The current limiting should be set to the operating current of the motor, which for our case is about 0.7A.

A 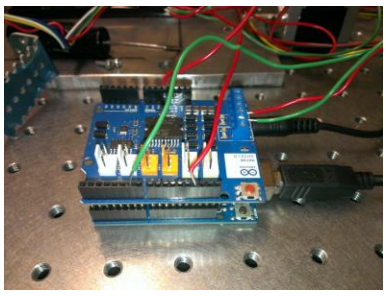 B 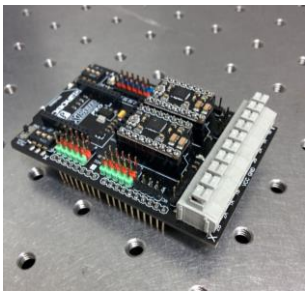 C 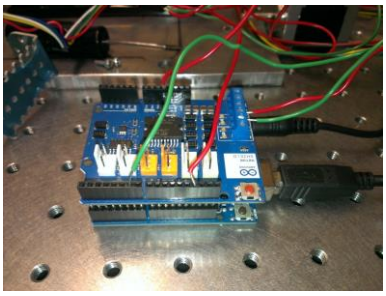

Figure 2.35 A) Two stepper motor drivers connected to Arduino microcontroller. B) the Dual Bipolar Stepper Motor Shield for Arduino C) DC-Motor driver shield stacked on the Arduino board.

Note that a third shield containing the LED drivers (which will be described in a later section) can be stacked with the other two forming a triple layer as shown in Figure 2.36. Note that in Figure 2.36 I have added additional cables labeled 1 to 4. Cables 1 and 2 I have soldered to the "enable pin" of the motor drivers. This allows me to enable or disable the motors via my software. Disabling motors can be useful because they can produce a lot of heat inside the incubator. Cables 3 and 4 go to the brightfield LED, cable 4 is the ground. Cable 3 is actually two wires that power the green and red components of the RGB LED. Note that these wires have incorporated resistances of 100Ω and 50Ω for these two colors of the light.

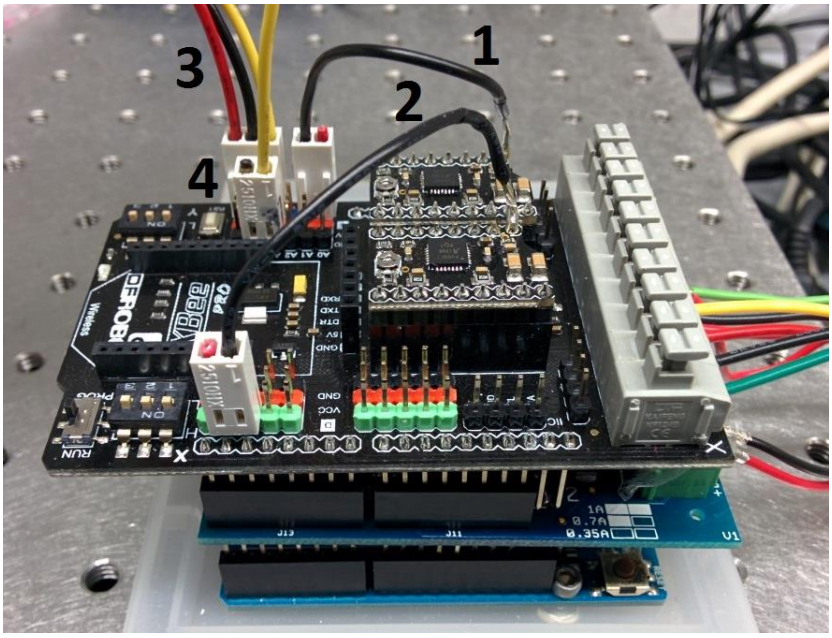

Figure 2.36 Close up of the motor shield showing additional connections for brightfield illumination and for motor control.

We can also use the A4988 stepper driver in combination with a PIC18F2455 but in this case we have to build the circuit ourselves. The following diagram illustrates the necessary connections between these two chips.

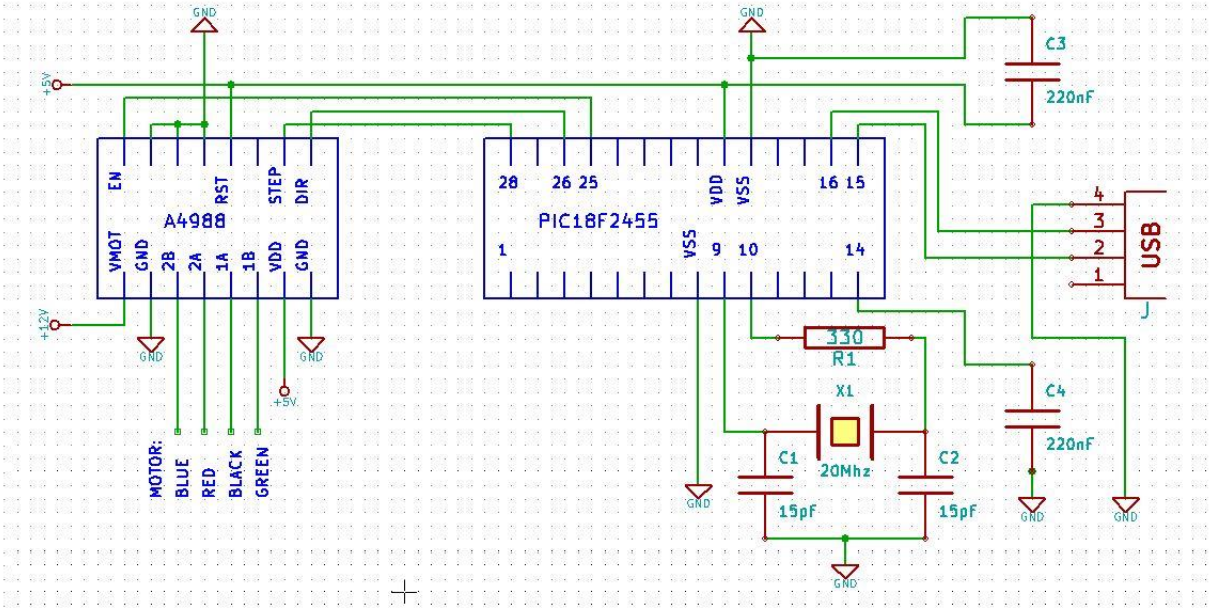

Figure 2.37 Schematic for a Pololu A4988 stepper driver controlled from a MicroChip PIC18F2455 and USB.

When using the DC motor, it is important to realize that when the controller tells the motor to stop, it continues to spin for some time until it stops completely. However there is a function to stop the motor by applying a brake. This is a function that is available on the motor shield. Even when we employ the braking function the motor still takes some time to come to a stop, and during this deceleration it is important to still count the pulses coming from the encoder. Additionally we don't want to send any serial communication to the computer during this deceleration to avoid interfering with the counting so we have to start a timer and send the message to the computer when the counter is over at a time when we are sure that the motor will have stopped completely. In my program I set up a counter that will count 40000 cycles which takes about one second which is enough time for the motor to stop moving. The motor will overshoot

its target by about 90 encoder pulses, but given that there are several thousand pulses per revolution of the shaft, it is an acceptable value. Figure 2.38-A shows a Thorlabs stage that I have motorized with two DC motors for X and Y motion and a stepper motor for focusing in the Z axis. The stepper motor is chosen for focusing because of its increased accuracy while DC motors are chosen for the other 2 axis because of their speed. Figure 2.38-A also shows all the electronics driving the motors. Figure 2.38-B shows how this stage is coupled to a microscope and will be explained later.

A 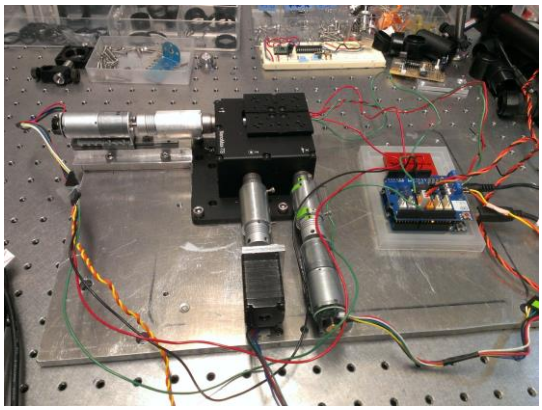 B 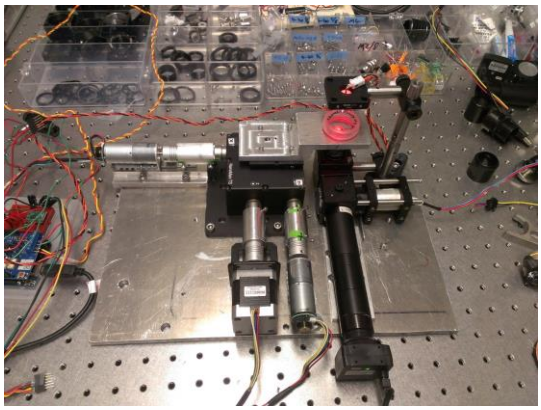

Figure 2.38 A) A stage with two kinds of motors and its corresponding electronics. B) The same stage coupled to a horizontal microscope (that will be described later).

Couplers to the micrometer knobs had to be machined from a 1 inch aluminum rod and made hollow with the use of a lathe and a drill (Figure 2.39-A). Figure 2.39-B shows the machining process of the stage that holds the dishes to be imaged using a CNC milling machine. It is manufactured from a single piece of aluminum because this is the best way to make sure that the focus will not change when moving the stage and that it will be horizontal to the micrometer stage.

A 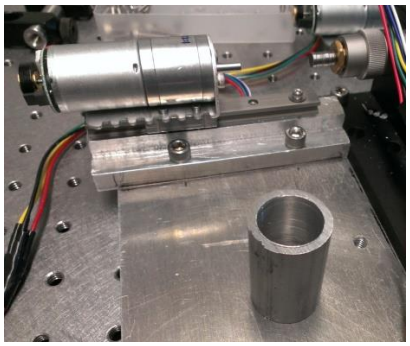 B 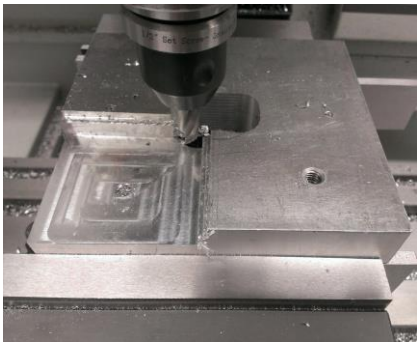

Figure 2.39 Machined parts included A) couplers and B) stage to support samples.

The disadvantages of the Thorlabs stage that I have described up to now is that it is very fragile and if you press on it, it will easily break. Additionally the travel distance is very limited. An alternative that I explored was to motorize a regular microscope stage such as the ones used in Olympus microscopes.

An option is to add motors that replace the knobs that serve to manually move the stage. This often requires the use of belts because the knobs share a single axis. Figure 2.40 illustrates my approach using stepper motors and belts.

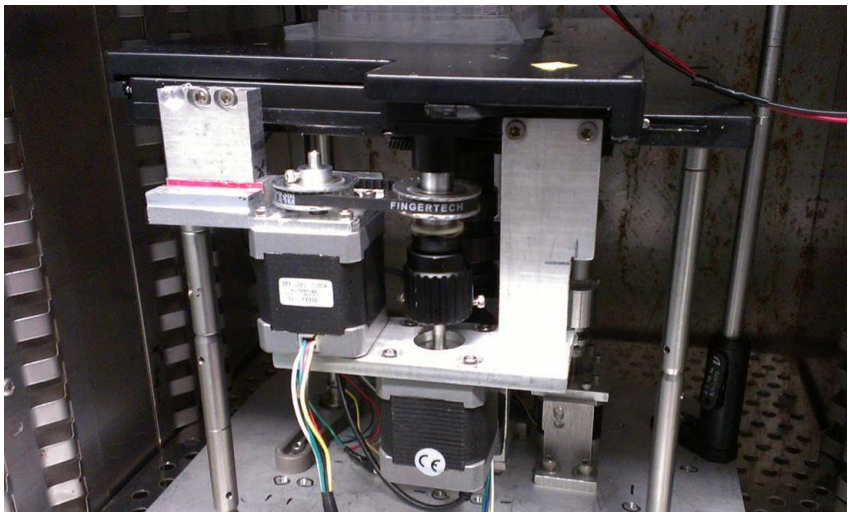

Figure 2.40 Stepper motors and belts attached to microscope knob. Aluminum parts were custom made.

For application requiring highly accurate movements I tried a different approach which involves moving the stage via lead screws. The first step is to attach a lead screw to a stepper motor and then attach this to the stage, once for each axis. (Figure 2.41).

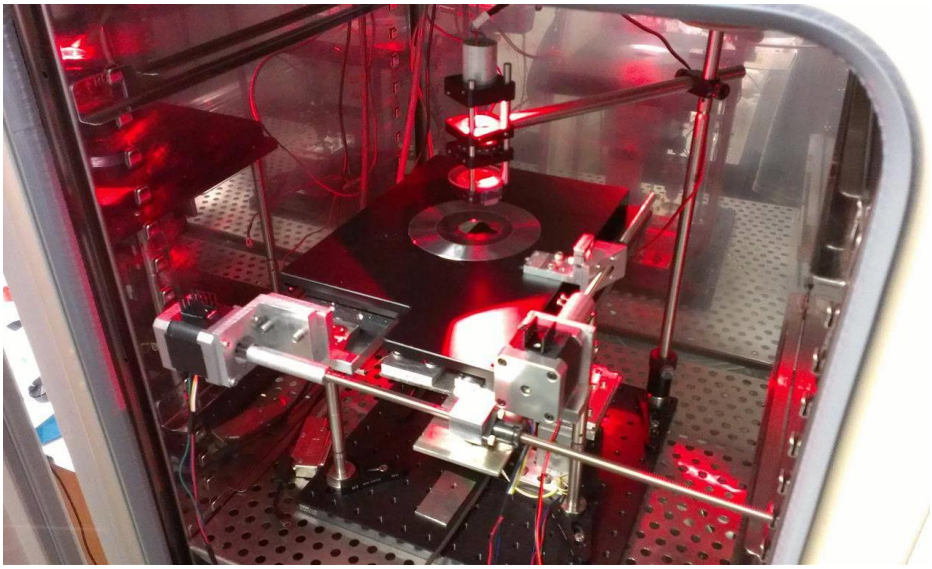

Figure 2.41 Motorization of a stage with stepper motors and lead screws.

Due to its size, however, this approach turned out to be less accurate than the smaller Thorlabs stages. An additional disadvantage of this approach is that there are a large number of aluminum parts that have to be custom machined to support the motors and attach to the stage. The advantage of this approach is that the travel distance is much bigger.

DVD Drive Stage

If you already have an old DVD drive stage then it can be a cheap option to build a translational stage with it. The drives have a built-in stepper motor that can be used to image multiple positions although it only moves in one direction. Four wires have to be hooked up with the motor and a support for the dish has to be installed. The same stepper motor driver that was used previously will work here except that we have to turn down the current to about 200mA because of the reduction in size of the motor.

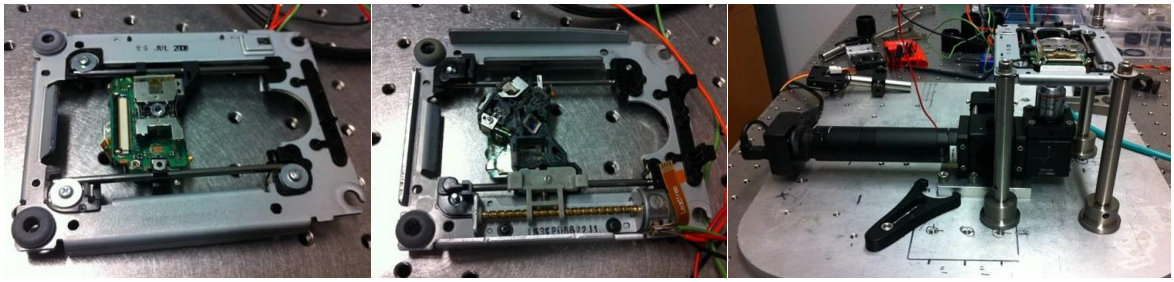

Figure 2.42 A DVD drive is shown (left) which has a motor underneath (middle) and can be used as a translational stage for the microscope (right).

The 1-Color Fluorescence Microscope

Figure 2.43 shows a top view of the main components of the horizontal version of the microscope.

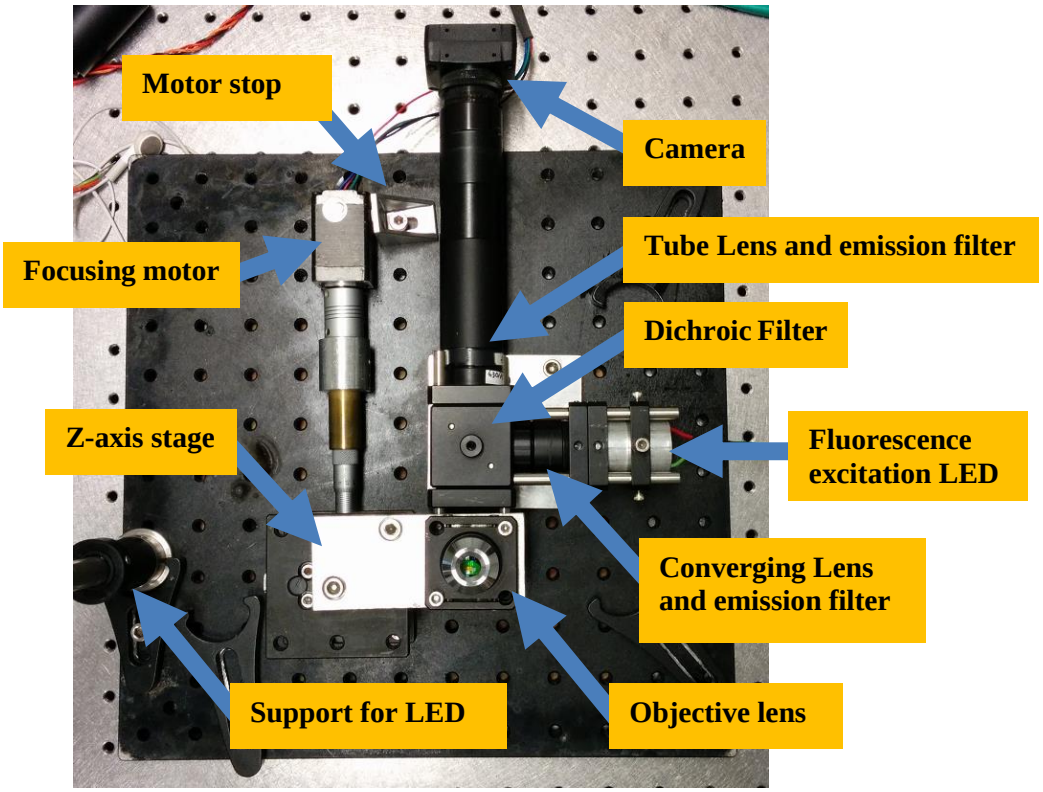

Figure 2.43 A top view of all the components of the horizontal version of the microscope.

The next figure shows the support for the brightfield LED. It is made by a combination of an LED holder (10mm Sparkfun COM-11148) and a Thorlabs SM05-Threaded 30 mm Cage Plate. The holder can screw into the cage plate. Thorlabs Stainless Steel Optical Posts make up the rest of the LED support. The LED itself is an RGB 10mm diffuse LED (COM-11120).

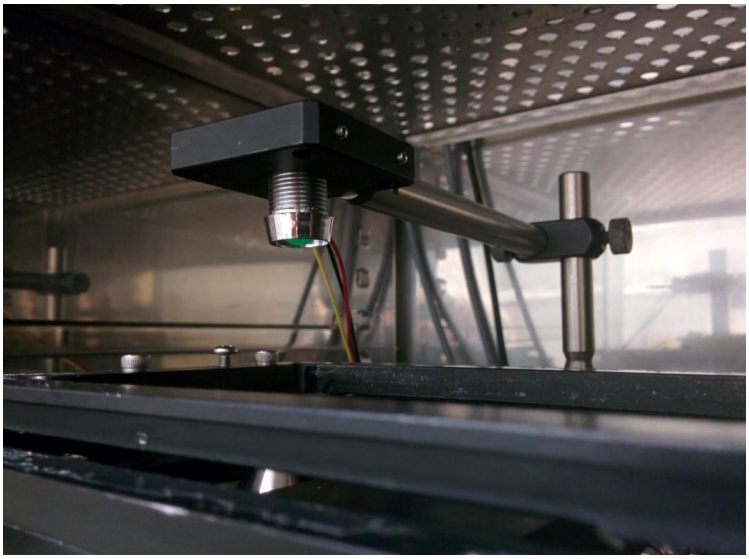

Figure 2.44 LED holder for brightfield illumination.

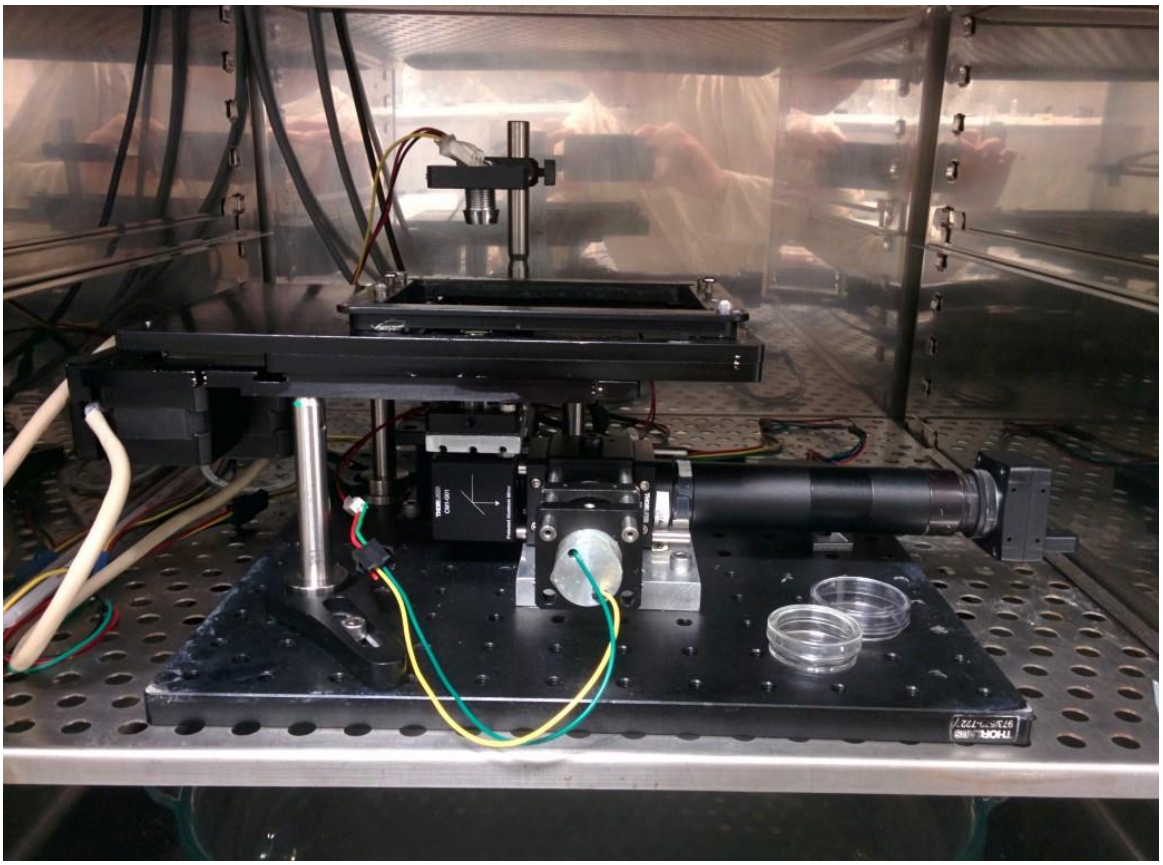

Figure 2.45 A side view of the final 1-color fluorescence microscope

The 2-Color Fluorescence Microscope

In order to go from a one color fluorescence microscope to a two color fluorescence microscope we have to have the ability to change four things: the dichroic mirror, the two filters, and the excitation lamp. I initially built a sliding mechanism to enable automatic exchange of filters (See Figure 2.46).

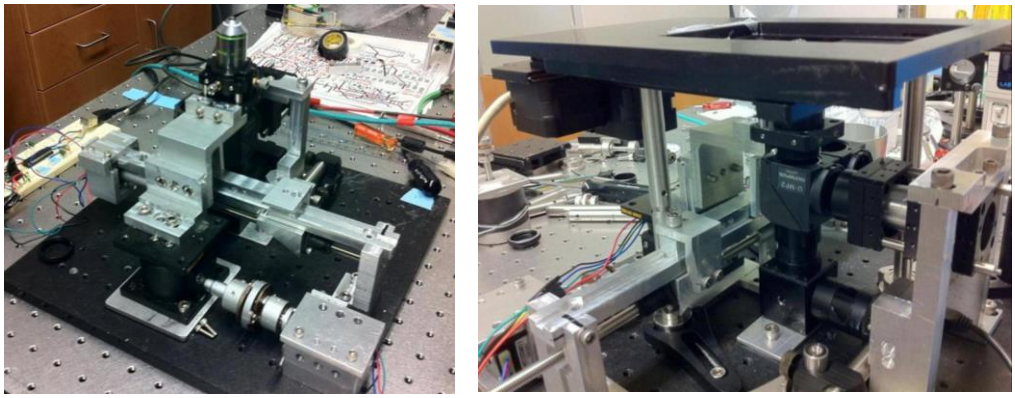

Figure 2.46 Two views of a sliding mechanism for filter exchange in a two-color fluorescence microscope.

This approach, however, didn't solve the need to change the excitation light source. Additionally a sliding mechanism would be too slow to take hundreds of images as required in some application. An alternative that I came up with was to make a two-color fluorescence microscope with no moving parts. This would allow for very fast switching between the two colors and a longer lifespan. To do this I double all the optical elements, I use two cameras and a total of three dichroic mirrors (illustrated in Figure 2.47).

A 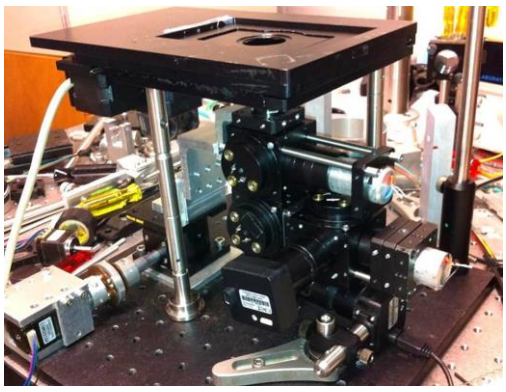 B 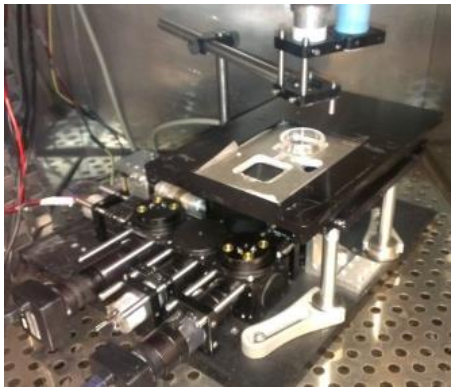

Figure 2.47 A) A prototype of two two-color fluorescence microscope. B) Final version of two two-color fluorescence microscope with a horizontal configuration (See Figure 2.48 for greater detail).

Figure 2.48 shows the location of the components of the two color fluorescence microscope in greater detail.

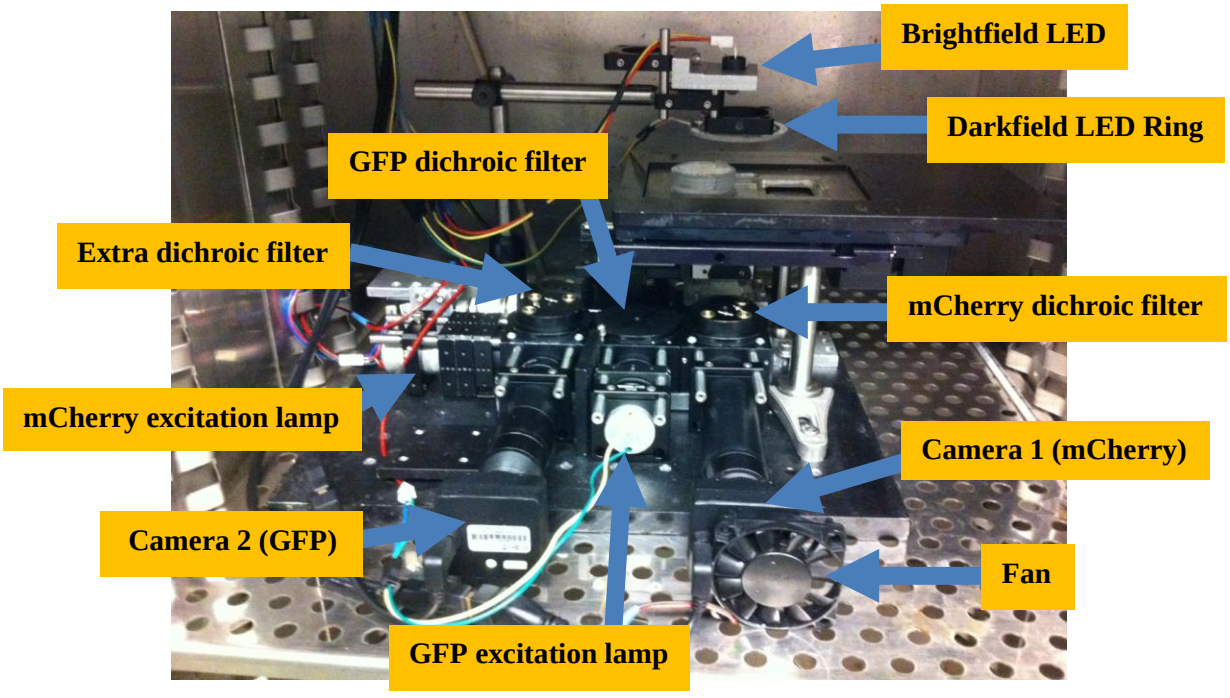

Figure 2.48 Main components of the two-color fluorescence microscope.

Other Aspects of the Microscope

Light Emitting Diodes and Electronics

There are two kinds of LEDs in use by the microscope: high power LEDs for fluorescence excitation that require 700mA of current and low power LEDs for brightfield illumination that require just 20mA. For this reason, they require different electronics. Due to the high current needed, the high power LEDs require an LED driver. For this we designed a circuit board which is illustrated in Figure 2.49 and Figure 2.50.

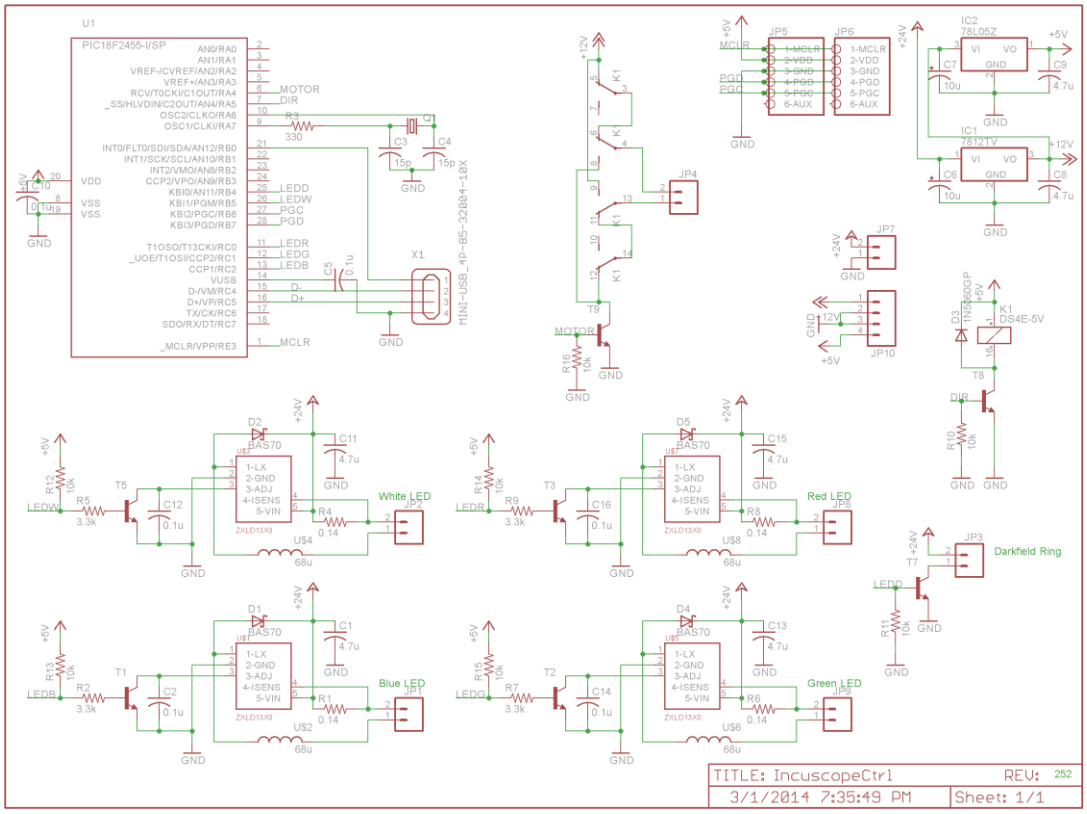

Figure 2.49 Circuit board schematics used for control of fluorescent excitation light via USB and the microcontroller PIC18F2455.

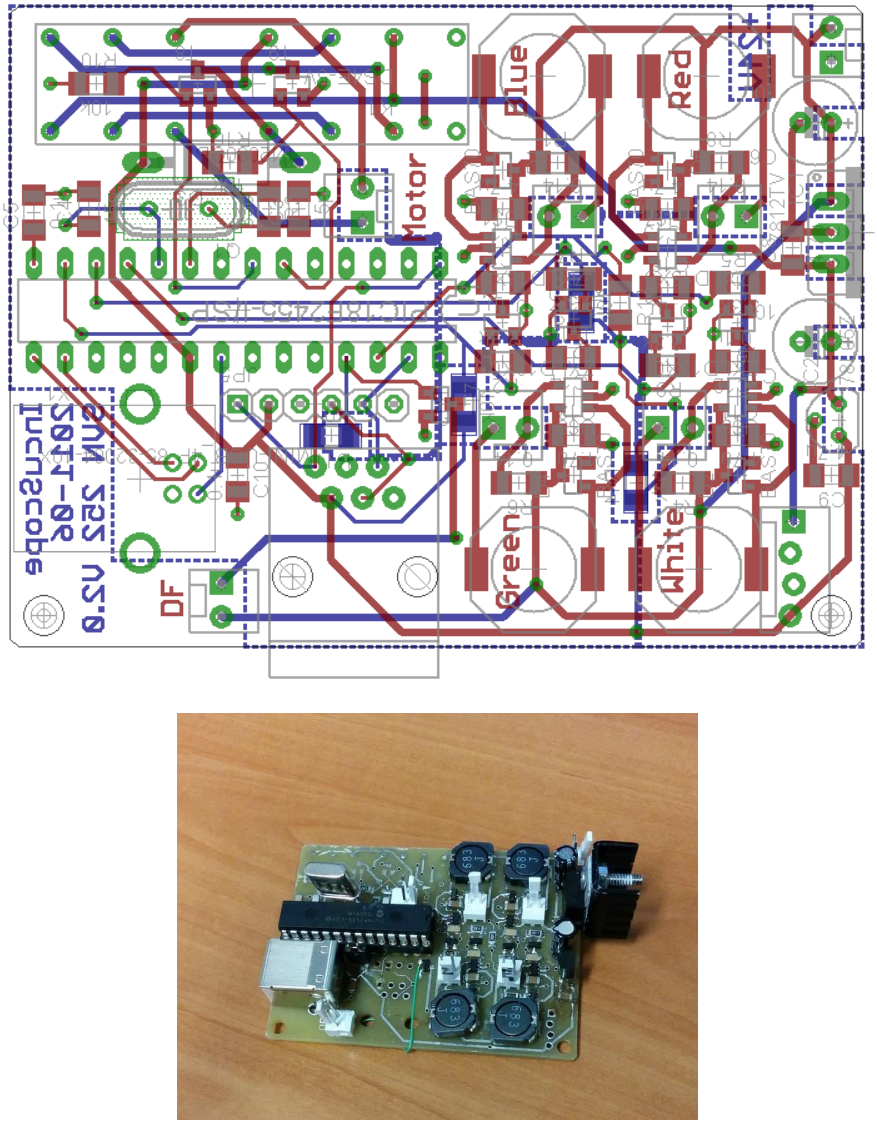

Figure 2.50 Circuit board schematics used for control of fluorescent excitation light via USB and the microcontroller PIC18F2455.

The board has to be programmed to receive instructions from the computer. This board appears to the computer as an HID (Human Interface Device) and thus requires that we assign a name to the microchip. This name must be known to the software that runs the program. The name of the microchip is "INCUSCOPE" just as the main application is called IncuScope.

The high power LEDs are Philips Luxeon Star (see Figure 2.51-A). Given that they consume a lot of power they quickly become hot, therefore they require a heat sink. I manufactured aluminum heat sinks that

additionally act as a support for the high power LEDs (Figure 2.51-B). The low power LEDs are tri-color diffused RGB LEDs that don't require heat sink and I operate them directly from a microchip with just the additional necessary resistors (Figure 2.51-C).

A B C

Figure 2.51 A) High power Luxeon Star LED. B) Aluminum heat sink. C) Low power RGB LED COM-11120.

An alternative to using a custom made board and a PIC18F2455 microcontroller is to use an Arduino microcontroller board with a 4 channel LED driver shield. This shield, however, is only manufactured in China by LEDSEE electronics and can take some time to ship, Figure 2.52. If using this shield note that you must solder together the two connections marked with 0.7A, which is the current that flows through the LEDs. Otherwise just 0.3A will flow through the LEDs. The shield and (LEDs) can be powered entirely from the Arduino board but the Arduino board must be powered to the mains. (Getting power from the computer's USB port is not enough to power the high power LEDs).

Figure 2.52 A 4 channel led shield for the Arduino UNO microcontroller board.

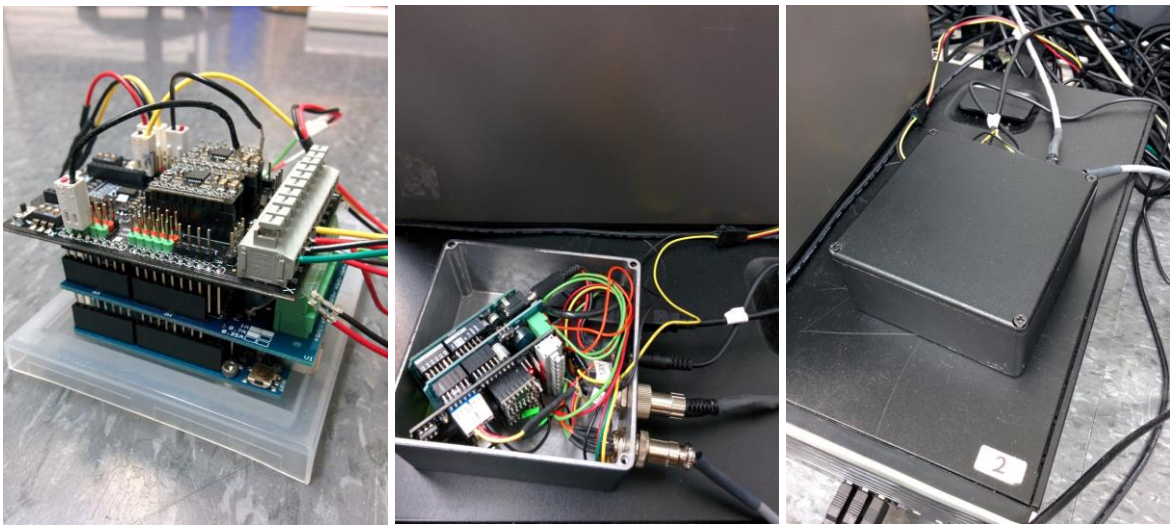

Figure 2.53 The electronics controlling the focusing motor and the LEDs can be stacked easily when using the Arduino microcontroller, and fitted into a box that connects to the computer and to the incubator.

Figure 2.53 shows the LED driver shield as the middle layer of a triple layer of electronics. The bottom layer is the Arduino UNO, and the third layer is the motor shield (this is the Dual Bipolar Stepper Motor Shield for Arduino (A4988) manufactured by Dfrobot, which was mentioned earlier in the section on motors). Note that this triple layer has two sources of power, one for the Arduino and LED shield, and another for the motor shield.

Upright Microscope

The microscope that I have described is an inverted microscope which means that the objective is below the sample. There are some situations in which it would be advantageous to have the objective above the sample, for example when the cells are cultured over an opaque surface. (This would be the case for cells cultured in opaque minerals that represent bone, which I have had to carry out). This is called an "upright" microscope. My microscope can be relatively easily converted into an "upright" microscope by turning it upside down as shown in Figure 2.54.

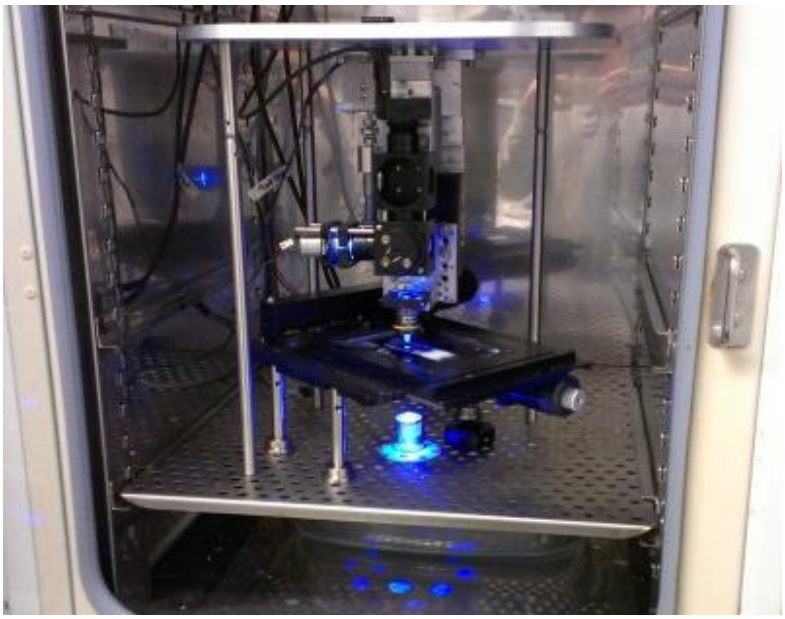

Figure 2.54 The inverted microscope can be converted into an upright microscope when turning it upside down.

Reduction of hot pixel noise

When CCD cameras operate they can get hot and certain pixels can become white. The high temperature inside an incubator aggravates this effect. The fan connected to the camera as illustrated previously in Figure 2.48 cools down the camera. Without the fan, the CCD of the camera will reach a temperature of 54 degrees Celsius. The fan will reduce this temperature by about 4 degrees which is enough to produce a big difference in the pixel noise as illustrated in Figure 2.55.

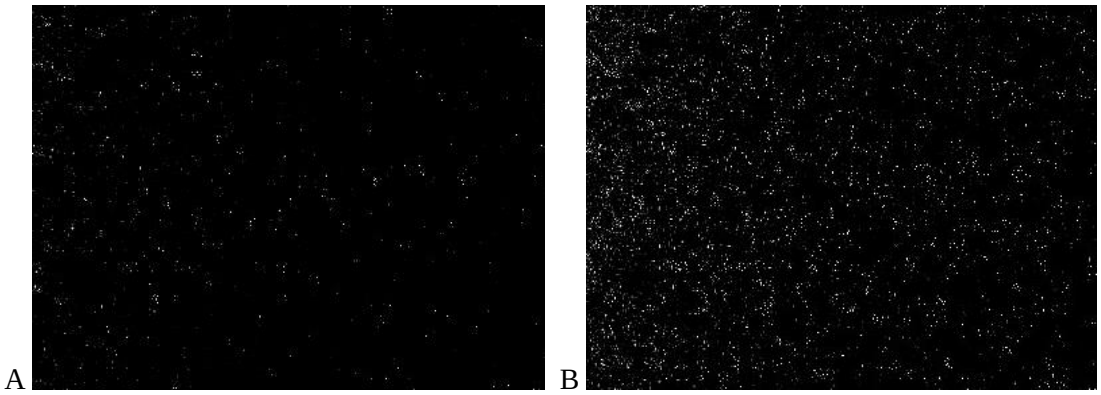

Figure 2.55 The pixel noise can be reduced when using a fan to cool down the camera, A) Image while using a fan attached to reduce the temperature of the camera. B) The same camera without a fan shows higher levels of noise. (1.2 second exposure).

The temperature of the camera depends on the rate of image acquisition. The rate of image acquisition of the image in Figure 2.55 was one image for every 7 seconds. This high rate of image acquisition is required when taking images at multiple positions. In other cases, it might not be necessary to utilize a fan to cool down the camera. Yet, even outside of the incubator the camera will remain at 40 degrees Celsius because the current that powers the camera also heats it. On the other hand, the amount of noise in the camera also depends on the exposure time. The previous images were taken with an exposure of 1.2 seconds, which is sometimes needed when imaging low intensity fluorescent cells. However, GFP fluorescent cells are usually bright enough that the exposure time is too small to observe any noise. This is why only one camera in

Figure 2.48 has a fan (the camera used for mCherry) while the other camera is used for GFP and therefore doesn't have a fan.

Calibration of the two-color microscope

In a microscope, the alignment of the optics is very important. In addition to this, in the case of the two color microscope, the two colors obtained from the two separate cameras have to overlap. I have added a function to the program to display a red mark at the center of the screen that serves as a bull's-eye when centering the two cameras which makes it easier to align the images (Figure 2.56). In order to align the images we have to follow a procedure step by step in the right order. First, the mCherry dichroic mirror has to be adjusted to a position in which we have a good illumination of the field of view with fluorescent excitation light. Then we switch to brightfield illumination and an arbitrary feature on the sample is aligned with the red mark on the first camera (camera 1, see

Figure 2.48) by moving the stage. Then the extra dichroic filter is turned and adjusted until the feature also aligns with the red mark while using the second camera. Then we turn on the blue fluorescence excitation light and adjust the GFP dichroic filter until we have a good illumination of the field of view with the blue fluorescent excitation light.

Figure 2.56 A red mark on the center of the program screen enables alignment of the two cameras of the two-color microscope.

If the two color images still do not fully overlap, they can be adjusted post-imaging and made to overlap via image processing.

Resolution

The resolution of a microscope under optimal conditions is the wavelength of light (λ) divided by two times the Numerical Aperture (N.A.) of the lens:

$$\text{Resolution, } \mathbf{R = \lambda / 2NA.}$$

Given that we typically use red light and an N.A. of 0.3, the maximum resolution that we can expect in this scenario is:

$$R = \lambda / 2\text{N.A.} = 0.7 / 0.6 = \mathbf{1.2\ \mu m.}$$

The microscope can perform close to this maximum resolution (Figure 2.57).

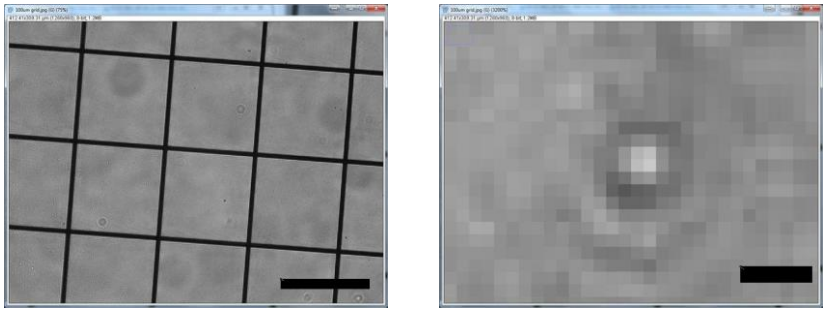

Figure 2.57 A 100 µm grid (left) indicates that we obtain 3 pixel per µm, and we can resolve an object that is approximately 1µm in diameter (right). Scale bar 100µm (left) and 2µm (right).

Condensation

Condensation that forms on the lid of dishes will hinder imaging. This was a problem for me until I realized that the source of the condensation was likely the heat that emanates from the motors. The biggest source of heat is from the focusing motors. The solution was to turn the focusing motors off after each

round of focusing. This largely solved the problem. However, it indicates that we can't use stage motors or focusing motors too heavily during an imaging session or else the heat will cause condensation.

Figure 2.58 A dish with condensation (left) and without condensation (right).

Condensation is caused by heat gradients and not by homogeneous heat. Even a small gradient will cause condensation over time. This is why cells are usually not affected by it. The fact that the condensation affects imaging (it only affects brightfield but not fluorescence) can be mitigated by either changing the lid when the condensation appears, or by adding a spacer between the lid and the dish which increases ventilation. If you choose to change the lid make sure the new lid has been conditioned to the appropriate temperature for at least 15 minutes before using it to prevent new condensation forming. If you see some images appear brighter and some images appear darker, then probably there are condensation droplets on the lid that are causing this effect and the lid needs to be changed.

Plastic versus glass dishes

In brightfield mode I did not observe any difference in image quality when using plastic or glass substrates to culture cells. On the other hand, the use of glass dishes is especially useful when using fluorescence and when we are interested in subnuclear structures. However, the increased contrast obtained with glass can make a significant difference to the computer algorithms that detect cells. Therefore it is recommended to use glass as a substrate whenever possible when using fluorescence and the difference is illustrated in Figure 2.59.

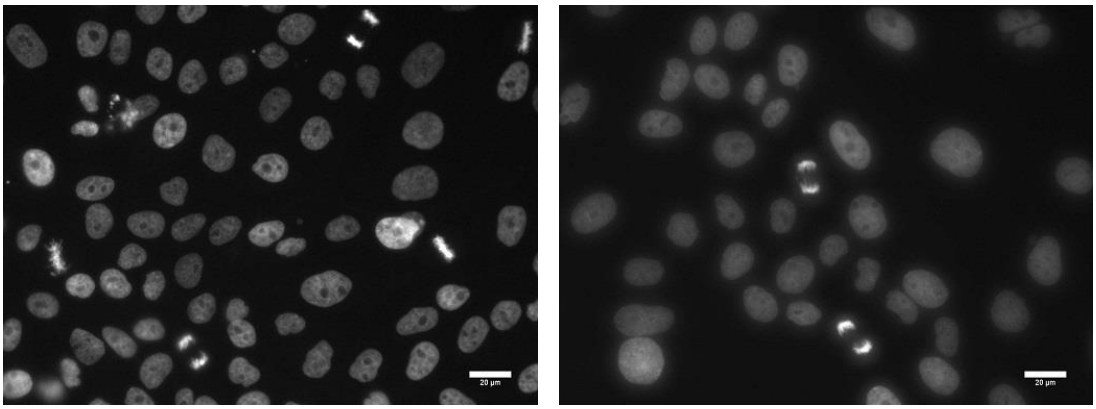

Figure 2.59 Cells grown in glass (left image), and plastic (right image). Even though glass is better, cellular nuclei can still be easily recognizable in plastic dishes. Scale bar 20um.

Incubator vibrations

We are placing a number of motors inside of the incubator and their movements will cause vibrations that can often be big enough to cause displacements in the sample and in the acquired images. Often the whole shelf of the incubator will vibrate which means that fixing the sample will not solve the problem. This effect can be especially troublesome in the case of fluorescent imaging, where long exposure times mean that if the sample moves the images will result blurred. However, it also poses problems for image tracking algorithms. A lot of the vibration happens because the shelves of an incubator are not fixed in place. A solution is to add a wedge to the shelves which will fix them and largely prevent them from vibrating. See Figure 2.60.

Figure 2.60 A wedge placed between the shelf and the incubator wall is essential when using motorized stages to avoid vibrations.

Putting wedges in all of the shelves instead of in just one will produce much better results because often the wall of the incubator itself is just a plate of metal that is removable for cleaning purposes and is not tightly fixed in place. Another thing to have in mind is to be careful when closing the door of the incubator as this on itself can produce vibrations that will blur the acquired images.

IncuScope – The Program That Runs The Incubator Microscope

The computer code developed for this thesis can be divided into three different parts: (a) the main application that captures and save images (which we call IncuScope), (b) the code that resides in the microchips which interfaces between the electronics and IncuScope, and (c) the code to process the images. In this section I will describe IncuScope, the main program that runs the imaging sessions for the incubator microscope. IncuScope is a Windows program that I have developed over the years, the latest version of which has been compiled with Microsoft Visual Studio 2013. I will now describe what the buttons mean and how to use it from the user perspective. The main window of IncuScope is shown in Figure 3.1.

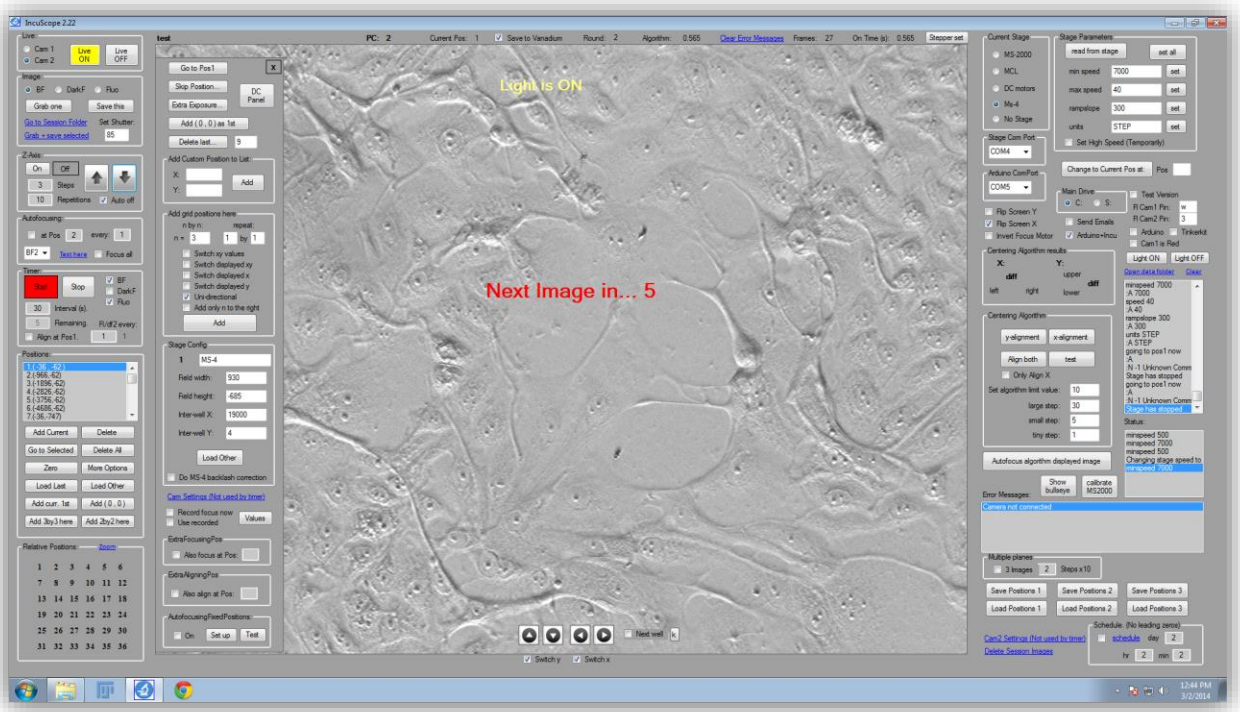

Figure 3.1 IncuScope: My application to control the microscope, including camera, stage, lights and focusing motors. Among its functionalities are autofocusing and the ability to carry out time-lapse imaging sessions in multiple user-defined positions.

The most frequently used buttons are placed on a panel on the left side of the window arranged in subpanels according to their function. This panel is always visible for ease of access (shown highlighted in red in Figure 3.2). There is a second vertical panel with additional buttons that is less often used which is only visible when it is required, thus avoiding clutter and maximizing the area available for the displayed images (highlighted in green in Figure 3.2). Above the displayed image is information about the current imaging session (highlighted in yellow in Figure 3.2). To the right of the displayed image is another panel with more advanced options and information about possible errors (highlighted in blue in Figure 3.2). Finally at the bottom of the screen, highlighted in gray, are buttons to move the stage up, down, left or right.

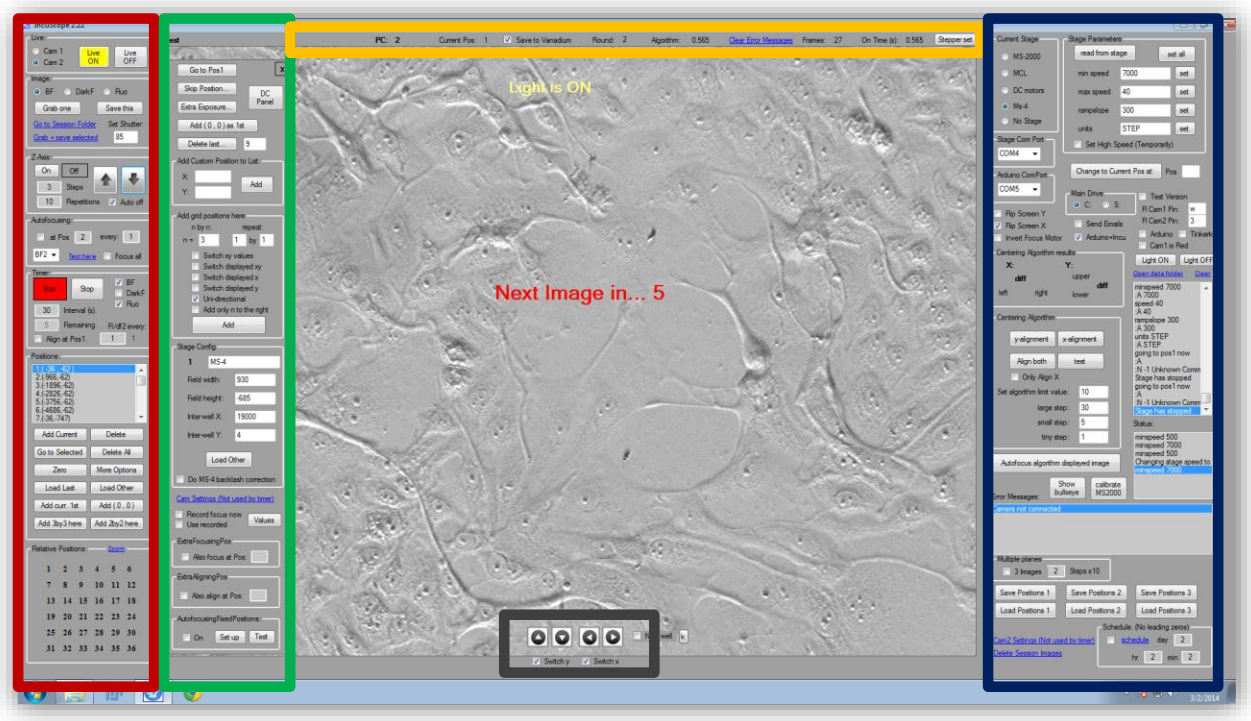

Figure 3.2 The main panels of IncuScope are highlighted in colors and explained in the text.

I will now describe in more detail some of the main functions that are available in the subpanels starting by the panel on the top left.

Main Functions

- In the Live subpanel (see Figure 3.3) we can select which camera we want to use. If we are using the 2-color microscope described in this thesis, Cam 1 will be set to image GFP and Cam 2 will be set to image mCherry fluorescence. The other two buttons enable us to turn on or off live imaging preview which will show the cells in real time. Live imaging should be turned off before starting a programmed time-lapse imaging session. Using live preview with brightfield is perfectly fine for as long as you want, but it is not recommended to use live preview when using fluorescence excitation because it can damage the cells. Additionally given that fluorescence LEDs are high power they can quickly heat up inside the incubator so it is best to try not to keep them on for more than a few seconds at a time.

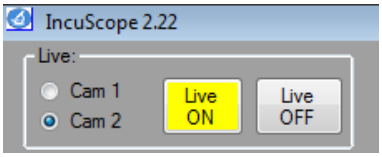

Figure 3.3 Live subpanel

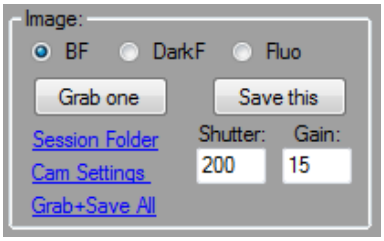

Figure 3.4 Image subpanel

- In the Image subpanel (see Figure 3.4) we can select one of three imaging modes which will be used for the live preview: brightfield, darkfield or fluorescence. The next two buttons allows us to grab one image and save it. Grabbing one image is only necessary if live preview has been turned off, but as mentioned earlier, grabbing one image at a time is the recommended way of previewing in fluorescence mode. Next are two numbers that we can change: the shutter time in milliseconds, and the camera "gain". Increasing the gain will increase the brightness of the image but it is recommended to first increase the shutter time. However, increasing the gain is useful when using fluorescence to avoid damaging the cells because the shutter time is linked to the LED lights, meaning that a longer shutter time will result in a longer time during which the lights will be on. Notice that these two numbers will be saved for each imaging mode and for each camera. Therefore if you change the imaging mode or camera, the numbers will change, but the values will be saved. On the left side of the subpanel are three links. The first one takes you to the session folder of the current imaging

session (if you have started a session). The second one enables you to change settings in the camera (notice that this will override the shutter and gain numbers). The third one is a function that allows you to grab images in each imaging mode and with each camera and save them all, just with one click.

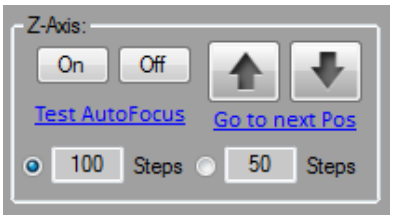

Figure 3.5 Z-Axis subpanel

- The Z-Axis subpanel has an on and off button to turn the focusing stepper motor on or off. The motor creates some amount of heat (which is proportional to the current that we have set to pass through it) and when we don't use it, it might be wise to turn it off with this button. In fact in the latest version of the program you might find that the motor is turned off automatically after some time for this reason. The arrow buttons move the objective up or down in order to focus on the sample, and the distance that they move with each click is given by the number of steps specified in the text boxes found below this button. I have added two text boxes so that we can quickly switch between a long set and a short step. The "Test AutoFocus" link will run the autofocus algorithm at the current position and the "Go to next Pos" link will move the stage to the next position if we have specified a list of positions (see next sections).

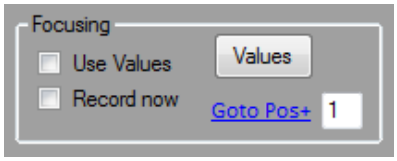

Figure 3.6 Focusing subpanel

- The focusing subpanel allows us to specify how the microscope will focus on our sample. Basically there are two ways of focusing. One is to tell the microscope how many steps it should move up or down at each position. The second way is to use autofocus. These two ways are not mutually exclusive. Using both together is useful when you know that there is a large vertical distance between two positions and you want to do a first quick approximation followed by a more effective use of the autofocus. The "Use Values" checkbox should be checked when you want to use the focusing capabilities of the microscope (either of the two methods previously mentioned). In either case we want to use the numbers specified in the window that opens when we click on the "Values" button. The "Values"

button will open the window shown in Figure 3.7 where we can set the number of steps to move at each position. On the right hand side of Figure 3.7 we can also specify which positions we want the program to try to autofocus by itself. Here, individual positions can be entered separated by commas, while ranges like 5 to 7 can be entered as "5-7". Below that, we can specify what happens in such intervals, for example, if we say "Do one every: 2" it will autofocus one position every two. This is useful because sometimes we have so many positions that performing autofocus on each one would take too much time. Note that the autofocusing will happen after the number of steps associated with that position has been executed. Note that when the program does autofocus on a position, it will automatically change the number of steps to focus next time at that position, so you may see the number associated with that position change over time.

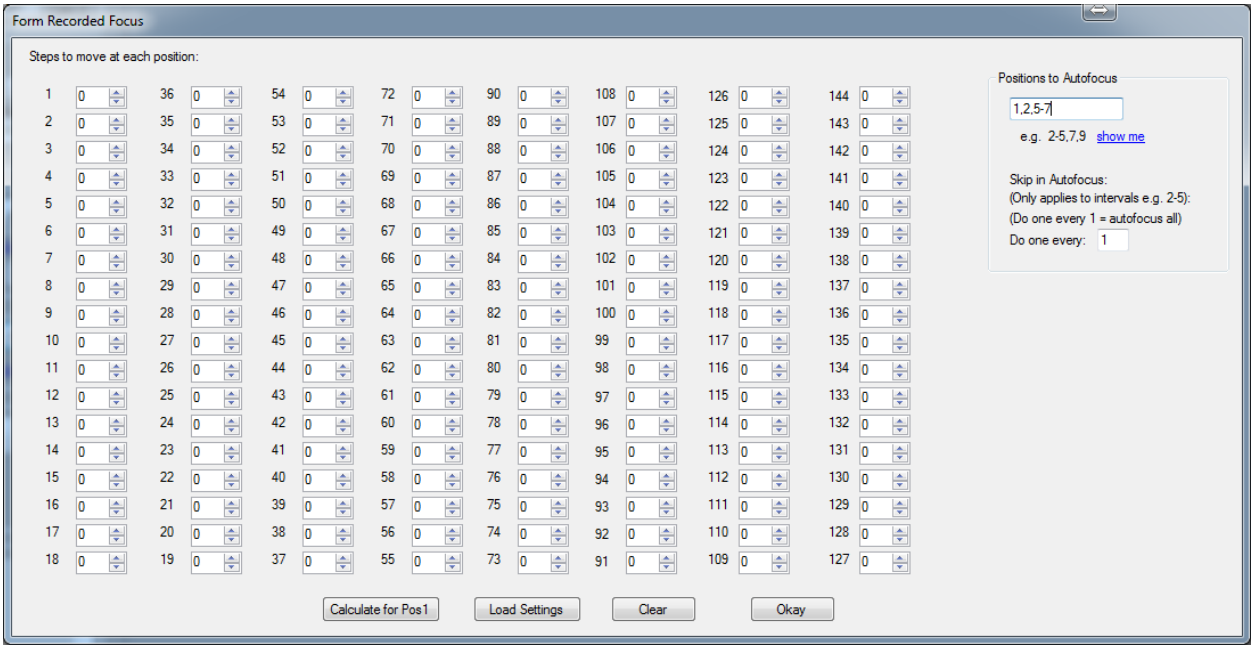

Figure 3.7 This is the form where you can specify the number of steps that the focusing motor should move at each position. The first number represents the position and the number that we can change is the number of steps. When automatic focusing is selected (autofocusing), these numbers will change automatically.

On the bottom of the window, the "Calculate for Pos1" button will calculate how many steps the motor should move when it gets back to position 1: this number should be the negative sum of all the other positions so that the focus returns to its original position after each cycle. The "Clear" button will set

everything to zero in case we want to start over. Finally when we are done we should click on the "Okay" button which will close the window and save all the values. Going back to the subpanel, the "Record now" checkbox is used to help us enter the values of Figure 3.7 semi-automatically. To do this we first focus at position one, then we make sure we have cleared all the values by clicking the "Clear button", then we check the "Record now" checkbox and we focus each position at a time using the up and down arrows of the previous subpanel. At the end, remember to click the "Calculate for Pos1" button. When you are done remember to uncheck "Record now" and to check "Use Values". The "Go to Pos+" link will move the stage to the next position and is the recommended way of going through all the positions in our list. Our list of position should first be specified in the "Positions" subpanel that I will describe soon.

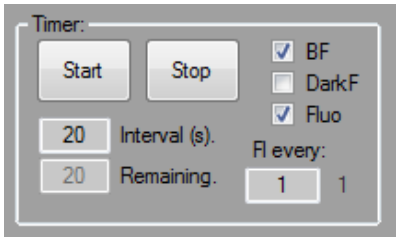

Figure 3.8 Timer subpanel

- The Timer subpanel is where we start or stop an imaging session. In an imaging session, all the positions specified in the list in the positions subpanel (see later) will be imaged indefinitely until we click the stop button. We can specify the time to wait in seconds after the final position has been reached before starting over at position 1. Make sure that this number is at least 10 seconds so that the stage has time to go back to the first position before starting another round. The checkboxes determine which illumination to use (all can be used at the same time). The "Fl every:1" text box specifies whether we want to take a fluorescence image for every brightfield image. If we set it to "Fl every:2" then a fluorescence image will be taken for every two brightfield images. This can be useful when you want to avoid damaging our cells with too much fluorescent excitation light, and it allows us to take a large number of brightfield images when we want to image fast cellular phenomena, while taking fluorescent images at a lower rate.

When we click on the "Start" button a new window will pop up that will ask us to specify more information about the current session (see Figure 3.9).

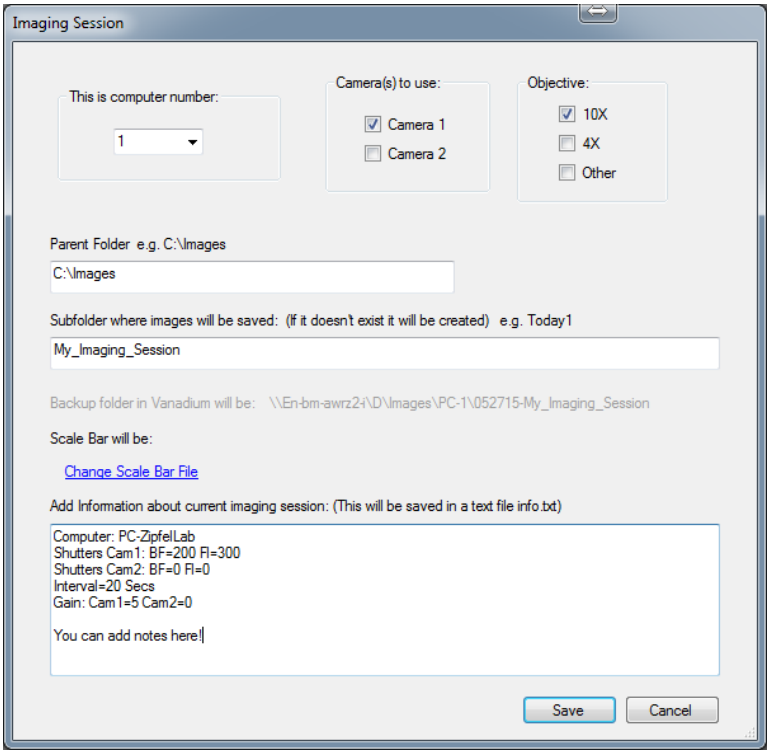

Figure 3.9 The "new imaging session" window lets us add information about the current imaging session, including name of session, cameras to use, and other useful information.

On the top left is the computer number. In the Zipfel Lab we had at least 3 computers and each is identifying with a number. Images obtained in these computers are automatically sent to a central computer called Vanadium. Choosing a number in this window will determine to which folder of the vanadium computer the image will be transferred to. For example, choosing number 1 will save the images to the folder named PC-1 in the Images folder of drive D of the vanadium computer. If you don't understand this don't worry because either way the images will also be saved to the computer that you are using.

Next in this window we can select the cameras to use and the objective type. While selecting the right cameras to use is crucial, select the wrong objective will only result in a different saved note.

The subfolder where images will be saved will be the name of the current session. You should change this for every new session that you start and the program will create the folder when you click save. Note that the program will automatically add the current date to the beginning of the subfolder name.

Finally at the bottom is an area where you can add extra information about your current session. This will be saved to a file named info.txt in your session folder. Note that this area is already populated with information that is added automatically that can be useful to you, such as the shutter for each camera, the interval, the gain, and name of the current computer. Once you click save, the window will close and another will pop up to remind you of whether your images will be transferred to the central computer or not, and giving you the option to cancel starting this session (which can be useful if you realize that you have made a mistake).

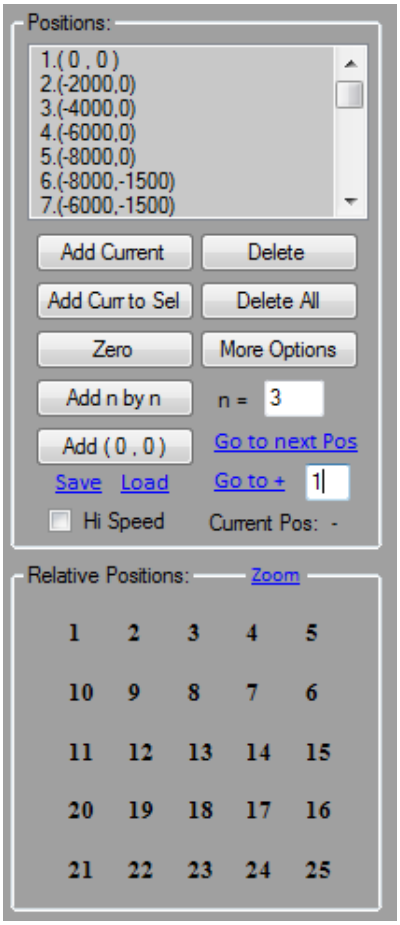

Figure 3.10 Positions subpanel

- The Positions subpanel shows a list of the positions to where the stage will move during each imaging cycle. Double-clicking an item in the list will move the stage to that position. The "Add Current" button will add the position that the stage is currently at to the bottom the list. "Add Current to Sel" will do the same but add it to the position on the list that you have selected instead of at the bottom of the list. "Zero" will set the current position to (0,0). Always make sure that the first position is (0,0). "Add n by n" will add n by n positions forming a square grid. "Save" and "Load" will perform the function for the whole list. The "Hi Speed" checkbox turns the high speed movement of the stage on or off. Note that it will be turned off automatically when you start imaging because high speed can cause unwanted movements in the sample. "Delete" will delete the position in the list that you have selected. At the bottom is a schematic representation of all the positions relative to each other which will dynamically change as positions are added or deleted. When clicking on "Zoom" button the schematic will grow in size which is useful when there are many positions close together in order to tell them apart. Clicking the button "More Options" will

show the second vertical panel that was previously highlighted in green in Figure 3.2 and which I will describe now.

Secondary Functions

- The second vertical panel (which opens when the button "More Options" of the first panel is clicked) contains a number of buttons which are options related to the list of positions that have just been described but they are placed in this panel because they are used less often. "Skip Position", which is used to skip certain position in the list, is useful when we have started an imaging session but we no longer want to image a certain position. This can be better than deleting the position from the list because the numbers will not change and therefore the folders were the images are saved won't change either. "Skip Position" will open a new window that is shown in Figure 3.12. The "Extra Exposure" button also bring up new window and is used to specify a longer exposure to certain positions. This can be useful when investigating the effect that different exposures have on the cells (with longer exposures typically being more detrimental to the cells). The "Extra Exposure" button brings up a new window that is shown in Figure 3.12. The "DC Panel" button brings up a panel to control DC motors. "Delete last…" is useful way of deleting a large number of positions at a time. We can add a custom position to the list of positions using the X and Y textboxes. This is not the preferred way to do add new positions, instead more often we move the stage to a new position either with the joystick or on-screen buttons and then add the position to the list by clicking the "Add Current" button in the left panel. The "Add grid positions here" subpanel is a more advanced way of adding positions forming grids. Not only can you add n by n grids but also add these forming larger grids by

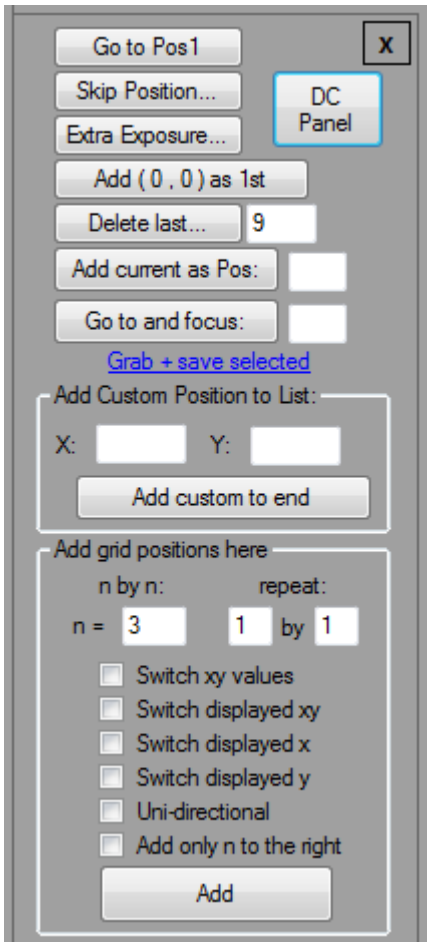

Figure 3.11 The panel that contains more option relating to the list of positions.

repeating them in the x and y directions. The various checkboxes relate to how these grids are displayed and the order in which the positions appear, and the "Add" button finally adds these positions to the list. Notice that the distance between the positions in the grids is specified in the next subpanel in the field-width and field-height textboxes.

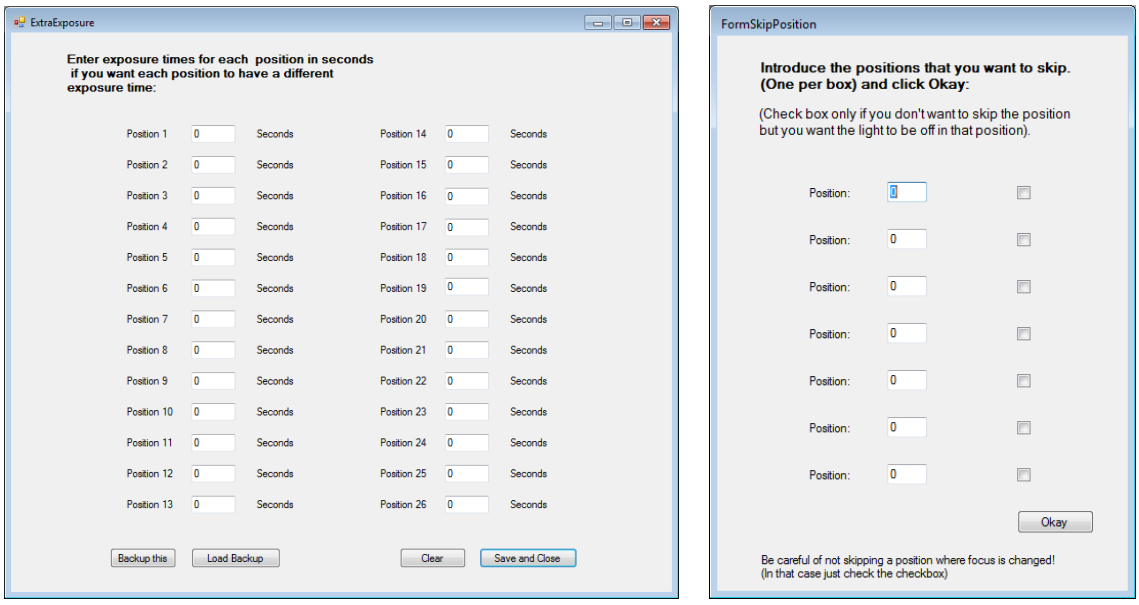

Figure 3.12 Additional forms are available in IncuScope to control the exposure of different positions or to skip certain positions.

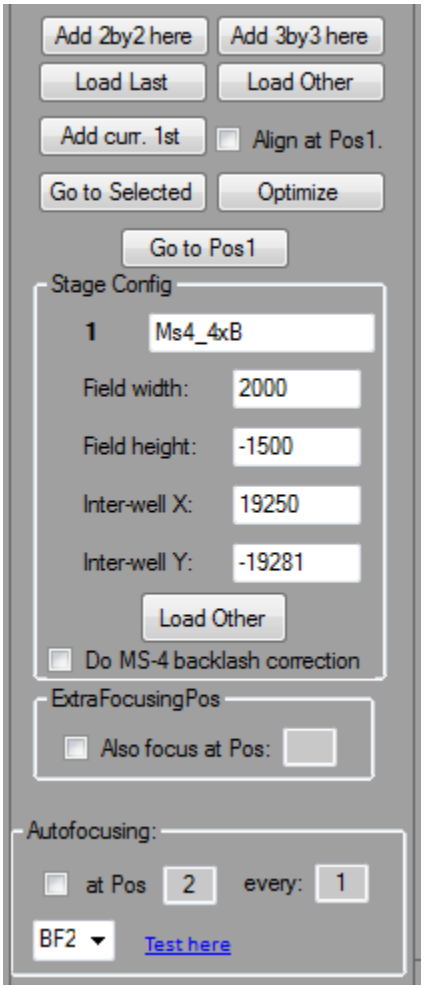

Figure 3.13 Continuation of the panel that contains more option relating to the list of positions.

- The lower section of the "More Options" panel is described here. The 2by2 and 3by3 buttons create grids of positions. "Load Last" and "Load Other" are ways of loading previously used lists of positions. "Align at Pos1" will start an algorithm at Pos 1 where a feature in the screen will be centered, this is used to avoid dish movements and will be described later. "Go to Selected" will move the stage to the currently selected item on the list of positions. A better way of doing this is to double click on a list item. The "Optimize" button will rearrange the positions in the list in such a way as to minimize the distance traveled. For example if position 3 is closer to position 1 than position 2, then position 3 will be swapped with position 2. This reduces the overall distance travelled, it reduces the time, and it reduces possible artifacts caused by excessive movements. In the "Stage Config" subpanel we specify the spacings: "field width" is the width of the field of view. It will also be the distance between positions in the grids mentioned previously. "Inter-well width" is the distance between grids as it was conceived for imaging sessions requiring multiple wells. Note that both Field and Inter-well distances are also used when moving the stage one screen at a time with the arrows found at the bottom of the main screen (described later). "Load other" will load previously inputted distances which is useful when using different kinds of stages. The "Do MS-4 backlash correction" checkbox implements a correction to the motion to counter the backlash that sometimes occurs during the motion of the stage. This backlash will be minimized if the distances between positions is low.

Figure 3.14 Buttons to move the stage

- These buttons located below the image were highlighted in gray in Figure 58 and move the stage one screen at a time with the values that were introduced in the left panel that was described previously. If the "Next well" checkbox is checked the movement will be one well at a time instead of one screen at a time, which makes it easier to move quickly between wells of a multiwell plate, or arbitrary large distances. The distances travelled when the checkbox is checked is the "Inter-well" width and height mentioned earlier while the distances travelled when the checkbox is unchecked is the "field" width and height. The "Switch" checkboxes flips the image horizontally or vertically to adjust to the relative orientation between the stage and the camera. The "k" button I created to be able to operate these buttons with the keyboard.

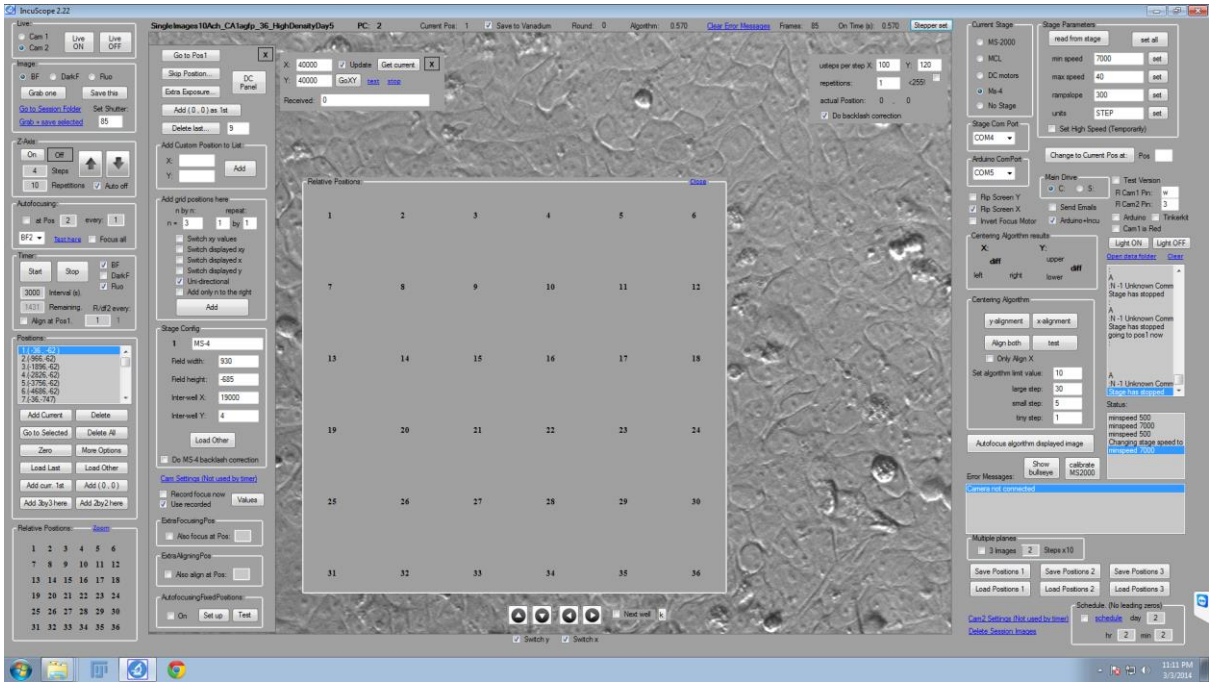

Figure 3.15 Screenshot of IncuScope showing all the panels including, the "zoom" of the diagram of the positions to be imaged.

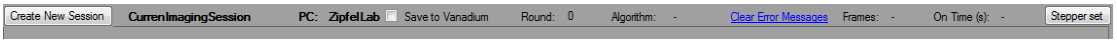

Figure 3.16 The top strip of the main window contains additional information and functions.

The strip found above the main IncuScope window (shown in Figure 3.16 and which was highlighted in yellow in Figure 3.2) has a button named "Create New Session" which performs almost the same function as the "Start" button that we mentioned earlier except that it will not actually start imaging. Therefore you can use this button to set up the current session before starting to image. Next it informs about the name of the current imaging session, followed by the pc name. The checkbox indicates whether the acquired images should be backed up to another computer in the lab via the network. Given that each image is copied and transferred as soon as it has been acquired, it reduces the wait times associated with transferring images at the end, as well as creating a backup of the images. Next is a number indicating the round of imaging (i.e. how many images per position have been taken). Then the values of the focusing algorithm is shown, then an option to clear all the error messages and the number of frames being captured by the camera. The last button serves to set up a stepper motor which is not currently used.

Next I will describe some of the options that are available on the panel that is situated to the right of the screen, which was highlighted in blue in Figure 3.2, and is shown in Figure 3.17. In this panel we can select the type of stage that we are using (Five options are available) although, at the time of writing this thesis, I only use the Ms-4 stage of A.S.I. (Applied Scientific Instrumentation). To the right we can set the parameters for the motion of the stage, with higher values typically indicating lower speeds. Next are the Stage Com Port and the Arduino Com Port. You can find which Com Ports you should use in Window's Device Manger, or you can select one from the drop down list, because only available com ports will be shown. There is an option to change the size of the display to fit smaller screens. There is a checkbox to "Autostart Imaging on Startup". This was originally created so that if the computer crashes and reboots it will automatically restart the imaging session. Also when you close IncuScope a message will pop up giving you the option to turn this feature off. Also note that for this feature to work a link to the program must be

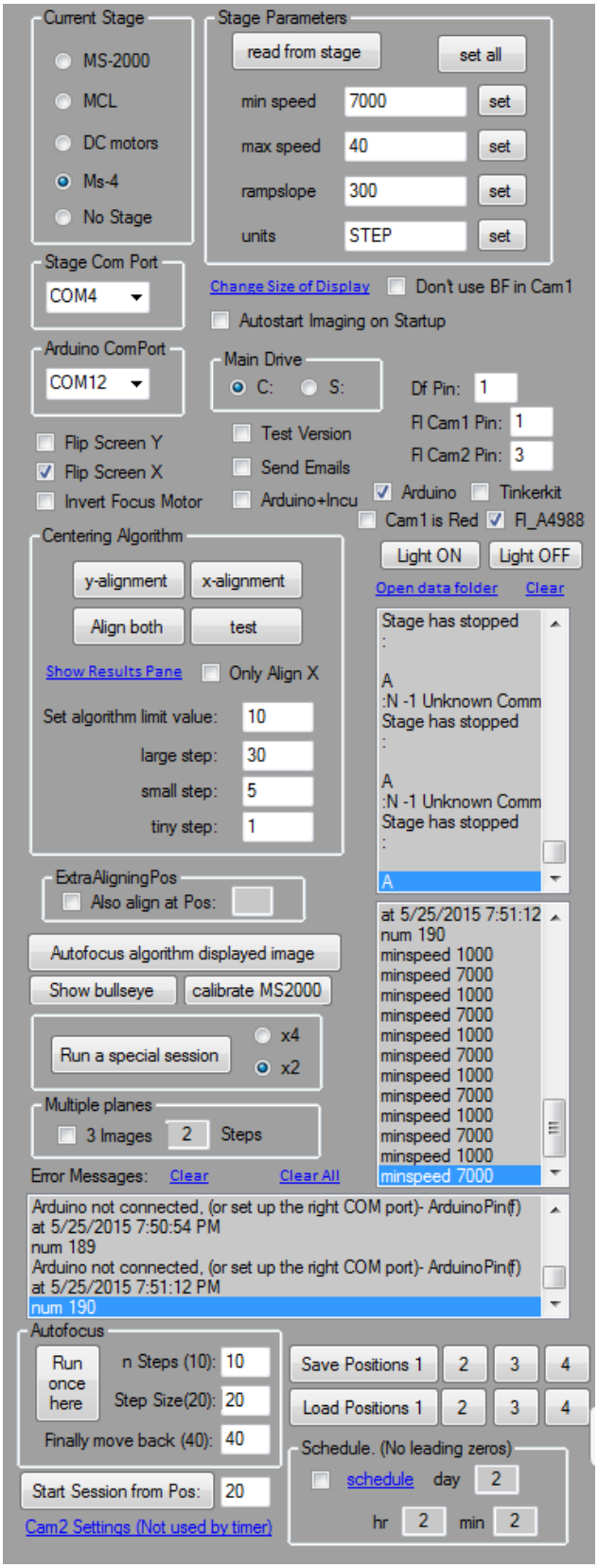

Figure 3.17 Advanced Options panel

placed in the Window's Start Up folder for the program to start automatically on startup. The three Pin textboxes to the right of the panel are important as they determine which pins of the Arduino microcontroller controls which LEDs. Notice that in Figure 3.17 there are two checkboxes that are checked (Arduino and Fl_A4988). Arduino must be checked in order to use the Arduino microcontroller and Fl_A4988 is to use the Arduino motor shield mentioned in a previous section. If we are using our custom board for the LEDs together with the Arduino then instead of Fl_A4988, you should check the Arduino+Incu checkbox. Further down, the results of the centering algorithm mentioned earlier are displayed and we can set up its parameters. Three different list boxes display information on the status of the stage and other algorithms and also display any error messages that may have occurred. The "multiple planes" subpanel takes three images at every position in case we want to take images above and below the focusing plane which is useful when imaging cells in 3D gels. The number indicates how far in motor steps these images should be. Next is the Autofocus subpanel where we can determine the number of steps, step size and final correction for the autofocusing

algorithm. The recommended values are the values displayed in Figure 3.17. Below that is an option to start the session from a position different than the usual position one. There are buttons to save and load the positions that the stage will move to (buttons labeled 1 to 4) and a subpanel to schedule certain tasks such as to stop imaging at a certain time on a certain day.

When IncuScope detects an error it can send an email to alert you. For this to work the "Send email" checkbox should be checked. This can be very important because if there is an error while the illumination is on it could kill the cells. Errors can include things like camera disconnection, low memory, backup errors due to network disconnection, or even incorrect focusing. Next to it is the "Test Version" checkbox which is useful to troubleshoot the software without error boxes popping up.

Algorithms

Autofocusing algorithm

The program can automatically focus at every position that it images. This is important because usually the focus plane will change from position to position and the change is grater for positions that are far apart. Additionally when doing time-lapse imaging, the focus of a single position will almost always change over time. Usually the change over time is more pronounced during the first one or two hours of imaging. Prior to introducing autofocusing as a feature of the program I had to manually adjust the focus at each position once and then the program remembered the place of this best focus and moved to it for each position. However, it is very time consuming when there are many positions that we want to image such as in a multiwell plate. Additionally, to deal with changes in focus that occur over time, all the positions have to be refocused several times over the course of an imaging session. This is impractical and therefore I developed this autofocusing algorithm. The other mechanism is still useful in cases where the autofocusing cannot be used such as imaging 3D cultures of cells. Therefore I have maintained both ways of focusing in the program, which in fact are designed to work together.

With autofocusing the program can do it all on its own. To determine whether the image is in focus an algorithm runs on each image of a series of images at different heights. The algorithm results in a number and the greater the number the better the focus. At each x-y position the program takes ten images at ten different z-positions, five below and five above. It calculated the algorithm for each of those ten images and moves to the image that has the maximum number. If the maximum number is far from the original position (for example at the first or last position), it will run again taking ten images around this new maximum. This way it can find the focus even if the focus is more than ten steps away.

The actual algorithm takes each pixel of the image and finds the difference in value between the pixel and the neighboring pixels (one in the x-direction and one in the y-direction). The sum of the squares of the values of these differences across all the pixels of an image returns the numerical value which determines how well the image is focused.

Because the process of autofocusing can take some time, especially if it is done on every position in a multiwell plate, I have added the option to do the autofocus at specified intervals. This is required when doing for example migration analysis of cells which require relatively fast acquisition of very large number of cells. Figure 3.18 shows the results of the algorithm on 25 images of cells at the same position taken at different heights.

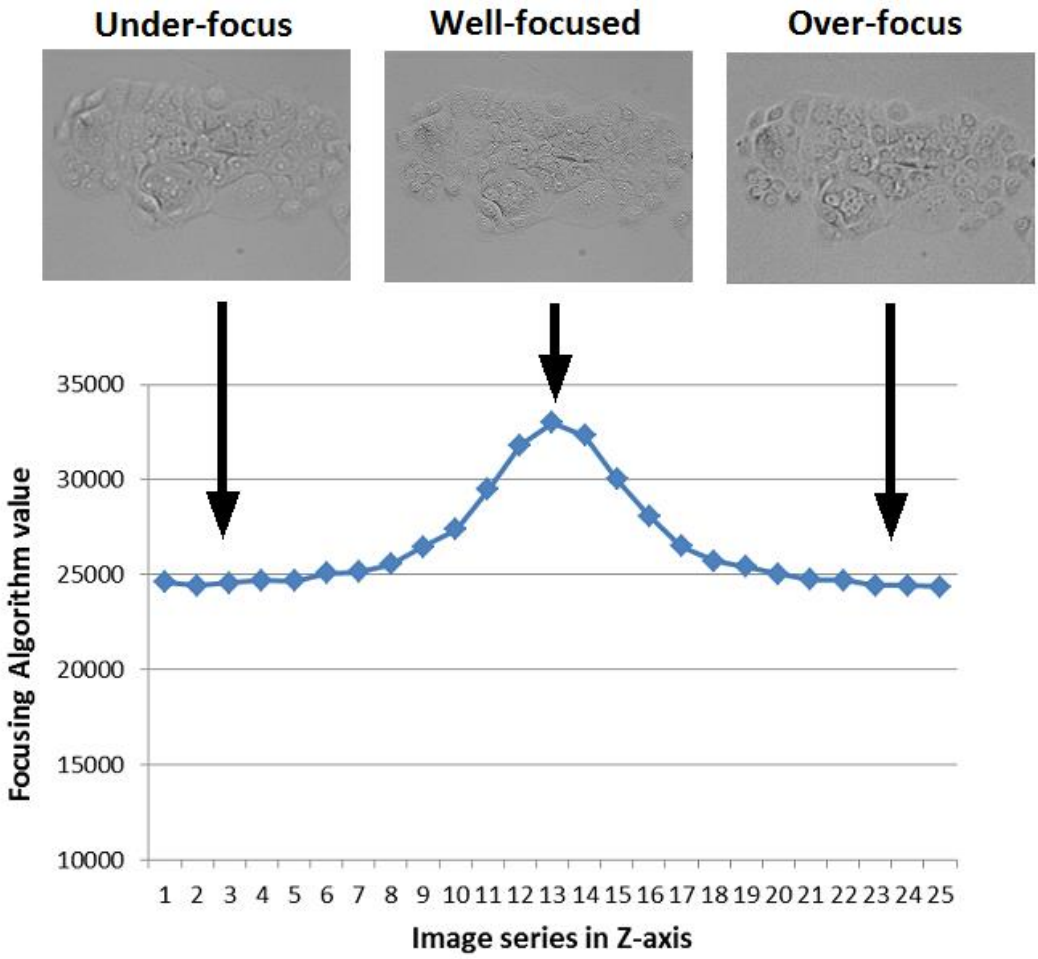

Figure 3.18 A plot of the values obtained from the focusing algorithm on a stack of images showing that the maximum value corresponds to the best focused image.

Algorithm for automatic optical position calibration

Microscope stages may sometimes not show the desired degree of positional accuracy in their X-Y translations. This may be due to several reasons which include the conditions of high humidity and high temperature inside the incubators, to small movements of the sample over time, or it could be just because we are approaching the limits of accuracy of the stage. To fix this kind of issue I have developed a method to automatically calibrate the position of the stage during the imaging session.

This is done by taking images of a predefined feature and moving the stage until the feature is centered on the screen. This feature can be a preexisting engravement on the substrate or a scratch performed with a needle. I employed the darkfield capability of the microscope to get high contrast images of the feature which greatly enhance the sensitivity of the algorithm.

The algorithm works by breaking up the image in two by the middle, comparing the average intensities of the pixels of each half, and then moving the stage accordingly so that the two halves become equal. This effectively centers the feature on the screen. This process is then repeated for centering the feature on the other axis as shown in Figure 3.19.

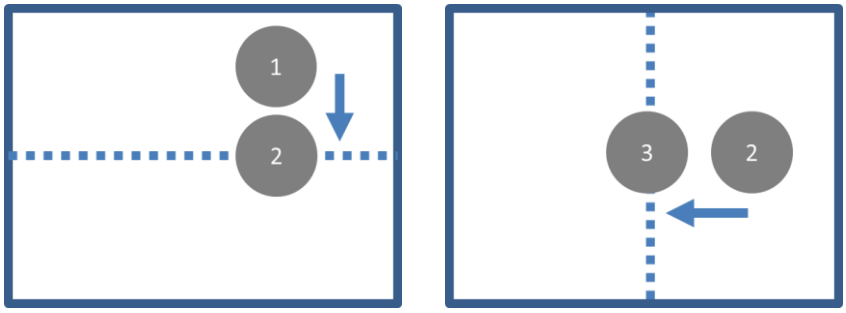

Figure 3.19 Centering of an object is done first vertically (left image) and then horizontally (right image).

The algorithm is designed to work no matter what object or feature we use. If the feature is a scratch on the surface of a plastic dish then the algorithm described above that uses the sum of the intensities of the pixels is what works best because scratches on plastic are extremely bright under darkfield imaging. If, however, we cannot make a scratch because we are not using a plastic substrate (for example when using glass bottom dishes) then we have to use a different kind of feature such as a mark done with a felt tip pen. In this case greater contrast will be achieved with brightfield light instead of darkfield and I have developed a different algorithm for this case. In this case the algorithm works by doing the sum of the gradients instead of the intensities at all the pixels.

An alternative option is to have a fiducial mark on the stage itself. We can do this by manufacturing a hole next to the sample which holds a piece of transparent plastic with some visible features, as illustrated in Figure 3.20.

Figure 3.20 Machining of a support for two dishes with a smaller window for a fiducial mark for repositioning stage movement errors.

While it is advantageous to use the fiducial mark to correct the images during image acquisition, it is also posible to correct them after the images have been taken. For the post-imaging approach I employ programs that I wrote in the ImageJ macro programing language which I will describe next.

Image Analysis Programs Written In The ImageJ Macro Language

ImageJ is one of the most popular image analysis programs in the life sciences. It offers several advantages. It is a free program developed by the National Institute of Health. It is constantly being upgraded and new versions are being released. It is very popular and has a large user base which is active producing and sharing new algorithm for image analysis. Additionally it has a very intuitive macro language which can be very powerful and that I have used to write several programs for image analysis. Some of the programs that I have written and which I will discuss in this section go beyond the macro language and use java code or even code written for windows, which can be embedded within the macro language. Some of these programs will be described now.

Methods for tracking cells

A program for tracking multiple fluorescent cells

The largest program that I have written for the ImageJ macro language is more than a thousand lines of code and serves to track multiple fluorescent cells at the same time and display their tracks on a screen as well as a table containing their speeds, distance travelled, etc.

The main windows and results of tracking are shown in Figure 3.21. Each color represents a different cell.

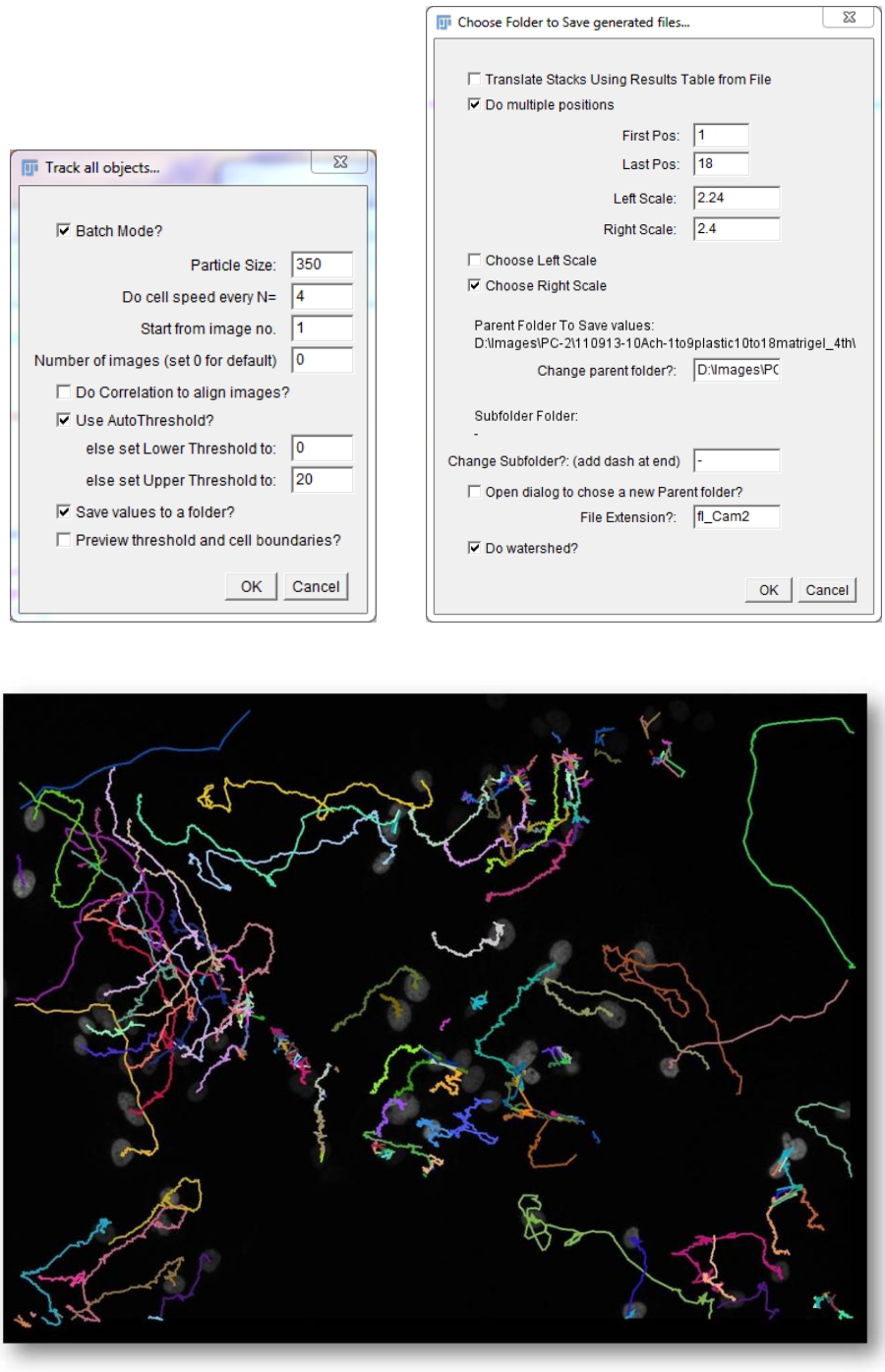

Figure 3.21 The main setting windows and results of a program for tracking multiple fluorescent nuclei of MCF10AT cells, written in the ImageJ macro language.

The progam follows a series of steps. First it does segmentation by automatic thresholding via a triangle method, followed by outlining via the Imagej analyze particles method, followed by a watershed algorithm step. A preview of these three steps is shown to the user before the tracking initiates in order to verify that the selected values are functioning properly. An example of this preview is shown in Figure 3.22.

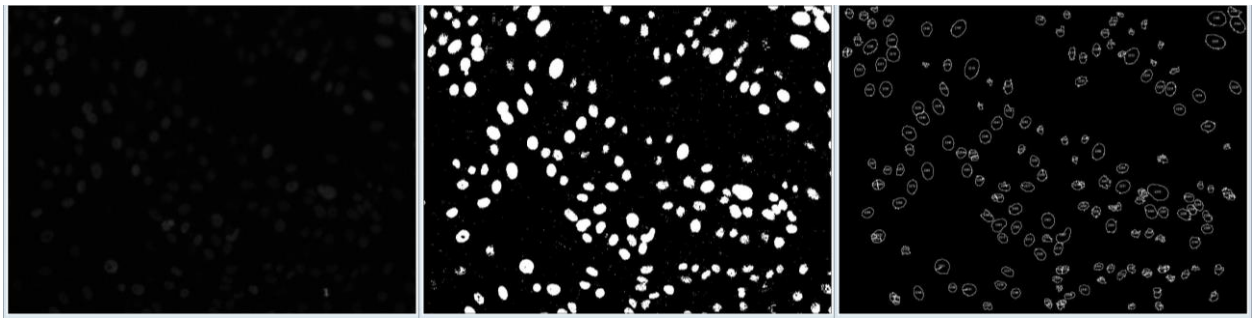

Figure 3.22 The three initial steps of the program that detects the position of cells are thresholding, segmentation and watersheding.

Sometimes cells have varying degrees of fluorescent intensity and this can be a problem to the detection algorithm (see Figure 3.23).

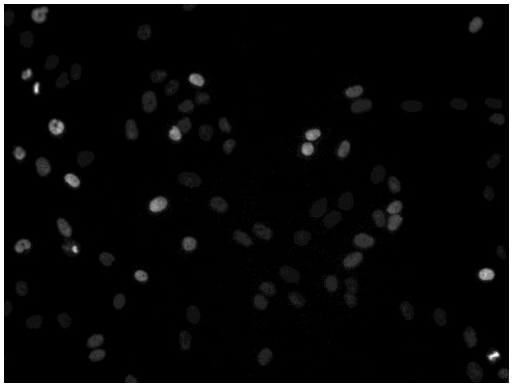

Figure 3.23 An example of different degrees of fluorescent intensity between cells contained within the field of view of a single image which can pose a problem to the detection algorithm.

This can be solved by watershedding (which will be described now), but the order of the steps have to be chosen carefully; Figure 3.24 shows that bright nuclei lead to merging during thresholding which can be solved by watersheding.

Figure 3.24 Original (left), thresholded (middle) and watersheded (right) images of bright. Notice the appearance of a black line separating the two cells on the right as a result of the watershed algorithm.

However, with dim nuclei, inhomogeneities show up when thresholding that lead to problems when applying the watershed algorithm.

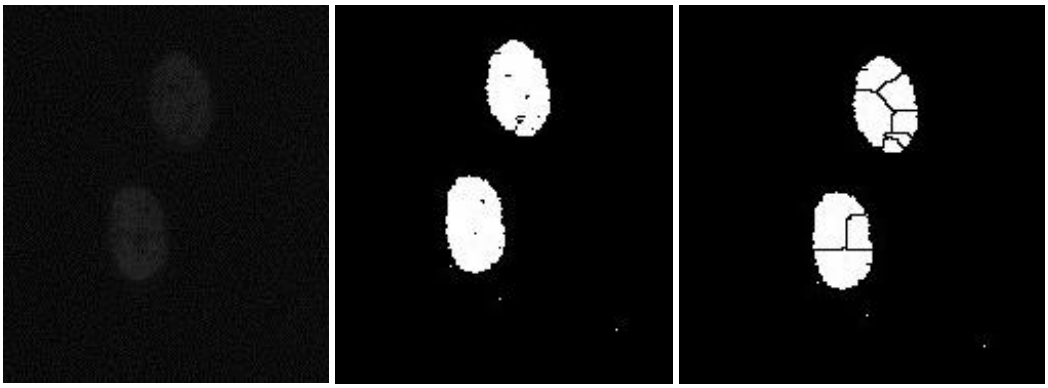

Figure 3.25 Original (left), thresholded (middle) and watersheded (right) images of dim cells.

This can be corrected by removing the inhomogeneities using ImageJ functions prior to the watershed function. More specifically by doing an additional "analyze particles" step just prior to watershed, as well as after it. Figure 3.26 shows that this method solves the problem presented in the previous figure.

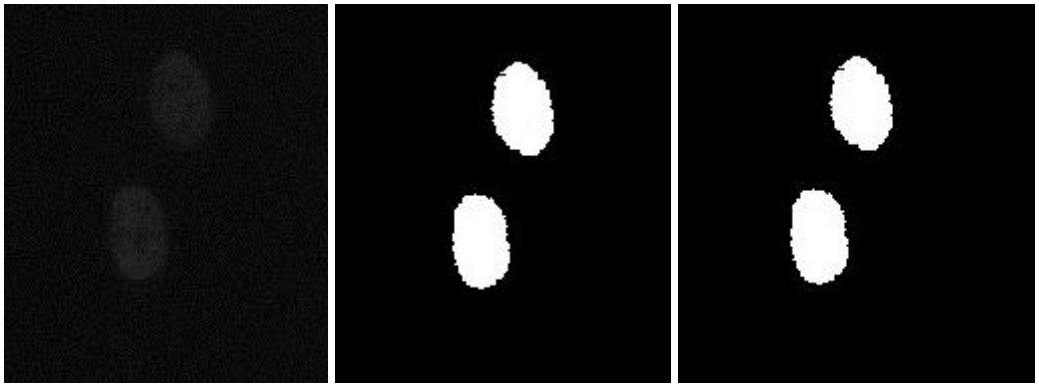

Figure 3.26 Original (left), thresholded (middle) and watersheded (right) with dim images of cells.

Dim cells can pose another problem: sometimes when the algorithm loses track of a cell, this loss will be detected by the program because there will be a jump in the position of the cell and so the program knows that this track should be stopped. Other times, however, a dim cell can lie just at the point where it comes quickly in and out of the detection threshold, making the program think that it is a new cell each time, as illustrated in Figure 3.27.

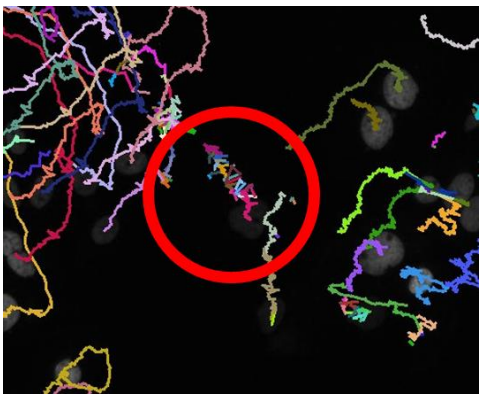

Figure 3.27 Aberrant tracking of a dim cell.

This can lead to aberrant values not only in the number of cells detected but also in the speed of this particular cell. The problem is mostly due to the fact that part of the cell will pass the threshold while part of it will not. To correct this problem I take longer intervals between coordinates while still tracking the cells at the lowest interval. In other words, I take images every 8 minutes and do tracking every 8 minutes

but I only take the coordinates every 24 minutes. This filters out location problems. Additionally this will also dampen stage vibrations that occur every time the stage moves.

However, stage vibrations are sometimes still present, and could lead to aberrant measurements of cell speeds. An example of stage vibration is shown Figure 3.28.

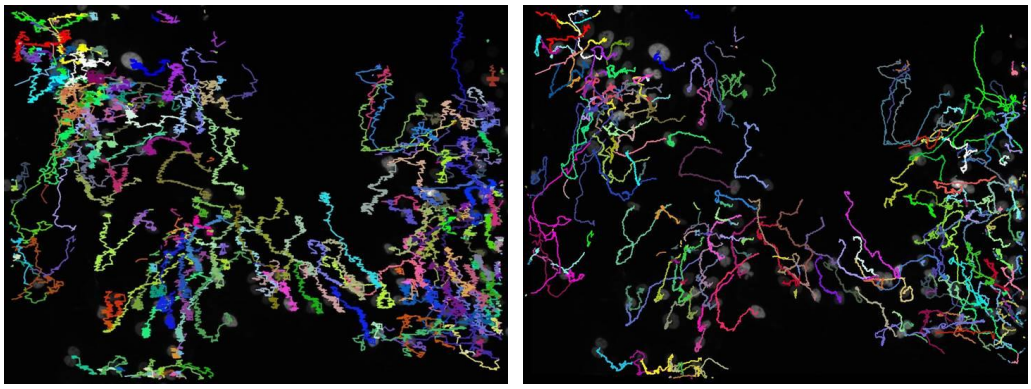

Figure 3.28 Vibrations show up on cell tracking (left image) but not after corrections are applied (right image).

The program has a built-in mechanism to deal with this vibration: It calculates the average vector displacement of all the cells at each time point and subtracts it to each cell. This helps to correct the problem. There are also other methods to correct vibrations post-acquisition that I will describe later.

Once the program is done with segmentation, locating cells and watershed, the actual tracking of the cells as shown in the previous figures can begin. The center of gravity of each cell is calculated and stored in memory. These coordinates are then compared to the coordinates of all the cells in the next image which should be about 8 or less minutes later. It calculates the distance to all those position and the shortest distance is assumed to be the new position of the cell. This new location is saved and a line is drawn between the two locations, keeping the color of the line consistent. This method works very well.

Other issues arise when tracking cells, for example, what to do when a cell exits the field of view. The algorithm will think that the cell moved quickly to the position of a different cell. This can be corrected after the tracking is finished by looking for two tracked positions that share the same coordinates, and

deleting one of them. This is done automatically. However, fast cells have a higher chance of leaving the field of view and thus not being tracked. This could result in biased results because we wouldn't be counting the fastest cells which are the ones that leave the image. The solution is to not just track the cells that were present on the image at the beginning of the imaging session but to also track cells that move into the field of view during the imaging session. If a cell appears at a new location where there were no cells previously (within a certain radius) the program assumes that it is a new cell and will start tracking its trajectory with a new color.

To simplify the use of the program I programed it so that most of the time there is only one parameter that is variable, and that is the lower limit of particle size. This value should be changed to match different cell types or different objective magnifications.

The program creates a lot of data that can be analyzed in different ways. Just one example is the distribution of cell speeds over time, shown in Figure 3.29.

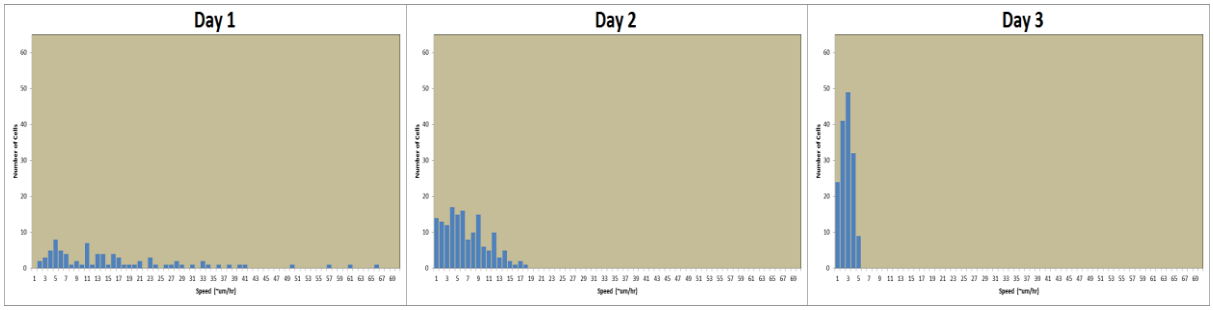

Figure 3.29 Distribution of cell speeds over time showing that cells decrease in speed over the first days in culture.

An alternative version of the tracking program is available for tracking single cells. Single cell tracking is sometimes the method of choice for non-fluorescent cells because in such cases it is not possible to localize all the cells automatically. The user just has to click on the cell that he/she wants to track and the program will do the rest. An example of this kind of tracking is shown in Figure 3.30 where a single cell that is not fluorescent is tracked and the green line shows the trajectory over time.

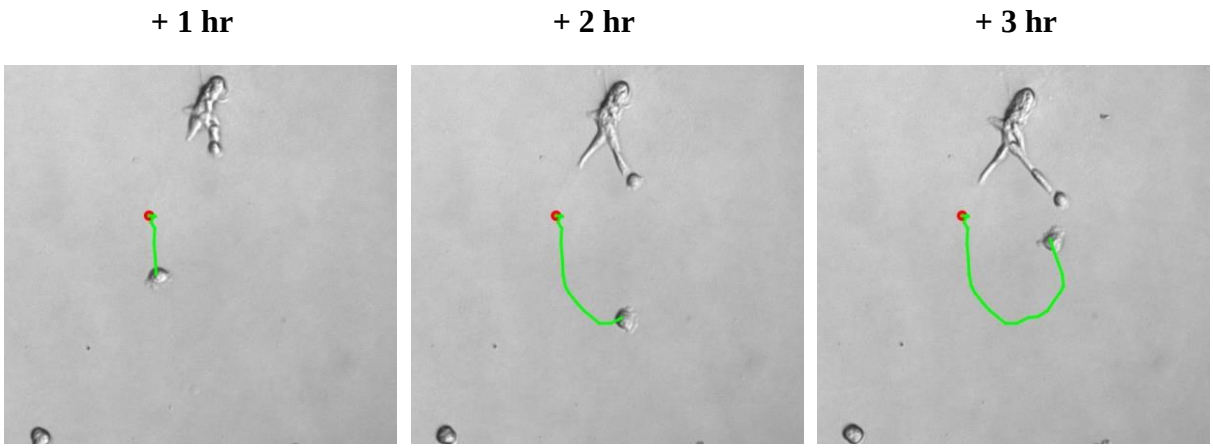

Figure 3.30 Three time point in a single cell tracking for non-fluorescent cells. The red circle is the initial position of the cell and the green line is the trajectory of the cell.

A program for semi-automatic tracking of non-fluorescent cells

Often, in the absence of fluorescent nuclei, the computer cannot tell how many cells there are in a group of cells. This limits the tracking options to single isolated cells because we can't identify cells within a group of cells. Moreover, single isolated cells don't last long especially in the case of cancer cells because they quickly divide and form pairs. Pairs of cells seldom dissociate from each other and often will move around as a pair or at least closely associated to each other. All of this makes fully automated tracking of non-fluorescent cells very difficult in cases requiring extended periods of time or involving high densities of cells. An alternative is to track each cell manually or in a semi-automated fashion. For this purpose I developed a program where the user only has to hover the mouse over the cell as the cell moves, and the data about the position and speed of the cell will be automatically recorded. Thus the user can obtain a lot of information without even having to click. Additionally, the user also has the option to click at specified intervals and obtain only those data points if desired. Alternatively a click of the mouse can indicate a cell division. Figure 3.31 shows an example where cells are tracked by this method and then the total relative movement of each cell is calculated and displayed in green lines in a new window.

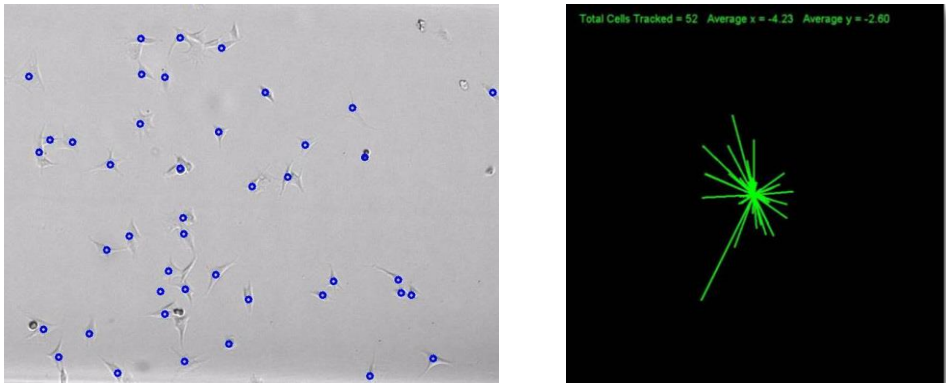

Figure 3.31 Blue circles indicate cells that have been tracked and whose total relative movement is shown on the right image as straight green lines.

This program was used to measure the migration of cells towards chemotactic agents and will be discussed later.

Performance of tracking algorithm on inaccurate stages

It is worth noting that when stage movement is not completely accurate it can lead to vibrations that can be interpreted as cell movements by the cell tracking algorithm. Fluorescent cells were fixed with ethanol so that they don't move and tracked to see whether we obtain a value of cell speed close to zero. In general there is more vibration the more the stage moves so movement of the stage was kept to just two wells of a 48 well plate. The stage used in this test is MS-2000, and the result is a 3.5 um per hour error in the movement detected. Therefore this stage was replace with a different one.

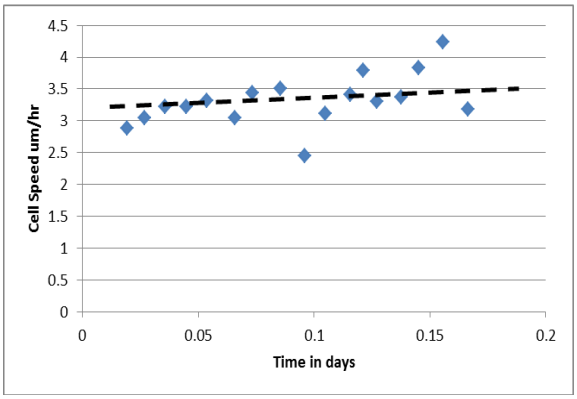

Figure 3.32 Fixing cells with ethanol is a good way to test if the stage is working well enough for the cell tracking algorithms. The chart corresponds to a poorly performing MS-2000 stage which shows residual cell movements when there should be none.

Methods for correction of vibrations via image alignments

The most common problem that I have faced when analyzing time-lapse images of cells is that the images are often not aligned with each other. There is a small random translation of each image which is often due to inaccuracies in the motion of the stage and which often is bigger with the distance travelled and it is the reason why I often choose to move the stage only for short distances. All of the stages that I have used (at least 7 different stages from different brands) display some sort of inaccuracy in their movement especially when placed inside an incubator. These misalignments often appear as vibrations in the acquired movies. However, even if the stage doesn't move at all, the images also can become misaligned at times. For example, the shelves inside an incubator are often not rigid and can vibrate when someone closes the door of the incubator, or even when the stage moves to a new position, which leads to misalignment of the images taken by the camera. Another example is when the dish or plate is not tightly secured to the stage. This is especially common with small dishes which can move over time. Finally on some occasions when we want to add new medium to the dish the dish might become misaligned even if we perform this operation inside of the incubator. Some of the methods that I developed to deal with these misalignments are computer vision object detection algorithms written in both the Microsoft .NET framework (described previously) and in the ImageJ macro language. The ImageJ methods are applied after

the images have been acquired, while the .NET methods are applied during the image acquisition. The ImageJ methods are based on either object recognition and tracking to re-align the images, or image alignments via Fourier transforms; whereas the .NET method made use of darkfield light in combination with immobile features of the plate. Additionally a method was embedded within my cell-tracking algorithm to deal with misalignments by subtracting the average vector translation of all the cells from each individual cell that is being tracked. This has been used in all the cell tracking that I have done and although it can deal with misalignment to some extent it is often not enough. I will now describe the two post-acquisition ImageJ based programs.

A program for post-acquisition stage motion correction

In cases where we want to track cell movements accurately, it is important to correct aberrant motions of the stage which might still be present after the images have been taken. The post-acquisition stage motion correction program creates a graph by tracking an immobile object using tracking algorithms previously discussed and then uses the values generated by this graph to translate the images in such a way as to correct the errors (Figure 3.33).

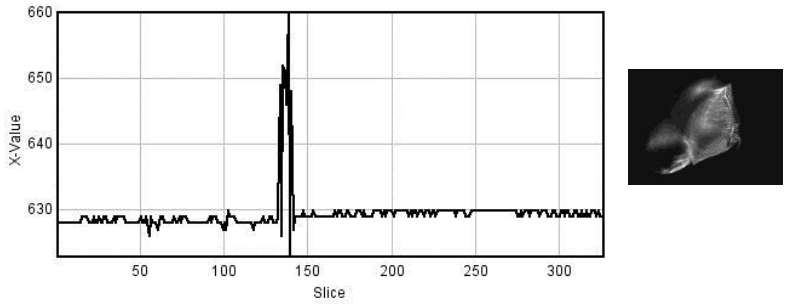

Figure 3.33 The graph shows post-acquisition tracking of the object shown on the right which is a needle puncture. The graph shows that at image number 140 of the graph, the object has suddenly moved, indicating that something caused an unexpected movement.

Even if we don't have any fiducial mark, it is possible to track immobile objects that are often present such as dead cells and use them to correct a drifting stage or a drifting dish. An example of such a situation is illustrated in Figure 3.34.

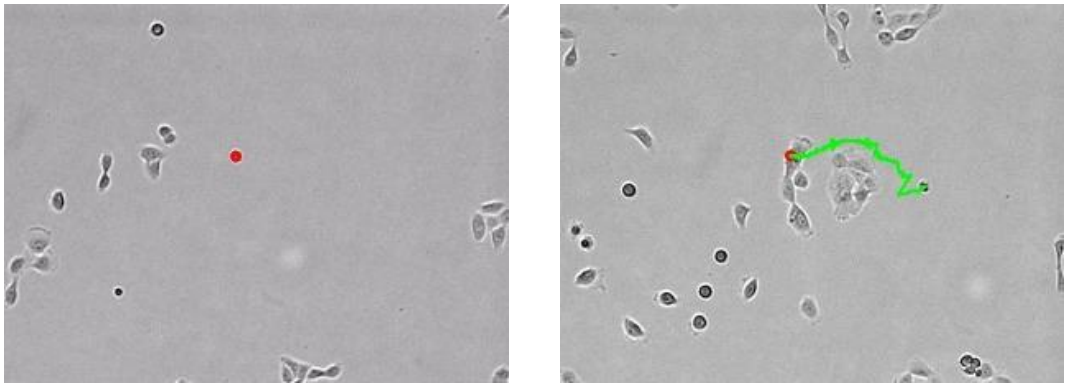

Figure 3.34 An object marked with a red circle (left) is tracked over time and the trajectory is shown in green (right).

A disadvantage of this approach is that to correct the drift we have to do image translations which will progressively reduce the size of the image. Careful programming of the algorithm can reduce this effect.

A program for stage motion correction by image alignment via Fourier transforms

An alternative way to deal with misalignments is to do post-acquisition image correlations via Fourier transforms (except when the misalignment is greater than the field of view, in which case live alignment is required). ImageJ has a function to do correlations but we still are required to write up to 60 lines of code in order to perform correlation on a stack of images and to do other tasks required for the algorithm to work. After doing the correlation we have to find the coordinates of the maximum values returned by the correlation and use them translate the images. This should align the images. An example of this code working in a real situation is shown in Figure 3.35 where a drift in the image has been fixed by applying image correlations via Fourier transforms. (The colored lines were obtained by cell tracking).

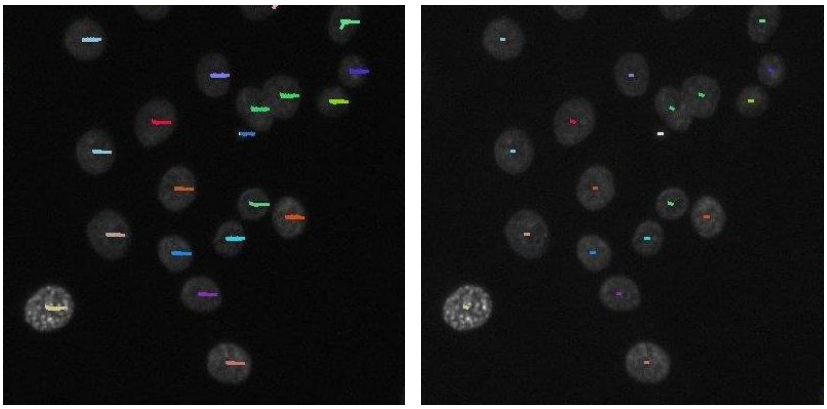

Figure 3.35 Image translation before (left) and after (right) image alignment with Fourier transform correlation. The colored lines indicate that there was a translation before we applied the algorithm which has been fixed.

Figure 3.36 shows a snapshot of the ImageJ macro code editing window (found in the FIJI version of ImageJ) which you can use to edit these programs.

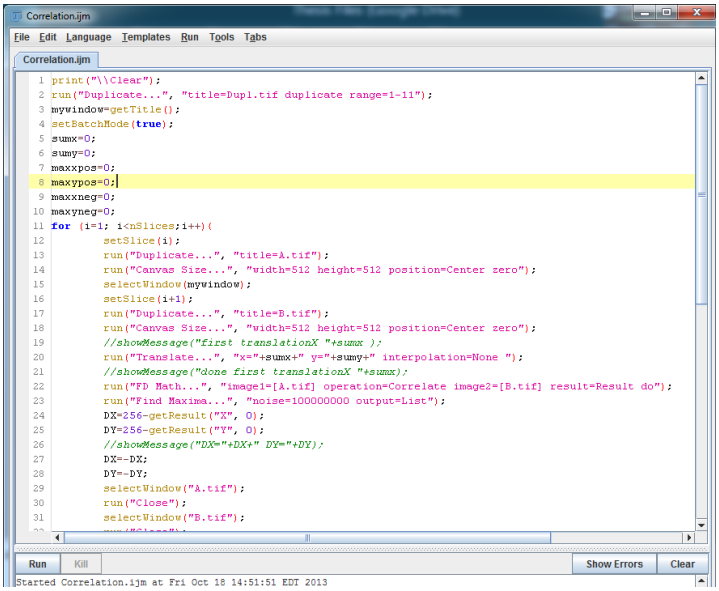

Figure 3.36 A snapshot of the ImageJ macro language showing Fourier transform code.

Other programs for image analysis

A program for detection of errors in the image acquisition or network transmission

If we are interested in cell speeds it is important that no image has been skipped during acquisition or saving. Image skipping can happen due to an error in the saving of the captured image or, more often, due to an error in the transmission of the image via the network (for example the receiving computer might have been restarted by someone or by software update). When dealing with large numbers of images as in time-lapse imaging, it is very useful to have a program that will look at all the hundreds of images and tell you whether there has been an image skipped. This program does that by looking at the intervals of time between images and displaying the results in a graph which makes it easy to see where there has been a skipped image. Figure 3.37 shows an example of the graph that is produced by the program which shows that there was an image skipped at image number 80.

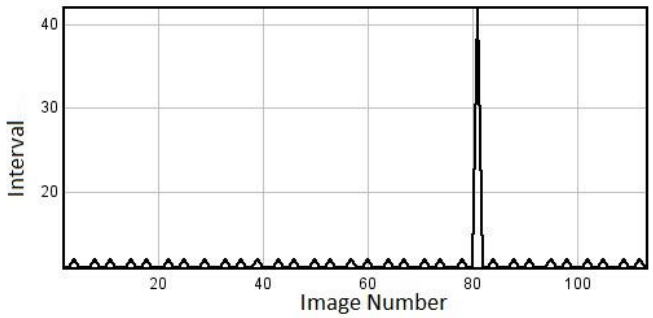

Figure 3.37 The graph indicates that there has been an image skipped at image number 80, such skipped images could pose problems in image analysis.

A program for detection of pulsations in cardiomyocytes

This program can detect the pulsations of cardiomyocytes in culture by looking at the values of the intensities in a given area, and the results can be displayed in a graph. When the cells contract the intensity values comes down, and when they relax the intensity increases, resulting in an accurate representation of the beating patterns. Figure 3.38 shows the cardiomyocytes in culture and a graph showing the pulsations as oscillations that occur over time.

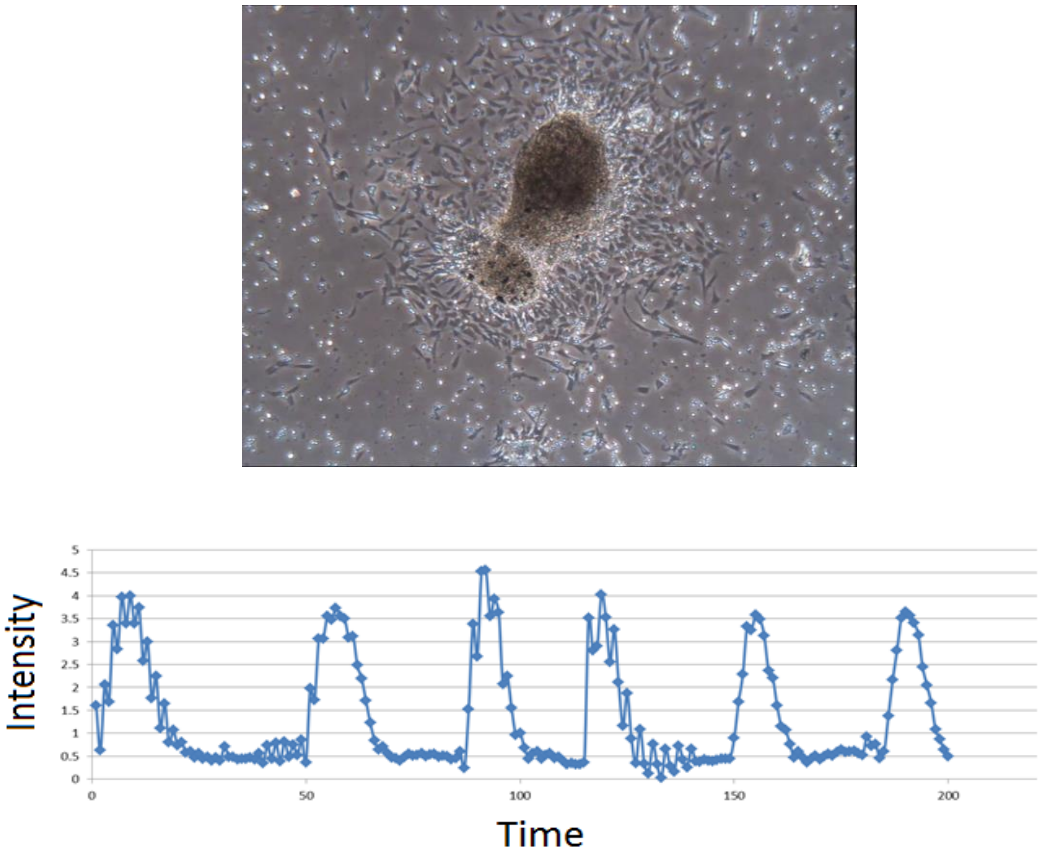

Figure 3.38 Cardiomyocytes in culture (top) and a graph that shows the intensity of the pulsations of the cells as a function of time (bottom).

Other programs

Other programs that I wrote for ImageJ include: A program for automatic montage of the images from different positions of an imaging session; A drag and drop feature to directly import imaging session folders to ImageJ; A program to merge the different colors of an imaging session; A program for counting cells automatically or manually; A program to transfer data to displayed trajectories; A program to automatically add lapsed time to images of a given session, and others. In some cases I enhanced the ImageJ program by adding plugins. For example, to retain the image names when merging colors. The plugins can then be called inside other macro functions. Figure 3.39 shows some of the graphical user interfaces for some of these programs.

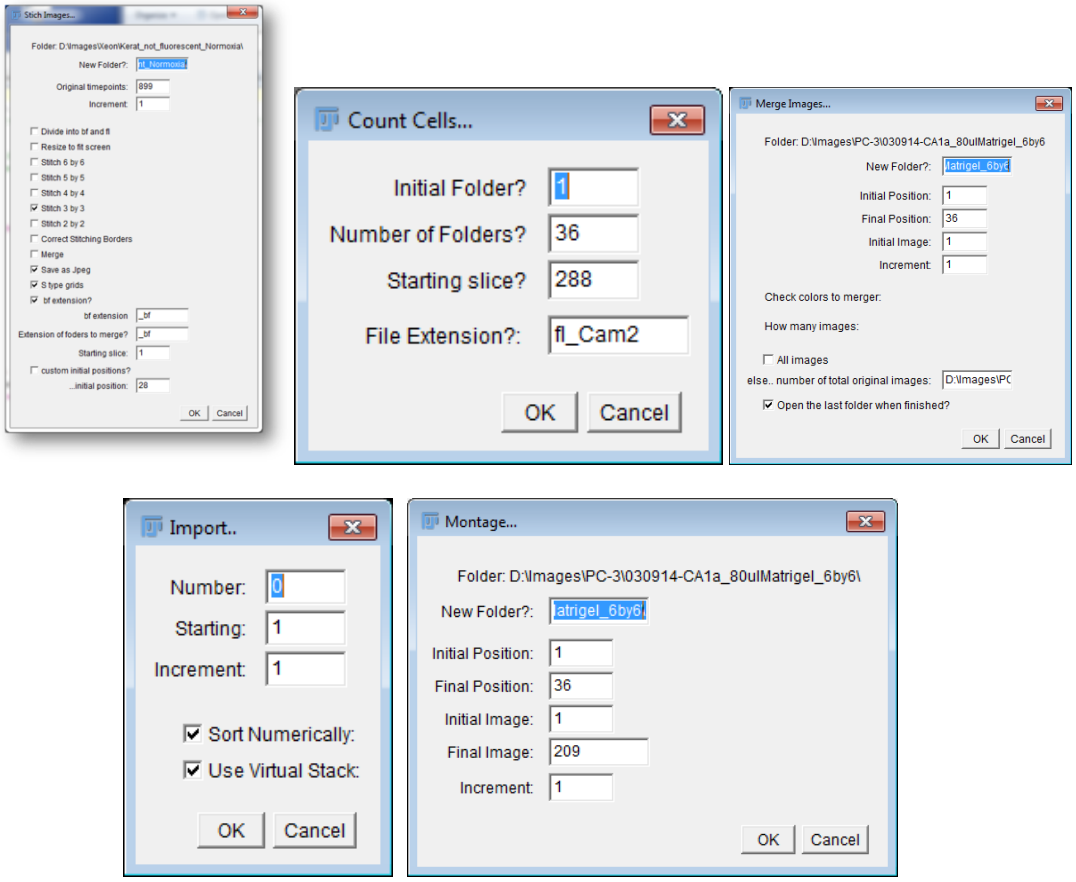

Figure 3.39 Some examples of other programs written for image analysis in ImageJ that I use frequently.

If, for example, we have obtained images arranged in a grid to cover a certain area of a dish, we can create a montage of these images so that we see the whole area in one larger single image. This technique I have used almost always in my biological studies as you will see in the next chapter of this thesis. It allows me to see very quickly what is happening in a large area of the dish. To create montages for imaging sessions that lasts days requires a lot of computation but that's why I created the programs in order to simplify the process.

CHAPTER 4: IN VITRO LONG TERM IMAGING STUDIES OF THE MCF CELL PROGRESSION MODEL OF CANCER

Abstract

Time-lapse analysis details how features unique to the MCF10CA1a cells, such as large nuclei, evolve over time. Tracing these large nuclei back in time reveals how they originate from mitotic errors. A progeny analysis reveals differences between cancer cells (MCF10CA1a) and normal cells (MCF1010A). A method is presented to quantify the absence of contact inhibition in the growth of the CA1a cells. Coculture studies show that CA1a cells affect the morphology of nearby 10A cells. When grown in Matrigel, acini formed by CA1a cells show outgrowths that invade into the surrounding space. Three processes that promote these invasions are identified: medium renewal, serum starvation, and exposure to epidermal growth factor. Finally, in cocultures, CA1a cells are found to be the leader cells of the invasive strands.

Introduction

The main focus of my studies has been the MCF10 cell progression model of cancer, which is composed of three cell lines: MCF10A, MCF10AT and MCF10CA1a (which I will refer to as 10A, 10AT and CA1a respectively). The 10AT cell line derives from the 10A cell line, and the CA1a cell line derives from the 10AT cell line. Given that they all originate from the same cell line, they share a common genetic background which is an advantage in the study of cancer progression. The malignancy or tumorigenicity of these cell lines increases as shown in **Figure 4.1**.

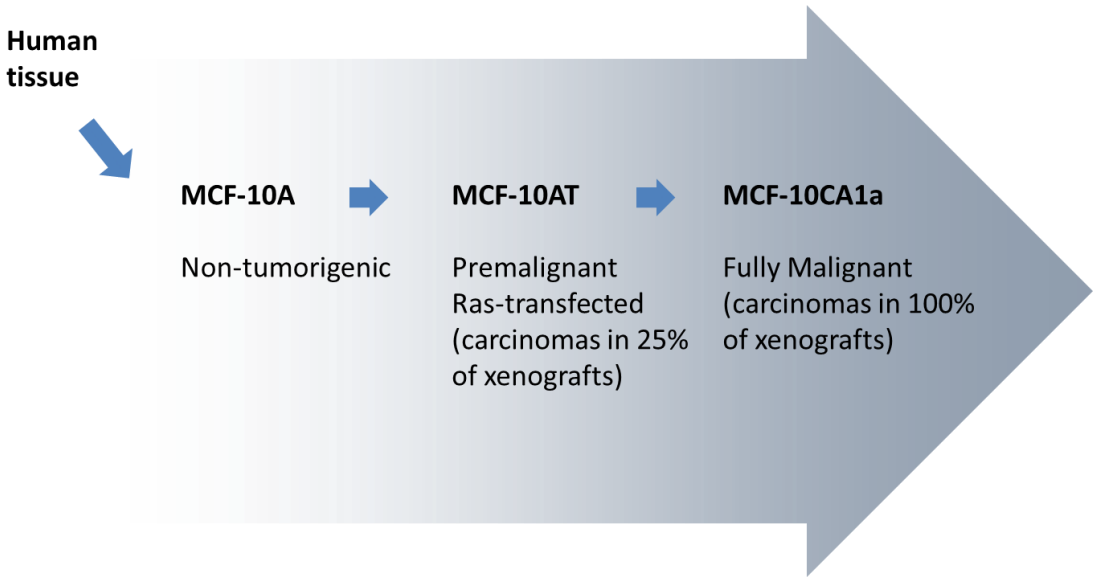

Figure 4.1. Diagram of the MCF10 cell human breast epithelial model system which represents a spectrum of cancer progression from non-tumorigenic breast epithelial cells (MCF10A cells) to malignant cells capable of metastasis (MCF10CA1a cells).

The MCF10A cell line is an immortalized, but non-tumorigenic, epithelial cell derived from human fibrocystic mammary tissue. More precisely, the MCF10A cell line derives from MCF10 cells that spontaneously became immortalized.[8] It is widely used as an example of a "normal" non-malignant cell line and is mentioned in over 700 PubMed articles. MCF10A cells are not considered tumorigenic because they do not form tumors in nude mice.[8] They are near-diploid, and have a stable karyotype.[8,9] They lack anchorage-independent growth and their growth in culture is controlled by hormones and growth factors.[8] Additionally when grown in a reconstituted basement membrane they form acini-like spheroids that recapitulate several aspects of in vivo tissue architecture.[10]

The MCF10AT cell line was created by transfecting MCF10A cells with the T24 c-Ha-ras oncogene, which is a constitutively active Ras variant that has a single base mutation. When injected subcutaneously into nude mice MCF10AT cells progress to invasive carcinomas 25% of the time.[11] Ras is important in human cancers: according to one study about half of human breast tumors have a 2 to 6 fold increase in Ras expression.[12]

The MCF10CA1a cell line was derived from MCF10AT tumors which were sequentially xenografted into nude/beige mice until they developed into a highly aggressive phenotype. Subcutaneously injected MCF10CA1a cells form tumors 100% of the time and the tumors grow more rapidly than when the MCF10AT cells are injected.[13] Upon intravenous injection in SCID/beige mice, the cells formed numerous metastasis in all mice. MCF10CA1a tumors are typically described as poorly differentiated and aggressive. The cell line has more chromosomal instability than the parental cell lines. They have some chromosomal modifications with respect to MCF10A cells, including extra copies of the long arm of chromosome 1, the chromosomal region that is most often duplicated in human breast cancers. With respect to the previous cells from which they were derived, there are differences in morphology in culture, karyotype, and typically display anchorage-independent growth.[13] A microarray analysis of the expression of 42,000 genes revealed about 3000 genes that were over two-fold up regulated in MCFCA1a cells compared to MCF10A cells, with an approximately equal number down regulated.[14] Additionally, spectral karyotyping of these cell lines revealed a number of translocations, deletions and duplications in the chromosomes, but, interestingly, these did not correlate with the gene expression changes observed in the microarray indicating that epigenetic factors probably played a more important role in these differences.[14] Morphological differences between these three cell lines were first observed by Imbalzano et al.[15] They showed that all three cell lines form epithelial layers when cultured in a petri dish, but MCF10CA1a cells contain some very large and vacuolated cells that are not seen on the other cell lines (**Figure 4.2**).

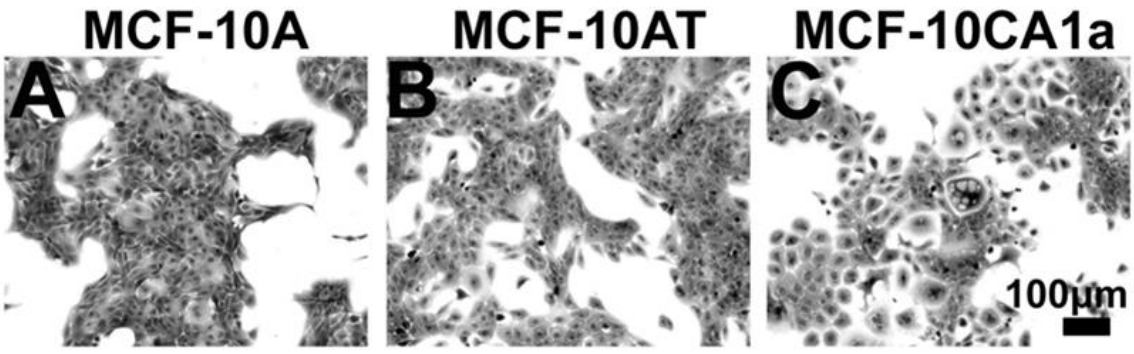

Figure 4.2. Images of the three MCF10 cell lines. Large cells are only present in the CA1a cell line. Taken from Imbalzano et al.[15].

Imbalzano et al. also showed that when cultured in Matrigel (a three-dimensional basement membrane culture) MCF10A cells and MCF10AT cells form acinar structures and exhibit growth arrest (MCF10AT cells does so later). On the other hand MCF10CA1a cells do not exhibit growth arrest, and form irregular overgrown structures that do not resemble the regular spherical acini found in the less aggressive MCF cell lines (as shown in **Figure 4.3**).

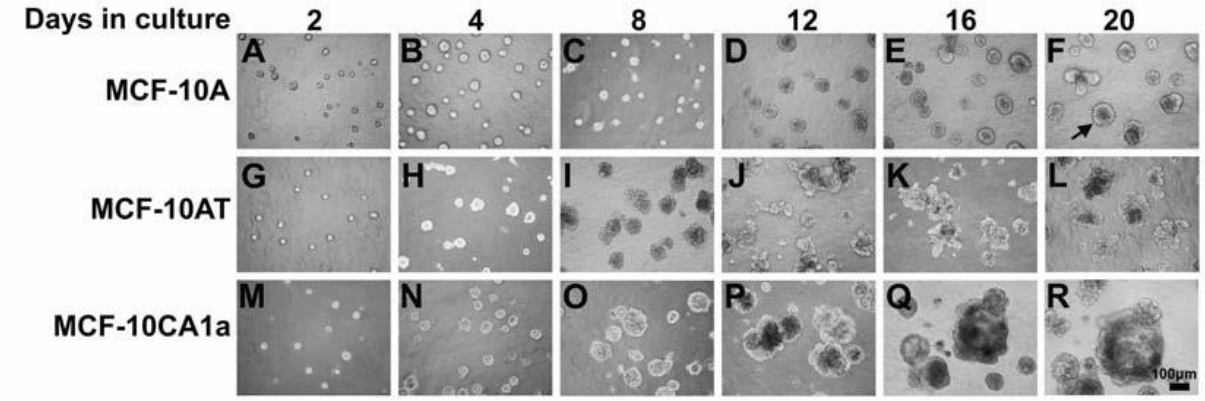

Figure 4.3. Images of the three MCF10 cell lines when cultured on Matrigel. After 20 days in culture the MCF10CA1a cells continue growing while the other cell lines maintain smaller acinar structures. (From Imbalzano et al.[15]).

The images in **Figure 4.3** where obtained by plating the cells on top of a thick layer of Matrigel and then adding Matrigel to the solution. Interestingly, when they did not add Matrigel to the solution, the MCF10AT cells and MCF10CA1a cells produced interconnected branches between the acinar structures, whereas MCF10A cells did not.[15] This difference attracted my attention and I decided to look more closely at this phenomenon using time-lapse imaging because Imbalzano et al. did not perform continuous time-lapse imaging experiments which would provide insight into how the characteristics of these cells develop.

Results

Cellular features characteristic of MCF10CA1a cells.

The images from Imbalzano et al. show that there is one main morphological difference between the CA1a cells and the other cells types: the CA1a cultures contain some cells that are enlarged. Using the incubator microscope described in Chapter 2, I carried out a series of experiments to more closely examine the differences between CA1a cells within the same culture. **Figure 4.4** shows CA1a cells under brightfield light as well as the fluorescence originating from their nuclei.

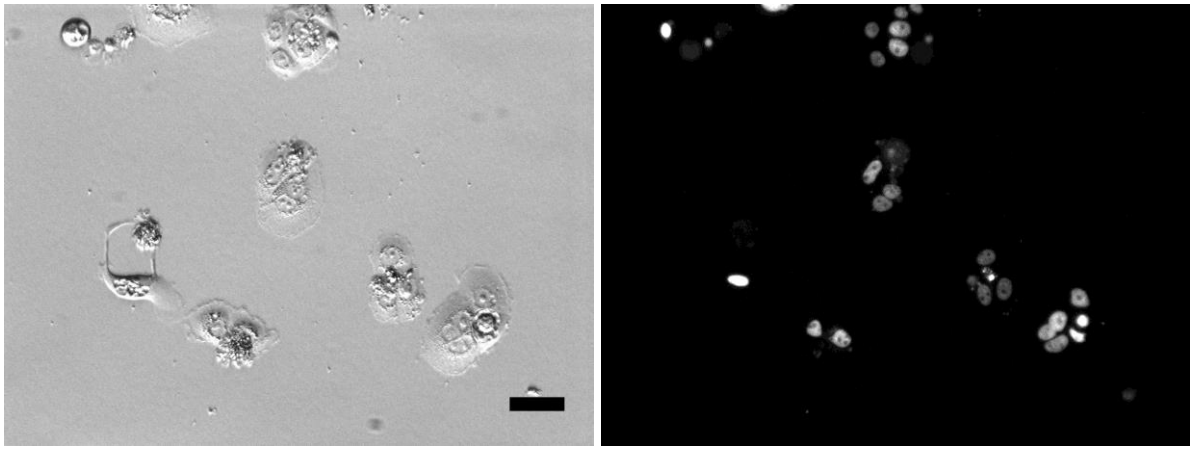

Figure 4.4. **Images of CA1a cells one day after plating.** Left image: Brightfield. Right image: Nuclear fluorescence originating from labeled histones (H2B-mCherry**)**. Scale bar is 50µm**.**

I made use of lentiviral transfection of histone H2B-mCherry which binds to chromatin and makes the nuclei fluorescent. This allows me to obtain a clear picture of the nuclei in order to characterize nuclear morphologies. **Figure 4.5** shows the merged image from the data in Fig. 3.4 and represents the morphological features that I have found to be characteristic of CA1a cells that are not commonly found in the other MCF cell types.

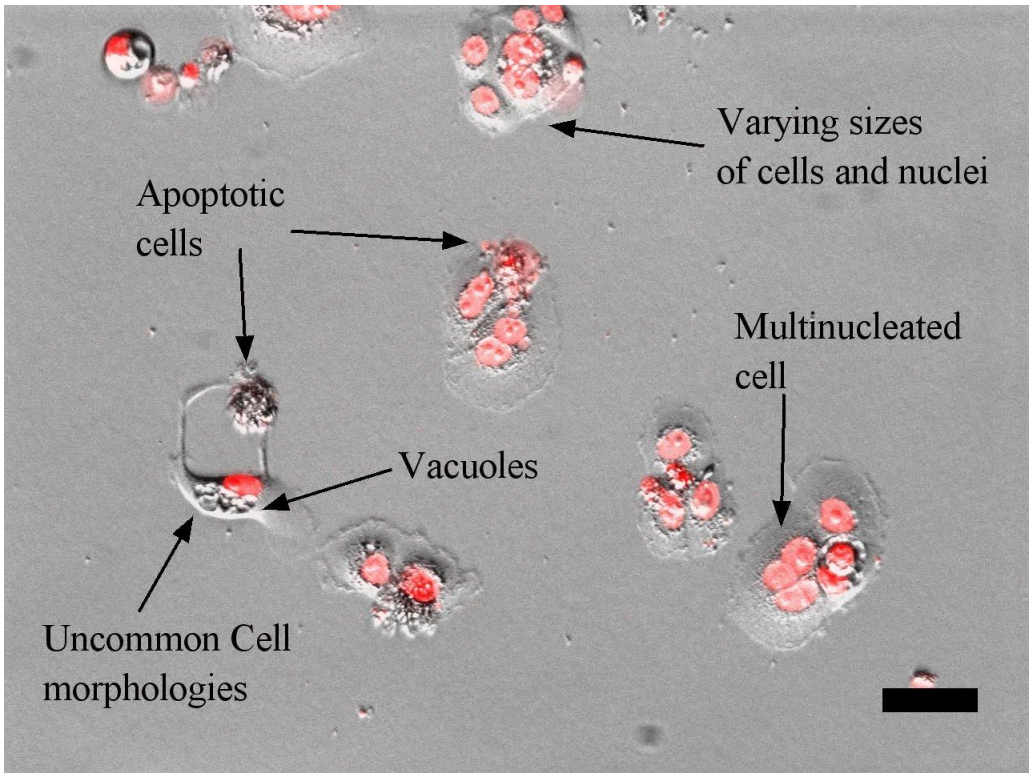

Figure 4.5. A merged image of brightfield and nuclear mCherry fluorescence. Labels show features that are often found in CA1a cells. Scale bar is 50µm.

The ability to do time-lapse imaging allowed me to see how these features characteristic of the CA1a cells evolved over time. The cells shown in **Figure 4.5** were imaged continuously for 4 days at the same position. By Day 4 the vacuoles that were present on Day 1 had grown in size. Additionally a significant fraction of the cell nuclei became enlarged. There is also evidence of continued apoptosis and irregular shaped nuclei, as well as nuclear fragments (indicated by labels in Figure 4.6).

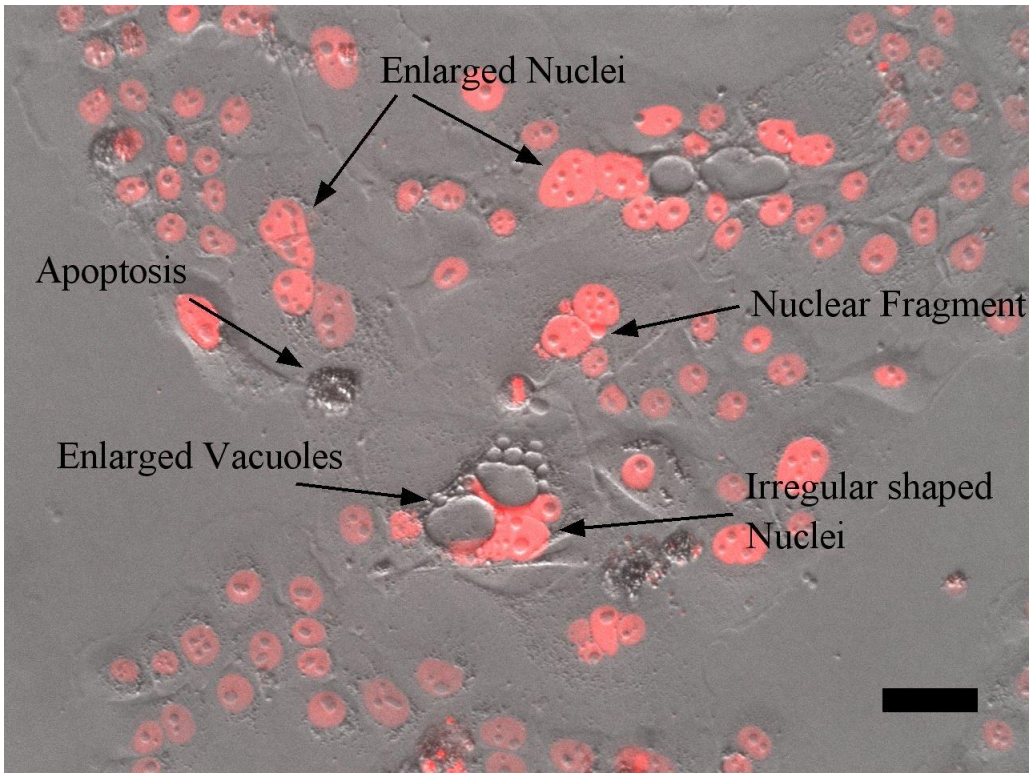

Figure 4.6. Same position as shown in Fig 3.5 at day 4. Labels show newly emerged features of the CA1a cells that have appeared after 4 days of culture. Scale bar is 50µm.

Time-lapse imaging of chromosomal instability in an anomalous CA1a cell

Given that so many CA1a cells appear "anomalous", as illustrated in the previous figures, and that they constitute a relatively large fraction of the cells, it was of interest to follow single cells to understand the developmental events that can happen to such a cell over time. One example would be the cell marked with the label "Multinucleated cell" in **Figure 4.5** This multinucleated cell first undergoes what seems to be a tripolar division whereby the replication of the DNA occurs in 3 poles instead of the usual 2 poles. The result of this aberrant division is that one multinucleated cell has become two cells that now have large and amorphous nuclei. This is shown in **Figure 4.7**.

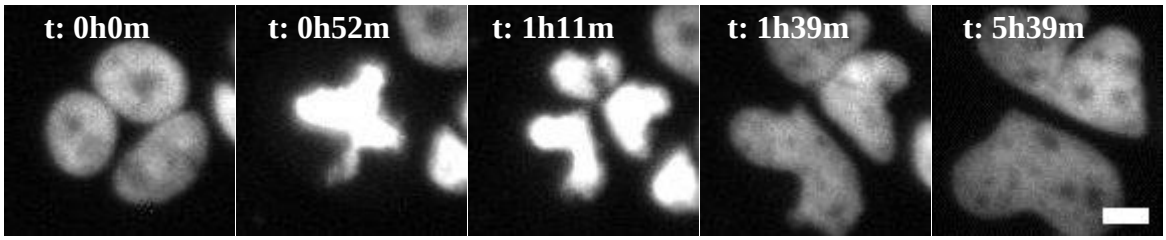

Figure 4.7. Fluorescent DNA of a multinucleated CA1a cell undergoing a multipolar mitosis event and producing large nuclei. Scale bar 10µm.

The phenomenon of tripolar divisions has been previously described by Ganem et al[16] and I provide more statistics on tripolar divisions in a later section. The resulting nuclei are larger than the original and have a more amorphous shape, a characteristic commonly used by pathologists when grading tumors. To verify that an observed multinucleated cell is a single cell and not several cells close together, I used the brightfield images obtained using oblique illumination merged with the nuclear fluorescence from images taken as the cell rounds up to initiate the replication phase. The nuclei of the multinucleated cell fuse together when entering mitosis and demonstrate that it is a single cell (**Figure 4.8**A). 14 hours later, the two daughter cells condense their chromosomes for a renewed round of division (shown in **Figure 4.8**B).

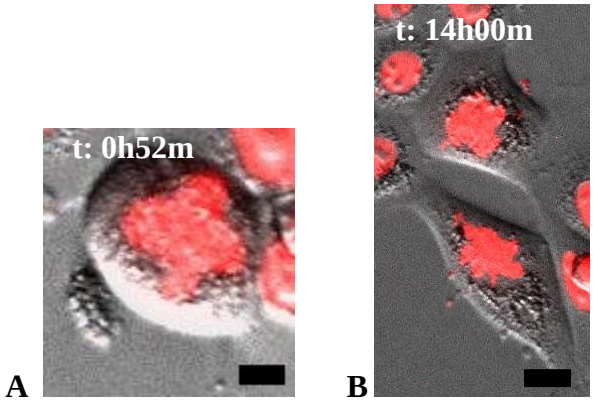

Figure 4.8. A) Another view of the cell of Figure 4.7 as it rounds up to enter mitosis. B) It produces two daughter cells, shown here 14 hours later. The division of the multinucleated cell shown in A **has created two daughter cells that are each mononucleated**, shown in B**. Scale bars: A) 10µm, B) 20µm.**

If we continue following these two daughter cells, we find that they both have tripolar divisions again. Therefore, a tripolar division doesn't necessarily require a multinucleated cell, as it can also happen to

mononucleated cells. Interestingly, this time the tripolar divisions give rise to three daughter cells for each parent cell (whereas previously the tripolar division had given rise to just two cells). **Figure 4.9** shows how each cell undergoes a tripolar division into 3 daughter cells. One of the daughter cells eventually ends up in apoptosis and was marked earlier with the label "Apoptosis" in Figure 4.6. Since a tripolar division results in an uneven distribution of DNA to the daughter cells, it can compromise cell survival.

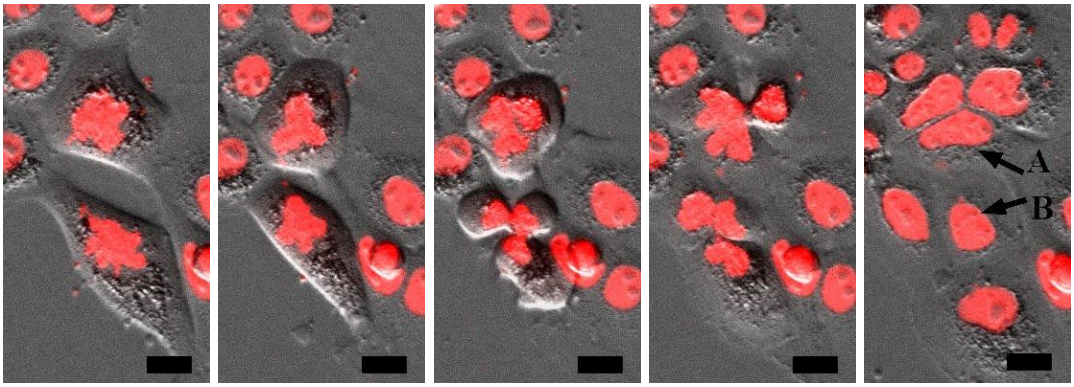

Figure 4.9. Two cells have tripolar divisions, giving rise to six cells. The daughter cells marked **A and B will** be followed in **Figure 4.10. Scale bar 20µm.**

Surprisingly, two of the daughter cells, labeled A and B in **Figure 4.9** then re-fuse into a single cell. The cells fuse together even though they come from two different parent cells (later we will see that two cells that come from the same parent fuse together more often). The result of the fusion is a single bi-nucleated cell with two closely packed nuclei (**Figure 4.10**). If we follow the three daughter cells we find that they fuse into one cell with three nuclei (I will show a more detailed view of this phenomenon later on). shows how this fused cell then undergoes a tripolar division into 3 daughter cells).

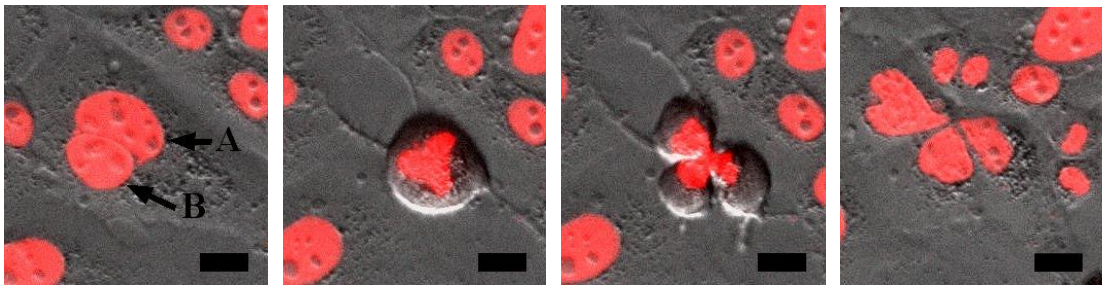

Figure 4.10. A binucleated cell (with nuclei labeled A and B), that has resulted from cell fusion, enters mitosis and has a tripolar division. Labels A and B are the same nuclei that were labeled in Figure 4.9. Scale bar is 20µm.

If we follow the three daughter cells we find that they fuse into one cell with three nuclei (I will show a more detailed view of this phenomenon later on). This cell then enters mitosis and this time the division is quadrupolar (4 poles that attempt to form 4 cells) which fails dramatically at cytokinesis and ends up as a single cell with a very big and amorphous nucleus (see **Figure 4.11**).

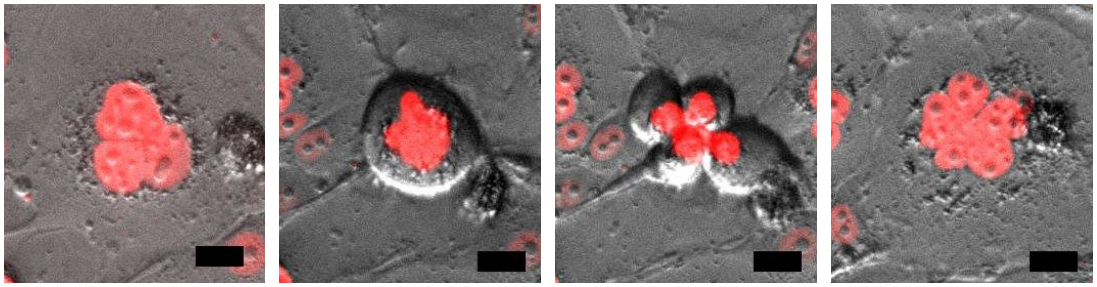

Figure 4.11. A multinucleated cell fails at mitosis and produces a large cell. The cell originated from the fusion of the three cells from the previous figure and attempts a multipolar division but instead produces a single large cell with an amorphous nucleus. Scale bar is 20µm.

Based on observations such as these, it is clear that a proportion of the giant cells commonly found in the CA1a cell line originate as a result of a number of complex and aberrant events that include multipolar divisions, cell fusions, and failed cytokinesis. Additionally, the amorphous nucleus now shows nuclear fragments (which were mentioned earlier as a feature of CA1a cells), which can be seen in the fluorescence image shown in **Figure 4.12**.

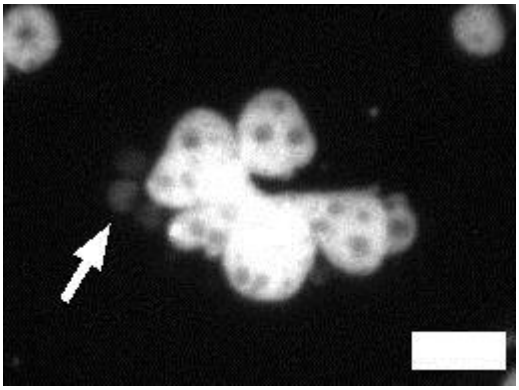

Figure 4.12. Close-up of the nuclear structure of the giant multinucleate cell shown in the last frame of Figure 4.11. Nuclear fragments are now visible with multiple small nucleoli. Scale bar is 20µm.

I found that cell fusions often precede failed cytokinesis events; however, one of the daughter cells shown earlier that did not undergo cell fusion also showed a failed cytokinesis event resulting in a single cell with a larger nucleus. The large nuclei seen are most likely explained by the fact that DNA replication has occurred and the cell now contains double the amount of DNA as a normal cell (**Figure 4.13**).

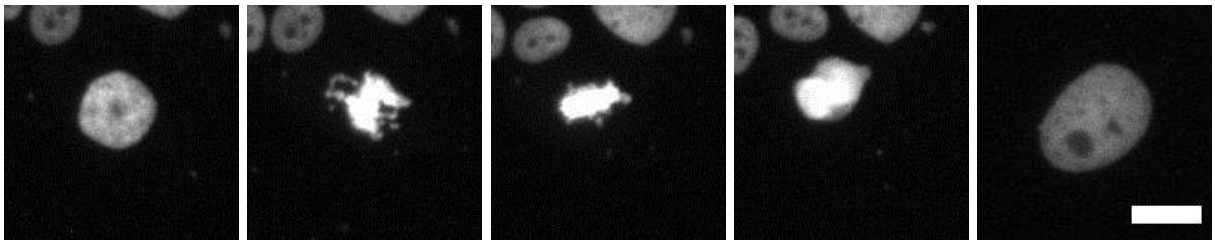

Figure 4.13. Failed cytokinesis in a cell leading to an enlarged nucleus. A cell enters mitosis and condenses the chromosomes but fails at cytokinesis. Scale bar 20µm.

Following the fate of the other two second generation daughter cells, I found that they fused and formed a bi-nucleated cell that quickly developed large vacuoles (**Figure 4.14**). Further tracking of these large bi-nucleate cells revealed that the vacuoles remained constant during at least the next three days.

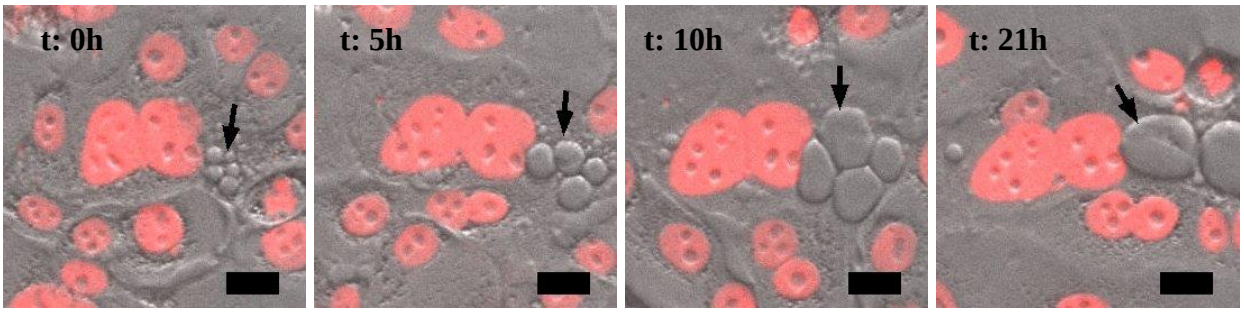

Figure 4.14. Formation and persistence of large vacuoles in giant MCF10A1a cells. Large vacuoles emerge within a short period of time. Scale bar is 20μm.

In summary, there is a chaotic disorganization of the nucleus and DNA structure following multipolar divisions and, additionally, there are cell fusions which appear to "scramble" the DNA even further. The cell fusions explain why after some tripolar divisions we sometimes see less than the expected number of three cells, which is due to the occasional fusion of the daughter cells a short time after the tripolar division.

Since DNA cannot be physically divided into three equal parts upon replication this process probably leads to severe aneuploidy. In any case, the cells are clearly defective cells (or at least their behavior and morphologies are not normal). Surprisingly there is often no apoptosis present in such states of disorganization. In the example field of cells used in the figures above, the only apoptotic cell occurred at an earlier time point. Some of the daughter cells arising from the aberrant divisions persisted for at least 4.5 days and would likely survive longer.

In conclusion, I have analyzed and tracked for 4.5 days the descendants that originated from a single multinucleated cell. Interestingly, all of the descendants are flawed in some way. By day 4.5, there were just three left out of the six possible descendants due to two cell fusions and one case of apoptosis. Of the three that survived, two have dramatically aberrant nuclei (one with big vacuoles) and the other one fails at cytokinesis repeatedly each time that it enters mitosis. At the end we obtain a giant cell and vacuoles, which are characteristics commonly found in this cell line. Therefore, these special characteristics of this cell line can emerge in a relatively short amount of time from other cells, via aberrant multipolar divisions, cell fusions and mitosis events that fail at cytokinesis. The propagation dynamics of a subset of MCF10CA1a

cells is chaotic and disorganized, and one would imagine that the increased genetic heterogeneity arising (termed genetic or chromosomal instability), could be responsible for its increased tumorigenicity.

I found that that large defective cells never go back to becoming smaller cells. However, the data indicates that the size of the nuclei is reset after passaging. Therefore the cells with large nuclei must die during the process of cell passaging by trypsinization and only the smaller, healthier cells survive. If we track a healthy-looking cell, eventually some of its progeny will therefore become large and defective, while other daughter cells will remain healthy, as this is necessary to maintain the observed equilibrium. In the previous section I tracked the progeny of a typical defective cell and found that all of its progeny was also defective. Next I will examine the dynamics of cells that initially look healthy and find that they can also give rise to defective progeny.

Time-lapse analysis of morphologically normal MCF10CA1a cells

Cells are designated as "morphologically normal" based on their appearance, which normally is very clear in contrast to the defective cells, which have amorphous nuclei, large vacuoles, and/or strange shapes. Immediately after plating the cells, one can easily tell the difference between defective, vacuolated cells and healthy cells. In **Figure 4.15**A all the cells that are labeled as "Vacuolated Cells" will die quickly during the following day and leave no progeny. On the other hand the cells labeled "Healthy Cells" proliferate.

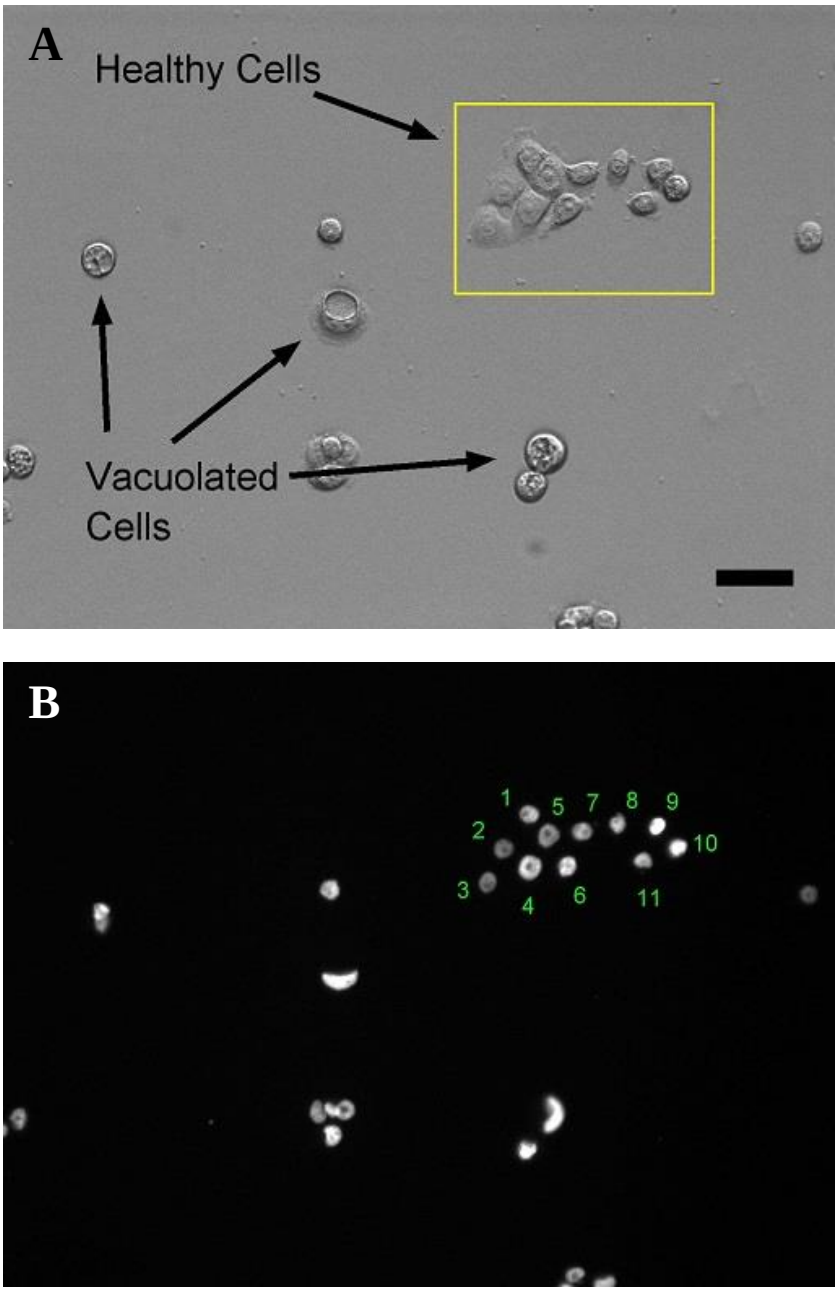

Figure 4.15. (A) CA1a cells on day 1 after plating. (B) Corresponding image of their fluorescent nuclei at the same time point. Scale bar is 50µm.

As expected, the fluorescence image shows that the nuclei of the healthy cells are rounded while the nuclei of the vacuolated cells have odd curved shapes (see **Figure 4.15**B). Additionally in the same figure, the nuclei of the healthy cells have been numbered to analyze their progeny and the number of resulting progeny for each cell is plotted in the bar chart in **Figure 4.16**.

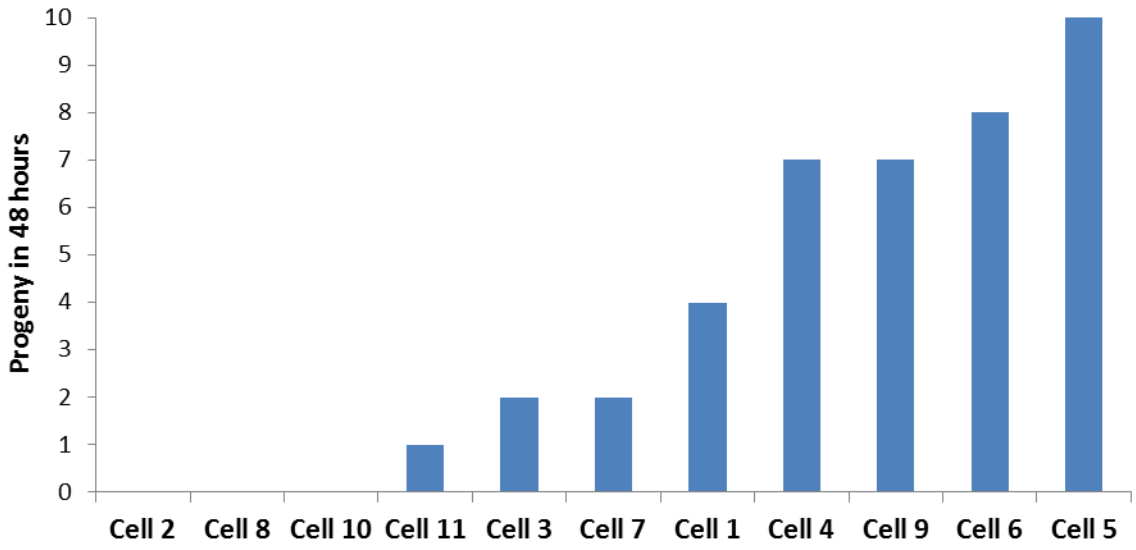

Figure 4.16. The number of progeny generated by a selection of CA1a cells in a 48 hour period. Cell number corresponds to the numbered cells in Figure 4.15.

Figure 4.16 shows that there is a large range of possible outcomes. All the eleven cells had good cellular and nuclear morphologies at the beginning, yet three of them died without leaving progeny and the others produced anywhere between 1 and 10 daughter cells. Additionally, by the end of the 48 hour period all the cells retained their good cellular and nuclear morphologies except one: cell 11 failed at cytokinesis and produced one large aberrant nucleus. Further tracking of this particular cell for 5 days reveals that it underwent several failed tripolar divisions and ended up producing only one very large cell, indicating that the origin of the giant cells found in MCF10CA1a cell cultures most likely arises from a failed cytokinesis event.

I expanded the previous study by looking at 30 additional MCFCA1a cells and 30 MCF10A cells for comparison purposes. Note that tracking these 60 cells and their progeny over 48 hours means that a total of 335 cells were tracked. The results are shown in **Figure 4.17** (the third bar plot is a superposition of the first two).

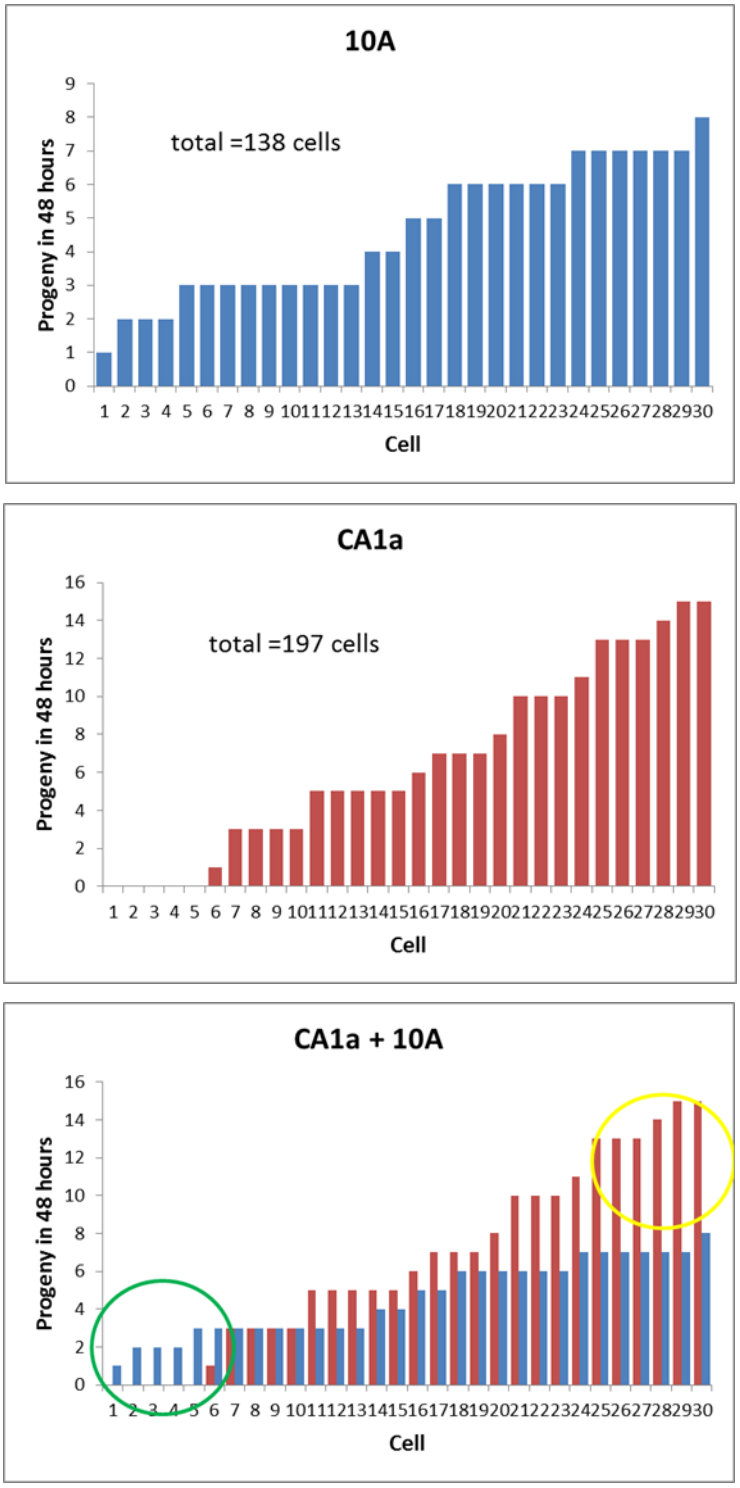

Figure 4.17. Progeny charts of 10A cells and CA1a cells. The third bar chart combines the data from both cell lines to show that some CA1a cells generate more progeny (yellow circle), while also a subset of CA1a cells create no progeny at all (green circle).

The bar charts of **Figure 4.17** show that some CA1a cells divide very quickly (marked with a yellow circle) but also some CA1a cells don't divide at all (marked in green). All of the CA1a cells that didn't divide died within the 48 hour period. In sum, 13 CA1a cells died whereas only one 10A cell did so. This suggests that 10A cells are healthier than CA1a cells. However, the number of cell fusions was similar, with 4 and 3 respectively (**Figure 4.18**).

	10A	CA1a
Deaths	1	13
Fusions	3	4

Figure 4.18. Cell Deaths and Fusions of the 335 cells that originated from 30 CA1a cells and 30 10A cells over 48 hours. CA1a cells show more deaths than 10A cells, but similar number of cell fusions.

It must be reiterated that the cells tracked were preselected as healthy cells (i.e. cells that looked defective were not tracked). Therefore, it appears that even the healthy and "normal looking" subpopulation of CA1a cells are in fact defective compared to normal cells since they die more often. However, they also have the potential to divide more often. Interestingly, the only 10A cell that died was the daughter of a cell that had undergone fusion. Moreover, this cell fusion resulted in a tripolar division, with three daughter cells instead of the usual two. Tripolar divisions are analyzed in more detail in a later section.

Two types of failed cytokinesis in MCF10CA1a cells

In the previous section, I identified a healthy cell which turned defective, and its first error was a failed cytokinesis event. This was done exclusively by looking at fluorescent nuclei. Closer examination by looking also at the brightfield images reveals that there are two types of failed cytokinesis. One is the failure to produce two distinct nuclei after mitosis which results in a single cell with a single nucleus (mentioned earlier and shown previously in **Figure 4.13**). The other type is when two distinct nuclei are produced at

mitosis that seem healthy, but are in fact not segregated into two daughter cells and therefore the product is one bi-nucleated cell. Two cells of the eleven cells analyzed in **Figure 4.16** (cell 4 and cell 5) which were previously categorized as being healthy fall into this category (**Figure 4.19** shows this event).

Figure 4.19. A CA1a cell produces a bi-nucleated cell. In this type of failed cytokinesis, two distinct nuclei are produced within a single cell. Unlike previous occurrences of bi-nucleated cells, this one is not the product of cell fusions. Scale bar is 20µm.

Interestingly, both cell 4 and cell 5 fail at cytokinesis after two rounds of good divisions. The resulting bi-nucleated cells later have failed multipolar divisions and increasingly defective giant nuclei. In sum, the 11 initially analyzed cells eventually led to three giant cells, all of which originated from failed cytokinesis, which then led to failed multipolar divisions. These three cells (cells 4, 5 and 11) are shown in Figure 4.20 at day 4.5 and are labeled with "Large Nuclei". An additional cell is labeled "binucleated cell", which is also a cell destined to become a MCF10A1a giant cell.

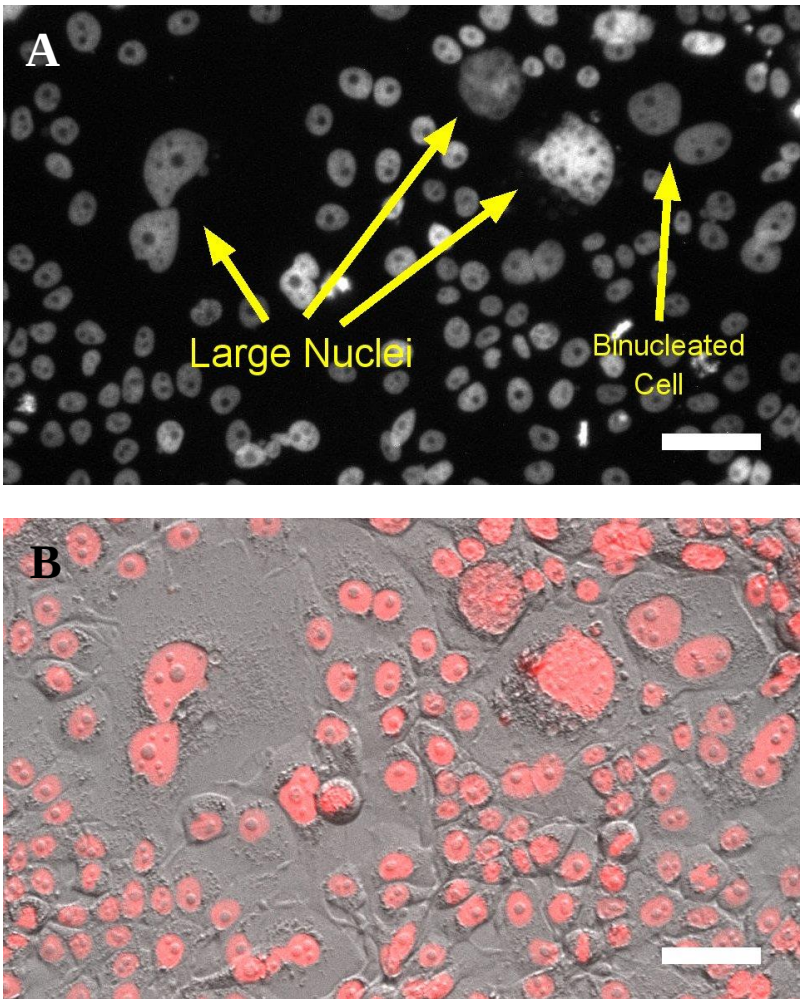

Figure 4.20. CA1a cells at day 4.5. (A) Fluorescent nuclei and (B) merge image of the CA1a cells. These are the daughter cells of the cells shown in Figure 4.15. Three large nucleated cells have developed as a result of failed cytokinesis and subsequent failed multipolar divisions. The cell labeled "Binucleated Cell" is also on its way to becoming a large cell. Scale bar is 50 µm.

Of the three giant cells, one is clearly bi-nucleated while the other two are mono-nucleated. Surprisingly the number of nuclei does not correlate with the original type of failed cytokinesis - the number of nuclei appears to be random. To illustrate this I looked at the parent cells of each of these three cells. The bi-nucleated cell resulted from a cell that was also bi-nucleated and had replicated its DNA several times without dividing. One of the mono-nucleated cells also resulted from a bi-nucleated cell. The other mono-nucleated cell resulted from a cell that had three nuclei and these three nuclei in turn came from a bi-

nucleated cell. Therefore a bi-nucleated cell can give one, two or three nuclei in a seemingly random manner.

In conclusion, tracking small morphologically healthy cells has revealed that the number of progeny is highly variable and some cells go on to produce the giant cells with amorphous nuclei seen in these cultures. Cells that produced many progeny, as well as those that produced few progeny, were equally capable of producing giant cells. The initial event in this transformation seems to be failed mitosis at cytokinesis resulting in either a bi-nucleated cell or a single mono-nucleated cell with probably twice the genetic content. In either case it leads to a cascade of multipolar divisions and cell fusions that eventually produce giant cells. Interestingly, before the failed divisions, the cells divided correctly like other cells, indicating that failed mitosis is likely a stochastic event. This is why there is always a subpopulation of cells that can divide correctly. However, this implies that all cells could fail at some point in time, but since the error occurs at mitosis, if the cells eventually become mitotically inactive, more giant cells would not develop.

The fate of the MCF10A1a giant cells

Given that giant cells do not survive the passaging procedure, it would be interesting to see what happens to them after a prolonged period of time without passaging. This would simulate what happens in an actual tumor. It might be that by passaging the cells we are not seeing what happens in real tumors where the giant cells could possibly survive. To answer this question I tracked 20 giant cells for a total of 9 days and found that half of them die and the other half survive. In general, the cells that die had more fragmented nuclei before dying. The fact that some giant defective cells survive for so long could mean that they play a role in cancer in vivo.

Analysis of tripolar divisions in MCF10CA1a cells

As shown in the previous sections, the chromosome marker histone H2B-mCherry (or H2B-GFP) allows us to clearly identify tripolar divisions in which the chromosomes are segregated into three parts during mitosis instead of the usual two parts, thereby producing three aneuploidy daughter cells. Ganem et al.[16] have looked in detail into this phenomenon (using the same marker) and have shown that it is present to some degree in most cell lines. I also detected triple divisions in the CA1a and 10A cell lines. An example of a triple division in a bi-nucleated CA1a cell is shown in **Figure 4.21**.

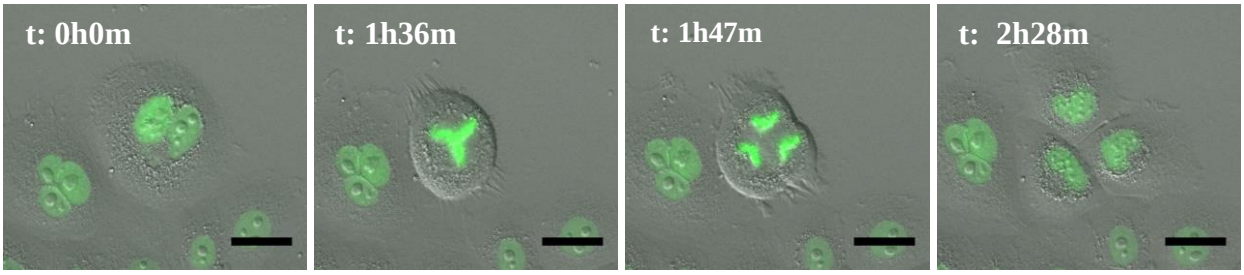

Figure 4.21. A CA1a cell undergoes a tripolar division resulting in three daughter cells. Green is histone H2B-GFP. A close up of the last frame is shown in Figure 3.23. Scale bar is 30μm.

Tripolar divisions also give rise to "chromosomal bridges" between the 3 nuclei (**Figure 4.22**), which can later break.

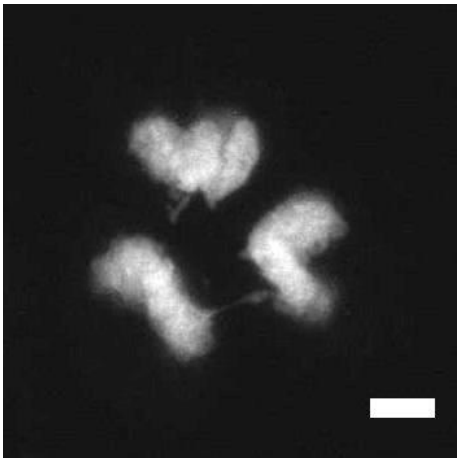

Figure 4.22. The tripolar division of the last figure at higher magnification. Connections or chromosomal bridges can clearly be seen between the two bottom nuclei. Another bridge joining the other two nuclei appears to have been broken. Scale bar is 10μm.

Previously I described fusion of daughter cells following a triple division. **Figure 4.23** shows another, but more extreme example in which a bi-nucleated cell rounds up and divides into three cells which then fuse again into a single cell.

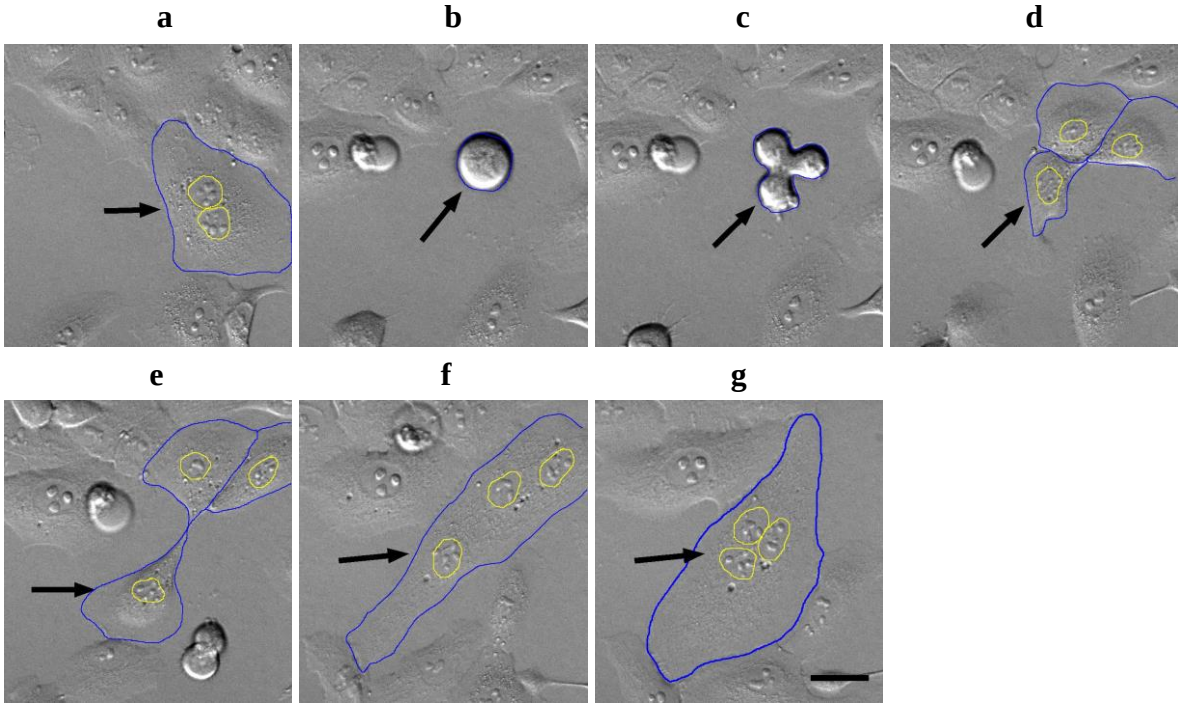

Figure 4.23. A tripolar division is followed by a fusion of all the three daughter cells into one single cell. For better visualization the nuclei are outlined in yellow and the cytoplasm is outlined in blue. A to G is the order in which the images were taken. Scale bar is 30µm.

To get statistics on occurrence rate of tripolar divisions, I counted the percentage of tripolar divisions in both 10A and CA1a cell lines and compared them to similar data from other cell types found in the literature. Surprisingly, 10A cells and CA1a cells have similar percentages of tripolar divisions (close to 1%) and this is low compared to other cancer cell lines. The data is shown in the following figure.

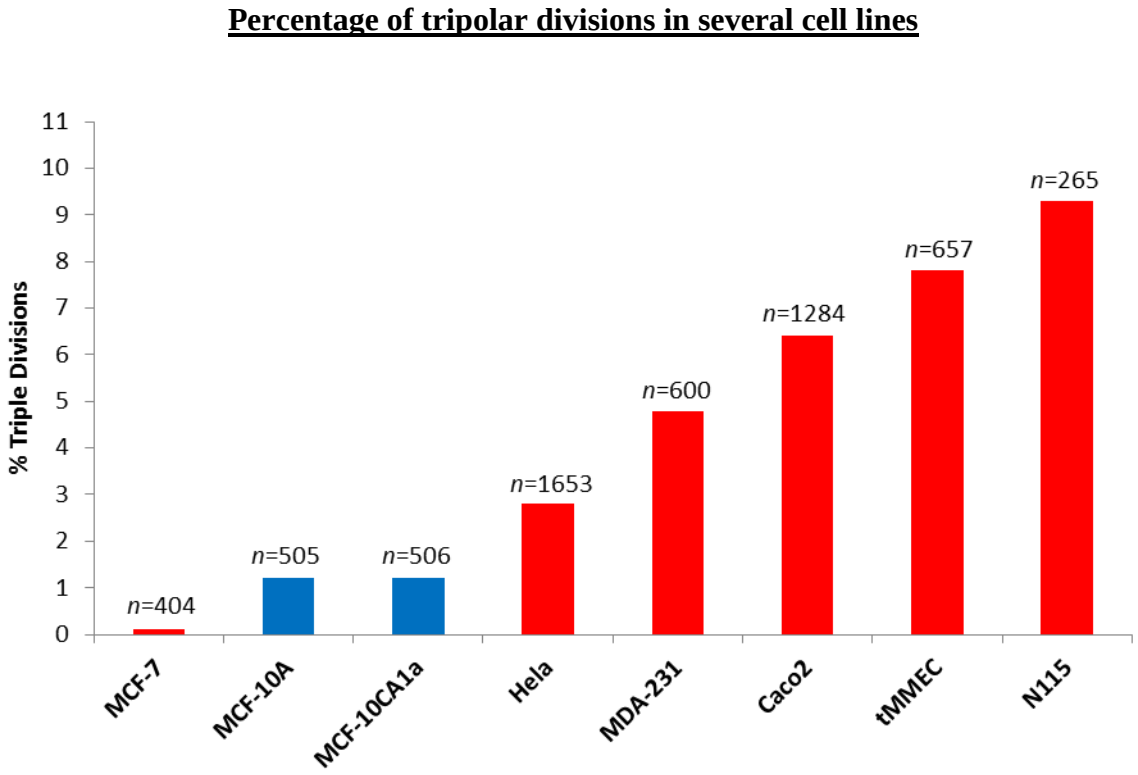

Figure 4.24. The percentage of triple divisions of MCF10A cells is similar to that of MCF10CA1a cells and it is low compared to other cell types. Data in red is taken from Ganem et al. [16]

We can conclude that 10A cells and CA1a cells have similar percentages of tripolar divisions, indicating that the increased tumorigenicity of the CA1a cell line is not due to a higher number of tripolar divisions. It has been previously suggested that tripolar divisions could be a source of chromosomal instability which in turn can lead to cancer.[1] This theory has been challenged by Ganem et al.[16] and my findings further support the idea that the presence of tripolar divisions is not correlated to tumorigenicity (since MCF10A1a cells are much more tumorigenic than MCF10A cells).

Origin of giant MCF10CA1a cells

To verify the claim made in the previous section that an error at mitosis initiates the production of giant cells which was made by looking at the evolution of the cells in one field of view, I looked at 15 other fields of view to get better statistics on this process. In total 18 giant cells were identified (at day 4.5 after plating) and tracked back in time until their first division on the first day after plating of the cells. The results, shown in **Figure 4.25**, indicated that in the majority of the cases (10 out of 18) the first division was a mono-nucleated cell becoming a bi-nucleated cell.

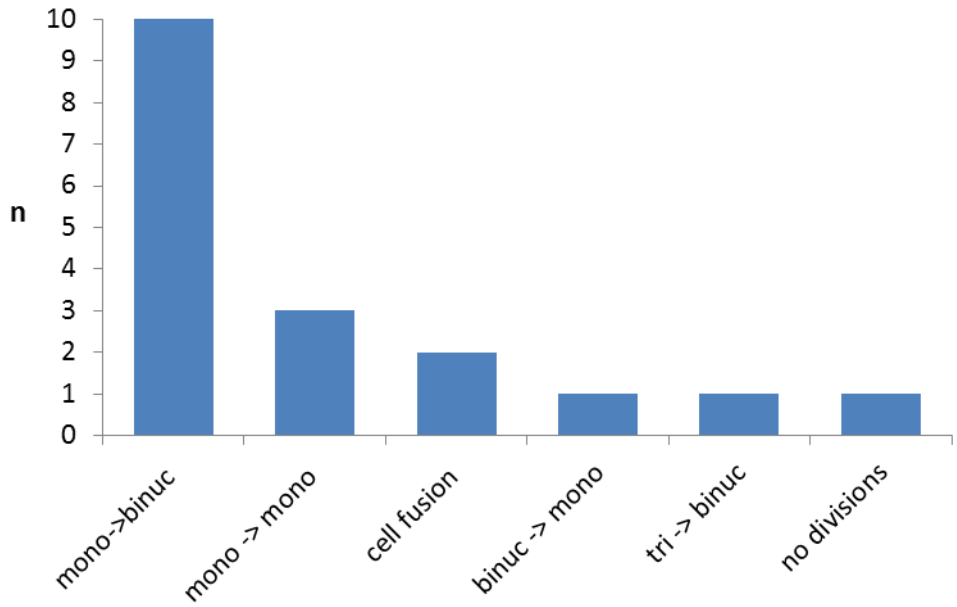

Figure 4.25. Giant cells tracked back in time (n=18) to identify the type of the first division. The first division of most of the cells that would later become giant cells was of the type "mono-nucleated cell that becomes bi-nucleated".

The data of **Figure 4.25** shows that a wide range of phenomena can occur. The two most common are: a mono-nucleated cell becoming a bi-nucleated cell (n=10) and a mono-nucleated cell becoming a mono-nucleated cell (n=3), with (presumably) increased ploidy. These are the two types of failed cytokinesis events that I described in the previous section. The third most common is cell fusion, which includes fusion of unrelated cells. Additionally I found cases of a bi-nucleated cells becoming a mono-nucleated cell and a

tri-nucleated cell becoming a bi-nucleated cell. Most intriguingly, there is a case of a cell that goes all the way from small cell to giant cell without attempting any divisions. It must be clearly stated that this data corresponds only to the first division of the cell and later divisions may happen in any combination of types.

Nuclear size dynamics in MCF10CA1a cells.

The analysis of the previous section indicates that the CA1a cell line contains some defective cells that have very large nuclei and their size increases with time after plating the cells. I have quantified this effect in **Figure 4.26** which shows that CA1a cells indeed have a higher proportion of large nuclei compared to 10AT cells, probably due to fusion events and failed mitosis. Interestingly, the nuclear size of 10AT cells also increases slightly with time. This could be due to the cells becoming flatter as they attach better to the substrate, but it is surprising that they keep increasing in size even after 15 hours.

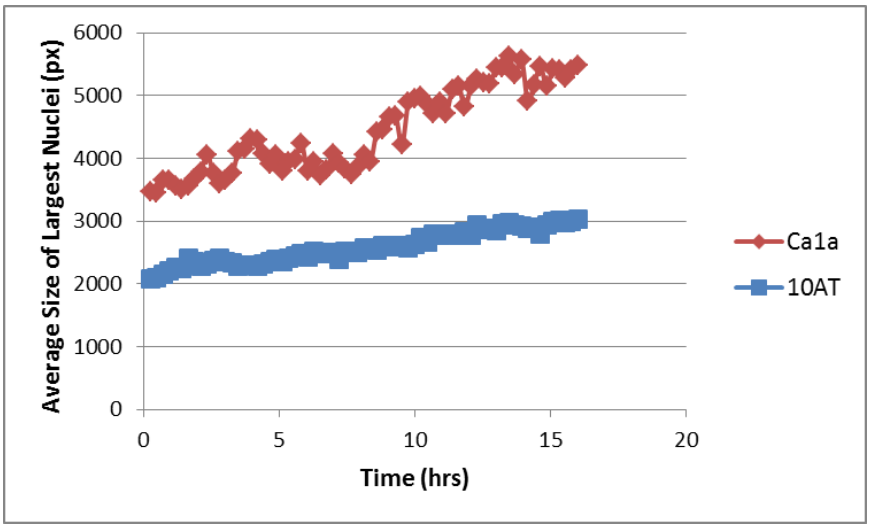

Figure 4.26. Nuclear size statistics in MCF10CA1 cells vs MCF10AT cells. The size of the nuclei of 500 cells of both CA1a and 10AT cells was measured and the average size of the largest nuclei for each frame was recorded. The results confirm that the CA1a cells have larger nuclei, and that the size of the nuclei increases with time.

I now show the distribution of nuclear sizes that we find when we plate cells in a cell culture dish and let them grow until they are near confluence. I used a computer program to automatically measuring the areas of 3000 nuclei of 10A cells and CA1a cells. I find that the CA1a cells have higher mean nuclear area and higher standard deviation. The CA1a cells have a higher number of very large (or multinucleated) nuclei which show up on the far right of the distribution (shown as >3500).

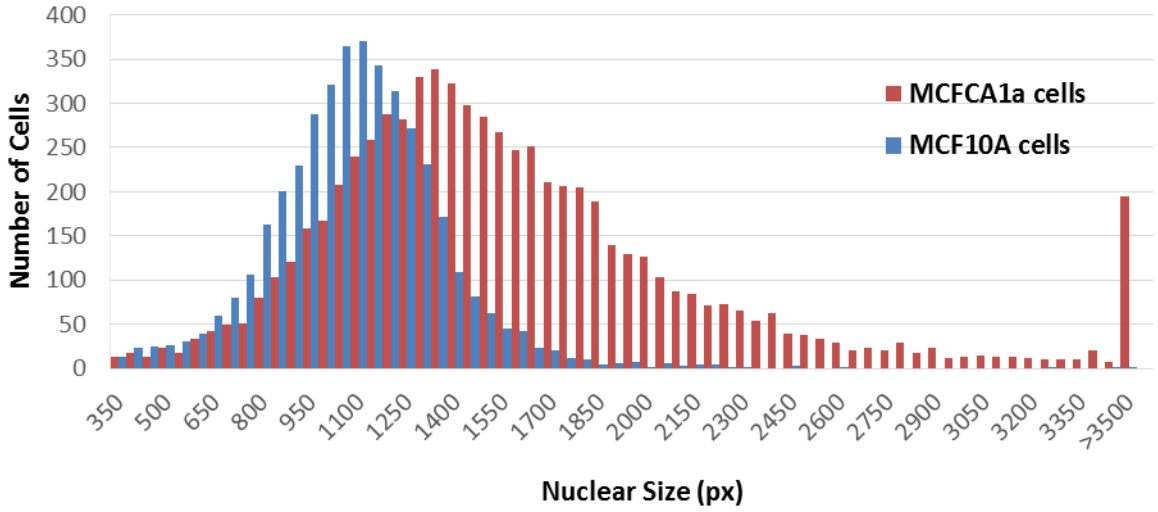

Figure 4.27 Size distribution of ~3000 nuclei measured in MCFCA1a cells (red bars) and MCF10A cells (blue bars). MCFCA1a cells have, on average, a higher nuclear size than MCF10A.

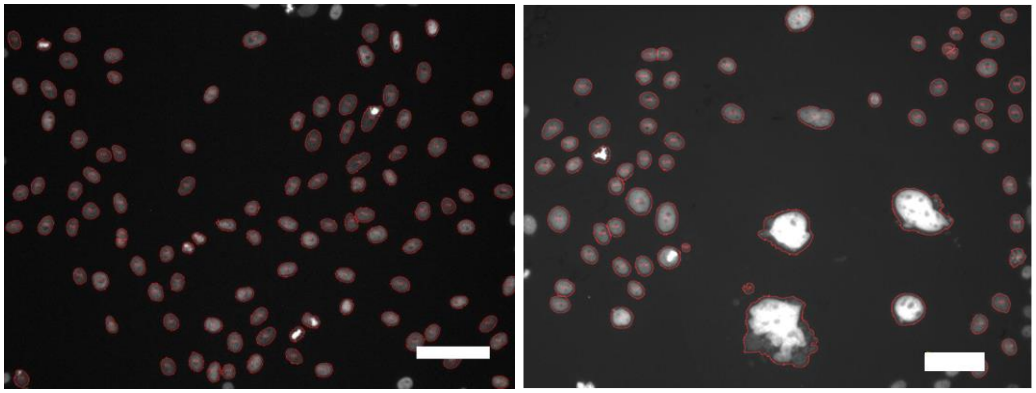

Figure 4.28. Example image from which the previous chart data was taken. Left: MCF10A nuclei, Right: MCFCA1a nuclei. (72 images were used in total. Scale bar is 50µm).

It has been previously reported that while the nuclei of normal cells have a rounded shape, cancers often have cells with nuclei that have irregular contours.[17] Large nuclei have been correlated with increased malignancy and pathologists regularly look at nuclear size for staging cancer.[18] In Pap smear tests for cervical cancer screening, the cancer cells display large nuclei and can also display vacuoles. I often see that large nuclei often have aberrant shapes and also have large vacuoles, all of which can be indicative of cell damage. For example, it is has long been known that carcinogens increase the nuclear sizes of cells.[19] Cancer associated viruses such as HPV26 can also increase nuclear size via endoreplication.[20]

Other features of MCF10CA1a cells

Bridges of DNA that link the nuclei in bi-nucleated cells

After a cell division, there is often a bridge of DNA linking the two daughter cells. **Figure 4.29** shows an example of one of these bridges linking the two nuclei of a large bi-nucleated cell. The bridge survives until the next division, even if the two nuclei are far apart from each other as shown in **Figure 4.29B**. When the chromosomes condense for the next round of division, the two nuclei come close together at the position of the bridge (**Figure 4.29D**).

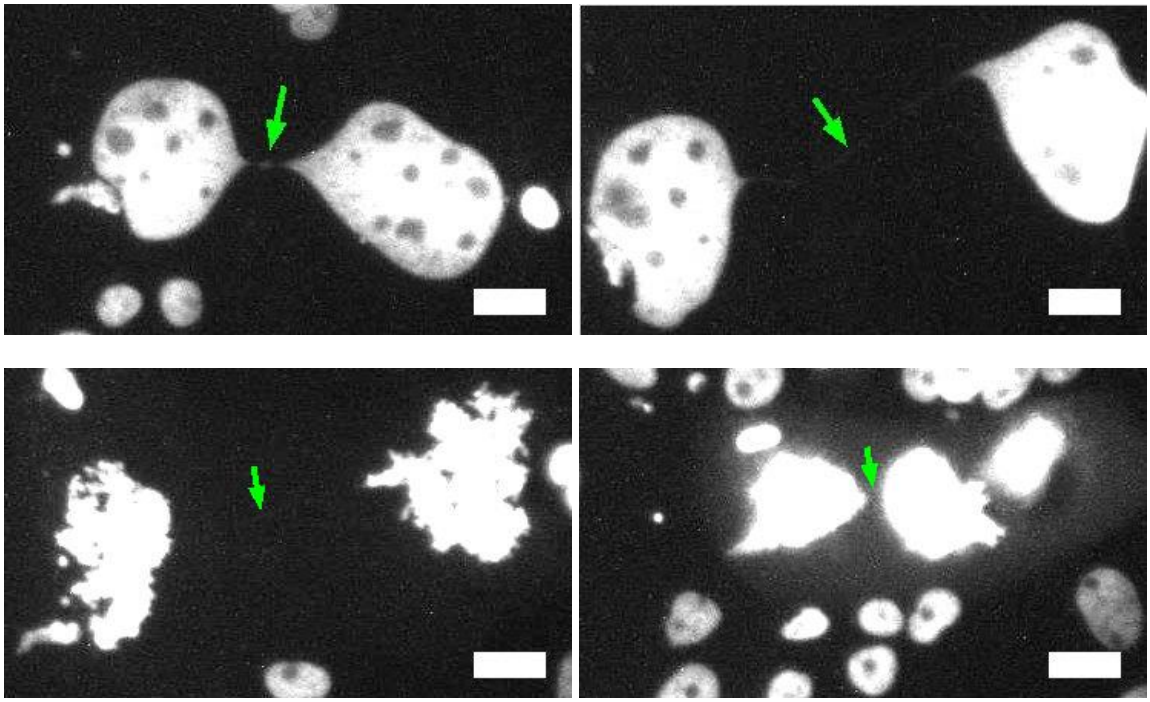

Figure 4.29. DNA strands that link the nuclei of a bi-nucleated cell. A,B,C,D are four consecutive time points showing a bi-nucleated cell with a bridge of DNA linking the two nuclei (see arrow). At image C the cell is entering mitosis. Scale bar is 20µm.

It is difficult to get statistics on the frequency of occurrence of DNA bridges because in many cases the bridge will not be visible. The bridges are very thin and often the two nuclei will be closely packed together. While it may be possible that the bridge is responsible for failed cytokinesis, the presence of the bridge doesn't always prevent cytokinesis from happening, because it often occurs that the bridge breaks during cytokinesis.

Whereas **Figure 4.29** was a very large cell, **Figure 4.30** shows that the same thing happens to small cells.

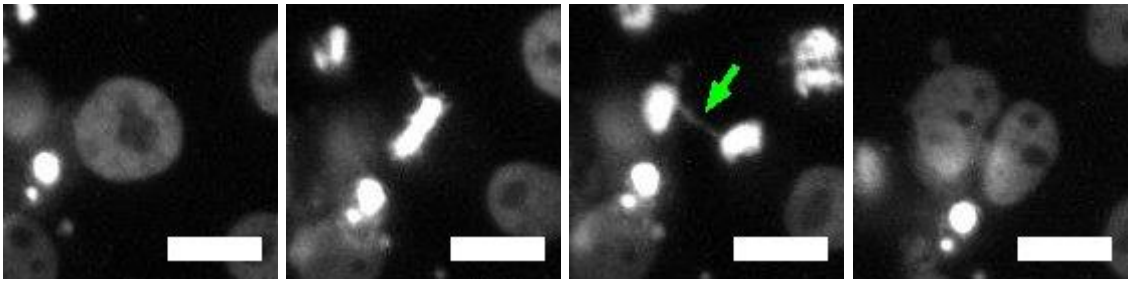

Figure 4.30. A cell enters mitosis and produces a binucleated cell. A DNA bridge links the two nuclei (green arrow). Scale bar is 20μm.

The chromosomal bridge shown in the previous section could be part of a feature commonly present in cancer cells called the Breakage Fusion Bridge Cycle (BFBC) which was first described by Barbara McClintock in 1941.[21] In BFBC, chromosomes fuse due to the loss of telomeres at the ends of chromosomes. Then during mitosis this fused chromosome is broken when the microtubules pull on the centromeres. This process can repeat over time, scrambling the genome, and possibly amplifying cancer genes. It is unclear whether the DNA is always broken upon in mitosis. The cases shown here support the idea that sometimes the bridge is not broken, and in fact could be the cuase of the formation of binucleated cells due to failed cytokinesis.

Quadrupolar and other types of aberrant divisions in MCF10A1a cells

Even though tripolar divisions occur at the same frequency in 10A cells as in CA1a cells, there are other events such as the existence of giant cells, defective divisions and amorphous nuclei that are unique to CA1a cells. Another example of an aberrant process that appears to be more common in the MCF10CA1a cell line is quadrupolar divisions, whereby a cell divides in four poles. **Figure 4.31** shows a quadrupolar division occurring at the same time as a tripolar division in the CA1a cell line.

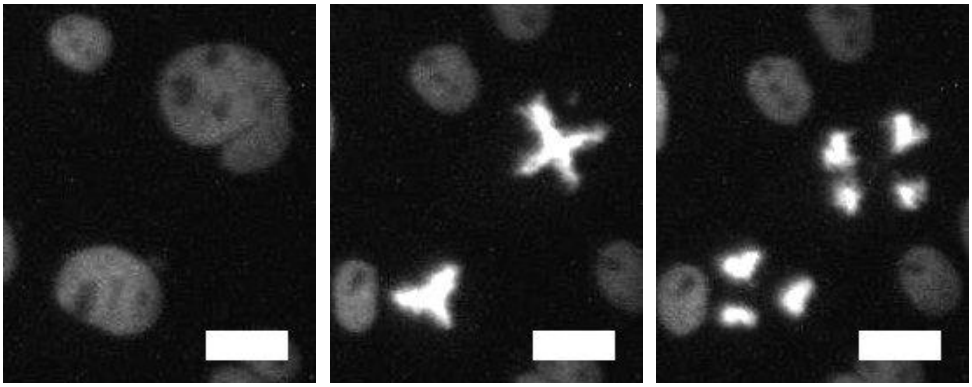

Figure 4.31. Time lapse of a tripolar (bottom left) and a quadrupolar division (top right). Scale bar 20µm.

Another example of an even more complex aberrant division present in CA1a cells but not in 10A cells is shown in **Figure 4.32**. The large multinucleated cell undergoes a highly aberrant multipolar division, producing oddly shaped nuclei with numerous chromosomal bridges.

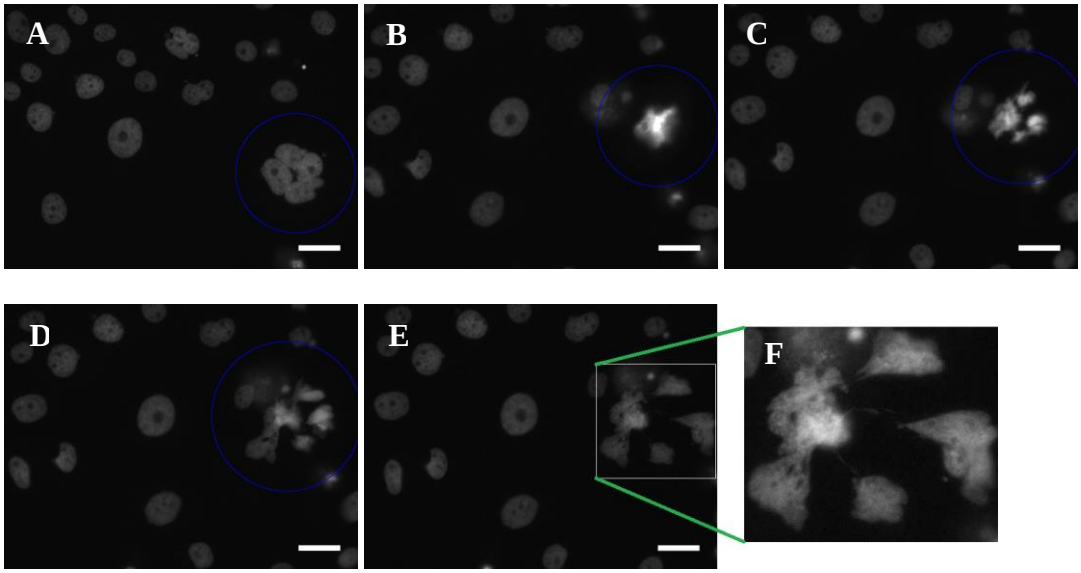

Figure 4.32. A multinucleated CA1a cell undergoes a highly aberrant division. A to E is a sequence of images during the division. F is a magnification of the box in image E, which shows the remnants of the highly aberrant multipolar division with numerous chromosomal bridges**. Scale bar is 30µm.**

Formation of Micronuclei in MCF10A1a cells.

It is possible that the nuclear fragments frequently found in CA1a cells are intact single chromosomes that have left the nucleus and form micronuclei. This has been described in the literature for cancer cells[22,23] where mitotic errors lead to lagging chromosomes during anaphase that then fail to segregate appropriately into the daughter cells.[23] Micronuclei can exist for several generations or can be re-incorporated into the primary nucleus. As they are more prone to accumulate DNA damage, they have been postulated to play a role in cancer.[22] An example of micronuclei in CA1a cells is shown in **Figure 4.33**, and **Figure 4.34** shows a binucleated cell with two micronuclei that condensate when the cell enters mitosis.

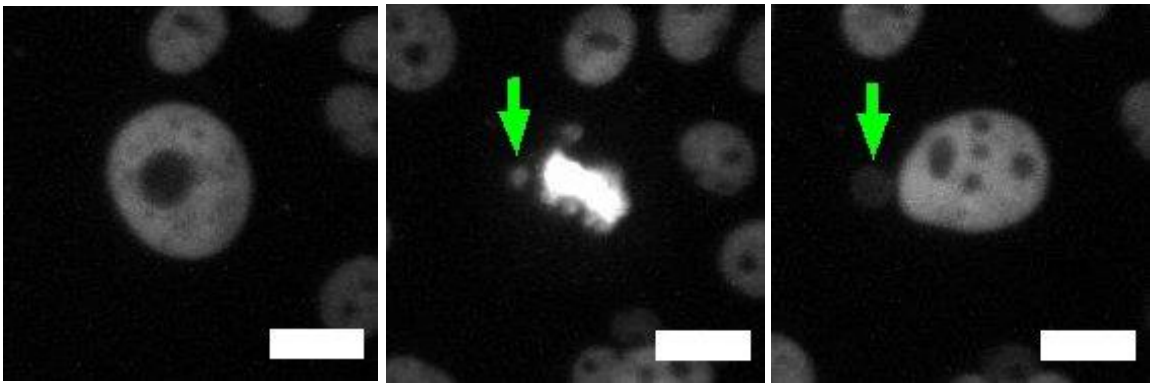

Figure 4.33. A MCF10CA1a chromosome forming its own micronucleus. Scale bar is 20µm.

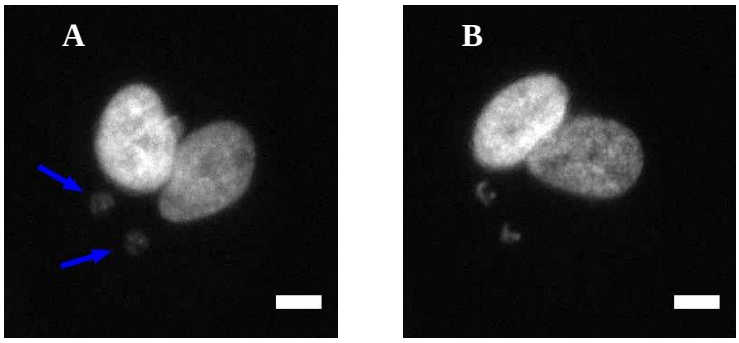

Figure 4.34. Example of a bi-nucleated cell with two chromosomes outside of the nucleus. A) Two micronuclei (blue arrows). B) The two micronuclei start to condense **at the same time as the rest of the chromosomes as the cell enters mitosis. Scale bar is 10µm.**

CA1a cells are more likely to detach from the culture dish

I cultured 10A cells or CA1a cells on a dish for 2 weeks. For the CA1a cells, the epithelial layer of 2 out of 5 dishes became detached (**Figure 4.35C** and **Figure 4.36**). Other plates with CA1a cells that did not detach showed high levels of vacuoles (**Figure 4.35B**). On the other hand, 10A cells looked morphologically normal and did not detach from their plates over the same time period (**Figure 4.35A**).

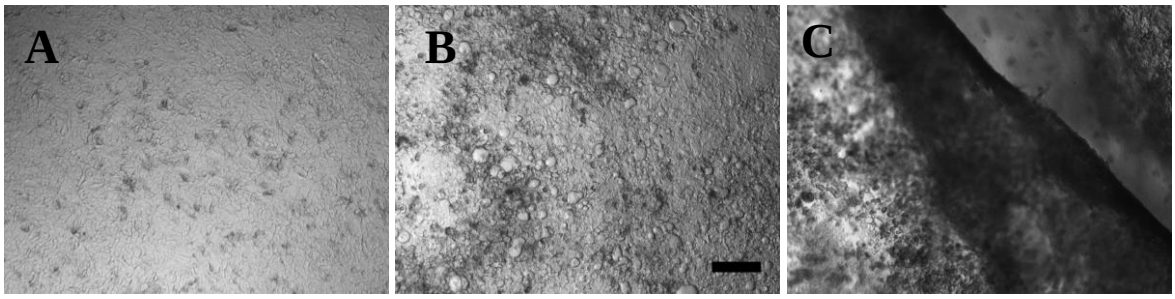

Figure 4.35. After 2 weeks of culture without passaging, CA1a cells either detach (C) or form large numbers of vacuoles (B). On the other hand 10A cells cultures are morphologically normal (A). Scale bar is 100µm.

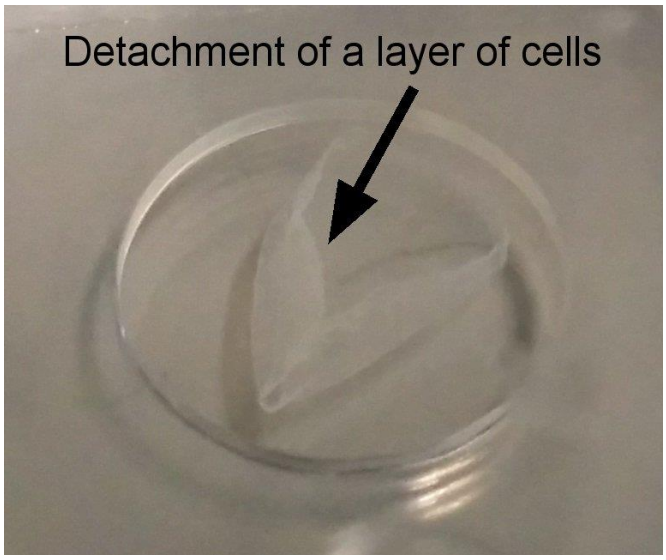

Figure 4.36 When cultures of cells reach a high density of CA1a cells, the epithelial layer of cells can detach from the culture dish.

A note about multinucleated cells

Binucleated cells are a form of tetraploid cells because they have double the number of chromosomes as a diploid cell, and one might assume that tetraploid cells are not healthy cells (at least in animal species where they are rare). However, some specialized cells in animals are commonly found to be tetraploid. Binucleated polyploid hepatocytes are normally found in all mammalian species[24]. For example, in humans, the number of polyploid cells in the liver is 20–30%.[25] Interestingly, any number of polyploidy can happen (4n, 8n, 16n and higher) both via cell fusion and via endoreplication that skips cytokinesis. Ploidy reversal where a polyploid cell becomes a diploid cell can also happen and has been described in the literature.[24] Therefore, polyploidy per se is not exclusively a feature of cancer cells. However, the cells that I have seen forming binucleated cells ultimately form giant cells with clearly defective nuclei, and these cells might therefore have a role in cancer due to their apparent chromosomal instability.

Experiments using co-cultures of MCF10A cells and MCF10CA1a cells

Since cancerous and non-cancerous cells coexist in vivo, it is possible that their interactions can influence the development of a tumor. It has long been known that the development of a tumor is affected by its micro-environment[26]. I attempted to co-culture 10A cells and CA1a cells to see if this would give rise to events that don't appear when the cells are cultured independently from each other. I started with a high number of 10A cells (to simulate a normal human epithelial tissue) and added to it CA1a cells at a low concentration (1 cancer CA1a cell to 1000 normal 10A cells) to simulate the initial stages of a tumor in which the cancerous part of the tissue is composed of only a few cells. Given that the two cell types had different fluorescent colors, I could track the progression of the growth of both cell types over time with my two color fluorescence incubator microscope. **Figure 4.37** shows the growth of CA1a cells in green (GFP) while co-cultured on 10A cells which have mCherry (red) fluorescence.

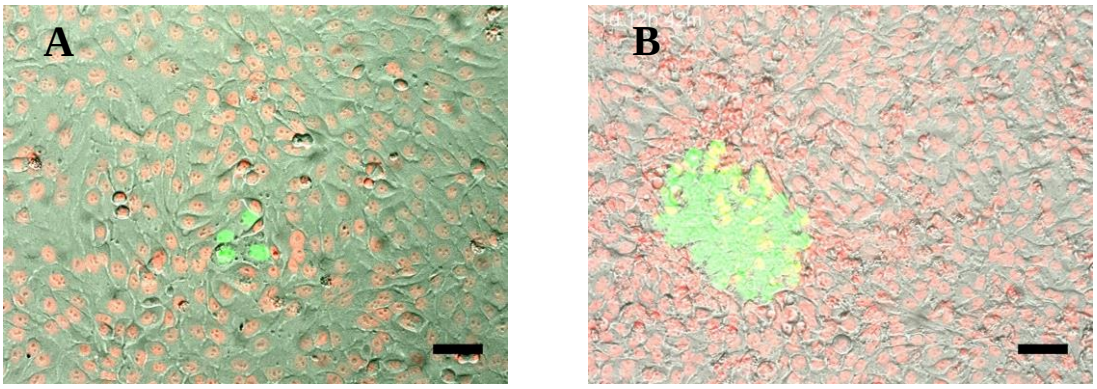

Figure 4.37. MCF10A cells in red and MCF10CA1a cells in green (mCherry and GFP, respectively). A) At day 2 after plating, just four CA1a cells lie on top of the 10A cells. B) By day 4.5 the CA1a cells have grown in number and form a tight clump of cells. Scale bar is 50 µm.

The CA1a cells don't always grow as a pack as shown in the previous figure. **Figure 4.38** shows the different types of growth rates that can be seen in a single dish after 7 days of culture.

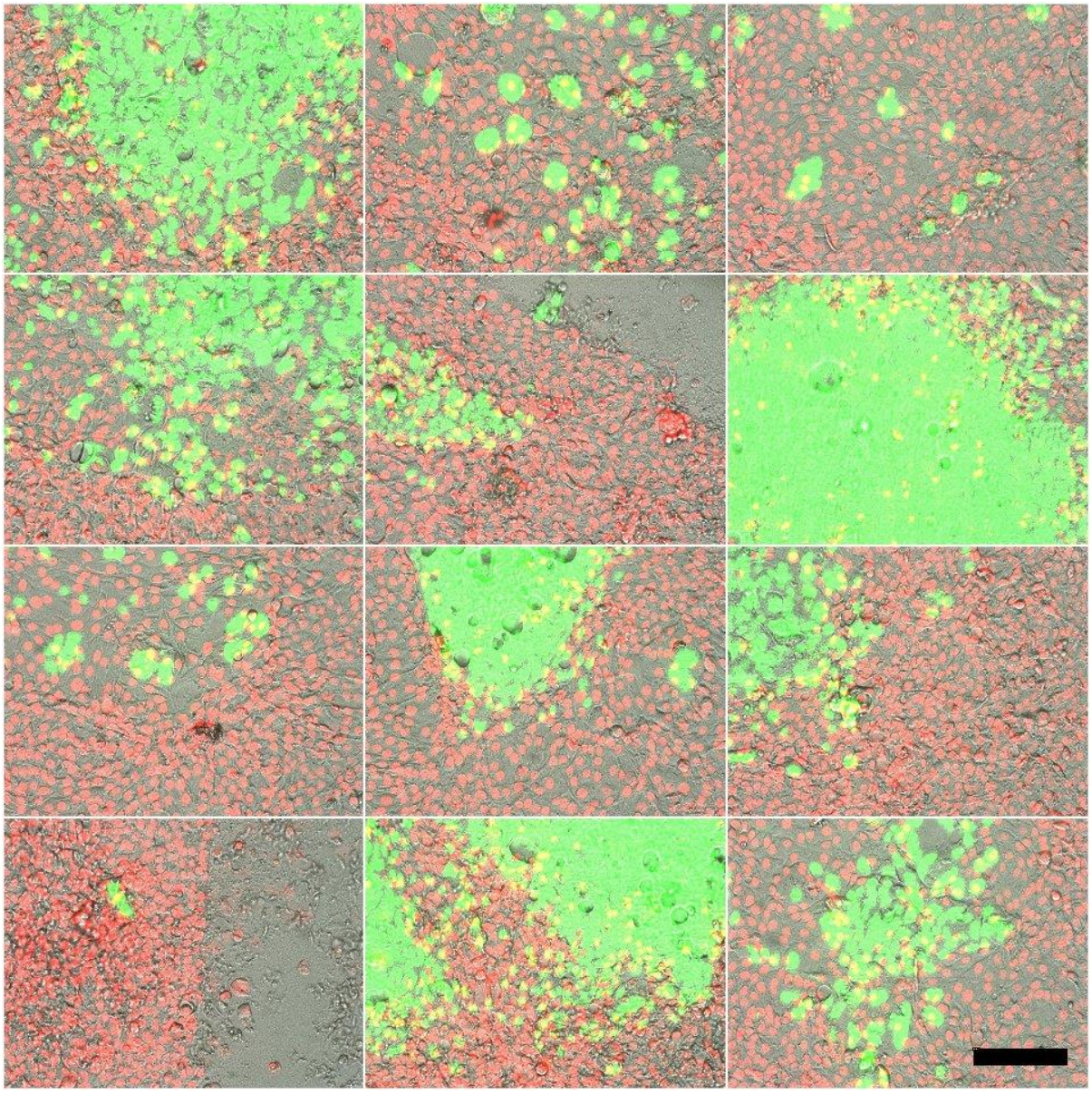

Figure 4.38. Different scenarios that can occur after 7 days of coculture. CA1a cells (green) were originally sparsely plated single cells co-cultured with densely plated 10A cells (red). After 7 days the CA1a cells show a variable degree of growth and variable degrees of compaction and size. Scale bar is 100µm.

When the CA1a cells grow in clumps they can form "domes", as illustrated by **Figure 4.39** which shows confocal images of domes formed after 3 weeks of coculture.

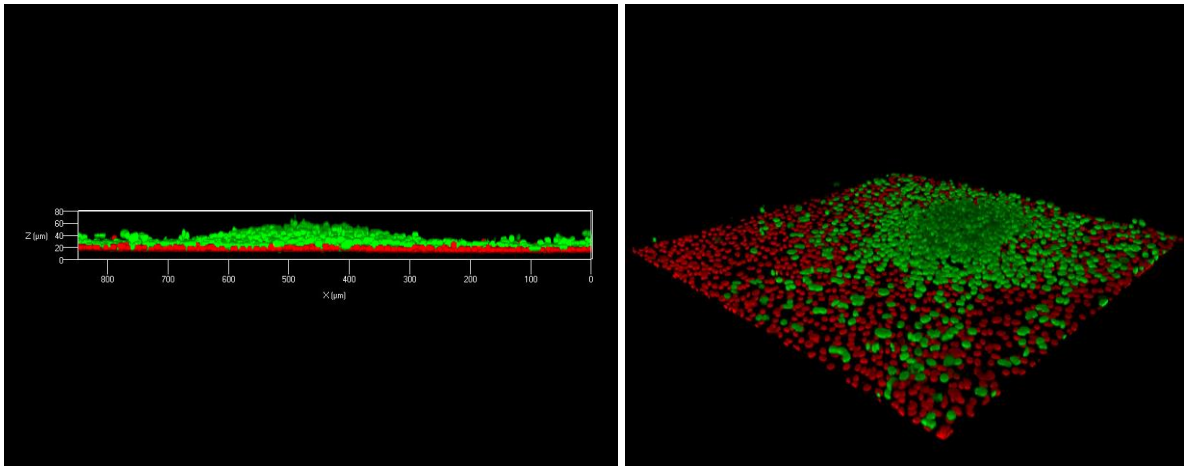

Figure 4.39. A dome is formed by tumorigenic CA1a cells. (10A cell nuclei are red, CA1a cell nuclei are green). Left image is a side view showing the profile of a dome. Right image is an oblique view of the same dome. (Taken using the Zeiss 780 Confocal)

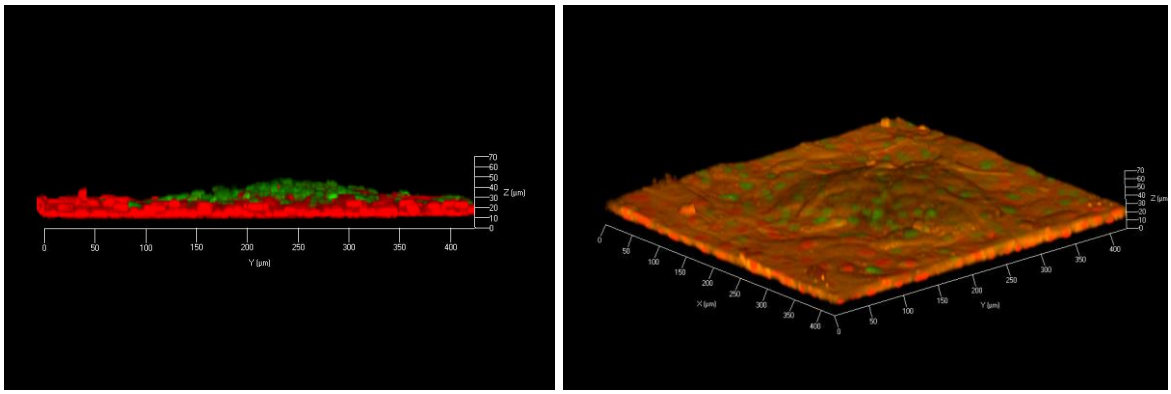

Figure 4.40. Another example of a dome, this time the cytoplasm of the cells has been labeled with Cell Tracker Orange so that the cytoplasm of the cells becomes visible.

Although the CA1a cells initially grow on top of the 10A cells, by the time they have formed domes, some of the CA1a cells (especially the ones at the center of the dome) start to infiltrate into the lower layer of 10A cells. This is shown in Figure 4.41, which shows slightly inclined 3D perspectives of domes so that the lower side of the layer of cells is visible.

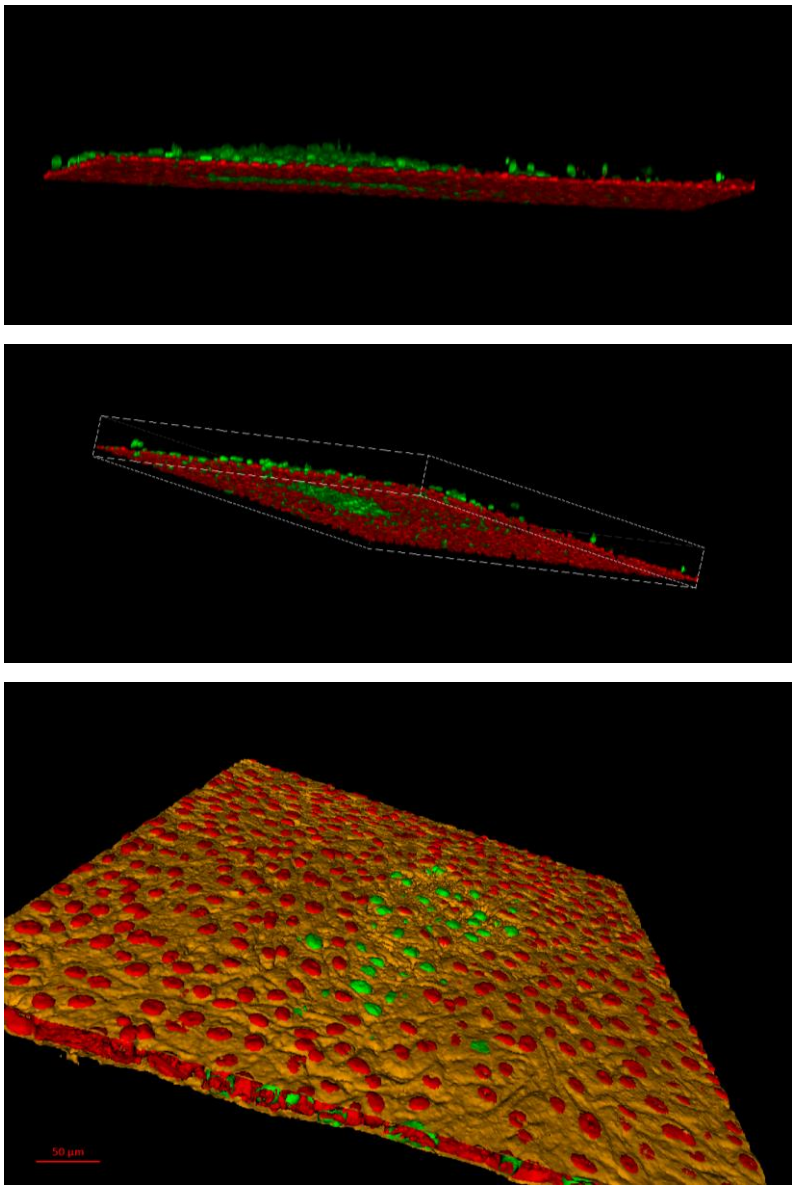

Figure 4.41. Inclined perspectives of the lower layer of 10A cells show infiltration of CA1a cells at the site of domes. (The third image is flipped; therefore the dome is underneath the visible layer).

The morphology of MCF10A cells is affected by the presence of MCF10CA1a cells

I found that the presence of CA1a cells has an effect on the morphology of 10A cells if co-cultured for a long enough period of time. In this experiment, 10A cells were first cultured to confluence and then CA1a cells were added on top of them at a low density as mentioned earlier. Images were taken four weeks after the start of the co-culture. The images show that 10A cells co-cultured with CA1a cells have larger cytoplasms (Figure 4.42B) than when they are grown alone (Figure 4.42A). (The top images are the control).

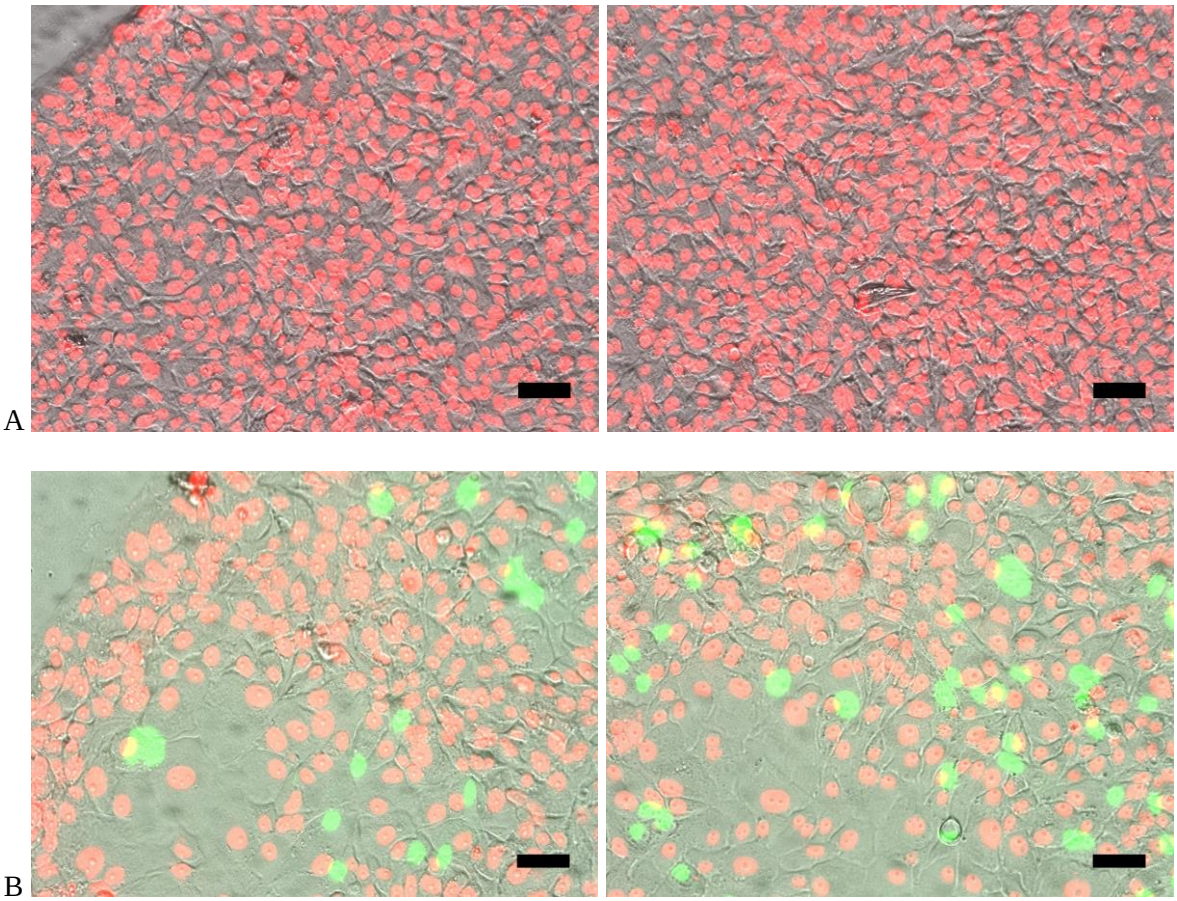

Figure 4.42. MCF10A cell size increases due to the presence of MCF10CA1a cells. A) 10A cells (red nuclei, grey cell bodies) cultured alone form a tight epithelial layer. B) 10A cells co-cultured with CA1a cells (green nuclei) still form an epithelial layer without gaps but they have enlarged cytoplasms which are visible in the gray channel. Cells were imaged 4 weeks after start of co-culture. Scale bar is 50µm.

An image montage made by tiling and stitching 15 images together reveals that the effect that the CA1a cells have on the 10A cells is local and limited in distance (Figure 4.43).

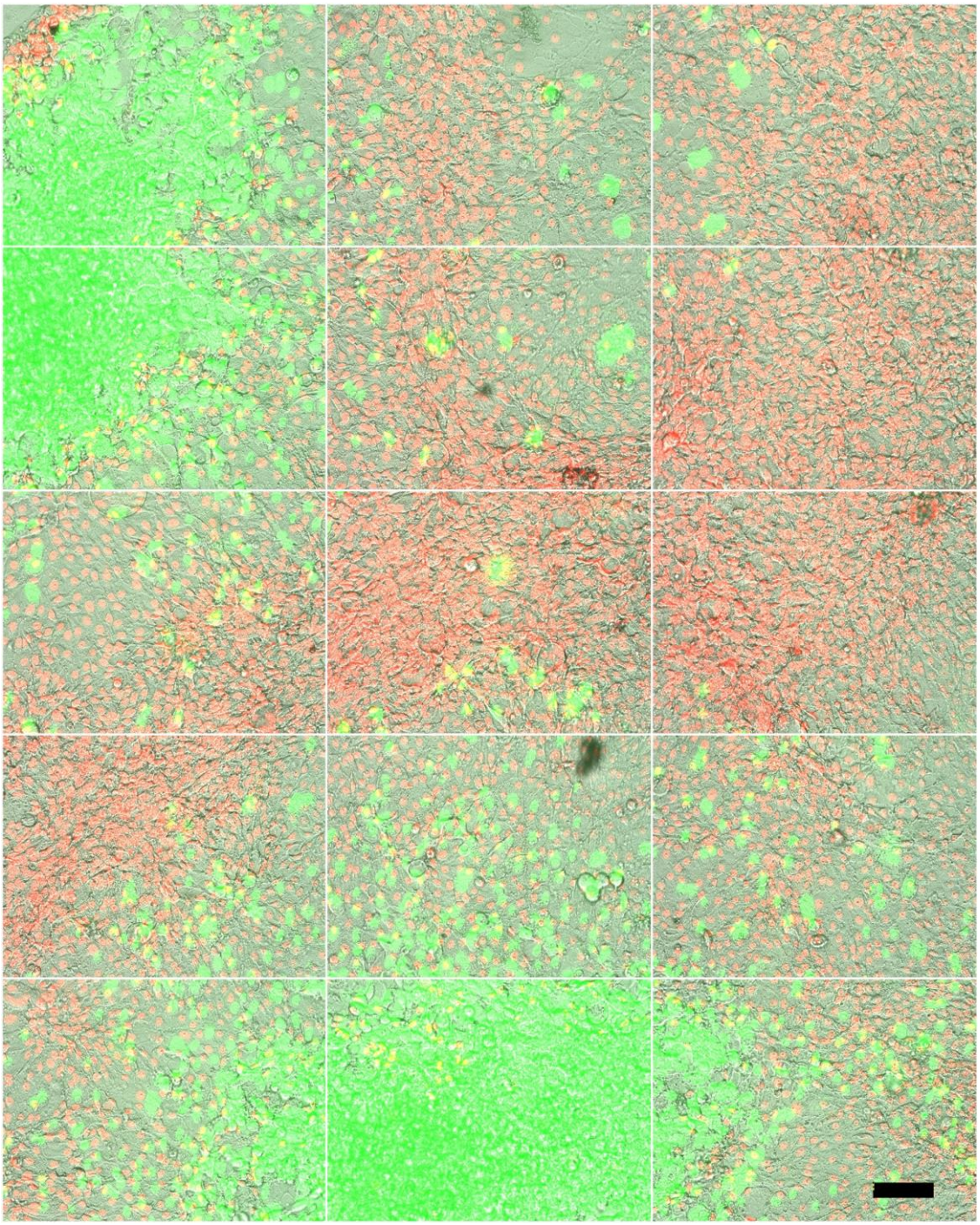

Figure 4.43 A large field of view of a co-culture of 10A cells (red) with CA1a cells (green). CA1a cells have an effect on nearby 10A cells noticeable by the lower density of 10A cells near CA1a cells. Images were acquired after 4 weeks of co-culture. Scale bar is 100µm.

An even larger field of view image which comprises the whole culture area of the dish (approximately 1cm by 1cm) is shown next. Again, the density of 10A cells appears to decrease in the proximity of CA1a cells (Figure 4.44).

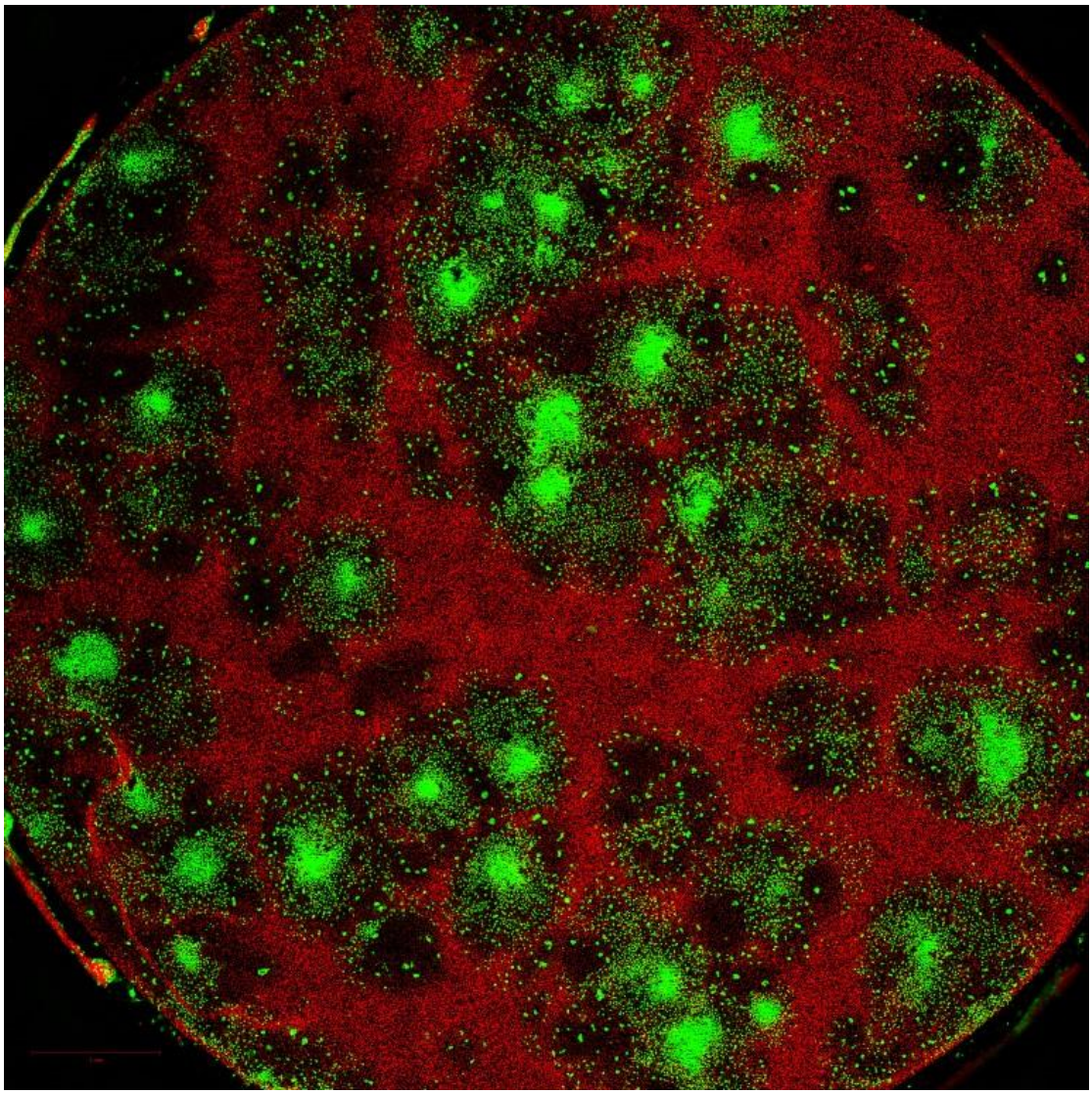

Figure 4.44. MCF10CA1a cells locally decrease the density of MCF10A cells. This is a confocal image of the whole culture area of the dish showing how CA1a cells (green) affect nearby 10A cells (red) illustrated by the dark areas that surround the green cells. Areas appear darker due a reduced density of red nuclei in those areas due to larger MCF10A cell size. Scale: Width of image is 1 cm.

Co-cultures show contact inhibited growth in 10A cells and 10AT cells, but not in CA1a cells

Here I show that co-culture with normal cells is a suitable method for detecting contact inhibited growth of malignant cells. By plating malignant or premalignant cells on top of a confluent layer of normal cells, and using different fluorescent colors for the different cell types, I can track the growth of the malignant cells and compare it to the growth of the premalignant cells. Figure 4.45 shows that only the malignant CA1a cells grow in such a co-culture.

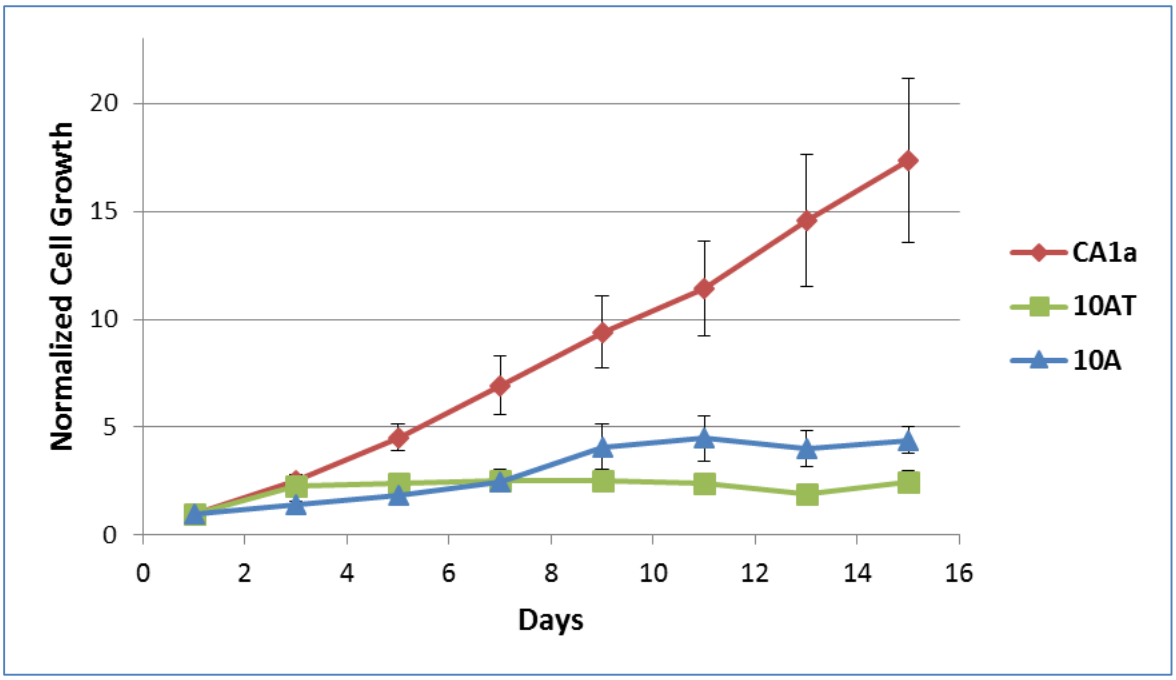

Figure 4.45. CA1a cells show a remarkable ability to grow when cultured at low density on top a confluent layer of normal 10A cells, as compared to the other cell types. (Errors bars are standard errors of 5 independent experiments).

What makes this large growth of the CA1a cells in a co-culture environment surprising is that when cultured alone, the malignant cells don't grow more than the other cell types. This is illustrated in **Figure 4.46**.

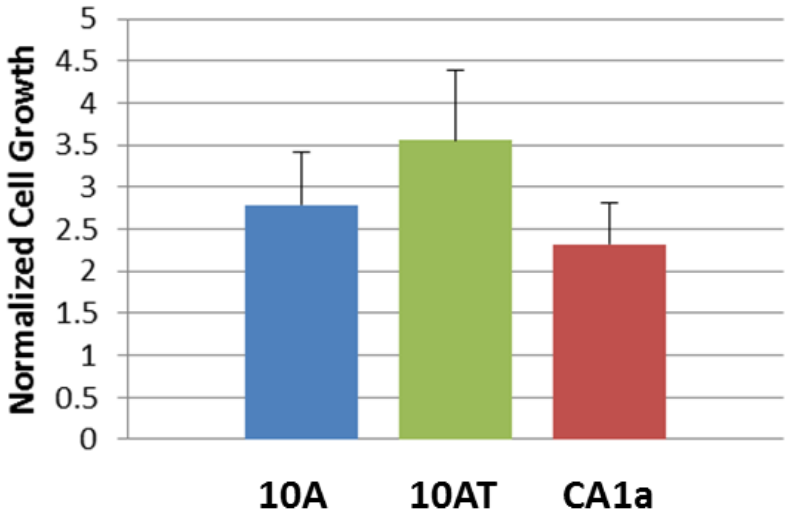

Figure 4.46. Comparison of growth rates of the three MCF cell lines used in this study. MCF10CA1a cells did not grow more than the other cell types when cultured alone in contrast to their growth in a co-culture environment. (Errors bars are standard errors of 4 independent experiments. 1 day growth).

In conclusion, even though the malignant CA1a cells grow slower than the other cell types when cultured alone, they have an ability to continue growing in an environment that makes the other cells to stop growing. Contact inhibition of growth is known to be disregulated in cancer cells. However, it is usually associated with the formation of domes in confluent cultures. Here I have shown that this absence of contact inhibition is more easily quantifiable in a coculture environment. I have also shown that the absence of contact inhibition is a unique characteristic of CA1a cells, which is absent in 10A cells and 10AT cells.

Confocal laser overexposure of CA1a cells reveals cytoplasms

While performing confocal laser imaging I discovered that even though the cells are only fluorescently marked in the nucleus, if the detector exposure and intensity of the laser is high enough, the cytoplasm of the cell also becomes visible. I used this technique to locate the cytoplasm of giant CA1a cells. **Figure 4.47** shows an example of using this overexposure to locate the area covered by the cytoplasm of CA1a cells.

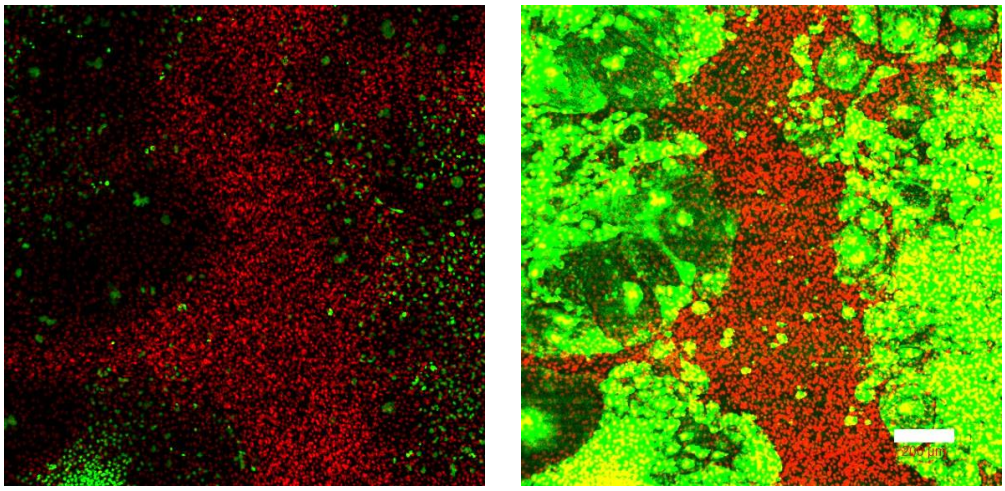

Figure 4.47. Increasing the laser power reveals the extent of cytoplasms in a coculture of CA1a cells (green) and 10A cells (red). Left and right images are the same image except for different exposure and laser intensity. Left image: regular exposure showing the green are red nuclei. Right image: overexposure in the green channel reveals the CA1a cell's cytoplasm. Scale bar 200μm.

I used this technique in conjunction with confocal transmission to reveal that 10A cells are flattened out underneath the giant cell while maintaining their epithelial attachments to other cells in the layer. This explains that their reduction in density is in fact due to a larger area covered by cells that are underneath the CA1a cells (this is illustrated in Figure 4.48.).

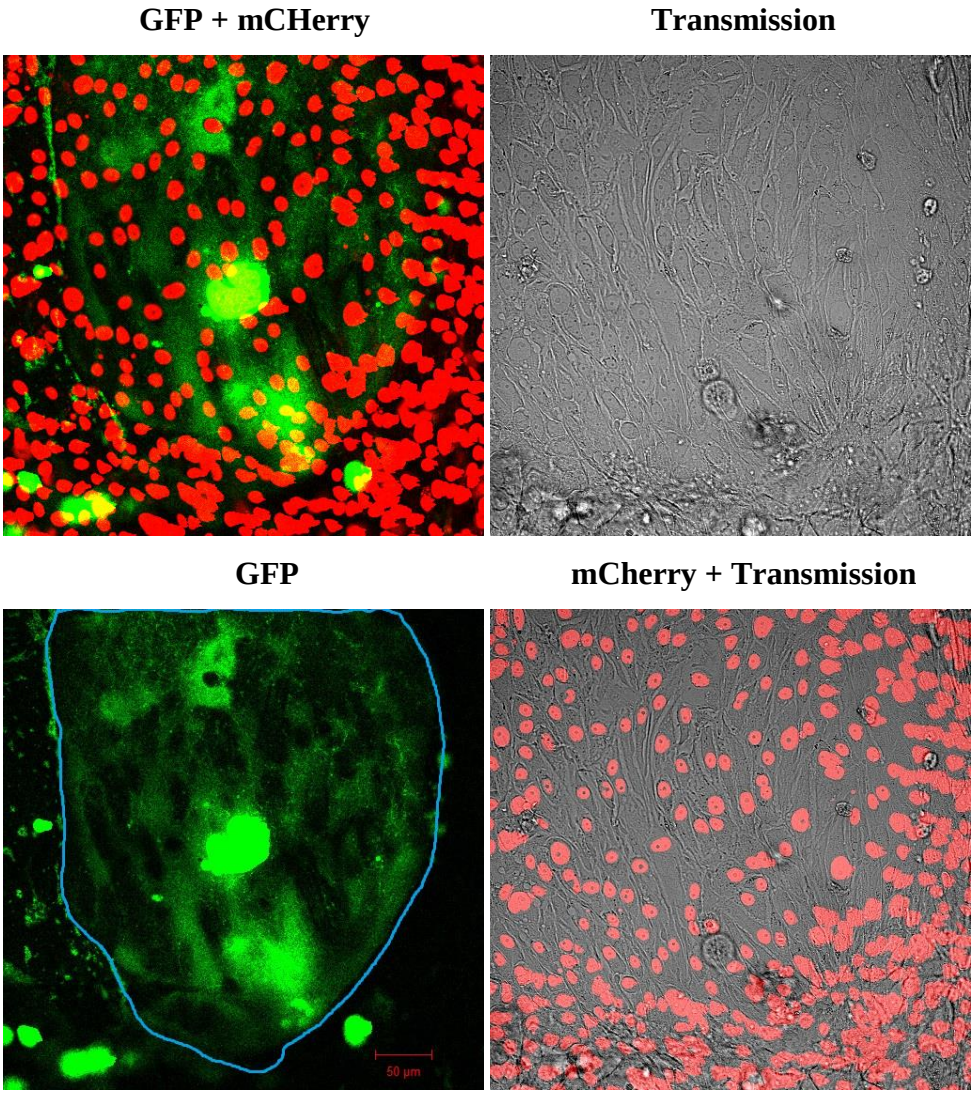

Figure 4.48. Images of one giant CA1a cell (green and outlined in blue) on a layer of 10A cells (red). The four images correspond to different fluorescence or transmission channels at the same location. The transmission image shows that the density of 10A cells is lower below the giant cell but higher toward the edges of the image. The 10A cells are forming a continuous epithelial layer but their cell bodies have been flatten out by the presence of the overlying giant tumorigenic cell. Scale bar 50µm.

Laser ablation of a CA1a cell

Now I perform laser ablation on the giant CA1a cell and I find out that its local effect on 10A cells is reversible. In other words, the 10A cells regain a normal morphology and homogeneous distribution after the CA1a cell has been ablated. For this I used a two photon laser. The laser was focused on the nucleus of the CA1a cell (shown in green in **Figure 4.49**) which resulted in the ablation of the nucleus.

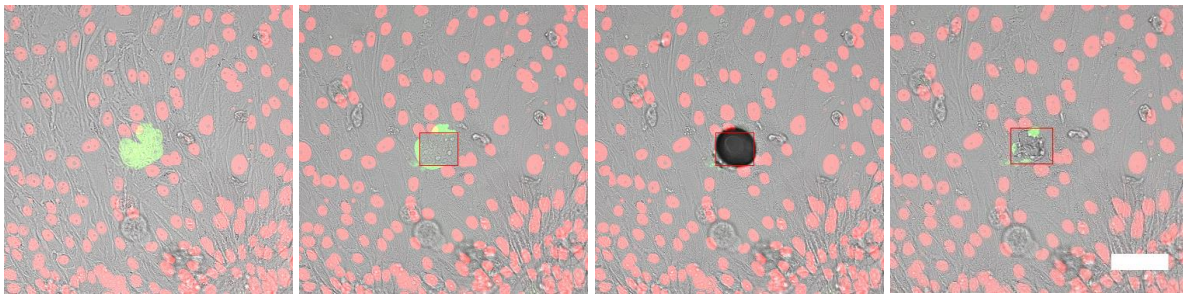

Figure 4.49. Laser ablation of the nucleus of the tumorigenic cell. The small red square is the area where the laser was focused which immediately results in bleaching of GFP fluorescence (second image). A few seconds later there is a small bubble (the black sphere in the third image). This bubble might be due to the heat of the laser, and subsides after a few seconds. Finally the fourth image shows that the nucleus has been destroyed. Scale bar 50µm.

The ablation of the giant tumorigenic cell's nucleus produces a rapid contraction of the cell and concomitant relaxation of the underlying epithelial layer of 10A cells. Indicating that the morphology and density of the 10A cells was likely mechanically affected by the presence of the cancer cells.

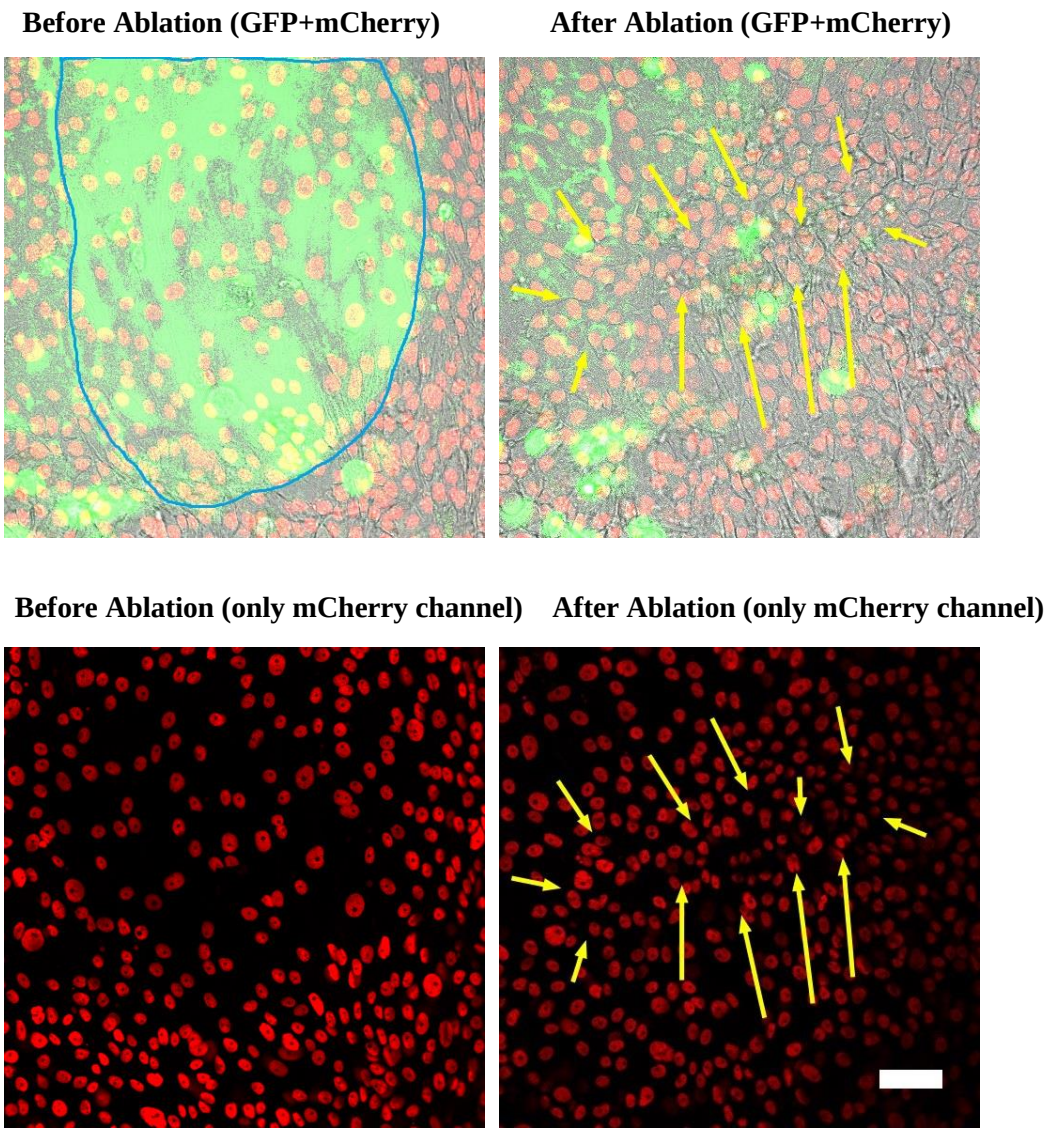

Figure 4.50. Images before and after laser ablation of the green giant CA1a cell (outlined in blue). The yellow lines indicate the trajectory of the underlying 10A cells as they regain a normal morphology and a homogeneous epithelial layer. Scale bar 50µm.

Growth of cells in Matrigel

When grown on a thick layer of Matrigel (~300 μm thick), the cells form spherical structures (known as acini) rather than the epithelial layers that I have described up to now. Cells can be cultured within the Matrigel or on top of the Matrigel. For imaging on a widefield microscope like the one that I have built it is more convenient to image the cells on top of the Matrigel, because the acini will lie on the same plane. When growing the cells on top of the Matrigel (and not within the Matrigel), Imbalzano et al. have shown that branching connections between the nodules occurs only for 10AT cells or CA1a cells but not for 10A cells.[15] See Figure 4.51.

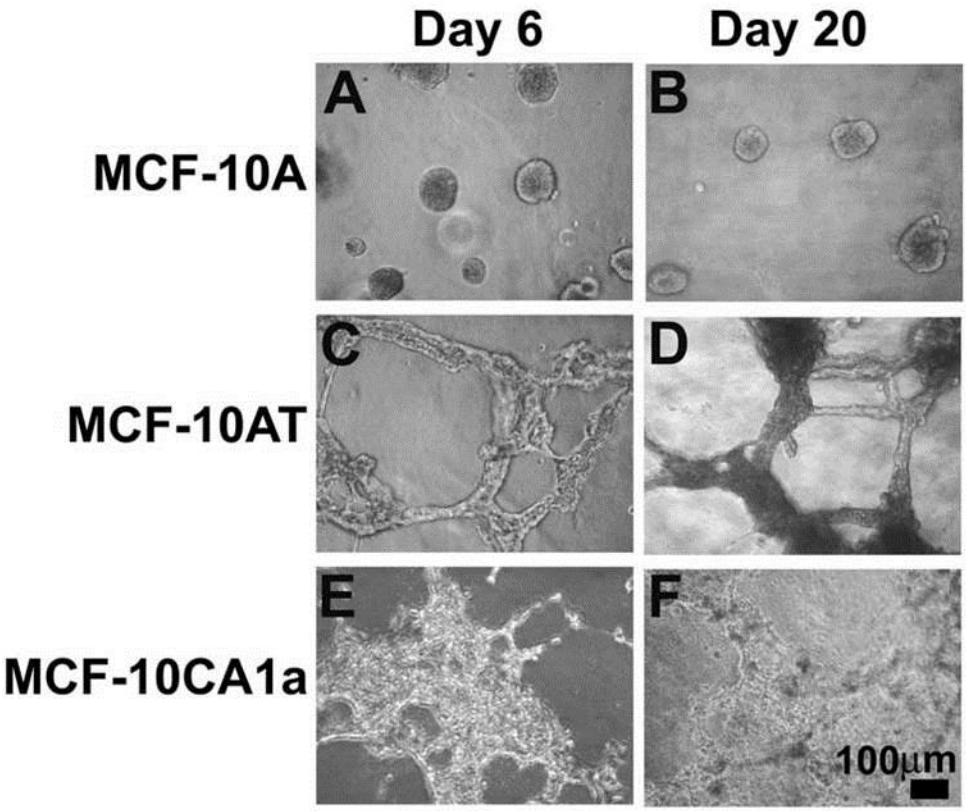

Figure 4.51. When cultured on Matrigel, branching connections between the acini occur only for 10AT cells or CA1a cells but not for 10A cells. (From Imbalzano et al).[15]

Effect of time and density on branching connections

I find that branching connections are formed as early as day 1 when plating 10AT cells or CA1a cells on Matrigel, and that the branches become more numerous when plating the cells at higher densities and become thicker as time passes (this is shown for 10AT cells in Figure 4.52).

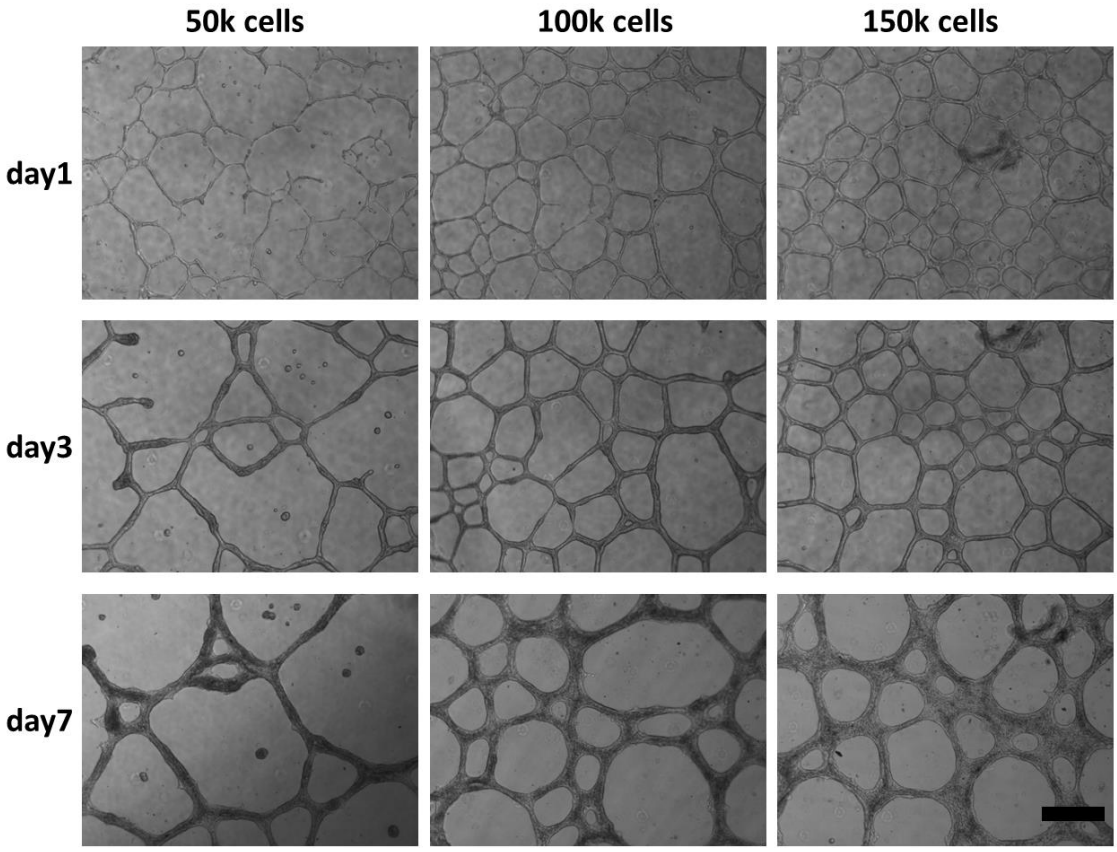

Figure 4.52. 10AT cells plated on Matrigel at different densities. Branches become more numerous at higher densities and become thicker with time. Scale bar 500μm.

The same is true for CA1a cells (Figure 4.53.), although in this case outgrowths of cells from the branches can be seen by day 7.

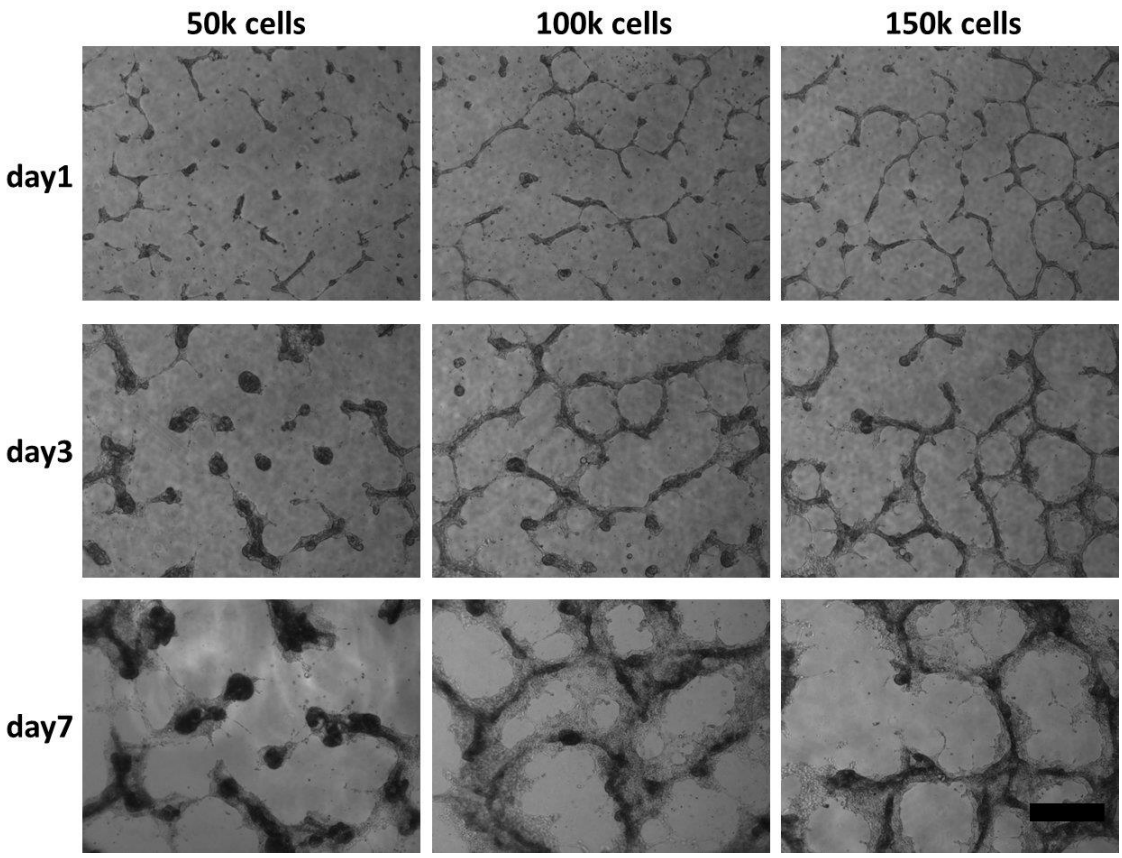

Figure 4.53. CA1a cells plated on Matrigel at different densities. Branches become more numerous at higher densities and become thicker with time. Additionally outgrowths growing from the branches can be seen by day 7. Scale bar 500µm.

If we go to an extreme and plate ten times more cells (~a million cells) the branching connections can form within just a few hours. This is illustrated in **Figure 4.54**.

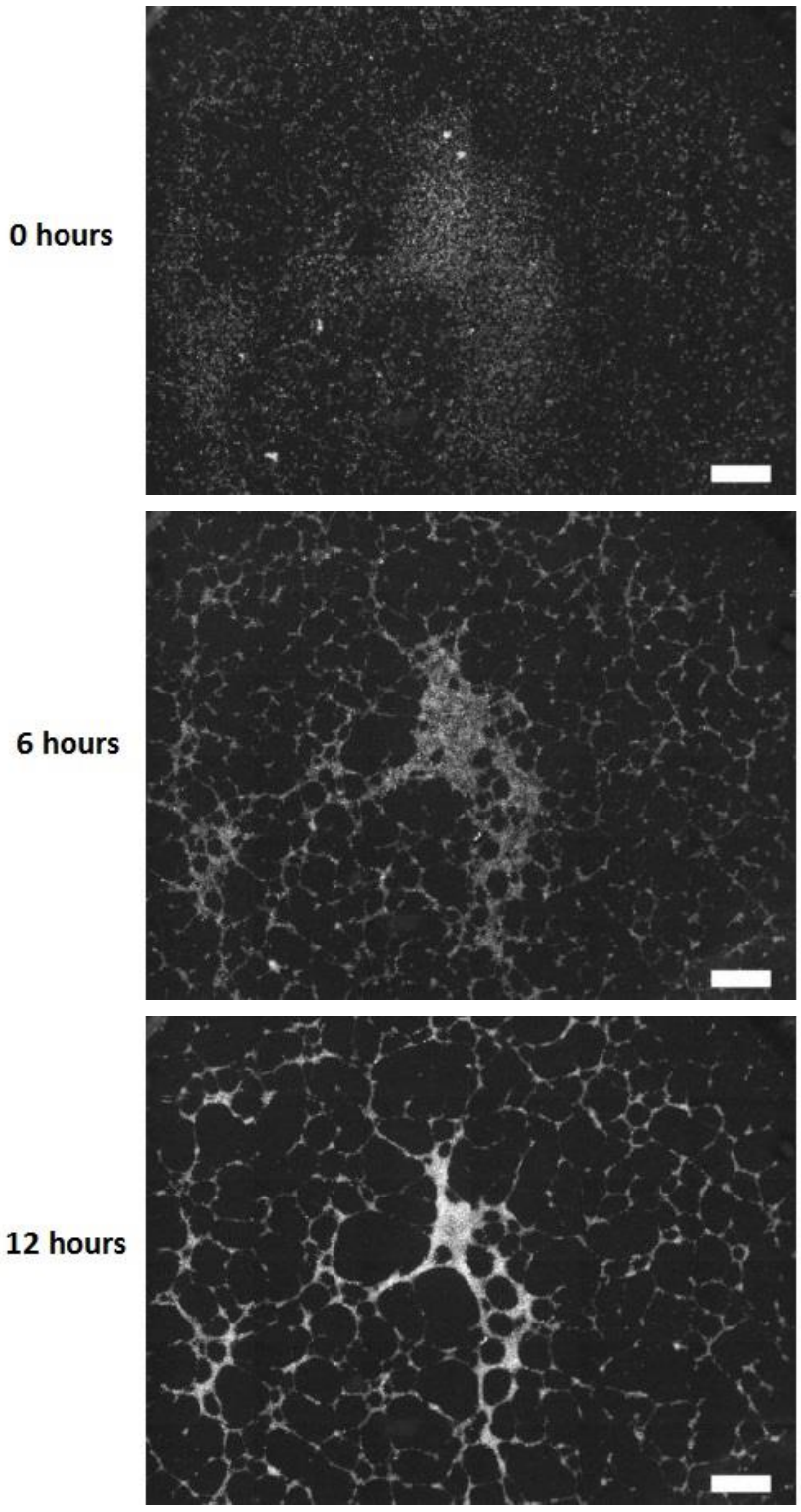

Figure 4.54. When plated at very high densities, the cells will form branches within 6 hours. (CA1a cells). Scale bar 1mm.

Long term culture of acini

Figure 4.55 shows long term culture (8 weeks) of 10A and 10AT acini. (CA1a cells typically cannot be cultured for so long and will be analyzed in a later section).

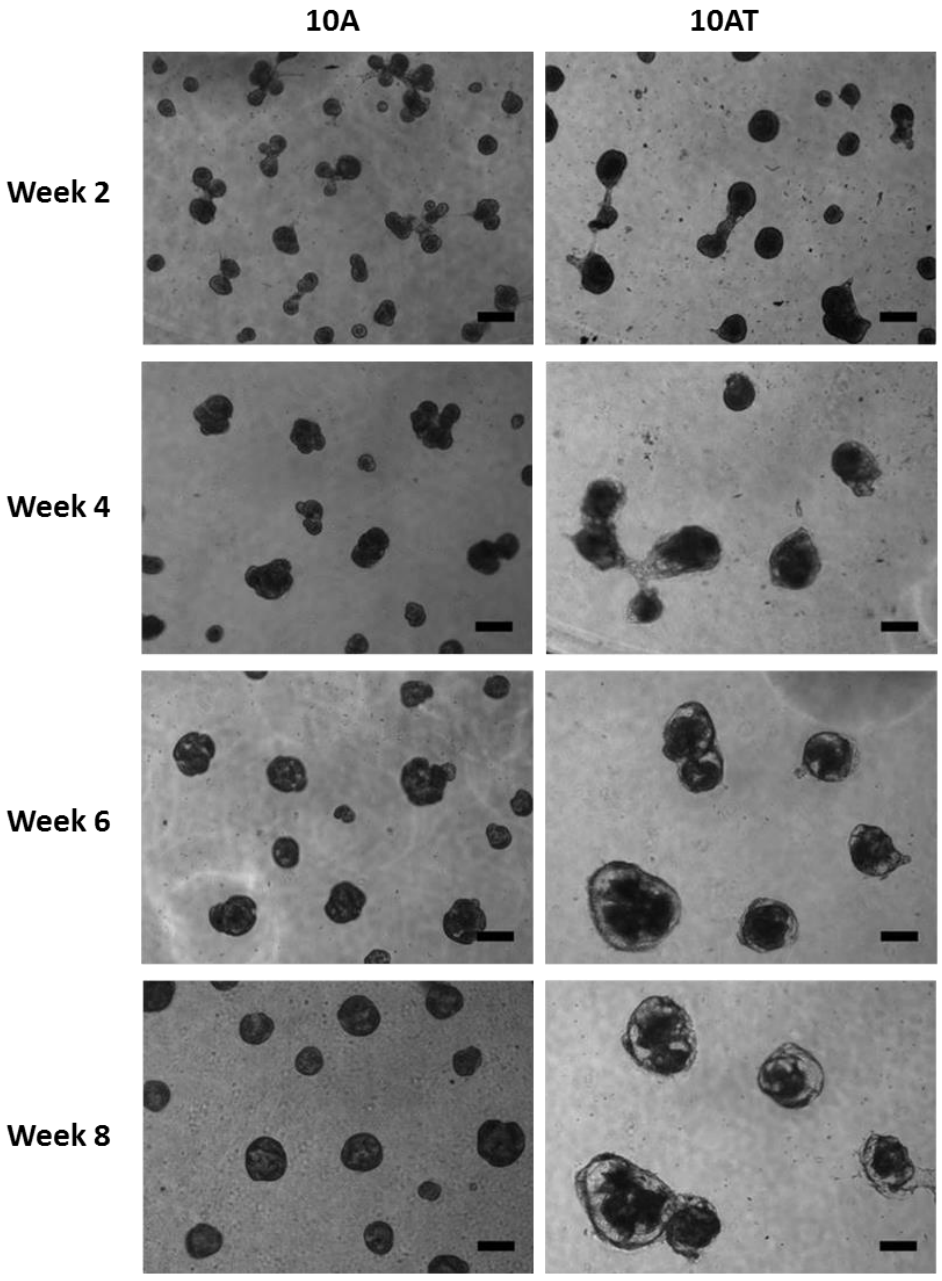

Figure 4.55. 10A and 10AT acini cultured for 8 weeks. The 10AT cells form larger structures than 10A cells. Scale bar 300μm.

The 10A acini stop growing around week 4 but 10AT acini keep growing in size up to week 8. The 10A acini maintain a more rounded phenotype than the 10AT acini. Also, the 10AT acini have white areas within the acini that are not present in the 10A acini. Histone-GFP confirms that these white areas are free of cell nuclei (Figure 4.56.).

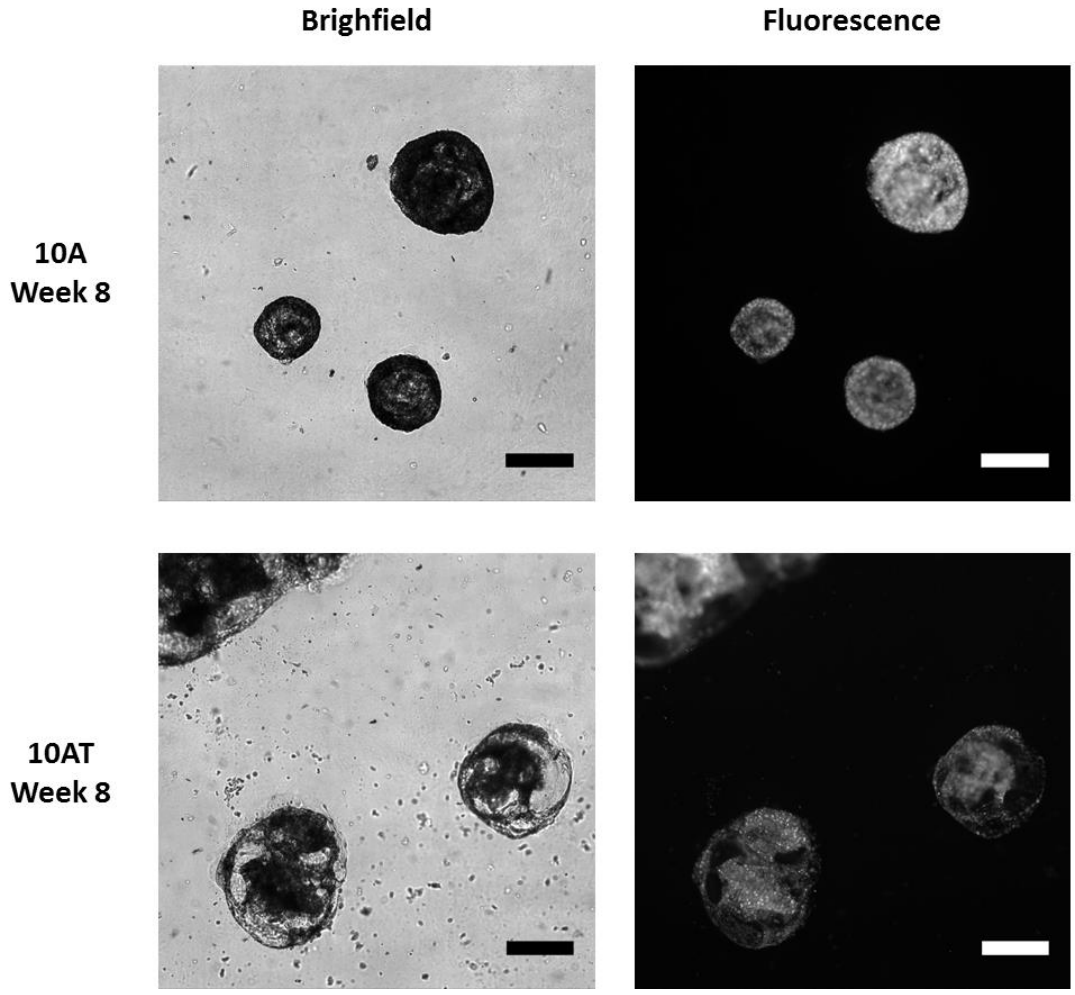

Figure 4.56. Brightfield and fluorescent images of 10A and 10AT cells after 8 weeks of culture. While 10A acini are homogenous, 10AT acini show an uneven distribution of cells within the acini. Scale bar 300μm.

Next I will show that when CA1a cells are cultured in acini, they often disassemble via migrating sheets of cell.

Migrating sheets of cells originating from CA1a acini

The CA1a cells usually form acini for the first 6 days. Then I often observe migrating sheets of cells originating from the CA1a acini. These are different from the branching connection that we saw earlier. These sheet outgrowths can happen spontaneously and I will later show what promotes their appearance. In Figure 4.57 sheet outgrowth (migrating sheets of cells) occur suddenly at day 6.5.

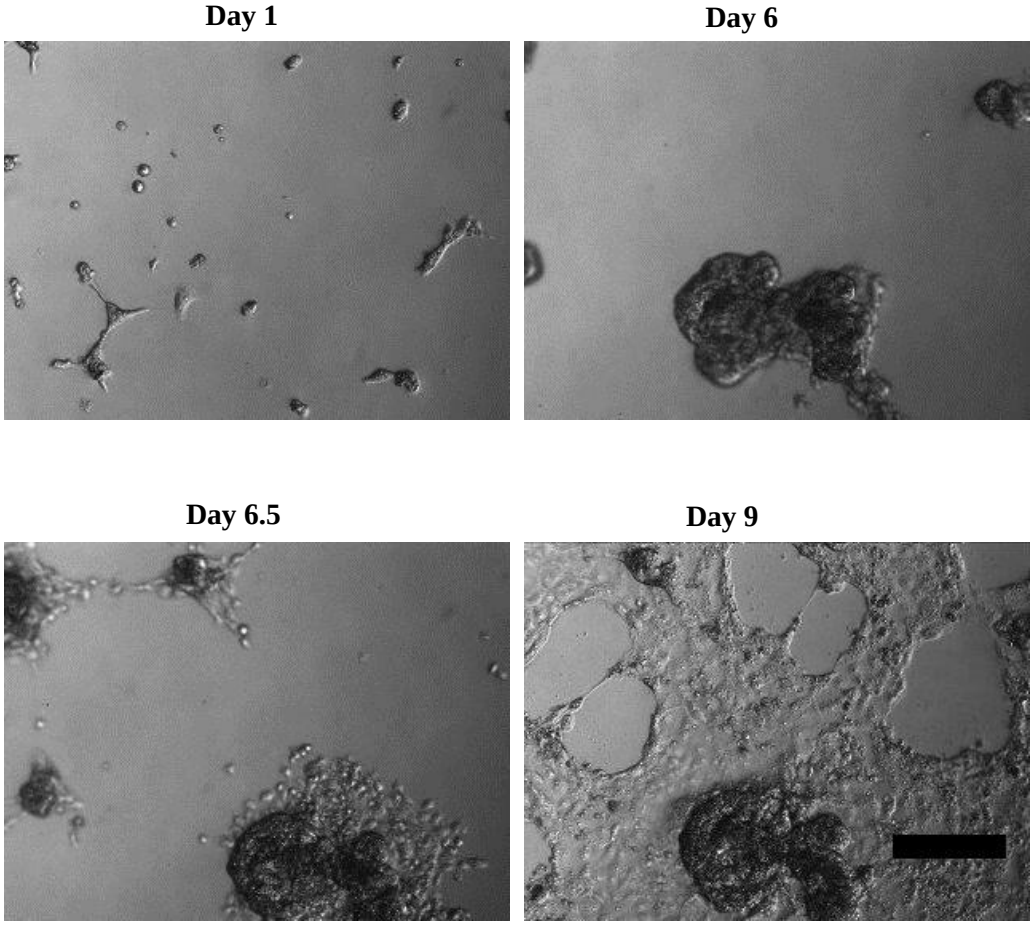

Figure 4.57. CA1a form acini by day 6. At day 6.5 the acini have sheet outgrowths. Scale bar 400μm.

These outgrowths are cells that are migrating out of the acini and form epithelial sheets on top of the Matrigel. In some cases, 10AT cells can also have sheet outgrowths like the CA1a cells, but they take longer

to do so and are less pronounced. Whereas CA1a cells can have outgrowths within 7 days, 10AT cells do so at day 16 as **Figure 4.58** shows.

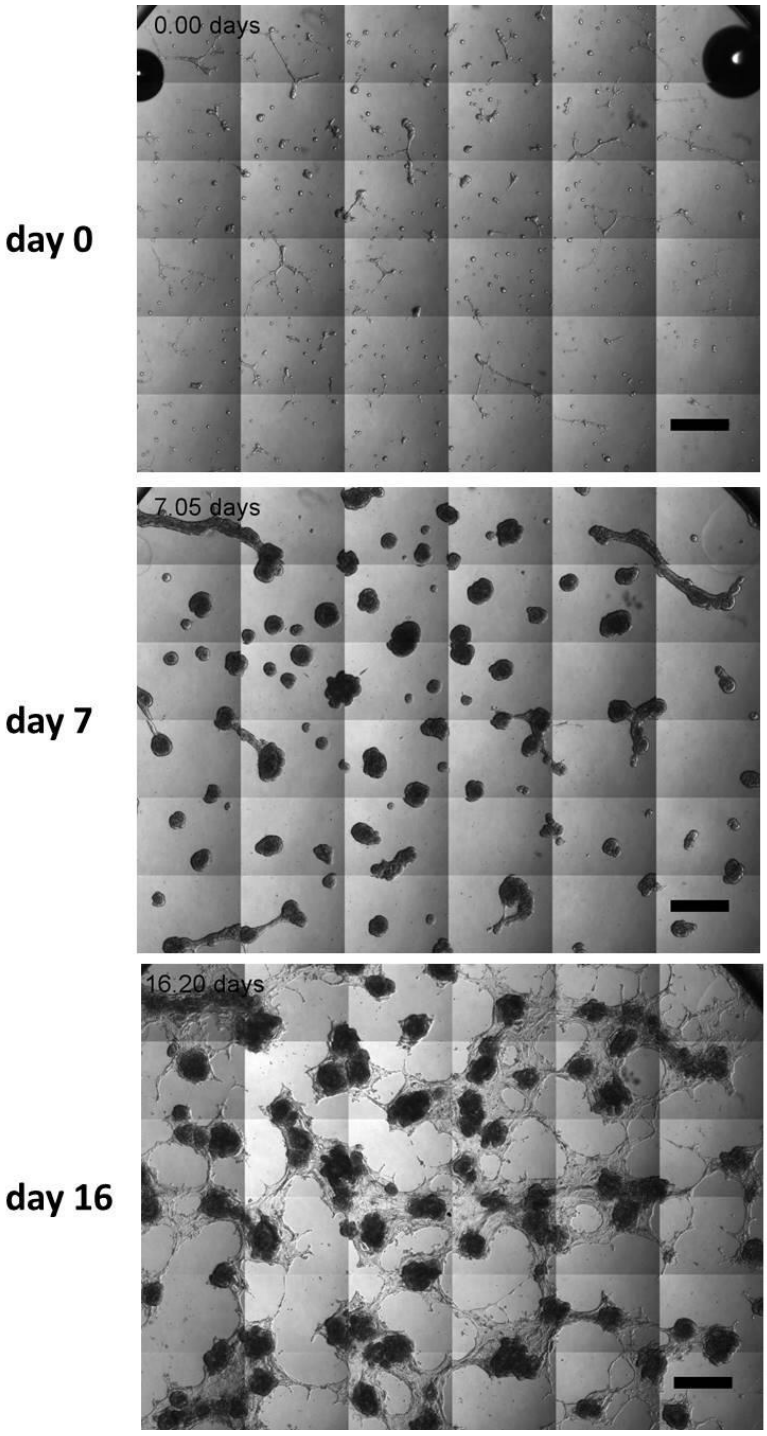

Figure 4.58. 10AT cells grown on Matrigel have formed acini by day 7. By day 16 some outgrowths emerge from the acini. The darker regions are the three dimensional acini, whereas the lighter regions are thin sheets of cells. The large number (layers) of cells in the acini cause them to appear dark. Scale bar 1mm.

Coculture of 10A cells and CA1a cells in Matrigel: Invasive strands

When 10A cells and CA1a cells are cultured together in the same dish on top of Matrigel they form acini that may contain both types of cells as well as acini that only contain one type of cell. No immediate differences are apparent between these acini, as Figure 4.59 shows.

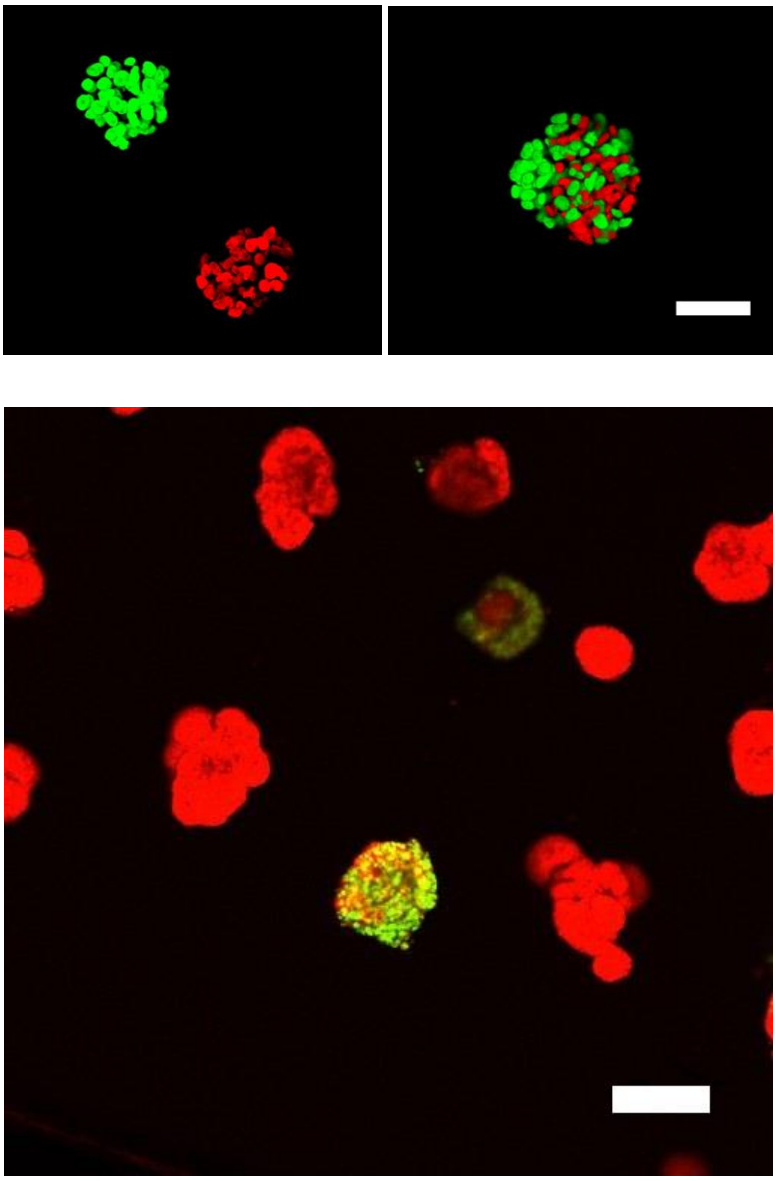

Figure 4.59. Images of 10A cells (red) and CA1a cells (green) cultured on Matrigel. Some acini have both types of cells, but no significant differences are apparent. Scale bars 50µm top, 200µm bottom.

CA1a cells are the leader cells of invasive strands in cocultures

A difference that emerges when the cells are cultured for long periods of time is that the tumorigenic cells create invasive strands in Matrigel. The leading cell of the invasive strand is called the leader cell. The leader cell tends to be highly motile and the other cells usually closely follow the leader cell (**Figure 4.60**).

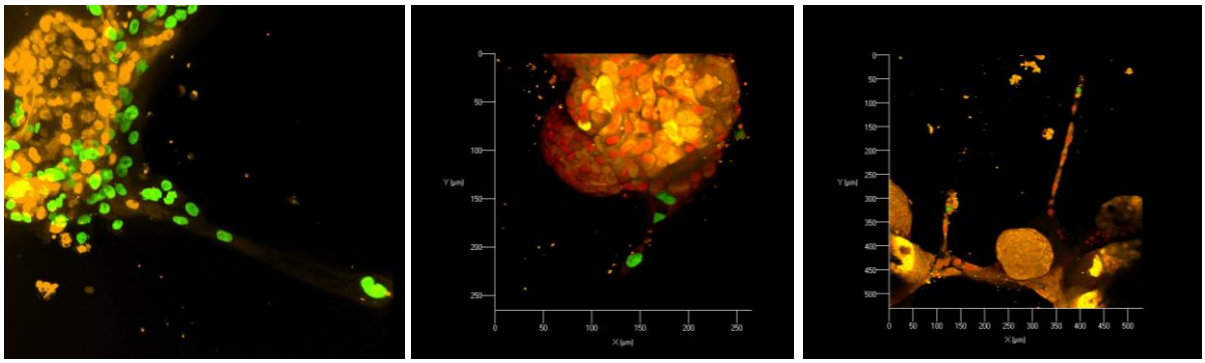

Figure 4.60. Examples of invasive strands in cocultures of cells on Matrigel. The leading cell of the invasive strand tends to be a CA1a cell (shown in green because of nuclear Histone-GFP). Red is 10A nuclei and orange is the cytoplasm cell tracker orange.

When coculturing 10A cells with 10AT cells (or CA1a cells) at a ratio of 4 to 1 (done so to simulate a real tumor environment) we find that the Ca1a cells are more likely to be the leader cell of invasive strands by day 6. (The cells were mixed and plated on top of a thick layer of Matrigel as described in the Methods section of the following section of this thesis). **Figure 4.61** shows that even though the cells start by being outnumbered by 10A cells (4 to 1), the CA1a cells are almost 100 percent of the time the leader cells of the invasive strand. On the other hand, 10AT cells are only about 50 percent of the time the leader cells. This is a striking difference between the aggressive CA1a cells and the premalignant 10AT cells.

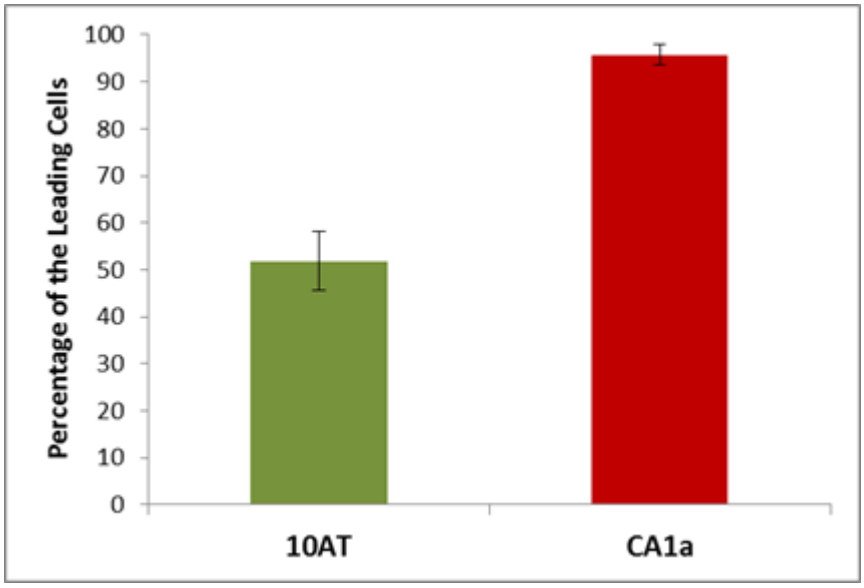

Figure 4.61. In a coculture with 10A cells, CA1a cells are the leader cells of invasive strands almost 100% of the time, while 10AT cells are only 50% of the time the leader cells. ($P<0.01$, n=9 independent experiments).

CA1a cells affects the morphology of 10A acini

Previously I showed that CA1a cells can affect the morphology of 10A cells when they are cocultured for long periods of time in a petri dish without Matrigel. Here I will do the same coculture but this time using Matrigel as the substrate instead of plastic (the Matrigel layer is several hundred microns thick to allow the formation of acini).

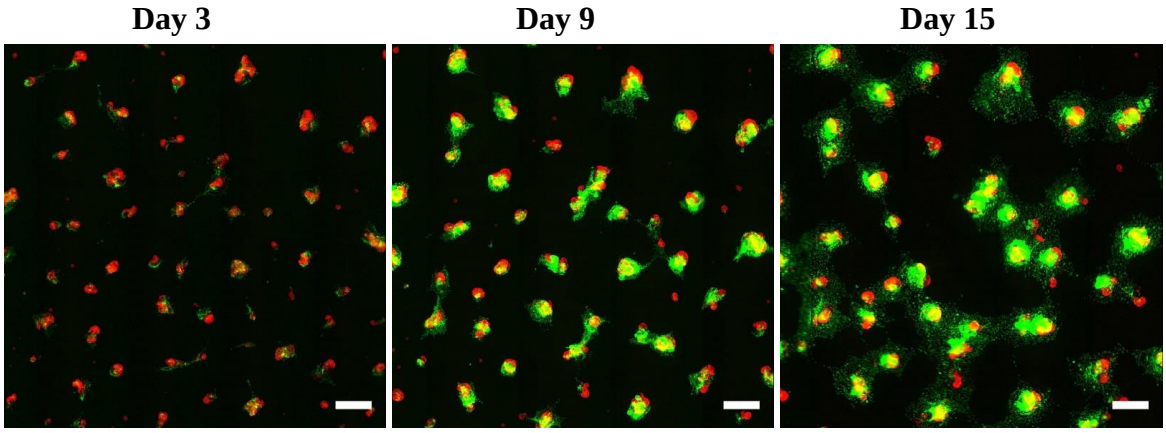

Figure 4.62. Coculture of 10A cells (red) and CA1a cells (green) plated at a ratio of 10:1 on top of Matrigel. Scale bar 1mm.

In Figure 4.62 10A cells and CA1a cells were plated at a ratio of 10:1 (10A cells outnumber CA1a cells by ten to one). Therefore during the first days there are more 10A cells (shown in red) than CA1a cells (shown in green). By day 9, the CA1a cells have overgrown the 10A cells. By day 15 it is clear that the CA1a acini have outgrowths extending from the acini.

By measuring the size of the 10A acini, we can tell whether the presence of CA1a cells affects the morphology of 10A acini. To see this clearly Figure 4.63 (A) shows 10A cells cultured alone (control) and (B) is the coculture of 10A cells and CA1a cells where only the 10A cells are fluorescent (red color) and the CA1a cells appear in grey.

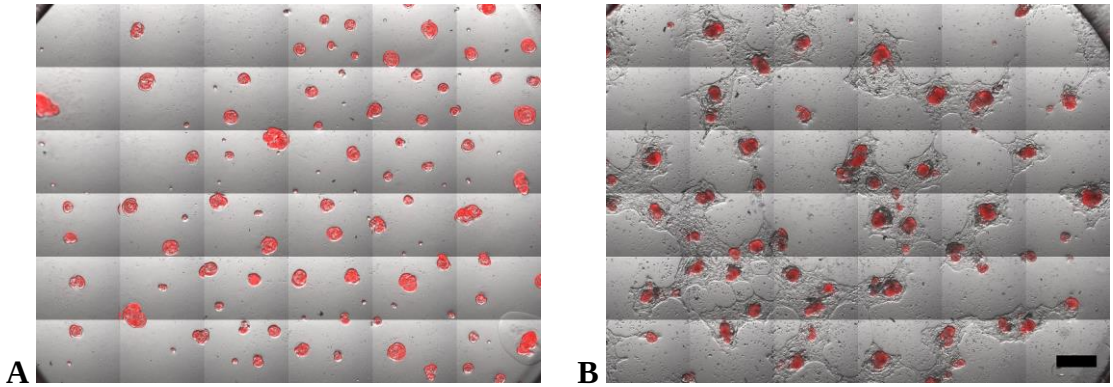

Figure 4.63. 10A cells were grown alone (A) or with CA1a cells (B). 10A cells are shown in red and CA1a cells are visible as non-fluorescent cells that spread out from the acini. (Day 12 after plating). Scale bar 1mm.

Figure 4.64 shows close-ups of the previous figures, additionally including cocultures of 10A cells with 10AT cells.

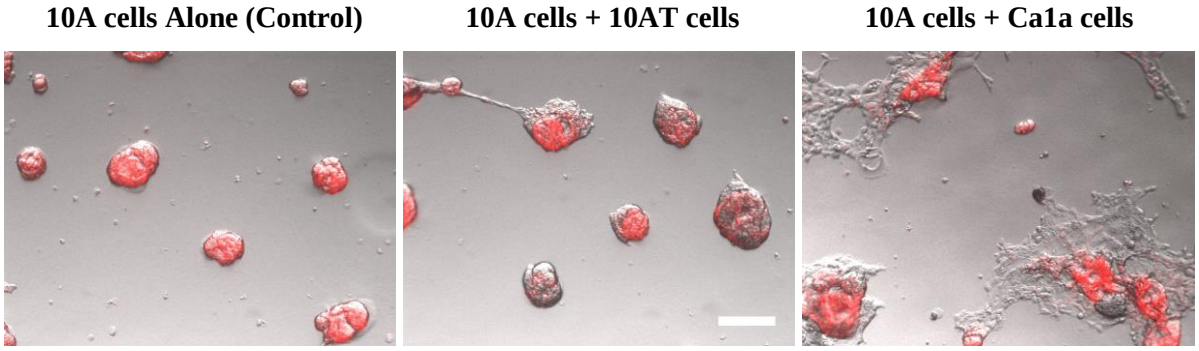

Figure 4.64. 10A cells alone, 10A cells + 10AT cells and 10A cells + CA1a cells were imaged after 6 days of culture on Matrigel. Only the 10A cells were fluorescent to show the area covered by the 10A cells under the effect of coculture. CA1a cells are seen spreading out from the acini and affecting the shape of the 10A acini. Scale bar 200µm.

From the images, it can be seen that the 10A cells are more spread out when cocultured with CA1a cells than when cultured alone. By performing measurements on the area covered by the 10A cells I confirm this observation and the results are shown in Figure 4.65.

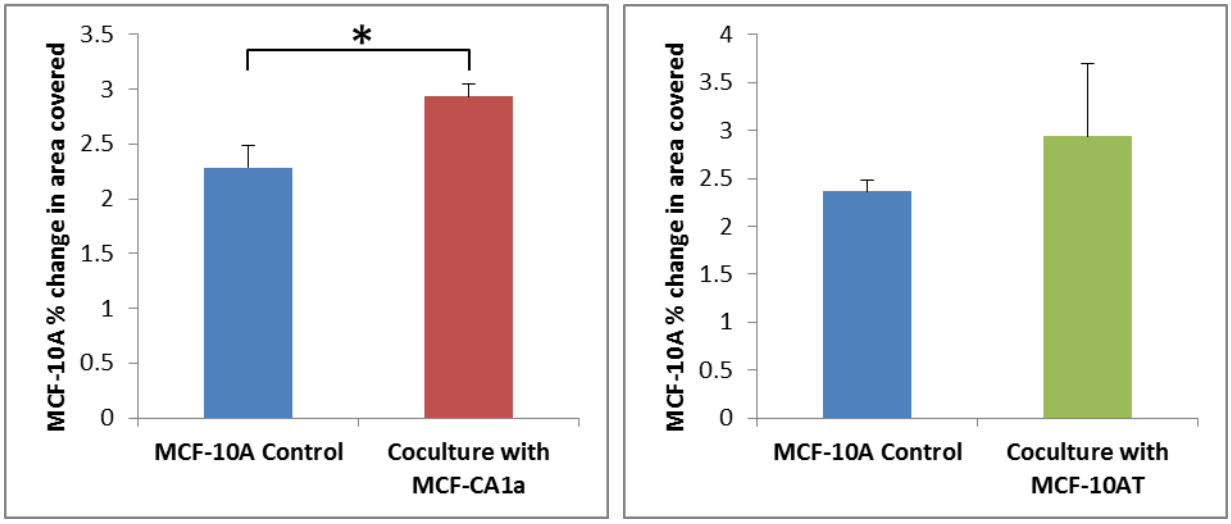

Figure 4.65. Left chart: The 10A cells were significantly affected when cocultured with CA1a cells as measured by the area covered by the cells. Each bar represents the average of 125 images taken in 5 independent experiments. * P<0.05. Right chart: When cocultured with 10AT cells, 10A cells also on average covered a larger area but the P value was not significant in this case.

Method: 10A cells were culture alone or were cocultured with either 10AT cells or CA1a cells at a ratio of 4:1. This ratio was chosen because in a real tissue normal cells outnumber cancer cells at least in the early stages of cancer. First, 80ul of Matrigel (BD Biosciences part # 356237) were placed on the glass portion of an In Vitro Scientific 29mm dish (part # D29-10-1.5-N). The Matrigel was allowed to solidify inside the cell culture incubator for 30 minutes. Then the cells to be cocultured were trypsinized, centrifuged and resuspended, and the cell numbers were counted with a hemocytometer. The cells were mixed at the ratio of 20000 normal cells to 5000 tumorigenic cells (or 25000 normal cells when cultured alone) before plating on the dishes and a total of 25000 cells was plated on each dish containing 2.5ml of medium. Each experiment was repeated on 5 different days. The dishes must be carefully shaken before the cells settle on the Matrigel to obtain an even distribution of cells. The dishes were placed in an incubator at 5% CO2. The medium was changed every 2 days by replacing half of the medium with new medium. The dishes were imaged with the microscope at days 3 and 6 using both brightfield and fluorescence. Fluorescence images of the normal MCF10A cells were used to quantify the area covered by the cells on the dish with the help of a computer program (NIH ImageJ).

Results: When normal MCF10A cells were cocultured with either the malignant MCFCA1a cells or the premalignant MCF10AT cells, the MCF10A cells covered a larger area after 6 days than when cultured alone (Figure 4.65). However, only the MCFCA1a cells showed a statistically significant increase under a paired t-test ($P<0.05$, $n=5$).

Sheet outgrowths reveal dynamic response of cells to new medium

Here I will show that the sheet outgrowths of acini happen concomitantly with medium change when the medium is renewed (typically the medium is renewed every 2 or 3 days). Analyzing the dynamics of established acini during several rounds of medium renewal reveals how this happens. To quantify this effect I used image analysis tools to automatically measure the area that is covered by the acini during time lapse imaging. Figure 4.66 is the result of measuring the area covered by the acini and their outgrowths over 30 days. The vertical green lines in the graph indicate the time points at which the medium was changed.

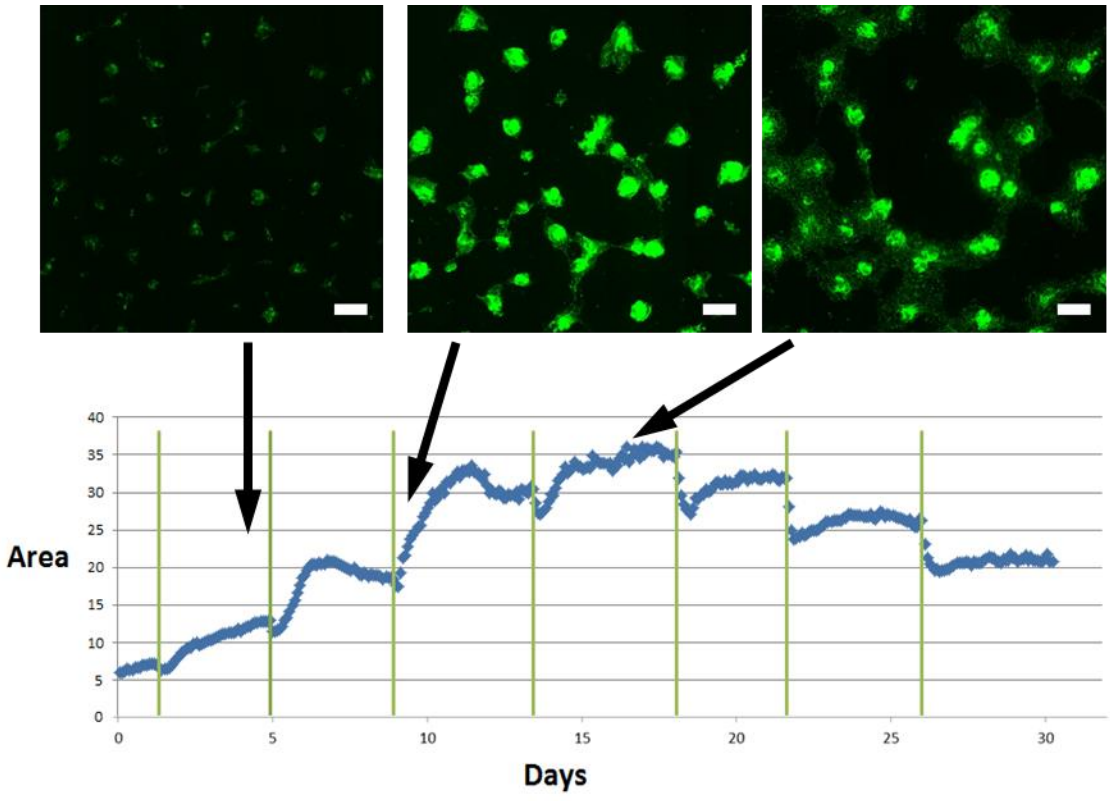

Figure 4.66. The area covered by the CA1a acini and their outgrowths over 30 days. The green vertical lines in the graph are the time points at which the medium is renewed. Each time the medium is renewed it causes the area to initially decrease slightly and then increases sharply. The black arrows point to the time points at which the three example images that are shown were taken. Scale bar 1mm.

The graph shows that the outgrowths of acini happen concomitantly with medium change. Each time the medium is renewed, the acini contract for a few hours before expanding strongly for the rest of the day. Then the expansion slows down for about another day until the medium is changed again.

It is unlikely that the outgrowths are exclusively caused by an increase in the number of cells since the time-lapse movies show that the cells are migrating.

To see if the area covered by the acini is affected by the frequency of medium renewal, I performed the following experiment: the medium was either changed 1.5ml every 2 days or 0.75ml every 1 day. This way the total medium changed is equal in both cases. The result is that changing medium every 2 days results in a higher area covered. See Figure 4.67. (Continuous means every 1 day and Stepped means every 2 days).

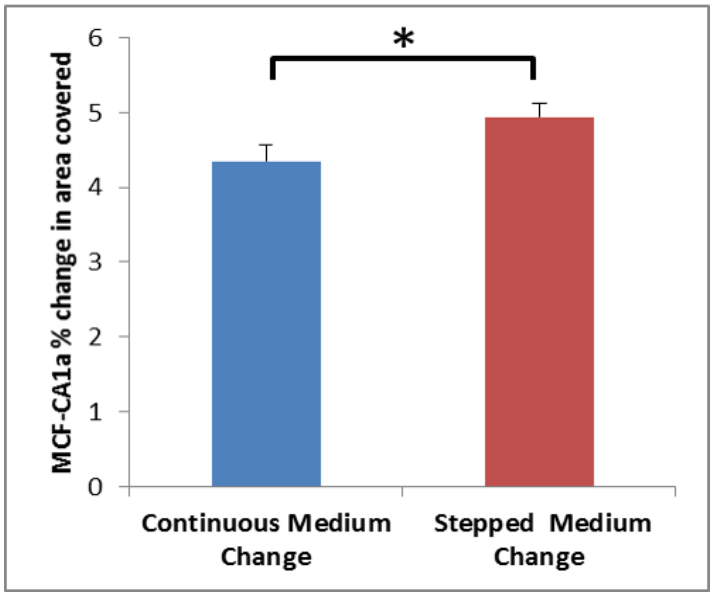

Figure 4.67. Changing the medium in a more continuous way results in a lesser expansion of the acini. (Where "Continuous" means medium renewal every day, "Stepped" means renewal every 2 days, but twice the amount of medium. Total medium change was the same in both cases). (*P<0.01 for paired t-test.)

Invasion is induced by serum deprivation and by EGF

Given that I have shown that changing the medium affects the invasive outgrowths, I set out to find out what the role of the FBS (serum) is on these invasions. Ye et al. have shown that serum starved MDA-MB-231 have increased invasion.[27] However, they use specialized Boyden chambers that use EGF as an attractant to measure invasion. Here I perform time-lapse imaging of acini on Matrigel and measure the maximum diameters as a way to quantify the invasion without the need to use any chemoattractants. (Where "maximum diameters" is the length of the largest invasive strand in each acini). "Invasion" is different from chemotaxis because only a subpopulation of cells invade and create an invasive strand in a random direction. The fact that these invasive strands are created within a 12 hour period allows us to rule out cell growth because the invasive strands are much larger than any possible growth during that period (also time lapse movies show that the invasive cells are migrating). 100,000 cells were plated on a thick layer of Matrigel as in previous experiments. At day 4 of culture the medium was replaced with either 10% FBS DMEM or 0%FBS DMEM. Imaging was performed for the next 12 hours. It is important to use time lapse (taking images every few minutes) because often acini will merge with each other, which will lead to erroneous measurements. We must only measure acini that have not merged with other acini. The results are shown in **Figure 4.68**, which shows that CA1a cells have a characteristic ability to invade when there is no serum, and this effect is not present in the other cells lines. In fact, the 10A cells contract when there is no serum.

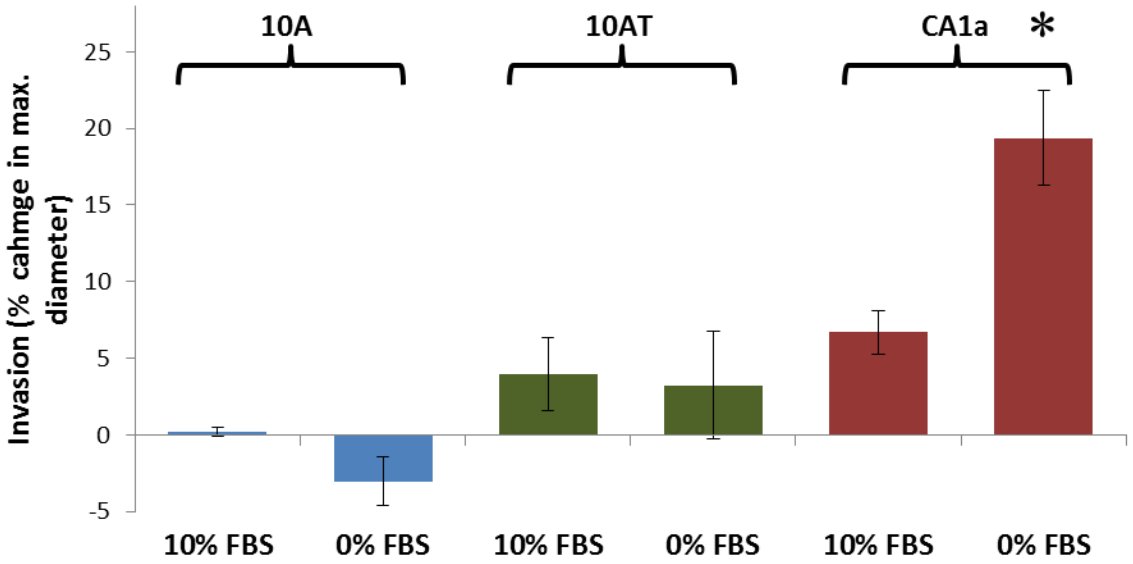

Figure 4.68. Removing serum from the medium results in an increase in invasion in CA1a cells but not in 10A or 10AT cells (* P<0.05 paired t-test, 25 acini measured in triplicates). The invasions were measured by the percent change in maximum diameter 12 hours after removal of serum.

If we repeat the experiment using EGF (human epidermal growth factor) instead of serum we find that the EGF also promotes the invasion.

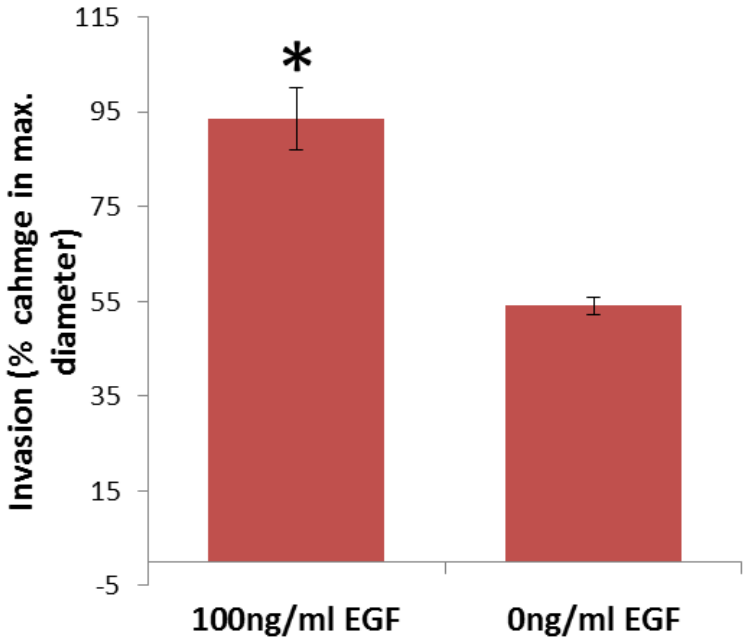

Figure 4.69. EGF promotes the invasion of CA1a cells.

We can conclude that both the absence of serum and the presence of EGF promote the invasion of CA1a cells (where "invasion" is quantified by measuring the change in length of the largest invasive strand of each acini over a period of 12 hours). It has been shown in the literature that EGF is a chemoattractant of a number of cell lines although it hasn't been shown for CA1a cells. Additionally these experiments involve the use of trans-membrane invasion experiments which have some limitations such as the absence of continuous data or the absence of invasive strands (because only single cells can migrate through membrane pores).[27] My results indicate that there must be a component within the serum that prevents the invasion of cells (that isn't EGF). Further experiments could determine what this component is and whether the invasion of the cells caused by serum deprivation is due to a deficiency in the nutrients that is detected by the cells.

CHAPTER 5: CONCLUSIONS

The microscopes and software described in chapters 2 and 3 of this thesis have become popular and valuable for a number of laboratories at Cornell University. Both the 1 and 2 color versions of the microscopes are often being used simultaneously and a calendar has been created for people to sign up to use them. With the instructions described in this thesis anyone with a background knowledge of optics and electronics could build these microscopes at a fraction of the cost of the commercially available microscopes, together with the software that I have created. Popular among users of the microscope has been the fact that it can be controlled remotely from a distant location (which requires a program for remote desktop connection such as TeamViewer which is free). Among the innovative features of the microscope is the horizontal configuration which reduces the height of the microscope and allows space for other trays in the incubator for cell culture. Also innovative is the ability to switch between fluorescence colors without mechanical movements, which extends the life time of the microscope and reduce the need for replacement parts. The use of inclined brightfield illumination has also proven to be useful as a means to increase contrast in a number of experiments. Finally the fact that the microscopes have survived the harsh conditions of humidity and temperature inside an incubator, with hundreds of long-term imaging sessions over the past several years, is a strong record which highlights the reliability of the microscope.

Chapter 4 describes the most notable results that I have obtained with the microscopes in the context of a progression model of cancer. Numerous other results that I have not delved into deeply, or that were not related to the progression model of cancer, have been relegated to the appendix. The appendix also includes collaborations with other laboratories at Cornell that have used my microscope and at least one paper published in the Cell Stem Cell journal. Chapter 4 begins with an analysis of the characteristics of MCF10CA1a cells which places emphasis on the morphological features of their nuclei with the help of fluorescent histones. I looked for features that were unique to the CA1a cell line that were not present in the 10A cells and 10AT cells from a morphological point of view. The only instance of such an attempt in

the literature is by Imbalzano et al.[15] They found that the CA1a cells contained giant cells, but they did not go into more detail on these giant cells other than mentioning that they exist. Therefore I decided to look in time lapse mode at the formation of these cells and I found that they form relatively quickly within five days from cells that looked morphologically normal at day 1 of culture. By looking at the first error at mitosis that preceded the formation of the giant cells I identified the most likely cause of the formation of the giant cells, which is the formation of multinucleated cells via incorrect segregation of the nuclei into distinct daughter cells at the cytokinesis step of mitosis. This process is not exclusively a feature of cancer cells. For example, binucleated polyploid hepatocytes are normally found in all mammalian specie[24] and, in humans, the number of polyploid cells in the liver is 20–30%.[25] Interestingly, any number of polyploidy can happen (4n, 8n, 16n and higher) both via cell fusion and via endoreplication that skips cytokinesis. However, I found that the events that can lead up to a giant cell are varied, but in most cases some kind of chromosomal instability is apparent. I find that the nuclear size of a subpopulation of cells in the cancer cell line increases dramatically during the first 5 culture days. Additionally, and interestingly, the nuclear size of all cells, including non-cancer cells increases constantly during the first day of culture. Both of these finding are not present in the literature. It is possible that the cells flatten out with time as they become better attached to the substrate. A case of increased cytoplasmic surface area in cells is the process of senescence.[3] The most widely used and most robust marker for senescence is the staining for beta-galactosidase.[3] However the test turned out negative on my giant cells (described in the Appendix).

By performing progeny analysis I found that cells are varied in their ability to give rise to progeny. Some cells give rise to 1 daughter cell whereas other cells can give rise to 8 daughter cells in a 48 hour period. This applies to both cancer and normal cells but the difference between them is that cancer cells have a greater range of possible outcomes because a subpopulation of cancer cells divide more often than normal cells and also a subpopulation divides less often. In the literature we find that there exists a subpopulation of cells within a tumor, so called cancer stem-cells, that have the ability to form new tumors.[28] However what I have found is not two distinct subpopulations but rather a continuum. Marusyk et al[29] have reviewed

cell to cell heterogeneity in cancer but I have not found a study where heterogeneity in division potential of single cells in cancer cells is compared to normal cells.

In the same study I find that the cancer cells have a higher degree of cell death than the normal cells. This is in line with some reports that indicate an increased degree of necrosis and apoptosis in cancer.[30]

In contrast to the previous findings, I find that the cancer cells and the normal cells have similar numbers of cell fusions and multipolar divisions. It must be said, though, that the aberrant, giant cells that appear after a number of days in culture would likely skew this result. Therefore it is likely that the number of multipolar or aberrant divisions increases with time for cancer cells. A study to confirm this would be straightforward and constitute an appropriate future direction.

I found that the cancer cells did not grow faster than the non-cancer cells in monoculture, but they did grow more in a coculture setting when cultured for an extended period of time. A classical hallmark of cancer is that the cells grow more than the normal cells because of self-sufficiency in growth signals (among other things) (Hanahan et al)[31]. However, another hallmark of cancer is the insensitivity to anti-growth signals.[31] Therefore my experiment indicates that what makes the MCFCA1a cells malignant is their insensitivity to anti-growth signals rather than their self-sufficiency in growth signals. This is because in a coculture setting (in which cells are confluent from the beginning) cell to cell contacts create inhibitory signals that suppress the growth of non-cancer cells, which does not happen in the case of cancer cells. Contact inhibition of growth has been extensively studied in the literature.[32] The novelty presented in this thesis is not only that this is absent in CA1a cells and present in the other cells lines but also the method that I have developed to quantify this effect using two color fluorescence is novel.

I have discovered that the cytosol of GFP labeled histone-transfected CA1a cells is fluorescent. This fluorescence, though low, can be detected if we use a high laser power and if we increase the sensitivity of the detector. This fluorescence was not expected because the histones are, in principle, only located in the nucleus of the cells. A future study could look at this phenomenon to figure out what is causing the fluorescence. It could either be GFP that has leaked from the nuclei or autofluorescence. To test this it

would be sufficient to image cells that have not been transfected with GFP-histone and see if they too are fluorescent. However, in a small number of cells I do have noticed cases in which leaking of GFP into the cytosol was apparent because the cytosol of these cells was highly fluorescent even under normal intensities of light. In the literature, the leaking of proteins from the cytosol to the nucleus has been observed in old cells.[33] I have not, however, found mentions of leaking from the nucleus to the cytoplasm except in cells that are necrotic (and my cells were not necrotic). It might also be interesting to compare this cytosolic fluorescence in cancer versus normal cells because if it is only present in the cancer cells it might indicate that they have some kind of nuclear defect.

With the help of laser ablation of the cancer cells I have discovered that the cancer cells affect the morphology and density of the normal cells that lie just underneath the cancer cells and that these regain their normal morphology and density when the cancer cell is killed. I have not found any similar examples of this in the literature as most coculture experiments in the literature involve coculture with fibroblasts or other stromal cells (because researchers are mostly interested in the interaction between the epithelial cells and the underlying stroma).[34] There are cases of stromal cells (or adipocytes)[35] affecting cancer cells and cancer cells affecting macrophage morphology[36], but I have not found cases of cancer cells affecting the morphology of epithelial cells as I have described.

For the cultures of the cells in Matrigel I followed Imbalzano et al.[15] and found, like they do, that the CA1a cells have invasive outgrowths. However, they did not quantify these outgrowths. I quantified the outgrowths and found several interesting additional things. In coculture experiments I found that the cancer cells are almost 100% of the time the leader cells of the invasive strands. In the literature, MDA-MB231 cells were shown to be the leader cells in cocultures with MCF10A cells in collagen[37]. The difference with my approach is that I have used MCFCA1a cells which are more similar to the MCF10A cells than the MDA-MB231 cells. Another difference is that I used Matrigel instead of collagen. Additionally I showed that the invasion of the cancer cells can change the morphology of the acinar structure of the non-cancer cells. Interestingly, leader cells of invasive strands have also been studied in a non-coculture setting in

collagen gels, where the leader cells were found to be a subpopulation of cells of the tumor that had spontaneously acquired invasive potential[38]. This could hold true for the MCFCA1a cells, since it is usually single cells that start the invasive strands, while the main bulk of the cells remain in the acini.

It would be interesting to find out if the leader cells of the invasive strands are related to the giant cells that are present in the 2D culture of CA1a cells. Although I have not identified giant cells in the 3D Matrigel cultures, I have seen some instances of leader cells that were larger and vacuolated. I have not, however, quantified this effect, but it could be interesting to do so. By looking at the movies it also seems that the leader cells are more active and more mobile than the rest of the cells of the invasive strand.

One of my most unexpected findings is the correlation between medium renewal and the invasions. The effect of medium on motility and invasion has been studied by Heylen et al.[39] They show that both conditioned medium and serum stimulate invasion. However, they use end point assays whereas I take continuous measurements which allows me to see that medium renewal causes a slight initial retraction of the invasions followed by a large stimulation of the invasion. Therefore I have found that the effect of medium renewal is time dependent. Additionally, my experiments indicate that the invasion is promoted when there are large changes in the medium because when the medium is changed in smaller intervals in a more continuous fashion, there is less invasion. In an attempt to identify the components of the medium that might be causing this effect I started by removing the serum. I found that when faced with serum starvation, 10A cells and 10AT cells retracted whereas CA1a cell invaded more (and this happens within 12 hours). It is likely that the effect of serum on invasion is also time dependent and that if cells are culture for a long time without serum they will stop invading because they will run out of nutrients. If, however, the cells are suddenly changed from a high serum to a low serum medium, I have shown that this triggers invasion of the CA1a cells. Ye et al.[27] have shown that this happens to MDA-MB231 cells. I have not only shown that this happens to CA1a cells but that the opposite effect happens to 10AT cells and 10A cells. Given that serum contains both nutrients and growth factors I decided to see what the effect of epidermal growth factor is on the invasion. I found that it has the opposite effect of serum in CA1a cells. Therefore it

is possible that there is another component of serum (that isn't EGF) that is inhibiting the invasion. An alternative possibility is that the invasion is caused by a genetically encoded starvation program that is activated when the cells sense low nutrient levels. A future direction for this research could be to culture the cells in a defined specially-formulated medium that is serum-free and then vary it's ingredients to identify the effect of each of them on the invasion (because the components of serum are mostly unknown).

APPENDIX A: OTHER ASPECTS OF THE 10A, 10AT AND CA1A CELL LINES

Other aspects of growth on Matrigel

I have noticed that when cells are grown in Matrigel, they attach to the Matrigel and pull on it. The force exerted by the cells on the Matrigel can be visualized when there are particles trapped in the Matrigel, as shown in the Figure 6.1.

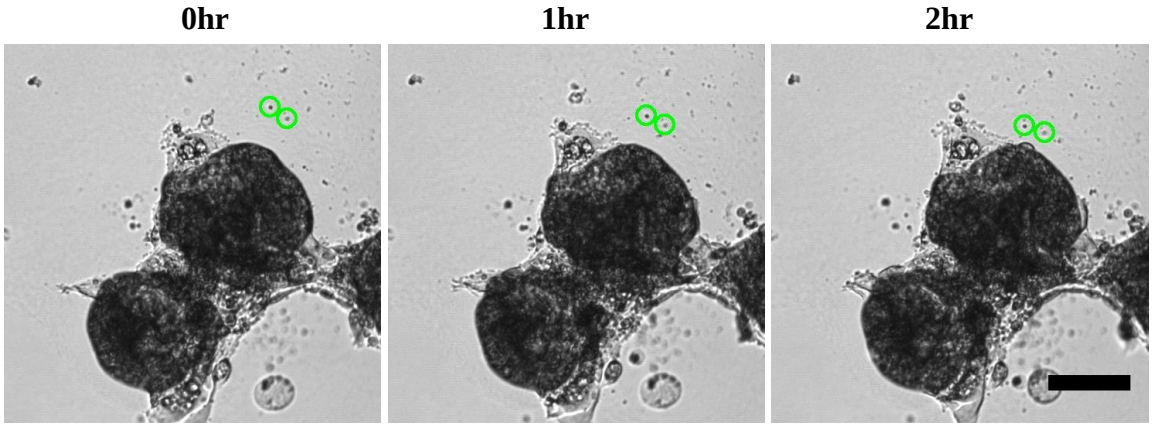

Figure 6.1. Highlighted in green are particles embedded in the Matrigel that are pulled toward the cells as the cells pull on the Matrigel. Scale bar 30 μm.

The cells not only pull on the Matrigel but apparently they also process it and consume it. Whether this process is intracellular or extracellular via enzymes is not clear. This can also be visualized by particles trapped in the Matrigel. After some days there is no Matrigel left close to the cells. Then the cells spread outward from the acini to the substrate that now lacks Matrigel. Figure 6.2 shows the cells starting to spread out from the acini at day 10.

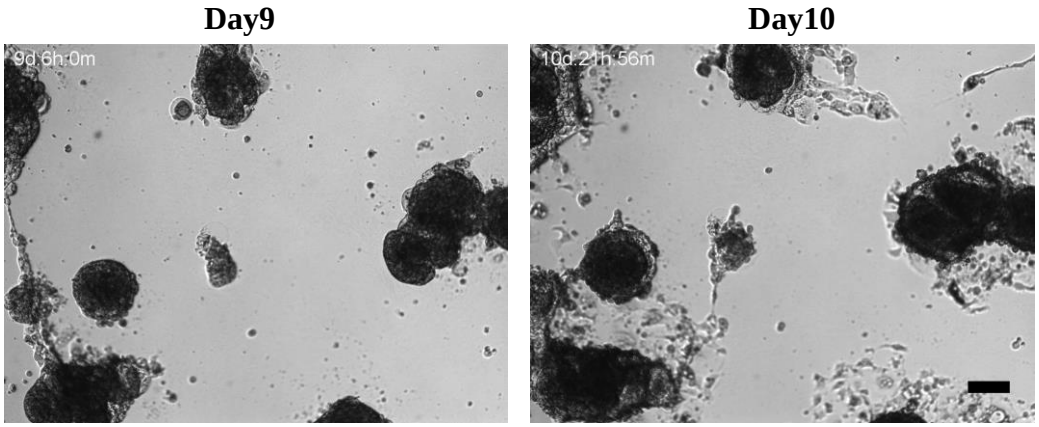

Figure 6.2. By day 10 (Image on the right) the Matrigel surrounding the cells has been consumed and the cells exit the nodules and spread out to form a layer on the surface of the plate. Scale bar 100 µm.

Since Matrigel is expensive I usually use small culture dishes and I plate the Matrigel only on the glass part of dishes that contain glass only at the center of the plastic dish. In this situation, the Matrigel will form a slightly curved surface on its own. This happens as it transitions from a liquid to a gel. The center of the dish will therefore have a lower thickness of Matrigel than the edges of the dish. The acini will spread out and disassemble when they come into contact with the glass substrate. This will only occur once there is no Matrigel left below the cells. Therefore acini will disassemble first on the center of the dish because that is where there is less Matrigel. This is explained in Figure 6.3.

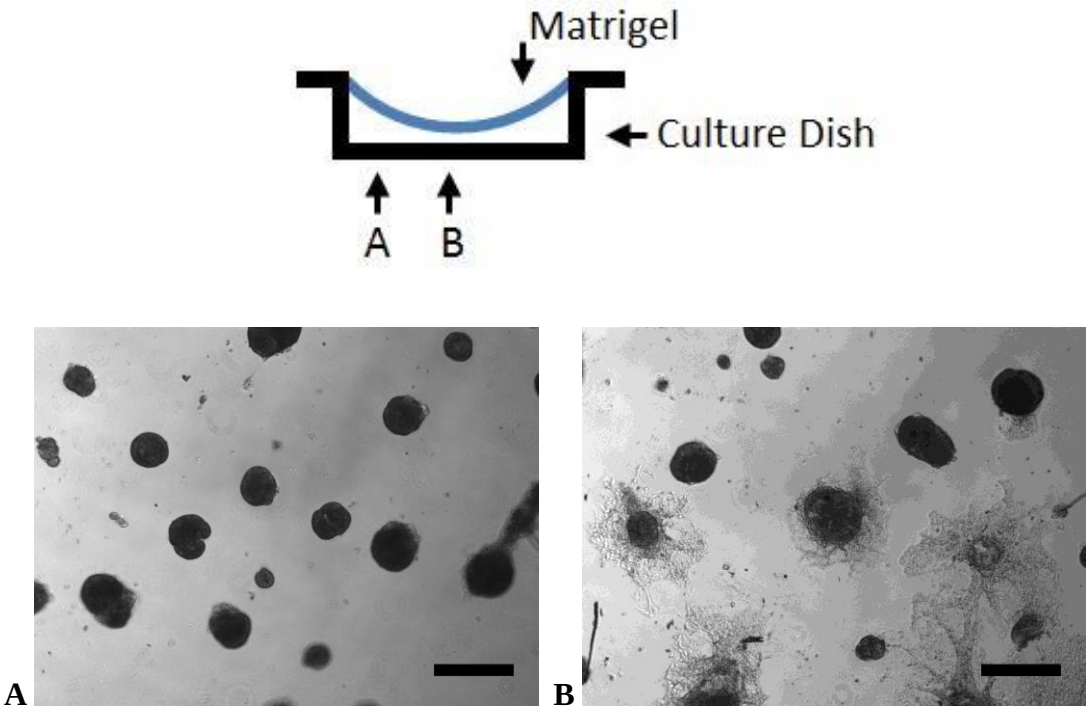

Figure 6.3. Disassembly of acini occurs at the center of the dish. A and B are two positions on a culture dish, A is on the edge of the dish and B is on the center. The width of the Matrigel was estimated at 400um on the edge and 300um at the center of the dish. Image A and B are taken at the same time point but B has a smaller amount of Matrigel because it is at a position close to the center of the dish, leading to disassembled acini occurring only at position B. Scale bar is 500µm.

It must be noted that the disassembly of the acini when they come in contact with the plastic is a different phenomenon to the spreading of acini seen earlier which is promoted by medium renewal.

Cell movements in Matrigel

I have found that cell movements of 10A cells are similar to CA1a cells when cultured in 2D. However in 3D Matrigel cultures some differences were apparent: There is more movement in the CA1a cells than in 10A cells and the highly motile cells are often vacuolated cells. Furthermore, these motile vacuolated cells often act as leader cells that eventually form the branching connections between the nodules.

Fast moving vacuolated cells are only present in the CA1a cell line and not in the 10A cells. Figure 6.4 shows the tracks of four highly motile cells which the cells can cover in under a day. Three of the four cells are vacuolated and one big and vacuolated cell acts as a leader cell to form a bridge. Additionally two of the cells die within one day, indicating that vacuolated cells are possibly damaged cells.

A 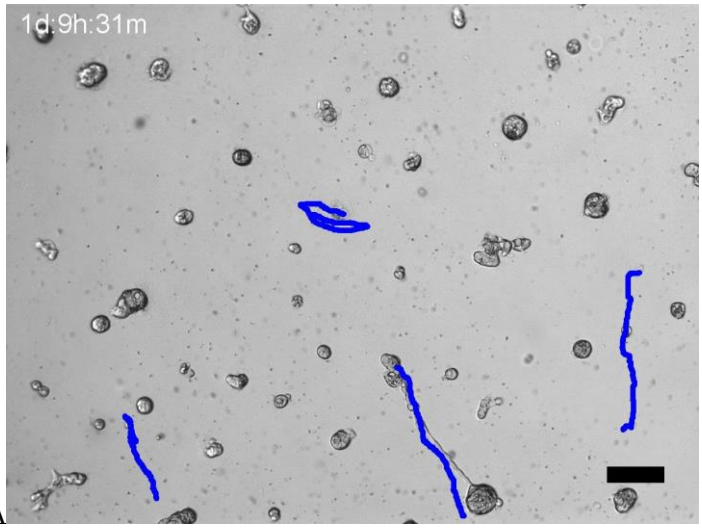

Figure 6.4. The trajectories of a subpopulation of fast moving cells are shown in blue. These distances are covered in under a day, and the rest of the cells will barely move during this time. Scale bar 100 µm.

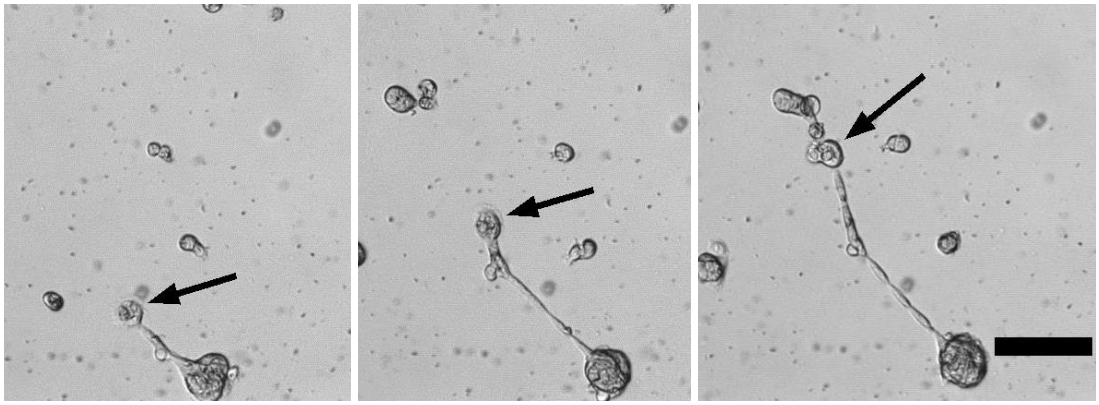

Figure 6.5. Three consecutive images taken every four hours of a large vacuolated fast moving cell acting as a leader cell that forms a branching connection between nodules. Scale bar is 100 µm.

Vacuolated cells emerge from the nodules (Figure 6.6**A**) even though they constitute a small subpopulation of all the cells (Figure 6.6**B**).

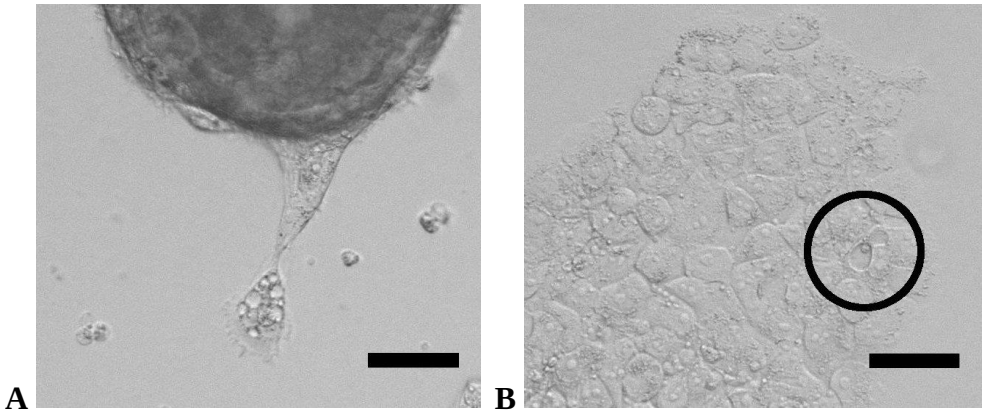

Figure 6.6. A) A vacuolated cell emerges from a nodule and acts as a leader cell. B) Cells from the same dish as A) that grew in monolayer shows a single vacuolated cell in the black circle showing that vacuolated cells are a small subpopulation within all the cells. Scale bar is 50 µm.

Hypoxia inhibits growth

I decided to see how hypoxia affect the growth of the cells. The cells were cultured on top of Matrigel in hypoxia (1% oxygen) and compared to their growth in normoxia (20% oxygen). Tubules formed in both

cases and no differences were detected after one day of exposure to hypoxia compared to normoxia (Figure 6.7).

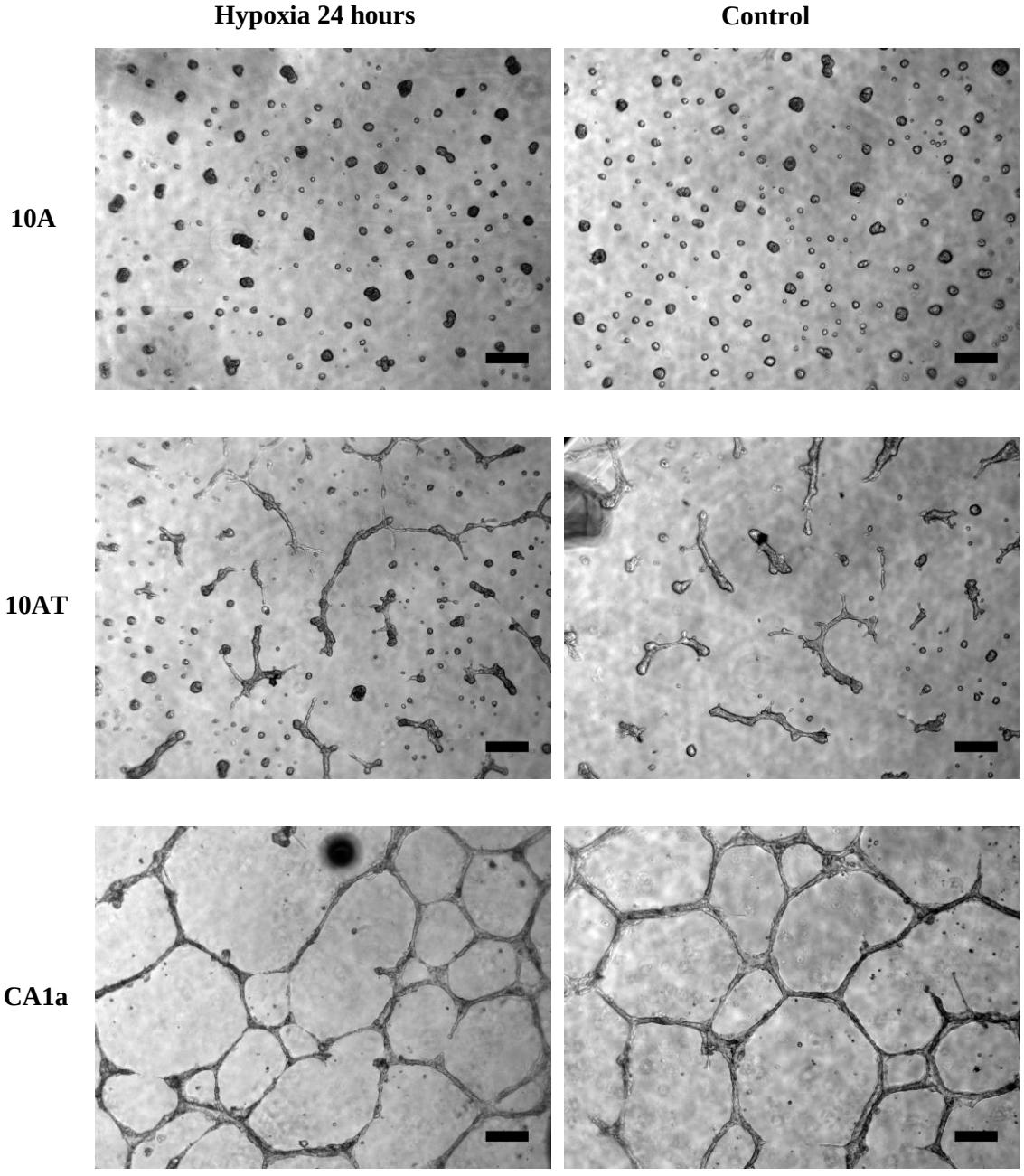

Figure 6.7. Images of 10A, 10AT and CA1a cells on Matrigel after a 24hour exposure to 1% hypoxia versus a control (normoxia). No differences are apparent. Scale bar 300µm.

However, after 4 days, the cells have grown less in hypoxic conditions for all cell types (10A, 10AT and CA1a), Figure 6.8.

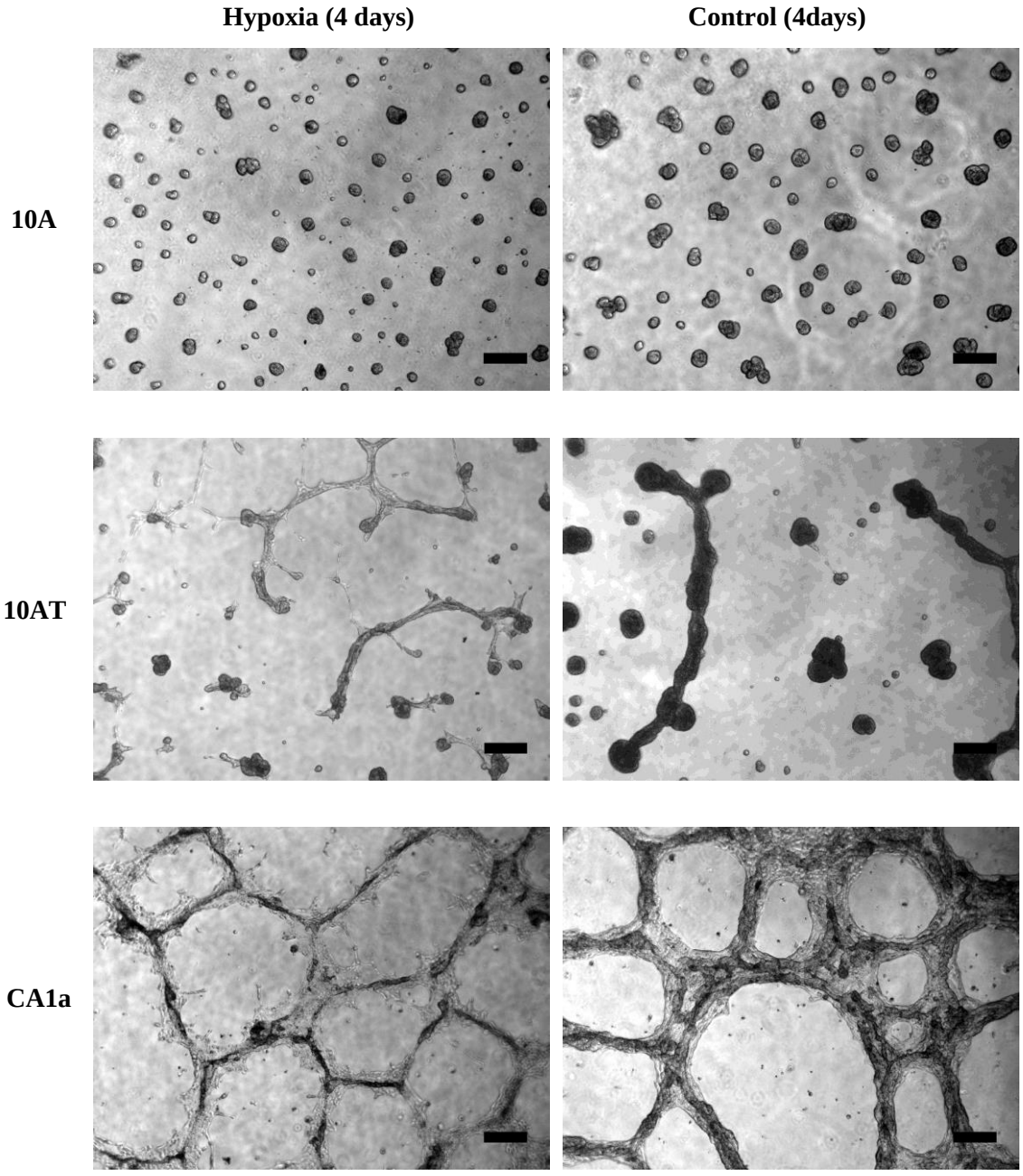

Figure 6.8. Changes are clearly visible at day 4. Cells grow less in hypoxia. Scale bar 300µm.

In sum, hypoxia seems to cause a slower growth of the acini, and this is visible by day 4 of culture.

Discussion on tubules

Historically, the formation of tubules in Matrigel was originally observed in endothelial cells forming vascular networks. Later it was observed that the formation of tubular networks also occurs with cancer cell lines.[40] The formation of tubular networks is sometimes termed vasculogenic mimicry (VM).[41] VM is more present in aggressive tumors and in some occasions it has been seen that fluids can flow through the tubules suggesting that the tubules act like a vascular network allowing blood and nutrients to reach the tumor.[42]

The fact that the formation of tubular networks only occurs when plating high numbers of cells, with better networks forming when the number of plated cells is increased, has been documented before.[40]

I have shown that there is an additional phenomenon that occurs when plating cells on top of Matrigel: sheet outgrowths, which happen after long term culture and are more pronounced in aggressive cells. These are independent of tubules as they can occur in acini where tubules are not present. They also show a pattern of outgrowth that very clearly depends on the state of the medium (seen when the medium is renewed). This dependence on the medium could provide a new method for understanding how the medium affects cells that would otherwise not be possible. The sheet outgrowths only happen for the most aggressive (CA1a) cell line and could represent a form of invasion that leads to metastasis.

Growth on Collagen

Up to now, we have seen that when plated on Matrigel, cells produce acini. When instead the cells are plated on collagen (instead of Matrigel), the growth is indistinguishable from growth on a 2D plastic surface and they form epithelial layers as shown in Figure 6.9.

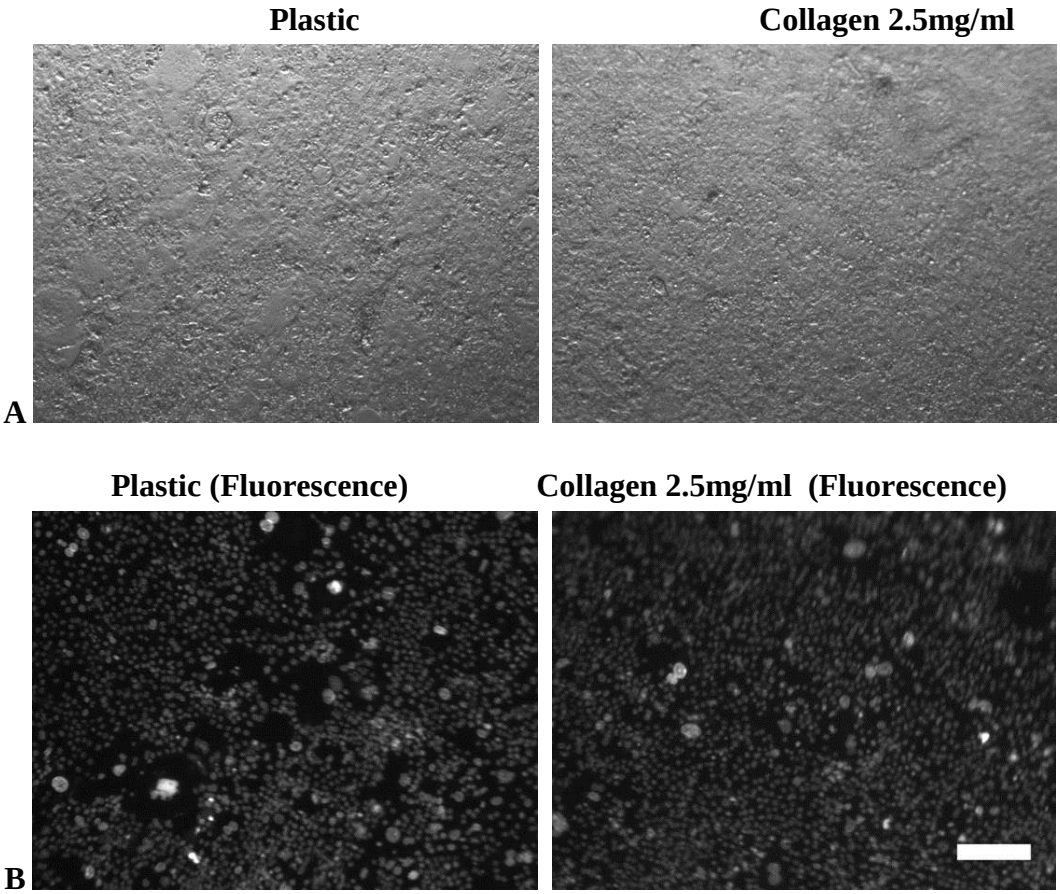

Figure 6.9. Cells have similar morphologies when cultured in plastic or collagen. (A) is brightfield and (B) is fluorescence. Scale bar 200µm.

I attempted variations in the density of collagen which yielded the same results. Therefore it seems that the formation of acini that we saw on Matrigel did not occur on collagen.

Effect of light on cell growth: MCF10A cells vs MCFCA1a cells

I compared the growth of cells under light to the growth of cells without light. The experiment was done for two kinds of fluorescence excitation light (yellow for mCherry and blue for GFP) to see if blue light has a negative impact on the growth of the cells. The experiment was done on 10A and CA1a cells to see if the more tumorigenic cell line is more susceptible to light (which has been demonstrated for certain melanoma cell lines).

The amount of light that the cells received was approximately 1 second of illumination every 5 minutes for 24 hours, which is equivalent to a typical fluorescence imaging session for tracking migration of cells. Approximately 800 cells were imaged in two wells of a multiwall plate. The experiment was repeated without light (just imaging at the beginning and end of the 24 hour period). This was repeated five times and the results are shown below:

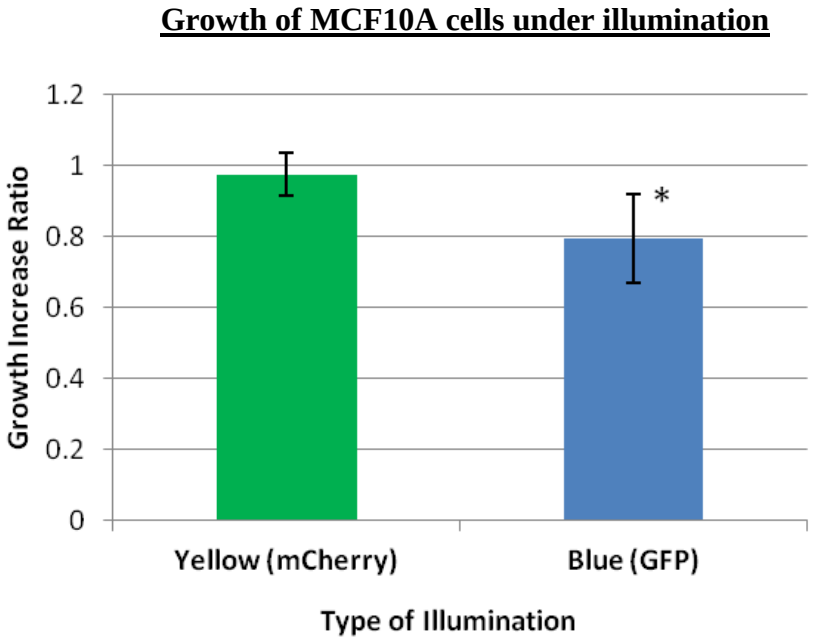

Figure 6.10. Growth of 10A cells for mCherry and GFP imaging sessions represented as a ratio with respect to the growth without illumination. Asterisk represents a P-value P<0.05 that GFP growth is lower than mCherry growth on a one-tailed paired t-test.

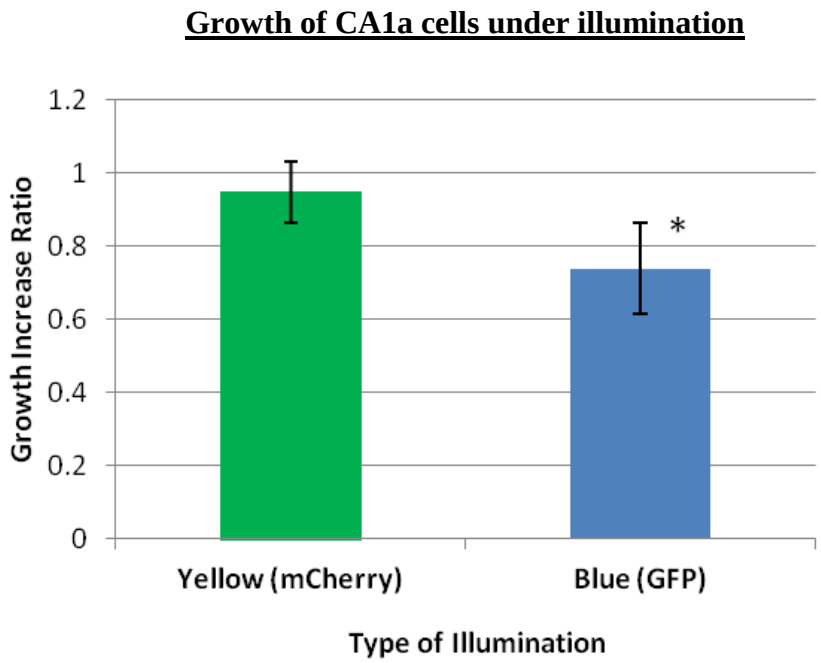

Figure 6.11. Growth of CA1a cells for mCherry and GFP imaging sessions represented as a ratio with respect to the growth without illumination. Asterisk represents a P-value P<0.05 that GFP growth is lower than mCherry growth on a one-tailed paired t-test.

Results

Growth under blue illumination was significantly lower than growth under yellow illumination with a $P<0.05$ for a one-tailed paired t-test. This was the case for both MCF10A cells and MCFCA1a cells. There was no significant difference between these two cell types.

Conclusion: Blue light can be detrimental to the growth of cells. Furthermore, there are no significant differences between the tumorigenic and the non-tumorigenic cell lines.

Sheet Migration: A problem to overcome when measuring cell migration speed

When plated on a regular plastic cell culture dish the cells will move around randomly in different direction. However, when the cells reach a certain density, they will form an epithelial layer where cells attach to each other via cell to cell contact. When cells are plate, if they are not well distributed in the dish, some areas will have higher densities of cells which will form epithelial layers quickly. These layers of cells can move as a whole. The motion is then not random but towards one direction. Generally the direction is dictated by cell pushing on other cells as they grow, due to lack of space. When for example the cells are close to the edge of the dish and the growth of the cells thus hits a wall, there will be a pressure to move in the direction opposite to the wall as the cells grow in number. This directed epithelial sheet migration also occurs in wound assays where a confluent cell culture is scraped with a pipet tip, as has been described in the literature. The gap formed is closed by migrating sheets of cells. Here I show that sheet migration is a problem that must be overcome when measuring the cell migration speeds of newly plated cells.

A difficulty when measuring cell migration speeds is the inherent variability in the speeds of the cells which requires taking images of many positions and then taking the average. Therefore in this experiment I imaged approximately 3000 cells which I divided into three sets of 1000 cells, each from a column of 5

wells (4 positions per well), which I named control 1, control 2 and control 3. I expected all the controls to result in equal values of cells speed. They were approximately equal for the first 10 hours but then one of them (control 2) increased in speed with respect to the others (which as I will show was due to sheet migration). See Figure 6.12.

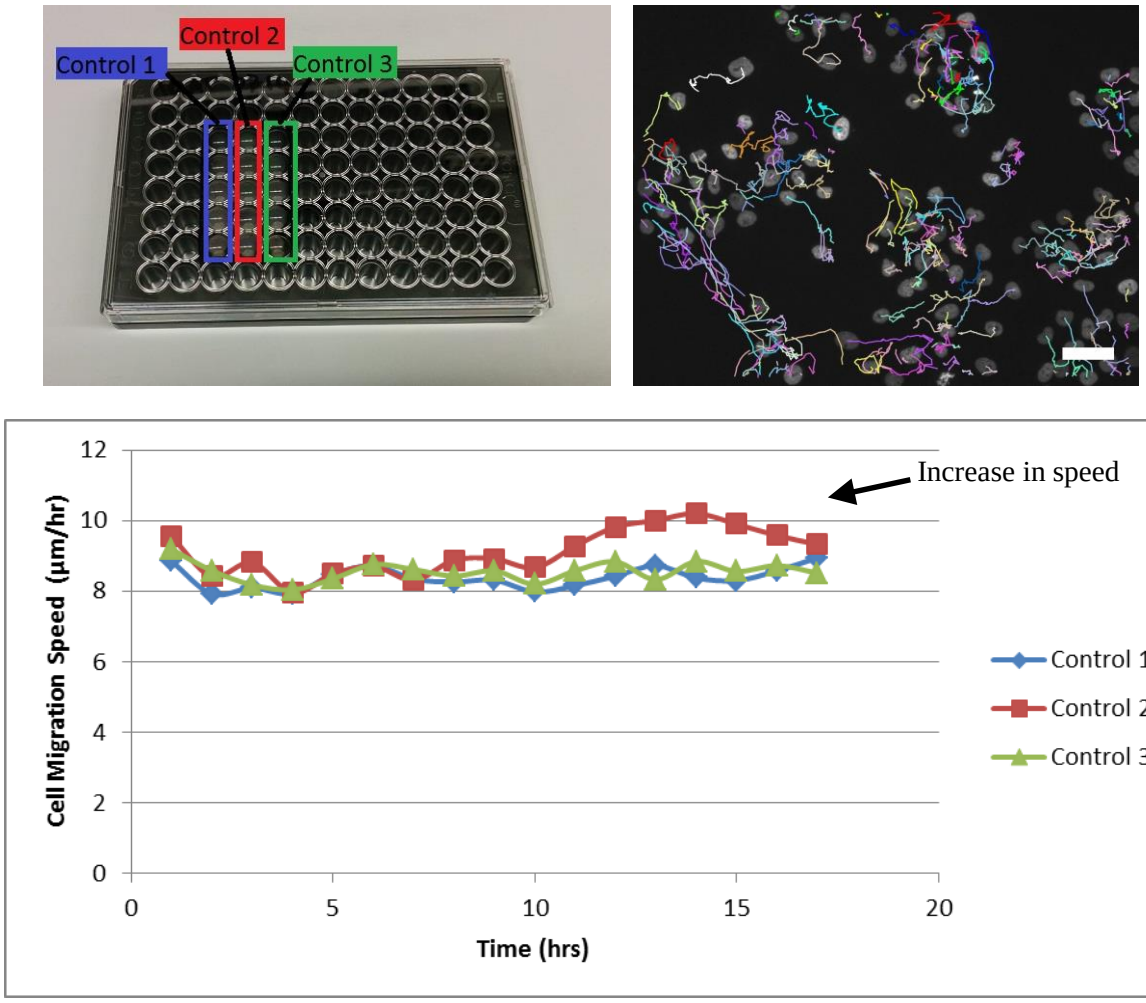

Figure 6.12. 1000 cells form each of 3 columns of a 96 well plate were tracked and their speeds are plotted. The red column shows a higher speed after 10 hours. Scale bar 50µm.

To investigate the source of this difference I plotted the speed of each of the 20 positions corresponding to the red column (control 2) to see which positions were giving rise to the discrepancy and then looked at the videos of these positions. This allowed me to find the source of the increase in speed: sheet migration of cells. When cells travel in sheets their migration speed can be much higher. The increase in speed in

sheet migration is due to cells pushing each other due to lack of physical space. See Figure 6.13. and Figure 6.14.

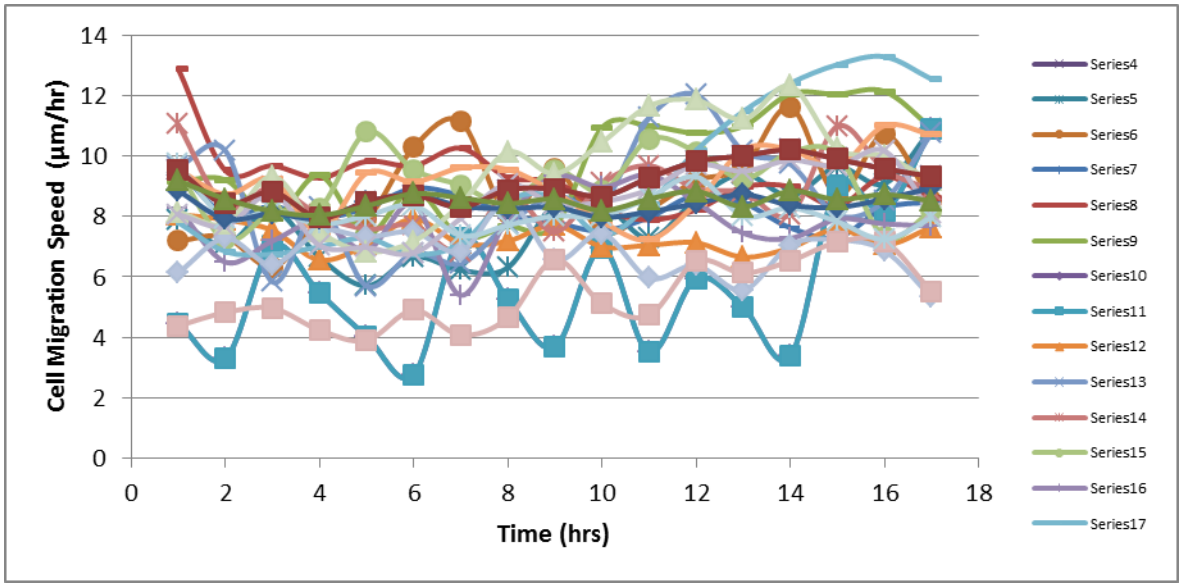

Figure 6.13. Decomposition of control 2 (column 2) of Figure 6.12. into each of the 20 positions to identify which is anomalous (for example, Series 17 is too high towards the end).

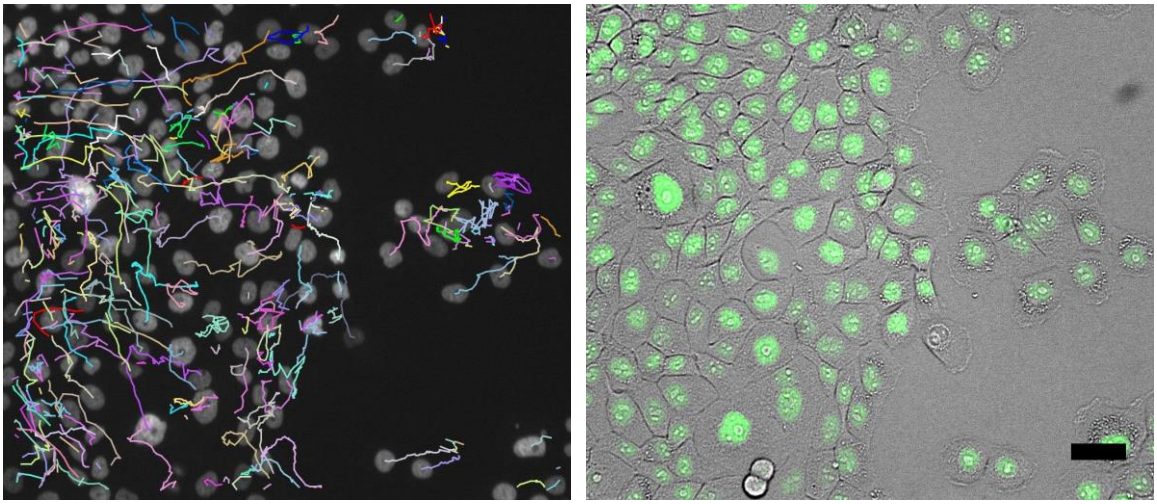

Figure 6.14. Images correspond to Series 17 of Figure 6.13. showing how a sheet of cells is moving towards the right (t=14hrs). Scale bar 50µm.

The appearance of sheet migration is often present in areas where there is high density of cells. It is also more likely to happen close to the edges of the wells. This is a reason to avoid small wells such as those found in 96 well plates when measuring cell migration speeds.

Average Migration Speed

While looking at the differences in cell motility between the MCF cell lines I came across an unexpected finding: the speed of the cells decreases sharply during the first three days, even before they reach confluence. Shown are the results of tracking 100 cells which grow to become 700 cells over the course of three days.

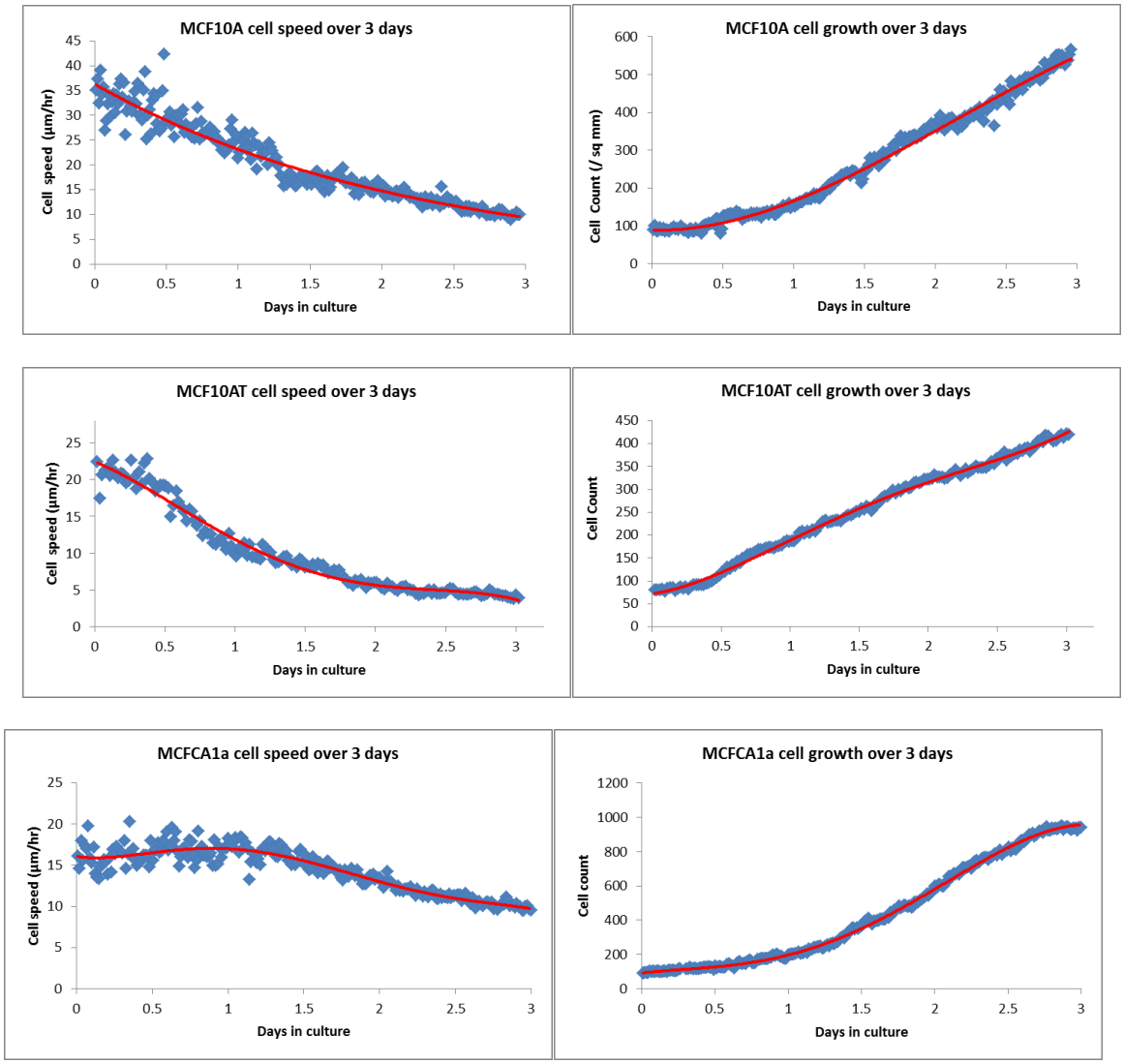

Figure 6.15. The cell migration speeds (Left) and cell growth (Right) of 100 cells of the 10A, 10AT and CA1a cell lines.

The following bar chart shows the comparison between the initial speeds of migration of the cells:

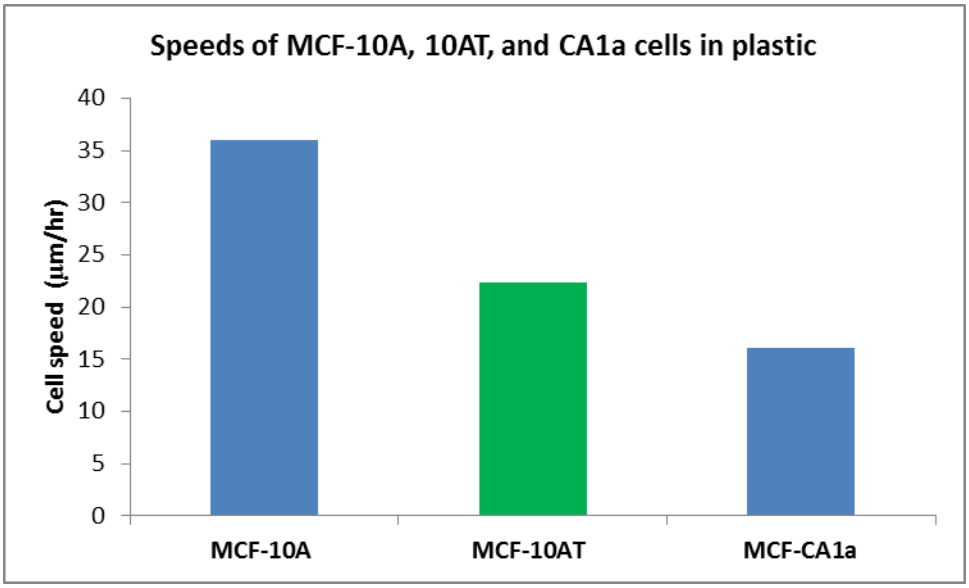

Figure 6.16. Initial average cell migration speeds of 100 cells of the 10A, 10AT and CA1a cell lines.

Distribution of Speeds

Analysis of the distribution of the migration speed of the cells reveals that initially the cells have a large range of possible random speeds. By day two of culture the speeds have largely been reduced to a small range of possible values, see Figure 6.17.

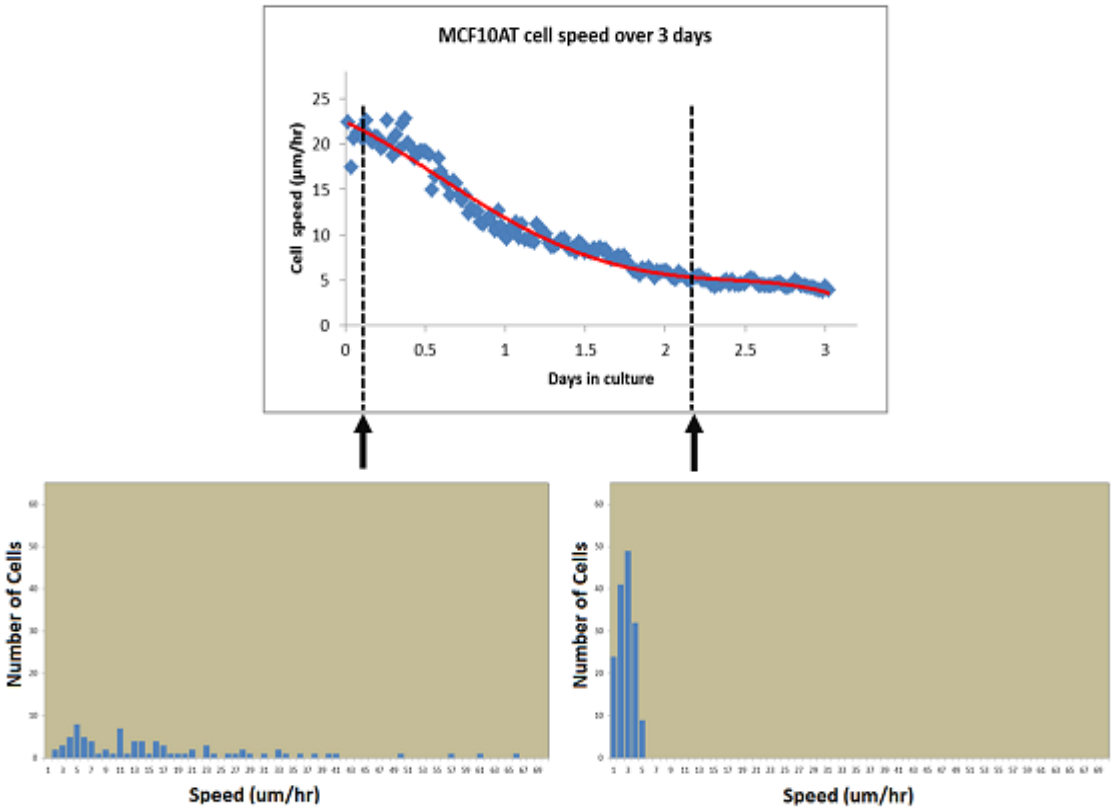

Figure 6.17. The distributions of cell migration speeds reveals that initially there is a large distribution of possible speeds. Later, the speed is only confined to lower values.

Test for cell senescence is negative

The appearance of large, flat cells is often attributed to the process of senescence. I wondered if the large cells present in the CA1a cell line are senescent cells. Cell senescence is a process by which cells loose proliferative capacity and acquire a large and flat morphology. It is caused by either short telomeres, by DNA-damage, or by activation of certain tumor suppressor pathways such as the ARF-p53 or the INK4a-RB pathways.[3,43] It is still unclear what determines whether a cell will become senescencent rather than the alternative which is to become apoptotic.[44] In the case of human cancer cells grown in vitro, chemotherapy often induces senescence at moderate doses and apoptosis at higher ones.[45] Senescence is considered to be

a mechanism to prevent cancer formation but there is evidence that cell senescence is present in some tumors. [3]

The most widely used and most robust marker for senescence is the staining for beta-galactosidase.[3] Figure 6.18 is taken form the literature and shows the difference between normal and beta-gal stained senescent cells. Figure 6.19 shows my cells before and after staining. Even though the cells have a senescent cell morphology, the staining was not positive for my cells, which might indicate that the cells are not senescent.

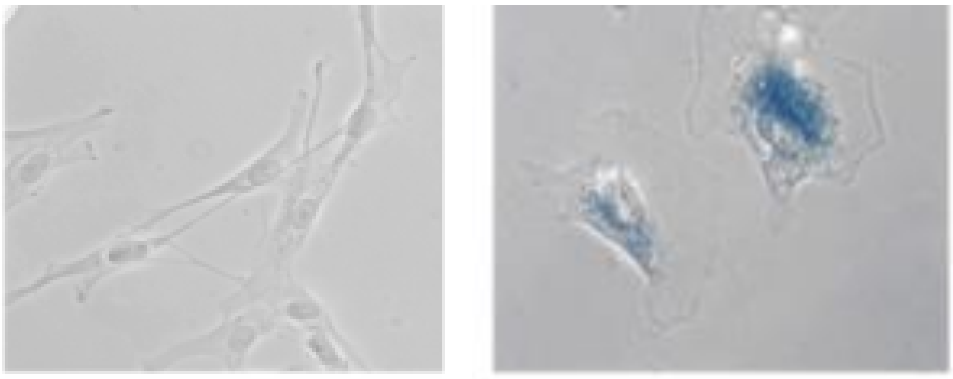

Figure 6.18. Literature example of non-senescent cell (Left) and beta-gal stained senescent cells (Right).[46]

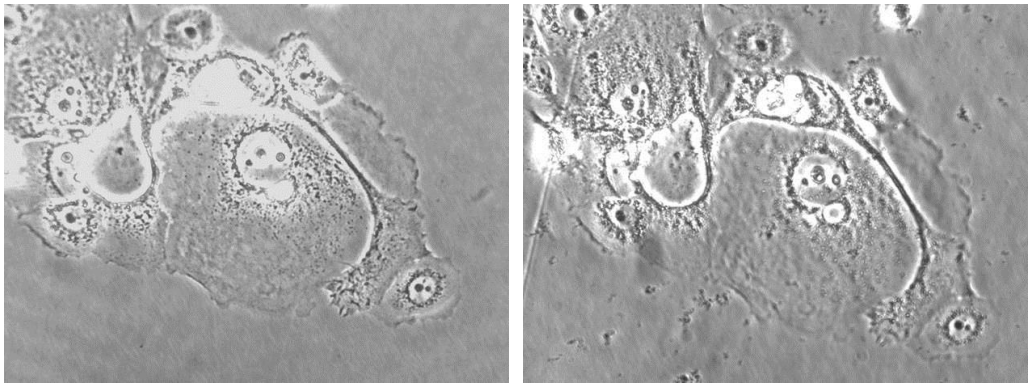

Figure 6.19. A large CA1a cell before (left image) and after (right image) beta-galactosidase staining. The absence of staining indicates that the cell might not be a senescent cell.

Search for markers of cancer stem cells

Cancer stem cells are defined as a subpopulation of cells whose characteristic is a largely increased ability to form cancers in mice compared to the non-cancer stem cells in the same population. Several studies have shown the existence of such cells and their increased ability to form tumors in mice.[47,48]

Aldehyde dehydrogenase activity

Aldehyde dehydrogenase is a stem cell marker whose activity can be detected with the Aldefluor assay. Charafe-Jauffret et al showed that several mammary cancer cell lines contain subpopulations of cells that express aldehyde dehydrogenase. [48] In the same paper they show that this subpopulation of cells is responsible for metastasis. By flow cytometry they determined that MCF10A cells have very low levels of aldehyde dehydrogenase. Here I show that in both 10A cells and CA1a cells, aldehyde dehydrogenase activity is detected only in a small number of cells inside vacuoles or other subcompartments of the cytoplasm.

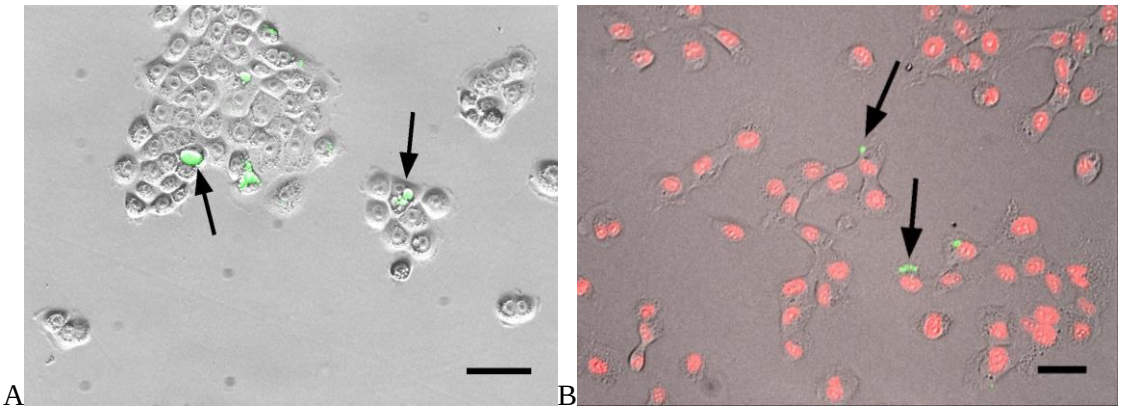

Figure 6.20. A) CA1a cells and B) 10A cells exposed to Aldefluor reagent show the location of greatest aldehyde dehydrogenase activity in green mostly inside vacuoles (10A cells were transfected with histone-mCherry to highlight the location of nuclei). Arrows indicate the position of aldehyde dehydrogenase activity. Scale bar 100μm.

Is Aldefluor present in vacuoles due to macropinocytosis?

Internalization of extracellular fluorescent markers has been attributed to the process of macropinocytosis. This was shown in the article "Vulnerability of Glioblastoma Cells to Catastrophic Vacuolization and Death Induced by a Small Molecule" whereby cancer cells show rapid incorporation of extracellular-phase fluid tracers and internalize it into vacuoles.

I attempted to see if macropinocytosis was present in CA1a cells by adding Dextran-TexasRed to the medium of the cells and see if it was internalized. The Dextran-TexasRed was not internalized into the big vacuoles of the cells indicating that pinocytosis is possibly not the cause of the vacuoles. See Figure 6.21.

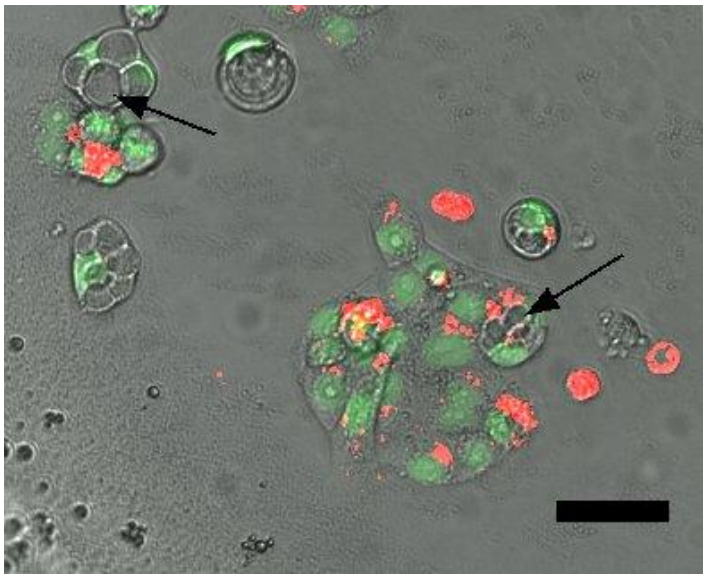

Figure 6.21. CA1a cells were exposed to Dextran-TexasRed. Arrows indicate vacuoles. The dextran seems to aggregate on dead cells but is not internalized into vacuoles suggesting that pinocytosis is not the cause of vacuoles. Scale bar 50µm.

Different modes of growth

While culturing the cells I have noticed that the MCF cell lines have shown different forms of growth. They can grow as individual cells that are highly motile and independent or they can grow as groups of cells that form immobile epithelial layers. Any combination of these two modes of growth is possible, and usually the growth is somewhere in between, with some cells forming groups and some cells migrating independently.

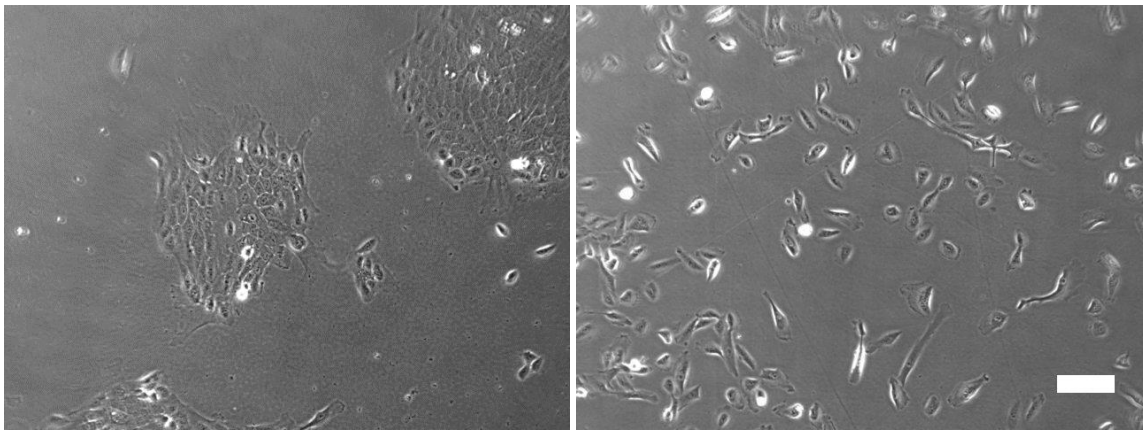

Figure 6.22. The MCF cell lines can grow as static epithelial layers (Left) or as scattered motile cells (Right) or in any combinations of these two modes. Scale bar 50µm.

This variability makes it difficult to obtain absolute results when measuring data relating to migration speeds as it can vary over time. How or why the cells switch from one mode to the other is unknown. In the literature such a transition is termed EMT (epithelial to mesenchymal transition) and a variety of factors have been identified that could lead to such a change, although in my experiments there seem to be a considerable degree of randomness involved.

The effect of a thin layer of Matrigel on 10A cells

Previously I cultured cells on top of a thick layer of Matrigel several hundred microns in height. I showed that the cells form acini in that case. However, if the layer of Matrigel is very thin the effects are very different from a thick layer because the cells will form epithelial sheets and not acini. Here I investigate the effect of a thin layer of Matrigel (just coating the surface) on growth and migration of 10A cells.

Figure 6.23 shows that the speed of migration is increased by the thin coat of Matrigel. On the other hand, cell growth is not affected by the Matrigel, as shown in Figure 6.24.

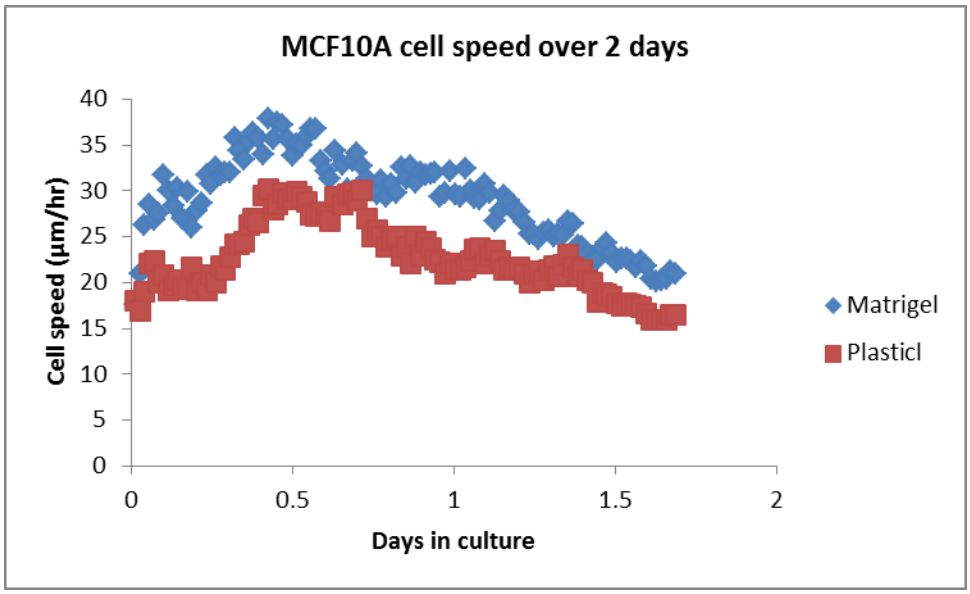

Figure 6.23. Coating a dish with a thin layer of matrigel increases the speed of migration of the cells.

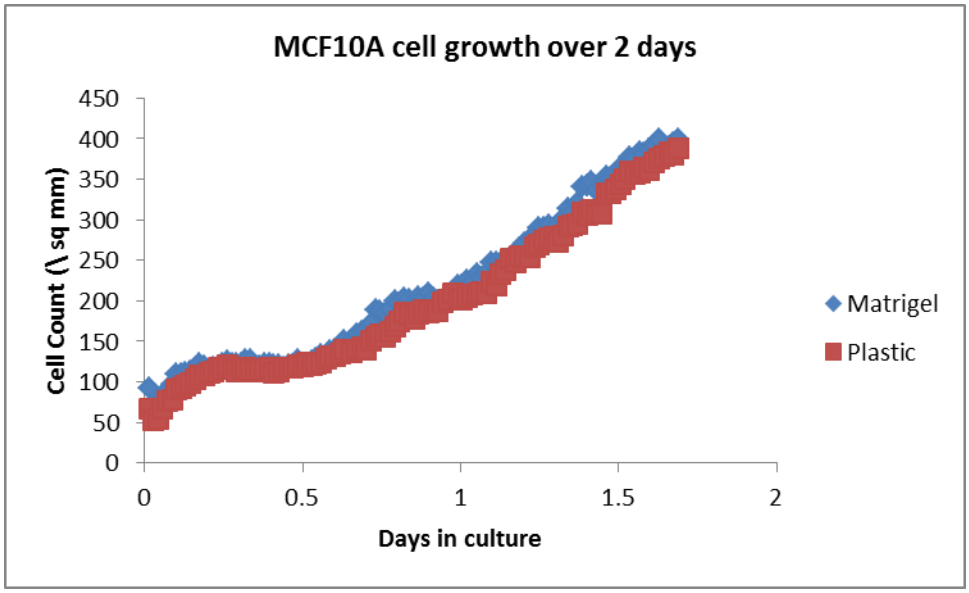

Figure 6.24. A thin layer of matrigel does not seem to affect the rate of growth of the cells.

Effect of density on cell migration speed and cell growth

Previously we saw that the speed of migration of the cells initially goes up, reaches a maximum and then decreases over time. The reason why this happens is clarified here. Figure 6.25 shows that when cells are plated at a lower density (red line) the cells take longer to reach the maximum migration speed. This suggests that the speed of the cells is dictated by the density at which they are plated.

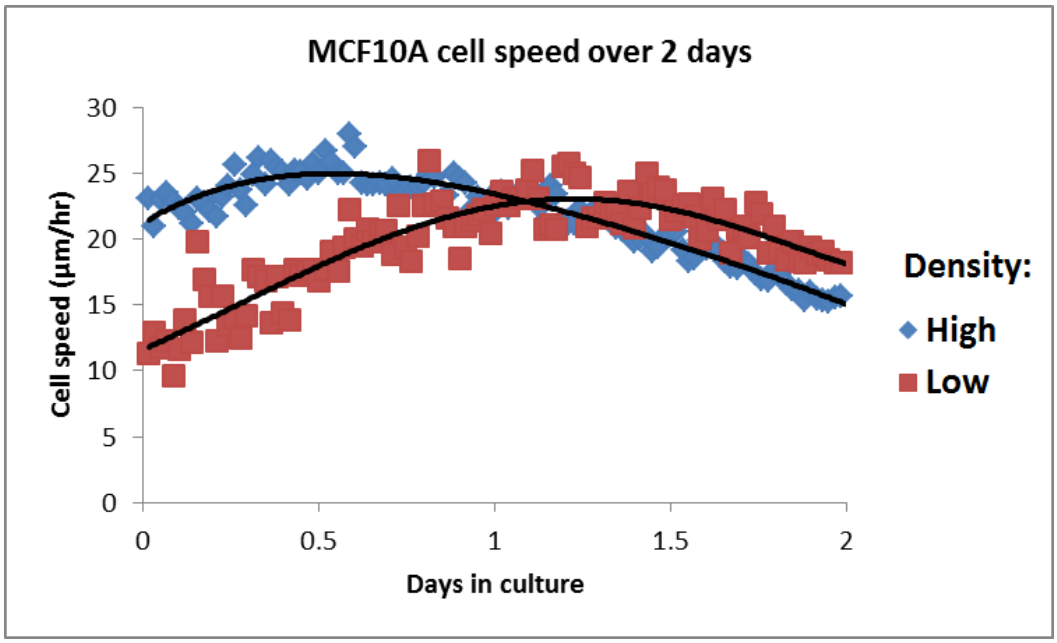

Figure 6.25. The effect on migration speed of plating cells at high (blue) and low (red) densities suggests that migration speed reaches a maximum at a certain density of cells. The next figure shows the correponding cell counts.

Figure 6.26 shows the cell counts for the same data as the previous figure, indicating that the maximum cell speed occurs at a cell count of approximately 150 to 200 cells per square millimeter.

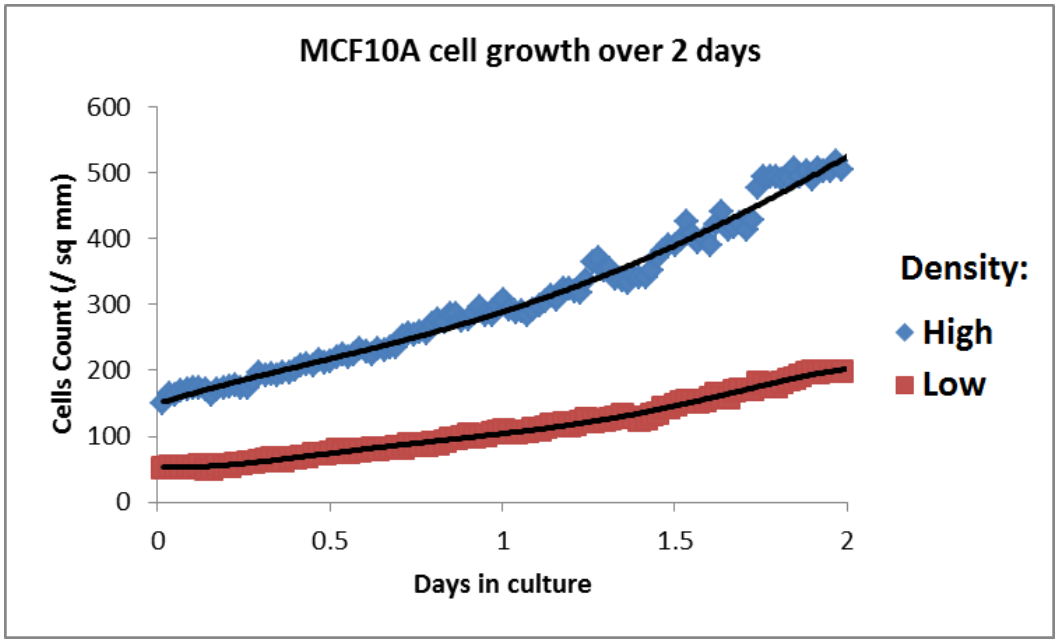

Figure 6.26. Cell counts at two different densities that corresponding to the previous figure.

Scratch assays

CA1a cells appear to migrate faster than 10A cells in scratch assays. Cells were plated and placed in the incubator until they reached confluence. Then a pipet tip was used to create a gap by scratching on the epithelial layer. The time for the gap to close was tracked with image analysis. The average of 48 videos is shown in Figure 6.27.

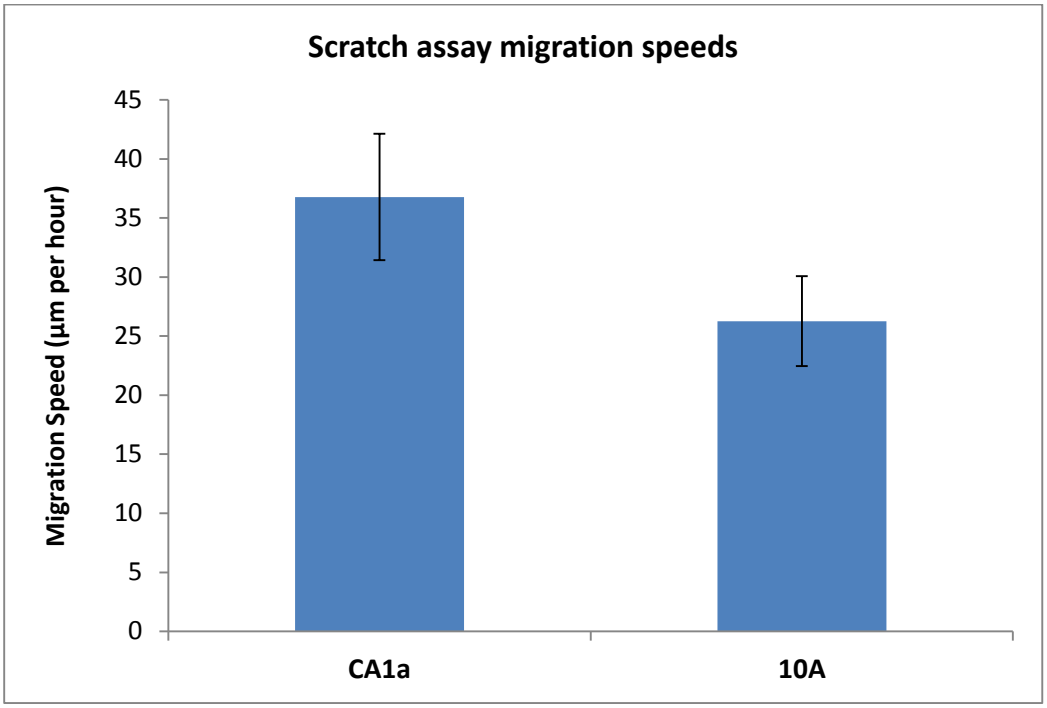

Figure 6.27. CA1a cells migrate faster than 10A cells in scratch assays (P<0.01).

The fact that CA1a cells close the gap faster is due to sheet migration. It also indicates that sheet migration is different from random migration of single cells, which is greater for 10A than for CA1a cells.

APPENDIX B: OTHER APPLICATIONS OF THE MICROSCOPE

Submitted co-authored Papers

A microRNA miR-34a-Regulated Bimodal Switch Targets Notch in Colon Cancer Stem Cells.

In this collaboration with Pengcheng Bu form the Shen Lab at Cornell I performed time-lapse fluorescence imaging of colon cancer stem cells with my microscope, the result of which is shown in Figure 7.1. This article was published in the journal Cell Stem Cell on May 2, 2013.

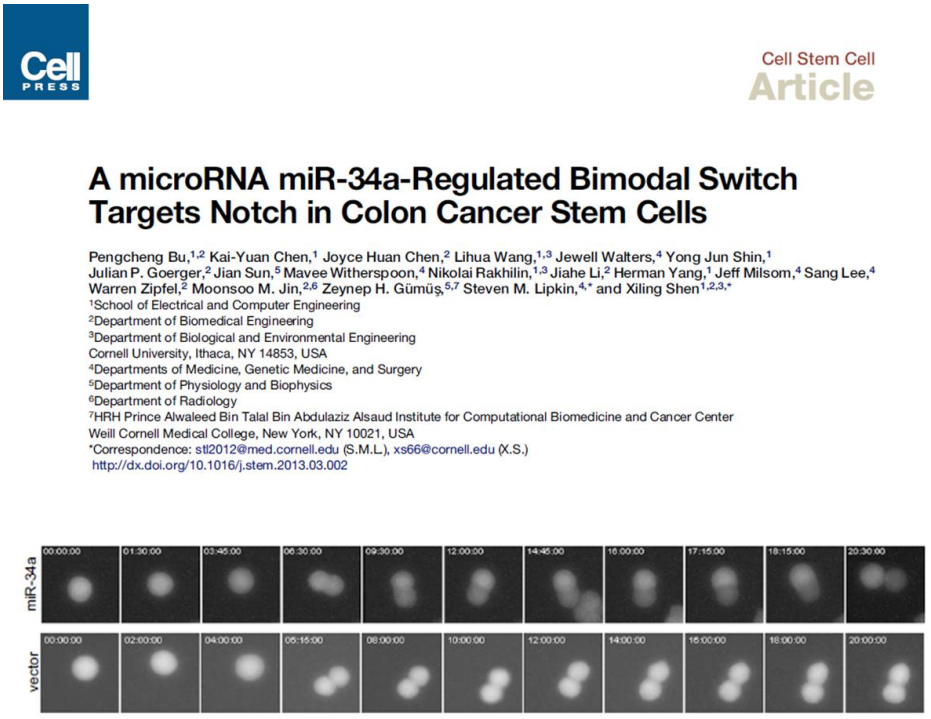

Figure 7.1 A figure contributed to the article.

Recruitment of mesenchymal stem cells by bone marrow concentrate and platelet rich plasma.

In this collaboration with Hannah Holmes from the Cornell Vet School Fortier Lab I performed time lapse imaging of horse mesenchymal bone marrow primary cells that were cultured in Ibidi flow chambers to study the chemotaxis of these cells as a response to growth factors and platelet rich plasma. The article has been submitted to Journal of Orthopaedic Research.

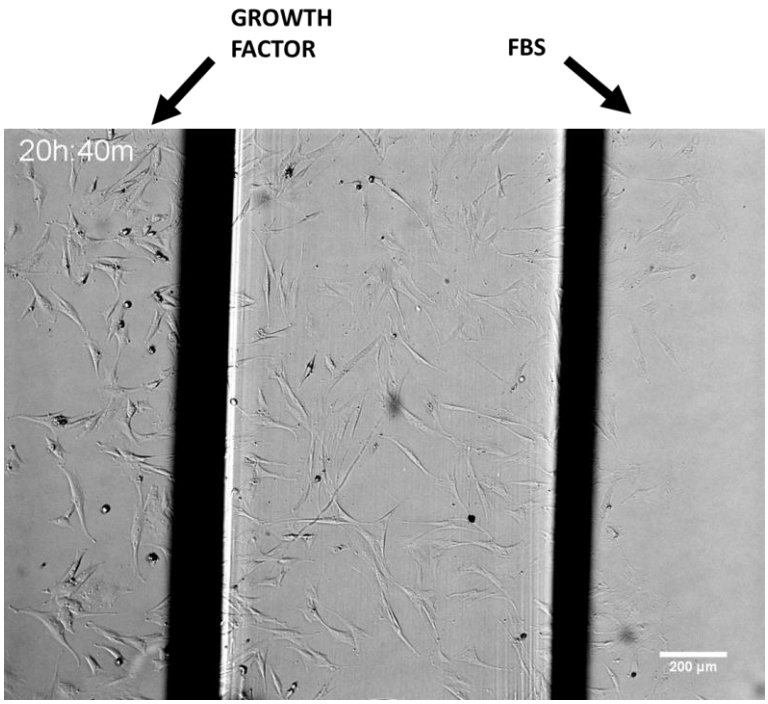

Figure 7.2 An example of the images acquired of horse mesenchymal stem cells in Ibidi chambers.

I was also involved in the analysis of the data by creating programs for tracking the cells (mentioned in an earlier chapter) and displaying results of migrating cells as shown in Figure 7.3.

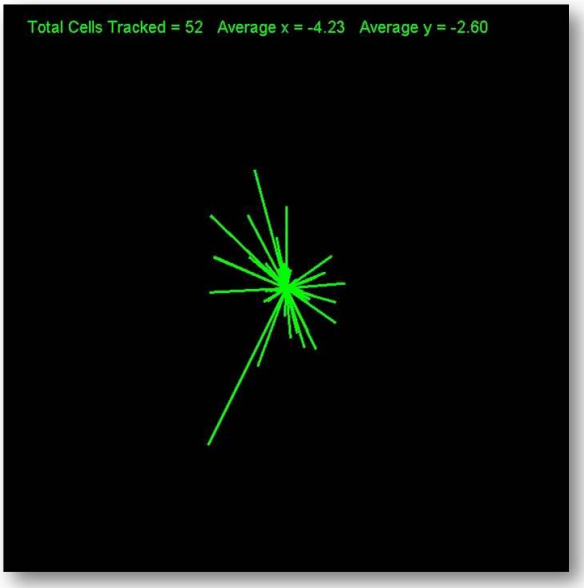

Figure 7.3 The tracks of individual cells are superposed and displayed along with the data of the tracking of the cells.

Other preliminary collaborative data

Triggering X-ray computed tomography with real time image analysis of heart beats in chicken embryo vessels

In collaboration with Cornell's Butcher lab I developed a way to trigger an x-ray machine via images acquired form pulsating blood vessels, in an effort to synchronize the x-ray images with heart beats to improve the quality of images of the heart. The system involves a lamp that illuminates the sample via an adjustable neck and a fiber optic bundle cable that transmits the image of the sample to an objective lens and a camera. There are motors to move the neck in 4 different directions because of the space constrictions inside the CT machine. Also because of space constrictions a mirror was added to the end of the cables. All of this is illustrated in Figure 7.4 and Figure 7.5.

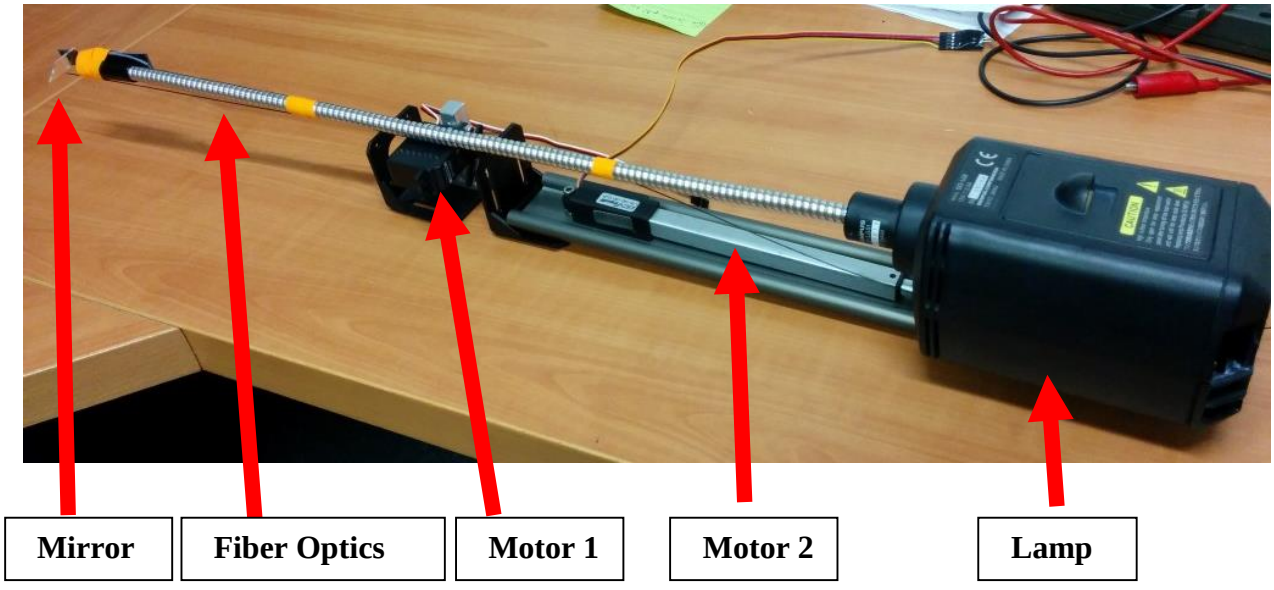

Figure 7.4 Illumination and image acquisition end.

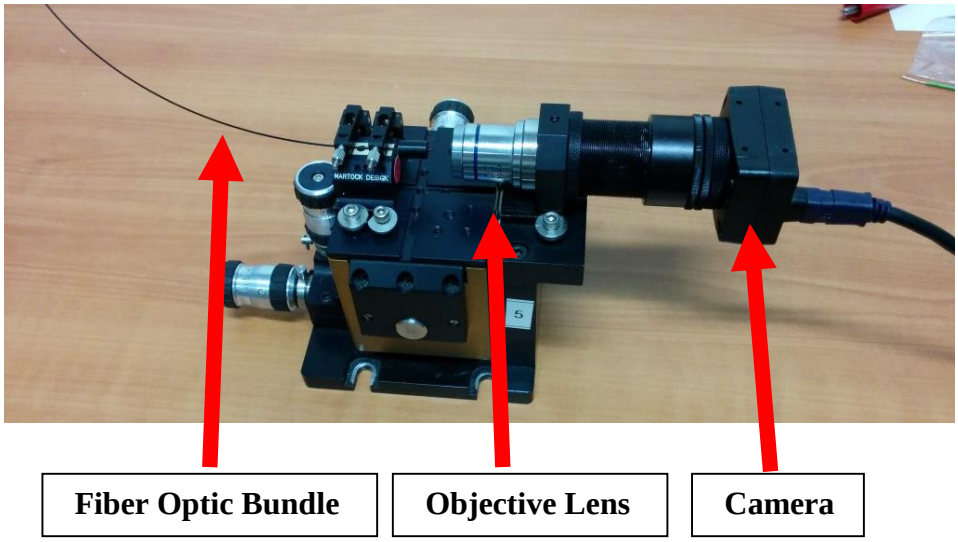

Figure 7.5 The back end of the fiber optic cable meets the objective lens and a camera. The knobs allow for precise alignment of the fiber with the objective lens.

Figure 7.6 shows how a chicken embryo is imaged within an egg through an opening in the shell. The images of pulsating blood vessels are analyzed by a computer program that I have developed. This program displays the images and a graph that represents the oscillations of the blood vessel. It triggers a signal for each pulsation which causes the CT-machine to acquire an x-ray image. See Figure 7.7.

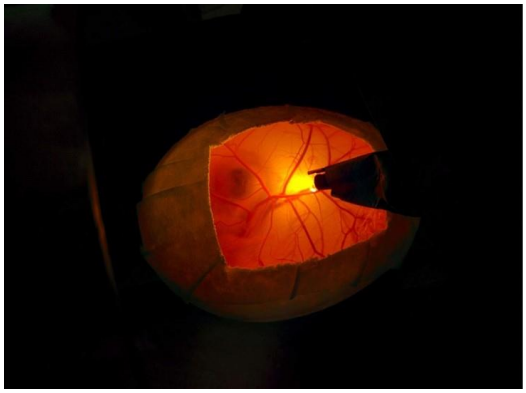

Figure 7.6 The fiber optic is placed close to a blood vessel of the developing embryo

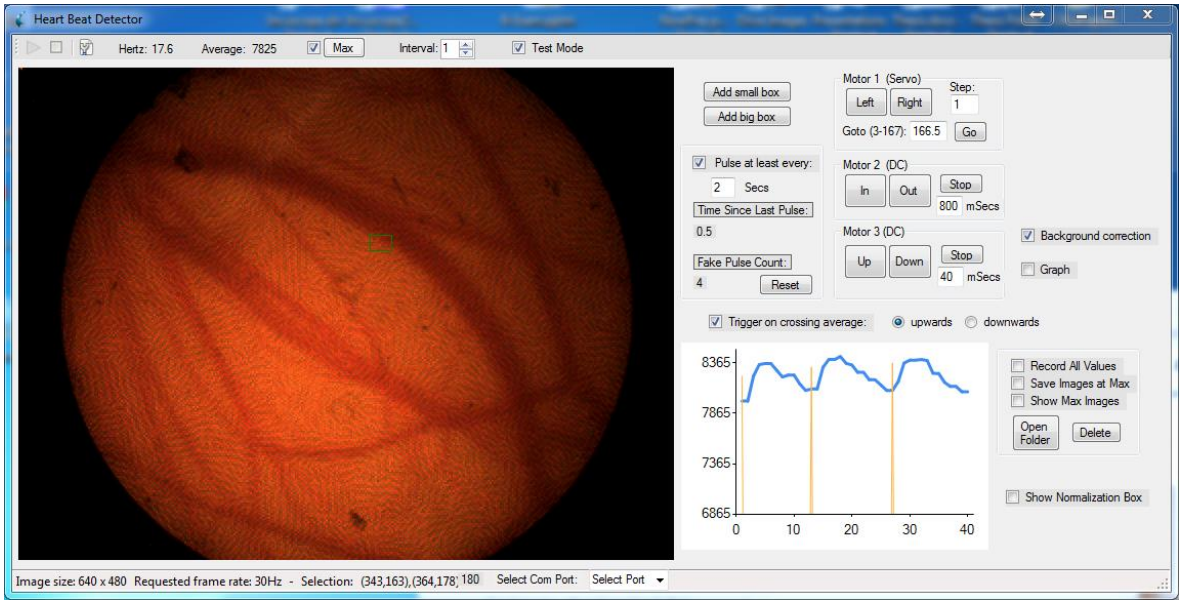

Figure 7.7 My program to detect pulsation of blood vessels. The pulsations are shown on the lower right. The red vertical lines in the graph correspond to automatically detected heart beats and trigger the acquisition of an x-ray image.

The user must first select the area on the image to be analyzed by a green rectangle. This must be placed at an edge of the blood vessel where the intensity oscillates with each pulsation. The blue line in the graph represents the intensity within this green rectangle. To detect each heart beat two algorithms are available. One detects the intensity maxima which is done by analyzing at the past 5 time point. The second algorithm is more sensitive and it triggers when the signal crosses the average of the last 20 points, the user can select if it will trigger when it's crossing it upwards or downwards. Due to the fact that the light might flicker, the values are normalized to the background intensity and this can be disabled by unchecking the checkbox labeled background correction.

Other features of the program are buttons to control the motors and buttons to save the values. Additionally the program can send signals at specified intervals because if the CT machine doesn't receive any signal after some time it will crash. At the bottom of the window is a drop box to select the COM port of the Arduino board. The program on the Arduino board must act when it receives an 'm' character (for "maximum") and set one of its pins to 5V which will signal the CT machine to acquire an x-ray image.

Horse mesenchymal bone marrow primary cells- Cornell Vet School Nixon Lab

Background

Primary cells from the bone marrow of horses where obtained from the Nixon Lab in the Cornell Veterinary College. Cells from young and old horses were imaged to compare the differences associated with age. Additionally, cells from passage 2 and passage 6 were imaged to assess the difference brought about by passage number. This is important to know for cell transplantation studies in cell therapy. For example, these cells are introduced into the joints of horses to regenerate their cartilage. If cells change from passage 2 to passage 6 it would mean that they might no longer be suitable for cell transplantation after passage 6. Additionally the effect of aging is also important to determine what age is suitable for cell transplantation.

Semi-automated cell speed determination

Because the cells are not fluorescent, we have to use a semi-automated method to track the cells. Figure 7.8 shows the movement of the cells during a 24 hour period. (Some cells are not tracked because they originate from dividing cells).

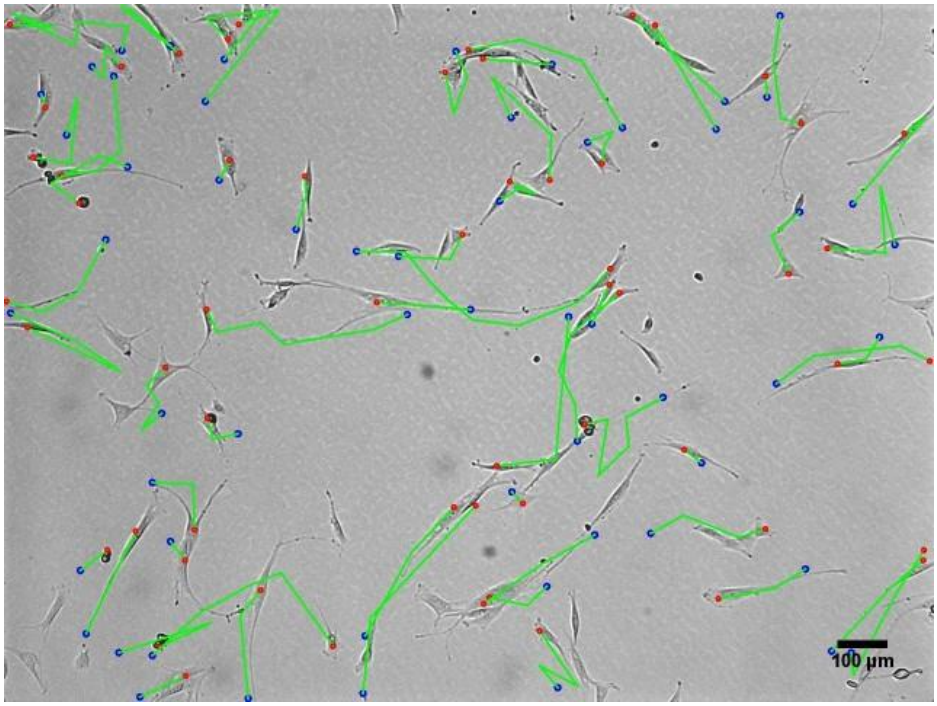

Figure 7.8 A semi-automated method for tracking mesenchymal bone marrow primary cells. Blue dots indicate the starting position of the cells and red dots indicate the finishing position.

Figure 7.9 shows the result of the tracking. Both passage number and age of horse affect the migration speed of the cells.

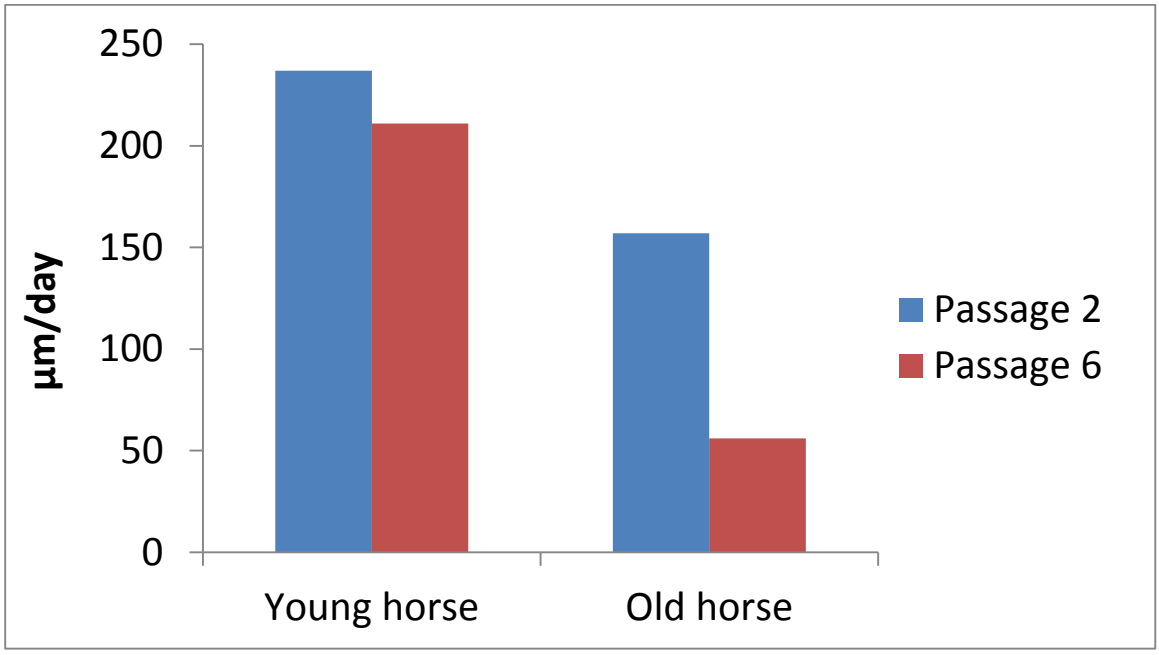

Figure 7.9 Preliminary data of tracking the horse mesenchymal bone marrow primary cells over a 24 hour period. Both passage number and age of horse seem to affect the migration speed of the cells.

Older cells also show an increase in size

Cells from old horses contain large cell that are not present in young horses (Figure 7.10).

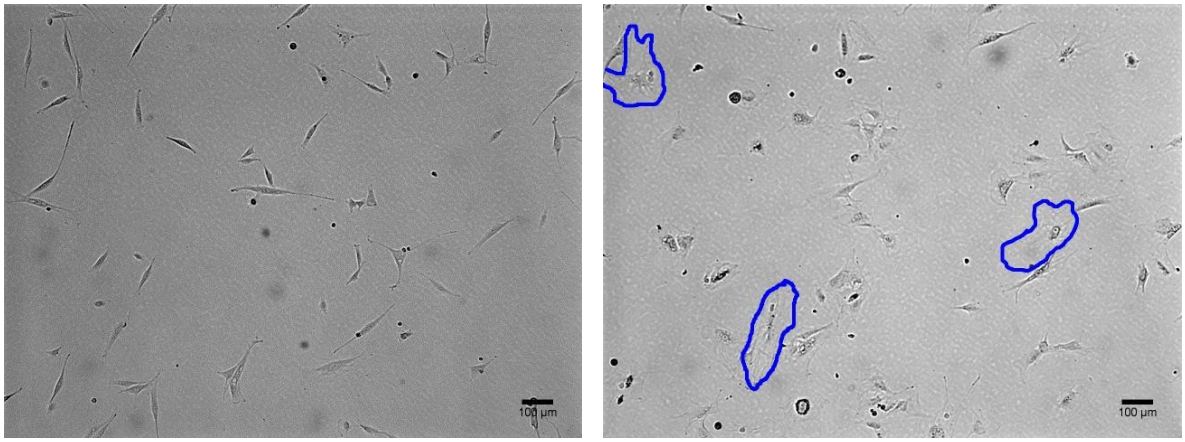

Figure 7.10 Large cells (shown in blue) appear in cells from old horses (Right) but are not present in young horses (Left).

Old horse bone marrow stromal cells seem to harbor high speed cytotoxic T-like cells

Small and highly motile cells were only present in the samples of hold horses. These have the characteristic morphology typically found in T cells (Figure 7.11).

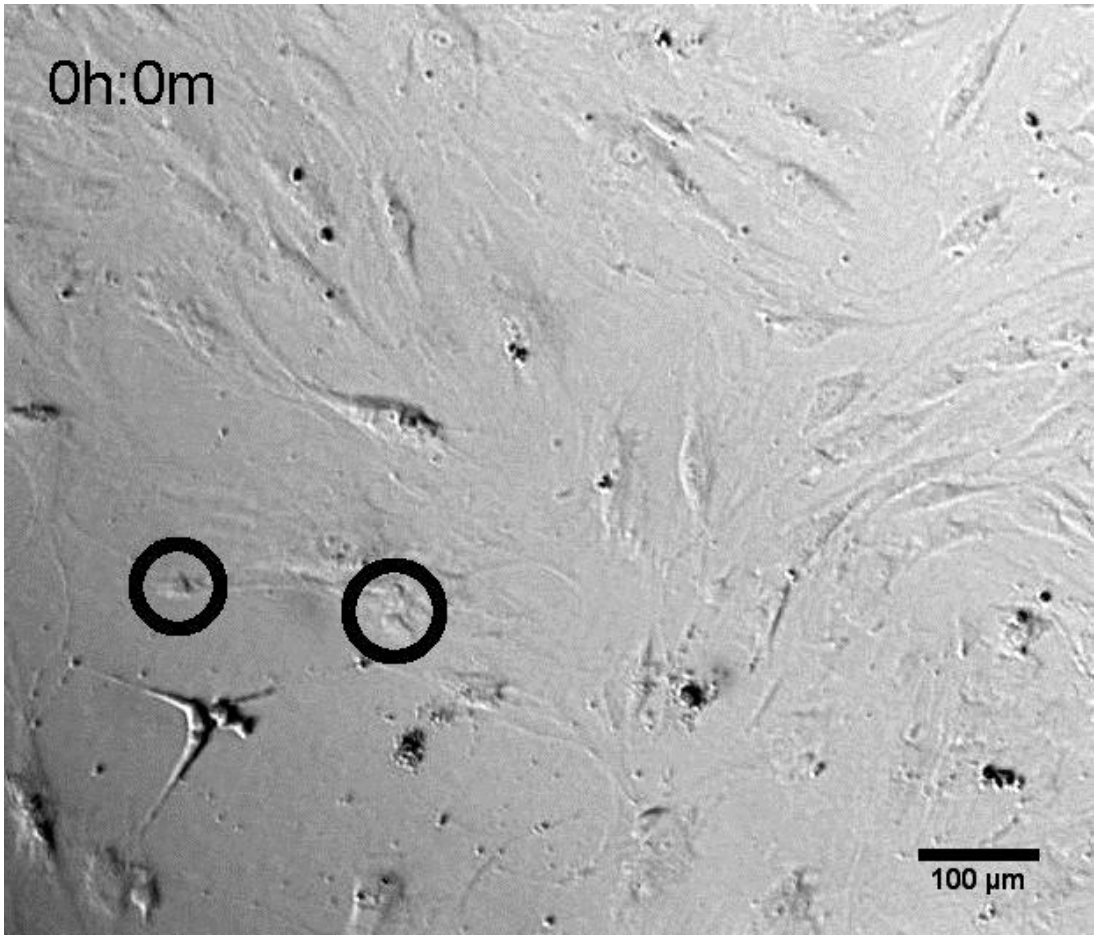

Figure 7.11 The circles indicate the position of two small and highly motile cells.

The speed of migration of the small T-like cells was orders of magnitude larger than the other cells (Figure 7.12).

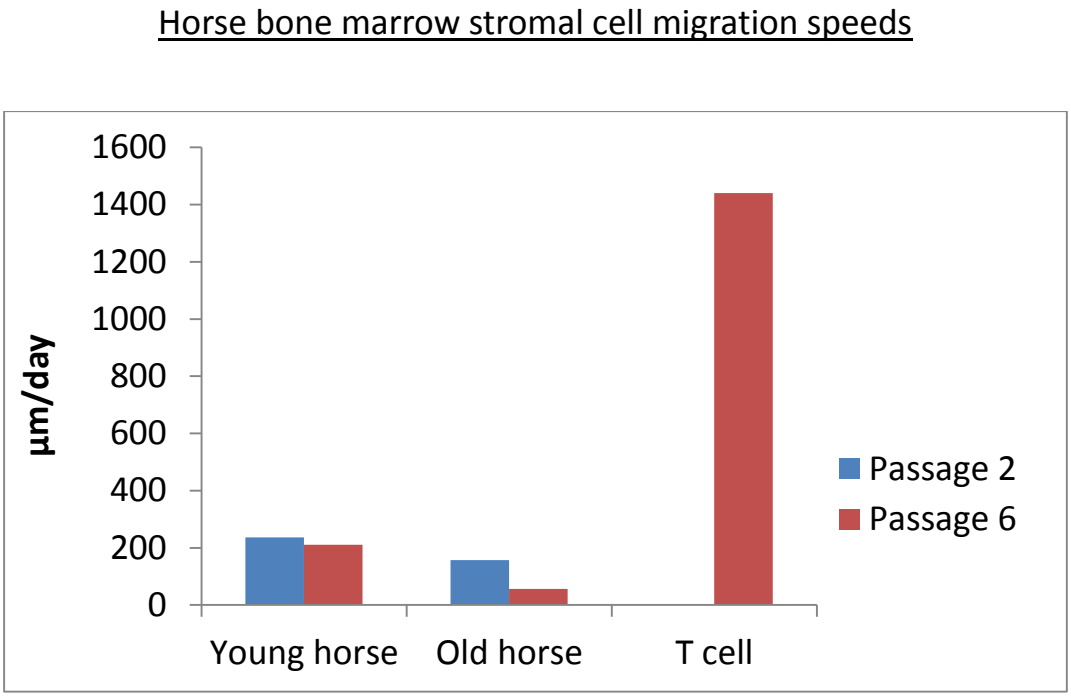

Figure 7.12 The data from the previous Figure 7.9 is shown here next to the speed of the T cells for comparison purposes.

T-like cells attack primary stromal cells

In Figure 7.13 the blue line indicates the area covered by cytotoxic T-like cells and the red circles show the cells that die within a 23 hour period. This indicates that the T-like cells are likely causing the death of the other cells.

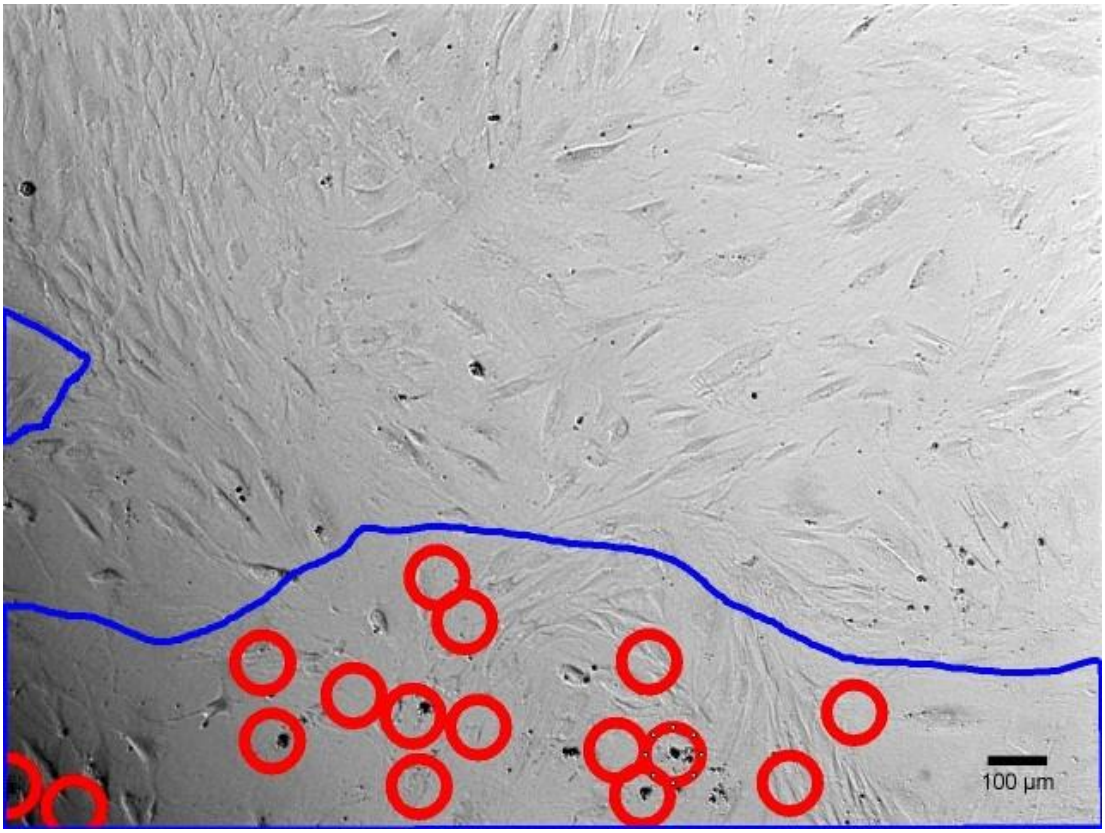

Figure 7.13 Blue line indicates the area covered by T-like cells. Red circles show the cells that die within a 23 hour period.

Cardiomyocytes and cell stress

In an alternative use of my incubator microscope, Cornell's Shuler lab used it to look at the contractions of cardiomyocytes over time. The contractions are very sensitive to temperature and therefore having a microscope inside the incubator is an advantage when performing these experiments. Figure 7.14 shows a colony of cardiomyocytes which contract in synchrony.

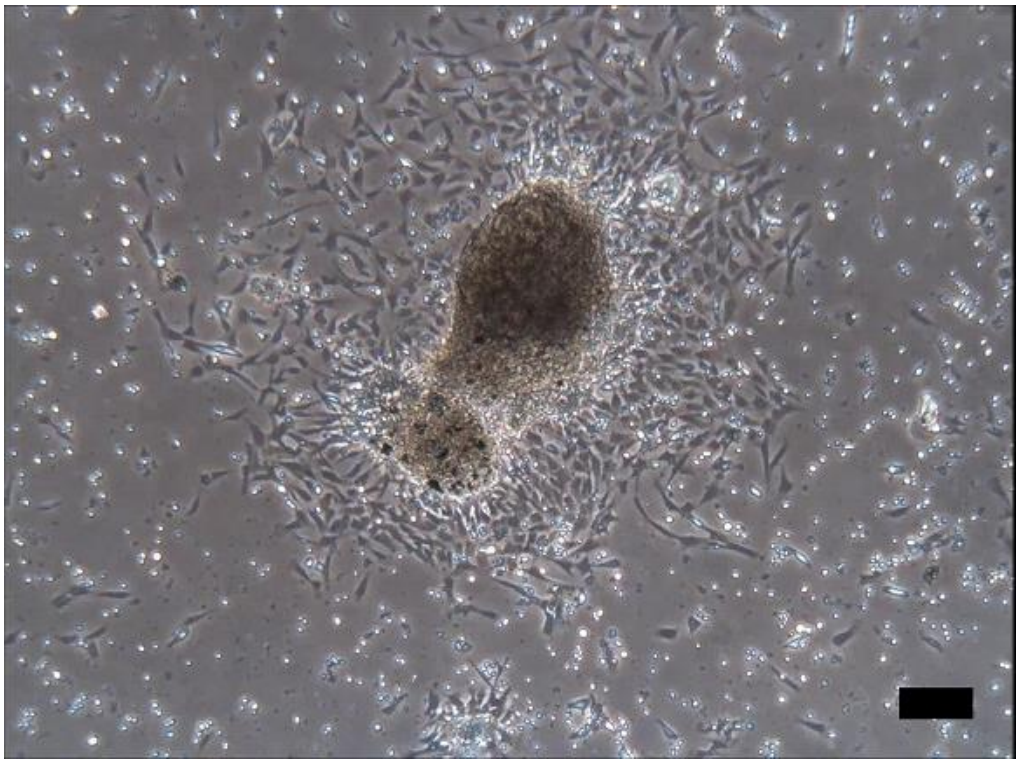

Figure 7.14 Pulsating Cardiomyocytes. Scale bar 50µm.

Additionally I created a computer program to automatically analyze and quantify the contractions of the pulsating cells from the images and create a graph from the data (Figure 7.15).

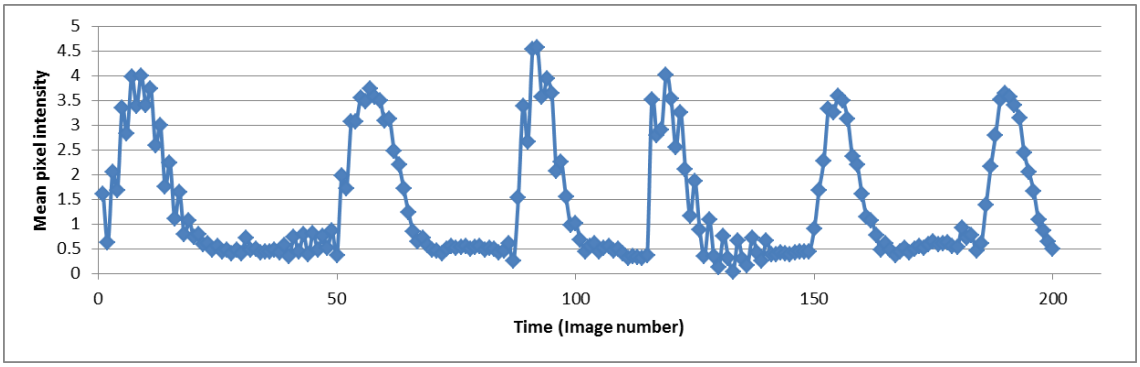

Figure 7.15 Profile of cardiomyocyte contractions over time.

We noticed that the pulses would become slower as soon as we took the cells out of the incubator, which indicates that the pulsations are very sensitive to temperature.

Therefore measuring the rate of pulsations could be a good way to know the state of the cells in real time.

This experiment could be used to very quickly identify which substances or conditions affect the pulsations of the cells and could inform us about the overall state of the cells and what conditions are toxic to them.

Unlike studies of cell growth, looking at pulsation can tell you whether the cells are undergoing stress immediately, without having to wait days for a result.

Cell retractions

Just as changes in conditions affect the pulsation of contractile cardiomyocytes, I asked myself whether this concept can be extended to regular cells that do not contract. For example the speed of migration of cells could also be an indicator of cell state or cell stress. However, from my experience, cell speed is vary variably random and often requires tracking fluorescent nuclei.

It is also possible to do time-lapse imaging of non-migrating cells to look at changes in morphology of the cells. This does not require fluorescent cells. I found out that the cells retract their cytoplasm within minutes in response to certain kinds of cell stress.

PBS stress test: I briefly changed the medium of 10AT cells from their original medium to 100% PBS without removing them from the incubator. Immediately the cells stopped membrane ruffling and started retracting their cytoplasm.

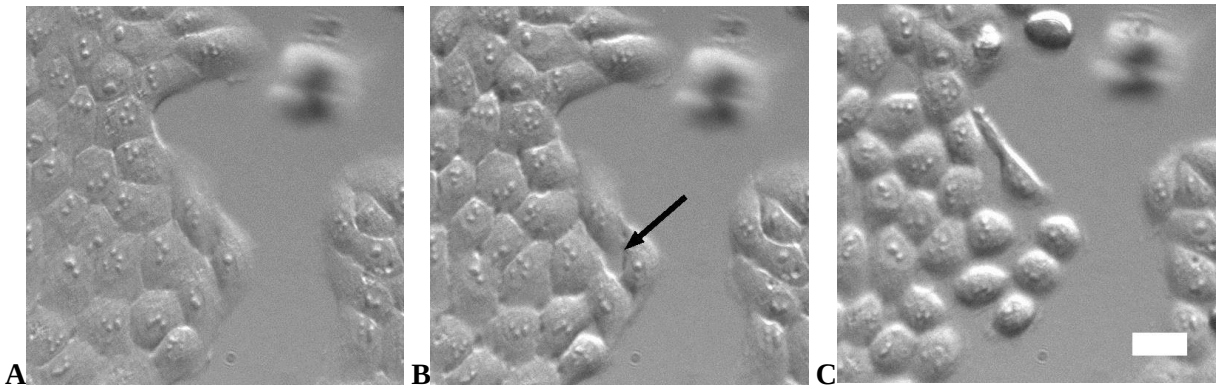

Figure 7.16 Effect of PBS on cells. (PBS is at 37C). A) 0min. B) 6min. C) 30min. The arrow shows that at 6min, a gap appears between the cells because the cytoplasms have started to retract. Scale bar 20µm.

When the PBS was replaced with the original medium, the cells resumed the membrane ruffling followed by cytoplasm extension.

I conducted similar experiments with CO2, changing medium, and ethanol. CO2 did not affect cell shape but changing medium did produce contractions that recovered 10min later. Ethanol seems to cause membrane blebbing but only in cells that are rounded up and not on attached cells.

Keratinocyte culture from Hair Follicle

Another area where my time lapse microscope could be useful is the study of the expansion of human keratinocytes from hair follicles. Recently this method has become popular for obtaining primary

keratinocytes for induced pluripotency studies where keratinocytes are transformed to induced pluripotent stem cells.[49] The original cells for these studies come from plucked hair follicles.

I was able to obtain cells from my own hair follicle and the result is shown in Figure 7.17, which shows how cells expand in a layer from the follicle.

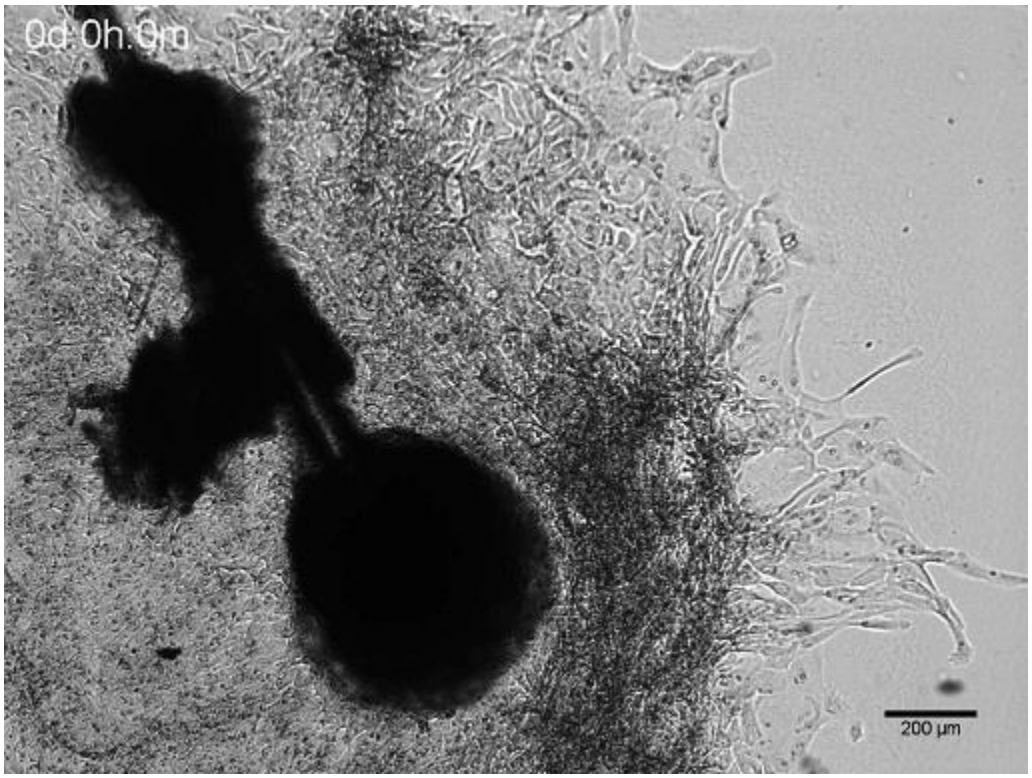

Figure 7.17 An epithelial layer of primary cells expands from a plucked hair follicle.

The resulting layer of cells is composed of two layers. Figure 7.18 is a higher magnification image showing these two layers as they advance over the culture dish.

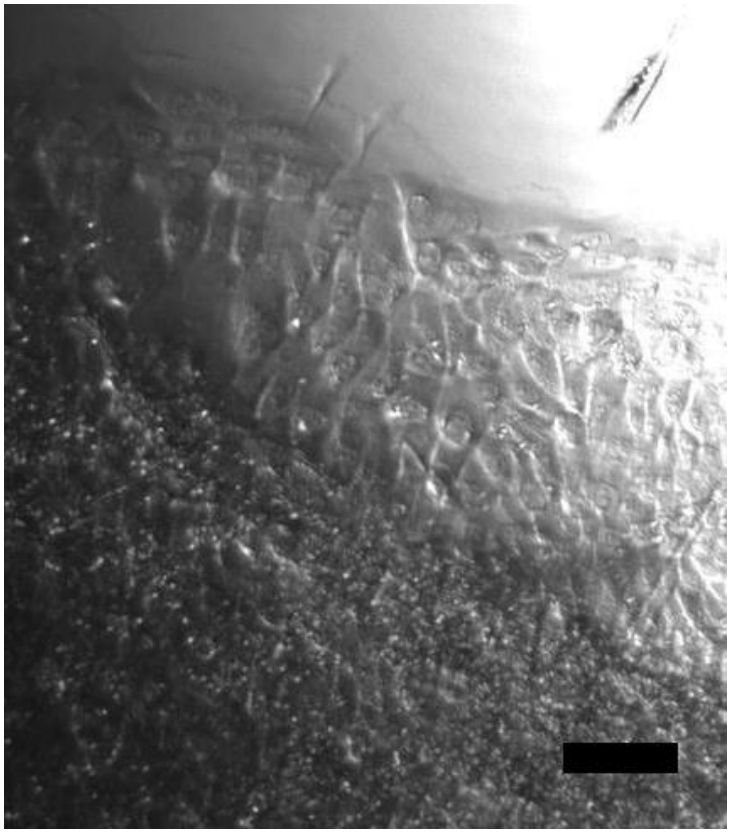

Figure 7.18 The advancing layer of cells is composed of an epithelial layer (top of image) and an additional layer on top of it (bottom of image). Scale bar 80μm.

Scratch assays reveal that migration inhibits division

While analyzing the videos of scratch assays performed on epithelial layers of cells I realized that there is a sudden increase in the number of divisions right after the gap made by the scratch is closed by the cels. Figure 7.19 shows an analysis of this effect.

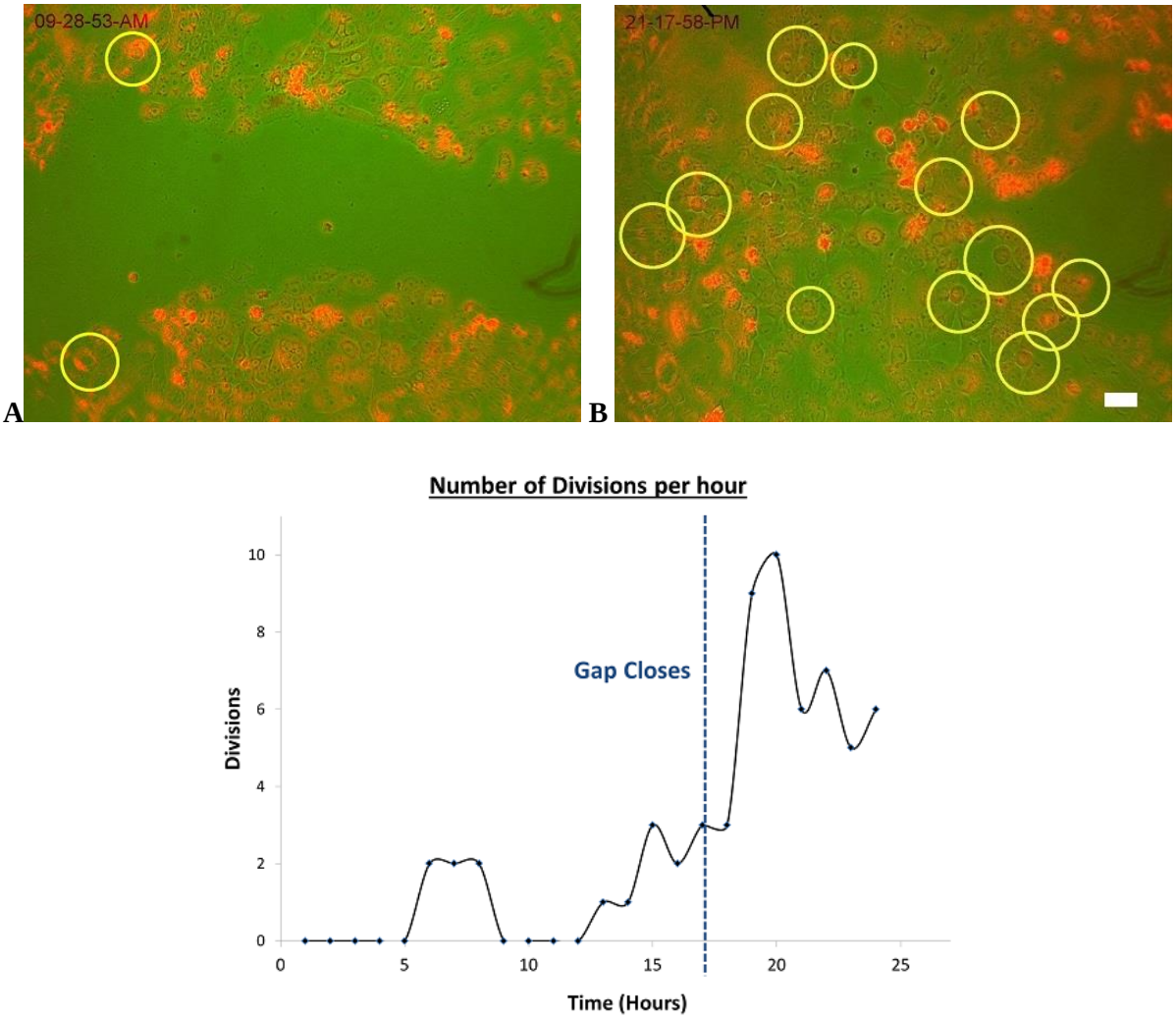

Figure 7.19 The graph illustrates that the number of divisions increases sharply after the gap in the epithelial layer has closed. Yellow circles indicate cells with active mitosis. Image (A): Before the gap closes. Image (B): After the gap closes. The number of divisions is normalized by the area covered by the layers of cells. Scale bar 50µm.

In my opinion, the increase in the number of divisions is due to the fact that the cells stop moving when the gap closes. When the gap is not yet closed the epithelial layers on either side of the gap are moving (this is clear when looking at the videos). It seems that the motion inhibits the entry into mitosis and therefore when the cells stop moving they are "synchronized" to enter mitosis all at the same time.

Darkfield illumination can detect subpopulations of primary cells

Darkfield imaging can be combined with brightfield for the detection of certain types of cells. In Figure 7.20 primary cells that we took from mouse mammary glands show a subpopulation of cells that appears bright under darkfield (shown in orange) while the majority of the cells only appear in brightfield mode (shown in green). The identity of the orange cells is unknown to me but the increase in darkfield contrast is probably due to vesicles in the cytoplasm of these cells.

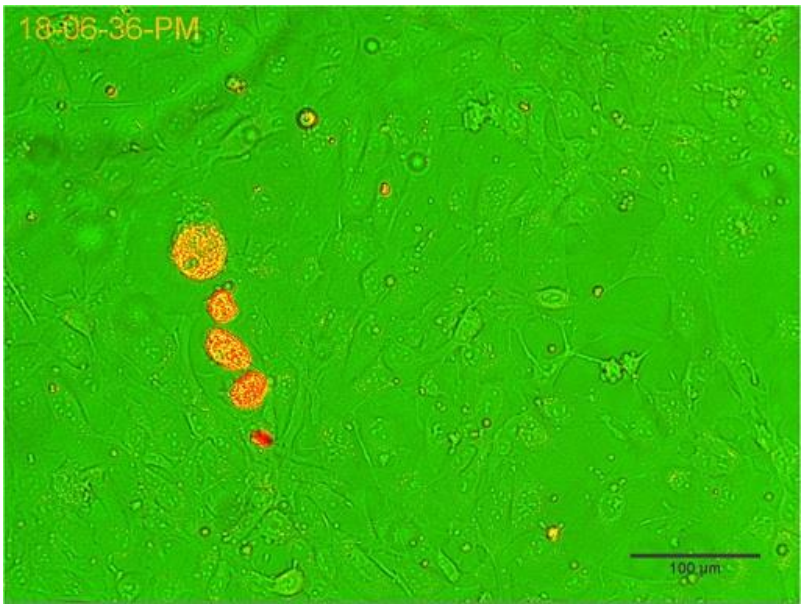

Figure 7.20 A brightfield image (green) and a darkfield image (orange) are combined into one image, revealing that only four cells are bright in darkfield mode.

Parts List for a simple non-fluorescent Microscope

Objective Lens: RMS4X RMS10X	**Most RMS lenses will work.** **The objective lenses that I use are listed here:** **Description:** 4X Olympus Plan Achromat Objective, 0.10 NA, 18.5 mm WD **Manufacturer:** Olympus/Thorlabs **Link:** http://www.thorlabs.us/newgrouppage9.cfm?objectgroup_id=1044 **Price:** $196 **Description:** 10X Olympus Plan Achromat Objective, 0.25 NA, 10.6 mm WD **Manufacturer:** Olympus/Thorlabs **Link:** http://www.thorlabs.us/newgrouppage9.cfm?objectgroup_id=1044 **Price:** $388
Camera: 	**Most PointGrey cameras such as Chameleon or Flea will work.** **The ones I use is listed here:** **Description:** Chameleon 1296x964px 1.3 MP Mono USB 2.0 **Manufacturer:** Point Grey **Link:** http://www.ptgreystore.com/search.aspx?searchterms=chameleon **Price:** $375
Two 2" 6mm Rods: 	**Description:** Two ER2 Cage Assembly Rod, 2" Long, Ø6 mm **Manufacturer:** Thorlabs **Link:** http://www.thorlabs.us/newgrouppage9.cfm?objectgroup_id=4125 **Price:** 2X$6.10=$12.20

Two 1” 6mm Rods: 	**Description:** Two ER1 Cage Assembly Rod, 1" Long, Ø6 mm **Manufacturer:** Thorlabs **Link:** http://www.thorlabs.us/newgrouppage9.cfm?objectgroup_id=4125 **Price:** 2X$5.40=$10.80
One Vertical ½ inch Rod: 	**Description**: One TR12 Ø1/2" x 12" Stainless Steel Optical Post, 8-32 Stud, 1/4"-20 Tapped Hole **Manufacturer:** Thorlabs **Link:** http://www.thorlabs.us/newgrouppage9.cfm?objectgroup_id=1266 **Price:** $10.82
Three Horizontal ½ inch Rods: 	**Description**: Three TR2 Ø1/2" x 2" Stainless Steel Optical Post, 8-32 Stud, 1/4"-20 Tapped Hole **Manufacturer:** Thorlabs **Link:** http://www.thorlabs.us/newgrouppage9.cfm?objectgroup_id=1266 **Price:** 3X $5.19= $15.57
90deg Clamp: 	**Description**: Three RA90 Right-Angle Post Clamp, Fixed 90° Adapter **Manufacturer:** Thorlabs **Link:** http://www.thorlabs.us/newgrouppage9.cfm?objectgroup_id=1985 **Price:** 3X $$9.48= $28.44
Pedestal: 	**Description**: PH3E Pedestal Post Holder, Spring-Loaded Hex-Locking Thumbscrew, L = 3.19" **Manufacturer:** Thorlabs **Link:** http://www.thorlabs.us/newgrouppage9.cfm?objectgroup_id=1268 **Price:** $24.00

Clamp: 	**Description**: CF125 Small Clamping Fork, 1.25" Counterbored Slot, Universal **Manufacturer:** Thorlabs **Link:** http://www.thorlabs.us/newgrouppage9.cfm?objectgroup_id=1268 **Price:** $8.75
2.5 inch Base Plate: 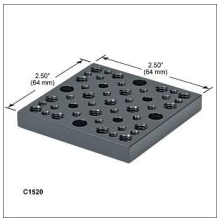	**Description**: C1520 Adapter Plate for Post Mounting Clamp, 2.5" x 2.5" **Manufacturer:** Thorlabs **Link:** http://www.thorlabs.us/newgrouppage9.cfm?objectgroup_id=169 **Price:** $29
Objective and Sample Support: 	**Description**: Three CP08 SM1 Threaded 30 mm Enhanced Clamping Cage Plate, 0.35" Thick **Manufacturer:** Thorlabs **Link:** http://www.thorlabs.us/newgrouppage9.cfm?objectgroup_id=2273 **Price:** 2X$19.00=$38
LED Support: 	**Description**: SM05-Threaded 30 mm Cage Plate, 0.35" Thick **Manufacturer:** Thorlabs **Link:** http://www.thorlabs.us/newgrouppage9.cfm?objectgroup_id=2273 **Price:** $16
Upper Lens Tube Spacers:	**Description**: SM1S10 SM1 Lens Tube Spacer, L = 1" **Manufacturer:** Thorlabs **Link:** http://www.thorlabs.us/newgrouppage9.cfm?objectgroup_id=3307

	Price: $12.00
Lower Lens Tube Spacers: 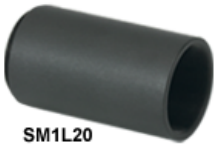	**Description**: **Two** SM1L20 SM1 Lens Tube, 2" Thread Depth **Manufacturer:** Thorlabs **Link:** http://www.thorlabs.us/newgrouppage9.cfm?objectgroup_id=3307 **Price:** 2X$16.50=$33
Tube Lens: 	**Description**: LA1433-ML Ø1" N-BK7 Plano-Convex Lens, SM1-Threaded Mount, f = 150.0 mm, Uncoated **Manufacturer:** Thorlabs **Link:** http://www.thorlabs.us/newgrouppage9.cfm?objectgroup_id=6276 **Price:** $31.03
Objective Adapter for RMS objective lenses: 	**Description**: SM1A3 Adapter with External SM1 Threads and Internal RMS Threads **Manufacturer:** Thorlabs **Link:** http://www.thorlabs.us/newgrouppage9.cfm?objectgroup_id=1524&pn=SM1A3#5081 **Price:** $16.75
Tube Adapter for Pointgrey Cameras: 	**Description**: SM1A9 Adapter with External C-Mount Threads and Internal SM1 Threads **Manufacturer:** Thorlabs **Link:** http://www.thorlabs.us/newgrouppage9.cfm?objectgroup_id=1524&pn=SM1A9#5082 **Price:** $19.75

LED Option 1: 	**Description**: TINKERKIT RED LED MOD 10MM **Manufacturer:** Arduino/Mouser Electronics **Link:** http://www.mouser.com T010118 **Price:** $6.95 This is not the recommended LED but it can be used and it simplifies the installation greatly if used with a TinkerKit shield. The recommended LED is shown next.
LED Option 2: 	**Description**: Diffused LED - RGB 10mm COM-11120 **Manufacturer:** Sparkfun **Link:** https://www.sparkfun.com/products/11120 **Price:** $0.95 This LED can be driven directly from Arduino pins, but requires the use of resistors. Also pictured is the LED Holder (10mm) COM-11148
LED Cable: 	**Description**: Cable Assemblies TOOLKIT WIRES 100CM MODULE **Manufacturer:** Arduino/Mouser Electronics **Link:** http://www.mouser.com T020080 **Price:** $4.95
LED Controller Arduino Board: 	**Description**: ARDUINO UNO REV 3 **Manufacturer:** Arduino/Mouser Electronics **Link:** http://www.mouser.com **A000066** **Price:** $25
Arduino Shield **(only when using LED Option 1)**	**Description**: TINKERKIT - SHIELD SENSOR V.2 MODULE **Manufacturer:** Arduino/Mouser Electronics **Link:** http://www.mouser.com **T020010**

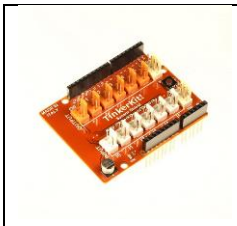	**Price:** $15.95
Optional **Arduino and Breadboard Holder:** 	**Description**: Arduino and Breadboard Holder **Manufacturer:** SparkFun **Link:** https://www.sparkfun.com/products/11235 **Price:** $3.95
Arduino Usb Cable: 	**Description**: USB Cable A to B - 6 Foot **Manufacturer:** SparkFun **Link:** https://www.sparkfun.com/products/512 **Price:** $3.95
Power Supply: 	**Description**: Wall Power Adapter: 5VDC **Manufacturer:** Pololu **Link:** http://www.pololu.com/catalog/product/1460 **Price:** $5.95

Figure 8.1 A simple non-fluorescence microscope designed by me for the Schuler Lab at Cornell University. Note that this is not the microscope described in this thesis as this is only a bare minimum microscope..

Additional Components needed for fluorescence and incubator use as described in the thesis

Fluorescence excitation LED light source:

Description: Red (627nm) Rebel LED, Pre-Mounted On A 20mm Star Base - 62 lm

Manufacturer: Luxeon Star

Price: $6

LED support:

Description: This aluminium cylinder that acts as a heat sink and as a support for the LED was built in-house. Alternatively it can be replaced by a Luxeon heat sink as shown next.

Description: 40mm Heat Sink.

LED can be glued to the bottom side of the heat sink

Manufacturer: Luxeon Star

Price: $7

(Optional) Mount for Objective Lens for manual focusing:

Description: Z-Axis Translation Mount for 30mm Cage Systems

Manufacturer: Thor Labs

Price: $177

Mirror Cube

Description: CM1-G01 30 mm Cage Cube-Mounted Protected Aluminum Turning Mirror

Manufacturer: Thor Labs

Price: $173

Dichroic Cage Cube

Description: CM1-DCH Holds a Rectangular Dichroic Mirror at 45°

Manufacturer: Thor Labs

Price: $ 158

Dichroic mirror and filters

Description: Filter set *GFP-3035D-000*

Manufacturer: Semrock

Price: $745

Convex Lens

Description: BK 7 Bi-Convex Lens, 25.4 mm Diameter, 100 mm EFL, 430-700nm *KBX064AR.14*

Manufacturer: Newport

Price: $50

Condenser Lens For Fluorescence Excitation

Description : Aspheric Condenser Lens, 32.5 mm Diameter, 23 mm EFL

Manufacturer: Newport

Price: $45

Lens tubes

Description: 1 inch LT Series, 1 inch and ½ inch length

Manufacturer: Newport

Price: $15x7 = $105

Vertical Translational focusing stage

Description: Melles-Griot 07TEZ704 Vertical Stage

Manufacturer: Melles-Griot

Stepper motor for translational stage

Description: Stepper Motor: Bipolar, 200 Steps/Rev, 28×45mm, 4.5V, 0.67A

Manufacturer: Pololu

Price: $19

https://www.pololu.com/product/1206

Shaft coupler to connect motor to stage

Description: Helical Shaft Couplers, M5 to M6.35

Manufacturer: makerstoolworks.com

Price: $10

http://store.makerstoolworks.com/motion/helical-shaft-couplers-set-of-2/

Supplementary Information

Suppl Info 1 (referenced in the text)

(A) or histone-GFP(B) were cultured in a 48 well plate. To 200ul of medium in the well I added 20ul of CD44-GFP (A) or CD24-PE (B). The wells were washed and replaced with new medium after 30min of incubation and were imaged in time lapse mode. The second image shows the fluorescent nuclei, while the third shows the antibody staining. We can detect some level of CD44 but no level of CD24. In relation to

Iliopoulos[47] et al. this would mean that these cells have some relation to cancer stem cells. 40ul was also tried with no increase in fluorescence. The fluorescence decreases quickly with time, making it not possible to track cells.

Suppl Info 2

This was also 20ul in 200ul medium but I also did 100ul in 200ul medium and 20ul in 200ul PBS with the same result (and for B I even did 100ul of antibody into 200ul).

Suppl Info 3

Aldefluor instruction:

-Add 5 µL of activated Aldefluor substrate per ml of sample and incubate for 30min

Aldefluor added to 10A cells: 5 wells of a 48well plate, added 0,1,5,3,3ul of Aldefluor stock solution, each to 200ul of the used medium except the last 3ul well which only contains 200ul of Aldefluor buffer. Waited 30min, removed old media add new media.

Programming codes for IncuScope, Arduino, ImageJ

All the code for the main IncuScope, electronics (Arduino) and ImageJ macro scripts will be available online at the GitHub website https://github.com/julian202/. Personal questions can also be addressed to me at julian202@gmail.com.

A program to sort PubMed results

When performing searches for articles in PubMed, the results are not order by impact factor. To me it seems very important to read first the most impactful papers, especially in cases when the results are thousands of papers long. For this I developed a program to automatically order article results from PubMed by impact factor. The user must only download the results file from PubMed and drag it into the program's main window and the results will automatically be displayed in order according to the impact factor of the journal in which the papers were published.

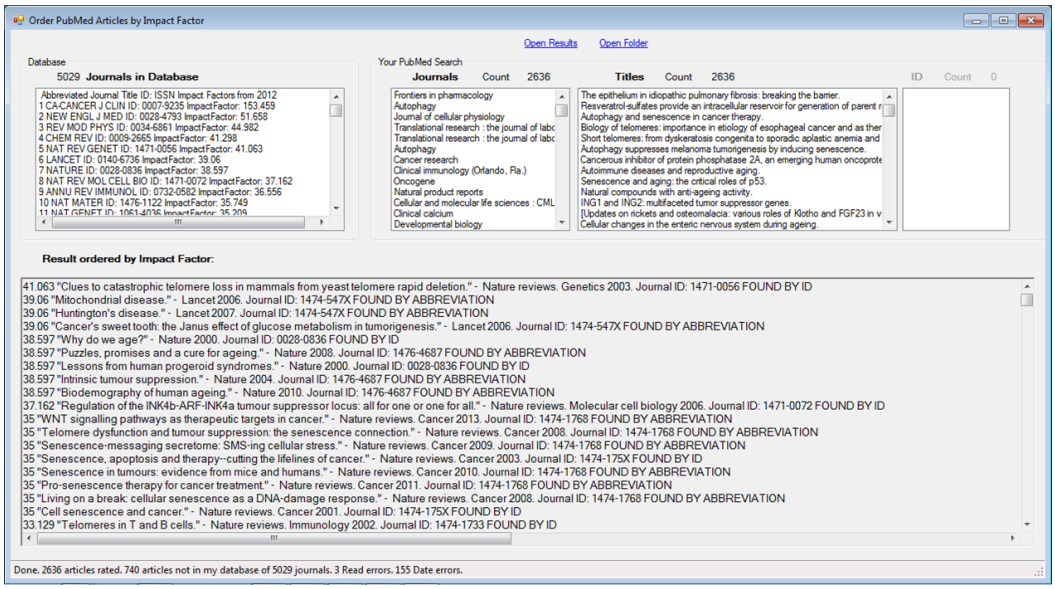

Figure 8.2 The program to sort PubMed results (Order Articles)

I will make this Windows program available online at the GitHub website https://github.com/julian202/, and personal questions can be addressed at julian202@gmail.com.

REFERENCES

1. Nigg EA. Centrosome aberrations: Cause or consequence of cancer progression? *Nat Rev Cancer*. 2002;2(11):815-825.

2. Cheung KJ, Gabrielson E, Werb Z, Ewald AJ. Collective invasion in breast cancer requires a conserved basal epithelial program. *Cell*. 2013;155(7):1639-1651.

3. Collado M, Serrano M. Senescence in tumours: Evidence from mice and humans. *Nat Rev Cancer*. 2010;10(1):51-57.

4. Bonatti S, Hochman B, Tucci-Viegas VM, et al. In vitro effect of 470 nm LED (light emitting diode) in keloid fibroblasts. *Acta Cir Bras*. 2011;26(1):25-30.

5. McDonald R, Macgregor SJ, Anderson JG, Maclean M, Grant MH. Effect of 405-nm high-intensity narrow-spectrum light on fibroblast-populated collagen lattices: An in vitro model of wound healing. *J Biomed Opt*. 2011;16(4):048003.

6. Azevedo LH, de Paula Eduardo F, Moreira MS, de Paula Eduardo C, Marques MM. Influence of different power densities of LILT on cultured human fibroblast growth : A pilot study. *Lasers Med Sci*. 2006;21(2):86-89.

7. Nikon Instruments I. Infinity optical systems. http://www.microscopyu.com/articles/optics/cfintro.html.

8. Soule HD, Maloney TM, Wolman SR, et al. Isolation and characterization of a spontaneously immortalized human breast epithelial cell line, MCF-10. *Cancer Res*. 1990;50(18):6075-6086.

9. Yoon DS, Wersto RP, Zhou W, et al. Variable levels of chromosomal instability and mitotic spindle checkpoint defects in breast cancer. *Am J Pathol*. 2002;161(2):391-397.

10. Debnath J, Muthuswamy SK, Brugge JS. Morphogenesis and oncogenesis of MCF-10A mammary epithelial acini grown in three-dimensional basement membrane cultures. *Methods*. 2003;30(3):256-268.

11. Dawson PJ, Wolman SR, Tait L, Heppner GH, Miller FR. MCF10AT: A model for the evolution of cancer from proliferative breast disease. *Am J Pathol*. 1996;148(1):313-319.

12. von Lintig FC, Dreilinger AD, Varki NM, Wallace AM, Casteel DE, Boss GR. Ras activation in human breast cancer. *Breast Cancer Res Treat*. 2000;62(1):51-62.

13. Santner SJ, Dawson PJ, Tait L, et al. Malignant MCF10CA1 cell lines derived from premalignant human breast epithelial MCF10AT cells. *Breast Cancer Res Treat*. 2001;65(2):101-110.

14. Marella NV, Malyavantham KS, Wang J, Matsui S, Liang P, Berezney R. Cytogenetic and cDNA microarray expression analysis of MCF10 human breast cancer progression cell lines. *Cancer Res*. 2009;69(14):5946-5953.

15. Imbalzano KM, Tatarkova I, Imbalzano AN, Nickerson JA. Increasingly transformed MCF-10A cells have a progressively tumor-like phenotype in three-dimensional basement membrane culture. *Cancer Cell Int*. 2009;9:7-2867-9-7.

16. Ganem NJ, Godinho SA, Pellman D. A mechanism linking extra centrosomes to chromosomal instability. *Nature*. 2009;460(7252):278-282.

17. Zink D, Fischer AH, Nickerson JA. Nuclear structure in cancer cells. *Nat Rev Cancer*. 2004;4(9):677-687.

18. Ikeguchi M, Sato N, Hirooka Y, Kaibara N. Computerized nuclear morphometry of hepatocellular carcinoma and its relation to proliferative activity. *J Surg Oncol*. 1998;68(4):225-230.

19. Clawson GA, Blankenship LJ, Rhame JG, Wilkinson DS. Nuclear enlargement induced by hepatocarcinogens alters ploidy. *Cancer Res*. 1992;52(5):1304-1308.

20. Hu L, Potapova TA, Li S, et al. Expression of HPV16 E5 produces enlarged nuclei and polyploidy through endoreplication. *Virology*. 2010;405(2):342-351.

21. McClintock B. The stability of broken ends of chromosomes in zea mays. *Genetics*. 1941;26(2):234-282.

22. Crasta K, Ganem NJ, Dagher R, et al. DNA breaks and chromosome pulverization from errors in mitosis. *Nature*. 2012;482(7383):53-58.

23. Thompson SL, Compton DA. Chromosome missegregation in human cells arises through specific types of kinetochore-microtubule attachment errors. *Proc Natl Acad Sci U S A*. 2011;108(44):17974-17978.

24. Duncan AW, Taylor MH, Hickey RD, et al. The ploidy conveyor of mature hepatocytes as a source of genetic variation. *Nature*. 2010;467(7316):707-710.

25. Guidotti JE, Bregerie O, Robert A, Debey P, Brechot C, Desdouets C. Liver cell polyploidization: A pivotal role for binuclear hepatocytes. *J Biol Chem*. 2003;278(21):19095-19101.

26. Liotta LA, Kohn EC. The microenvironment of the tumour-host interface. *Nature*. 2001;411(6835):375-379.

27. Ye Q, Kantonen S, Gomez-Cambronero J. Serum deprivation confers the MDA-MB-231 breast cancer line with an EGFR/JAK3/PLD2 system that maximizes cancer cell invasion. *J Mol Biol*. 2013;425(4):755-766.

28. Prince ME, Sivanandan R, Kaczorowski A, et al. Identification of a subpopulation of cells with cancer stem cell properties in head and neck squamous cell carcinoma. *Proc Natl Acad Sci U S A*. 2007;104(3):973-978.

29. Marusyk A, Polyak K. Tumor heterogeneity: Causes and consequences. *Biochim Biophys Acta*. 2010;1805(1):105-117.

30. Lowe SW, Lin AW. Apoptosis in cancer. *Carcinogenesis*. 2000;21(3):485-495.

31. Hanahan D, Weinberg RA. The hallmarks of cancer. *Cell*. 2000;100(1):57-70.

32. McClatchey AI, Yap AS. Contact inhibition (of proliferation) redux. *Curr Opin Cell Biol*. 2012;24(5):685-694.

33. Hetzer MW. The role of the nuclear pore complex in aging of post-mitotic cells. *Aging (Albany NY)*. 2010;2(2):74-75.

34. Miki Y, Ono K, Hata S, Suzuki T, Kumamoto H, Sasano H. The advantages of co-culture over mono cell culture in simulating in vivo environment. *J Steroid Biochem Mol Biol*. 2012;131(3-5):68-75.

35. Kuhbier JW, Bucan V, Reimers K, et al. Observed changes in the morphology and phenotype of breast cancer cells in direct co-culture with adipose-derived stem cells. *Plast Reconstr Surg*. 2014;134(3):414-423.

36. Hollmen M, Roudnicky F, Karaman S, Detmar M. Characterization of macrophage--cancer cell crosstalk in estrogen receptor positive and triple-negative breast cancer. *Sci Rep*. 2015;5:9188.

37. Carey SP, Starchenko A, McGregor AL, Reinhart-King CA. Leading malignant cells initiate collective epithelial cell invasion in a three-dimensional heterotypic tumor spheroid model. *Clin Exp Metastasis*. 2013;30(5):615-630.

38. Cheung KJ, Gabrielson E, Werb Z, Ewald AJ. Collective invasion in breast cancer requires a conserved basal epithelial program. *Cell*. 2013;155(7):1639-1651.

39. Heylen N, Baurain R, Remacle C, Trouet A. Effect of MRC-5 fibroblast conditioned medium on breast cancer cell motility and invasion in vitro. *Clin Exp Metastasis*. 1998;16(2):193-203.

40. Francescone RA,3rd, Faibish M, Shao R. A matrigel-based tube formation assay to assess the vasculogenic activity of tumor cells. *J Vis Exp*. 2011;(55). pii: 3040. doi(55):10.3791/3040.

41. Zhang S, Zhang D, Sun B. Vasculogenic mimicry: Current status and future prospects. *Cancer Lett*. 2007;254(2):157-164.

42. Basu GD, Liang WS, Stephan DA, et al. A novel role for cyclooxygenase-2 in regulating vascular channel formation by human breast cancer cells. *Breast Cancer Res*. 2006;8(6):R69.

43. Kuilman T, Peeper DS. Senescence-messaging secretome: SMS-ing cellular stress. *Nat Rev Cancer*. 2009;9(2):81-94.

44. d'Adda di Fagagna F. Living on a break: Cellular senescence as a DNA-damage response. *Nat Rev Cancer*. 2008;8(7):512-522.

45. Roninson IB. Tumor cell senescence in cancer treatment. *Cancer Res*. 2003;63(11):2705-2715.

46. Becker T. Molecular Mechanisms of Cellular Senescence, Senescence and Senescence-Related Disorders, Dr. Wang Zhiwei (Ed.), ISBN: 978-953-51-0997-6, InTech, DOI: 10.5772/54120.

47. Iliopoulos D, Hirsch HA, Wang G, Struhl K. Inducible formation of breast cancer stem cells and their dynamic equilibrium with non-stem cancer cells via IL6 secretion. *Proc Natl Acad Sci U S A*. 2011;108(4):1397-1402.

48. Charafe-Jauffret E, Ginestier C, Iovino F, et al. Breast cancer cell lines contain functional cancer stem cells with metastatic capacity and a distinct molecular signature. *Cancer Res*. 2009;69(4):1302-1313.

49. Aasen T, Izpisua Belmonte JC. Isolation and cultivation of human keratinocytes from skin or plucked hair for the generation of induced pluripotent stem cells. *Nat Protoc*. 2010;5(2):371-382.